Delft University of Technology

Msc Thesis

Modelling the equalizing process of rockfill dumps with a plough

subsea cut and transport processes

W. Kranendonk

Faculty Civil Engineering
Section hydraulic engineering

Version 1.1, June 17, 2011

Modelling the equalizing process of rockfill dumps with a plough

subsea cut and transport processes

Author:
Wouter Kranendonk

Thesis Committee:
TU Delft
Prof. dr. ir. C. van Rhee
Ir. G.L.M. vd Schrieck
Ir. H.J. Verhagen

Company Supervisors
L. Kok
S. Wezemer
M. Moens

Under the Authorisation of:
Koninklijke Boskalis Westminster N.V.
Van Oord B.V.

Acknowledgments

This thesis has been performed under the guidance of the section Dredging Engineering and is carried out under the authorization of PUMA, a joint venture of Royal Boskalis Westminster N.V. and Van Oord B.V. The scale tests were executed in the Speurwerkgoot at the faculty of Civil Engineering at the Technical University Delft.

I would like to use this opportunity to thank several people who were involved and helped me during my graduation period.

First of all I would like to thank my thesis committee for the helpful guidance during my research. Ir. G.L.M. van der Schrieck for the always interesting conversations we had during the individual meetings. The meetings gave me useful knowledge and the discussions resulted in new insights in the processes. Ir. Verhagen for guiding me, especially in the first period by keeping a good overview and giving me the right directions. My graduation professor, prof.dr.ir. C. van Rhee for the useful feedback during the committee meeting and the critical view on my work

I would like to thank Boskalis and Van Oord for the opportunity to perform this graduation research and the resources that where needed to execute my work. Leonard Kok for providing me useful practical knowledge behind the theory and supporting and motivating me during the individual and the committee meetings. Anna Kroon for helping me to explain and write some useful Matlab codes to quickly process the data obtained in the physical scale test. Henrik Keij for supporting me and providing me with useful insights on both a professional and personal level. Serge Wezemer and Joost Mol for sharing practical knowledge of ploughing. Dick Bodegom for the critical view and feedback during the conversations we had at the PUMA office. And all the other people at the PUMA office I did not mention for the conversations and great time I had working there.

For the practical execution of my research I would also like to thank Dingena Schott, from the section Transport Engineering & Logistics, for the opportunity to work with EDEM. I would also like to thank the staff members of the laboratory for the assistance during my physical scale test.

Finally I would like to thank my parents for supporting me through the years of my study. And my girlfriend for her patience and the interest she shows for my study and work field.

Abstract

A way to equalize granular rockfill dumps at a sea or river bed is the use of a plough. A plough can be modeled as a set of straight blades in sequence. Several cutting models for dry and saturated sand are present in the literature. In cutting coarse material, the increase in pore water pressures caused by dilatancy of the grain structure play a minor role. This results in a different shape of the layer cut than for traditional cutting methods in fine soils. The layer cut has a limited surface slope resulting in grains rolling down under the angle of repose η. Failure of the grain structure in coarse material depends mainly on the gravitational, shear and inertial forces between grains. This master thesis gives an analytical model for cutting rockfill larger than medium coarse sand with straight cutting blades (Chapter 4.2). A description is given of the important processes involved in equalizing with a plough and the different stages of filling. The analytical model is realized by use of models made by S.Miedema for cutting saturated sand and models for cutting dry sand by Hettiaratchi, and Reece (1966). The analytical model is verified by performing a physical scale model. The scale model is used to simulate the process in a discrete element computer model EDEM .

Contents

Nomenclature

A_{blade}	Area of blade tip	[m^2]
A_{stone}	Stone surface	[m^2]
B_{eff}	Width strip foundation	[m]
c_{μ}	Friction coefficient	[-]
C_m	Factor virtual mass ship	[-]
D	Diameter of particle	[m]
D_e	Equivalent core diameter	[m]
E_{kin}	Kinetic energy ship	[Nm]
F_d	Drag force	[N]
F_n	Normal force on blade	[N]
F_i	Inertia force ship	[N]
F_e	Propeller force ship	[N]
F_g	Gravitational force blade	[N]
F_s	Friction force shear zone	[N]
$F_{H,f}$	Horizontal force front blade	[N]
$F_{H,r}$	Horizontal force rear blade	[N]
$F_{V,f}$	Vertical force front blade	[N]
$F_{V,r}$	Vertical force rear blade	[N]
$F_{Friction}$	Friction force plough surface/soil	[N]
G_w	Mass soil wedge transporting	[N]
G	Mass soil wedge cutting	[N]
h_b	Height of blade	[m]

h_i	Cutting depth	[m]
h_w	Height of wedge in front of blade	[m]
I_{sd}	Point load strength	[kPa]
k	Elasticity wires	[mm/N]
K_2	Grain force on blade	[N]
L_b	Length of blade	[m]
L_w	Length wedge in x-direction	[m]
L_s	Length shear zone	[m
L_{eff}	Length strip foundation	[m]
m	Water displacement	[N]
n_0	Initial porosity sub layer	[-]
n_{wedge}	Porosity wedge	[-]
P	Failure Load (pressure x piston area)	[kN]
p_f	Bearing resistance soil	[Kpa]
p_w	Water pressure	[kPa]
T	Inertia force	[N]
ΔV_1	Overflow volume	[m^3]
ΔV_2	Exchanged soil volume wedge	[m^3]
W_b	Width of blade	[m]
x_m	Horizontal distance to mass centre	[m]
$\ddot{x}$	Acceleration of particle in x-direction	[m/s^2]
y_w	Vertical distance to wire attachment	[m]
α	Angle of blade	[degree]
α^*	Angle of boundary wedge	[degree]
β	Angle of shear line	[degree]
β_{lift}	Angle of suspension wire with x	[degree]

β_d	Angle of drag wire with	[degree]
δ	Friction angle between steel and soil	[degree]
λ	Friction angle between boundary wedge and Rankine zone	[N/m^3]
γ	Density of rockfill	[N/m^3]
μ_r	Coefficient of rolling friction of particle in EDEM	[-]
μ_s	Coefficient of static friction of particle in EDEM	[-]
ρ_s	Density of solids	[kg/m^3]
ρ_w	Density of water	[kg/m^3]
φ	Angle of internal friction	[degree]
η	Angle of repose	[degree]
$\ddot{\phi}$	Angular acceleration of particle	[rad/s^2]
σ	Total soil stress	[kPa]
σ'	Effective grain stress	[kPa]
σ_v	Vertical penetration stress	[kPa]
$\sigma_{v,blade}$	Vertical stress under the assumption the blade is penetrating	[kPa]
$\sigma_{v,stone}$	Vertical stress under the assumption the stone is penetrating	[kPa]
τ_s	Shear stress	[kPa]
$\tau_{s,critical}$	Critical shear stress	[kPa]
τ_δ	Steel/soil friction	[kPa]

List of Figures

List of Tables

Chapter 1 Introduction

As a result of flow or wave motion near the coast and in rivers sediment is transported. This sediment often consist of natural materials, like cohesive mud, silt and sand. When the water movement decreases the sediment settles on the bed, resulting in a decrease of the water depth or local shoals. A decrease in water depth is an unwanted effect for navigation. To maintain a good accessibility of the waterways, maintenance dredging is often carried out. The navigation depth is increased by removing the top soil layer. The bottom has to be equalized afterwards in order to guaranty the desired bottom level over the entire cross section. A method of equalizing the bottom, especially on places that are difficult to reach, is ploughing.

Ploughing is a method in which a harbour or river bed is equalized by use of a plough(bar). The plough is attached to a vessel or crane by wires and dragged along the bottom. During the ploughing process material is transported from higher lying peaks in the bed (dunes) to deeper lying areas (gullies). This is done by scraping/cutting material from a dune and transport this material in front of the plough. A more extensive description of the process of ploughing can be found in chapter 3.

A current development is using a ploughbar to equalize coarse sand and rockfill. The particle size varies from gravel to cobbles and boulders. The rockfill is dumped by vessels or cranes as a foundation for hydraulic structures. Due to positioning inaccuracies and wave motion during dumping the stones are not equally spread on the bottom. Irregularities in filter or foundation layers can cause problems for a good placement of the superstructure. Ploughing is currently used as a method to equalize these coarse rockfill layers.

This report is a research on the processes involved in equalizing coarse material and how to translate these processes into analytical models. A scale experiment is performed to visualize the plough and soil movement and to obtain quantitative information to validate these models. The report starts with a short introduction on the company the research is carried out for and a problem analysis is given (chapter 2). Chapter 3 gives an analysis of the processes involved in equalizing a sea or river bottom. After a literature study, the existing models for cutting dry and saturated sand from the literature (chapter 4.1) are used to create analytical models that are applicable for equalizing/ cutting coarse grains (chapter 4.2).

A comparison is made between the data obtained from the physical scale model and the calculations from the analytical models (chapter 6). The second model is a computer model using discrete element modelling (chapter 7). The EDEM computer model is validated by the observations and data obtained from the physical scale model and is performed after the derivation of the analytical models. The simulation is used to get more insight of the grain movement inside a layer cut and the occurrence of a shear plane.

Note that the word ploughing is used in this report in combination with other words like equalizing or leveling. The term ploughing is wide used in dredging companies. So although the word is technically not exactly right it will be used to describe the operation. Ploughing is an activity in agricultural operations in which the soil is penetrated and moved upward in order to create a loose sub layer well exposed to the air. This is in fact the opposite process as in dredging where the top layer is equalized and the underlying layers are hardly disturbed.

Chapter 2 Problem analysis

2.1 Motive research

In Rotterdam (Netherlands) a large land reclamation project is carried out along the coast. At the north side of the reclamation area a revetment is constructed to protect the harbour from incoming waves. The revetment consist of a granular rockfill deposited on top of a sand embankment. The embankment is made by trailing suction hopper dredgers using excavated sand from the North sea. The granular revetment is build in layers with increasing stone size consisting of respectively gravel, cobbles and boulders. On top of the boulders concrete blocks of 40 tons are placed to break the waves. The condition of the sub layers is important for the stability and filter properties beneath the blocks. These layers prevent erosion of the underlying sandy bottom and form a foundation for the blocks. The granular rock is deposited by side stone dumping vessels (SSDV). These ships shove rockfill from both sides of the deck by hydraulic cylinders setting walls in motion. Due to wave motion and irregular sliding of the rockfill high spots are created on the sea bottom.

The high spots differ in layer thickness and are effecting the next layer that is deposited, causing the bed level to deviate from the design level . The bed level is monitored using a multibeam. Each layer is inspected in order to ensure the filter properties. To remove the high spots, the bottom is equalized by a ship equipped with a 17 ton weighing plough as shown in figure 2.1.

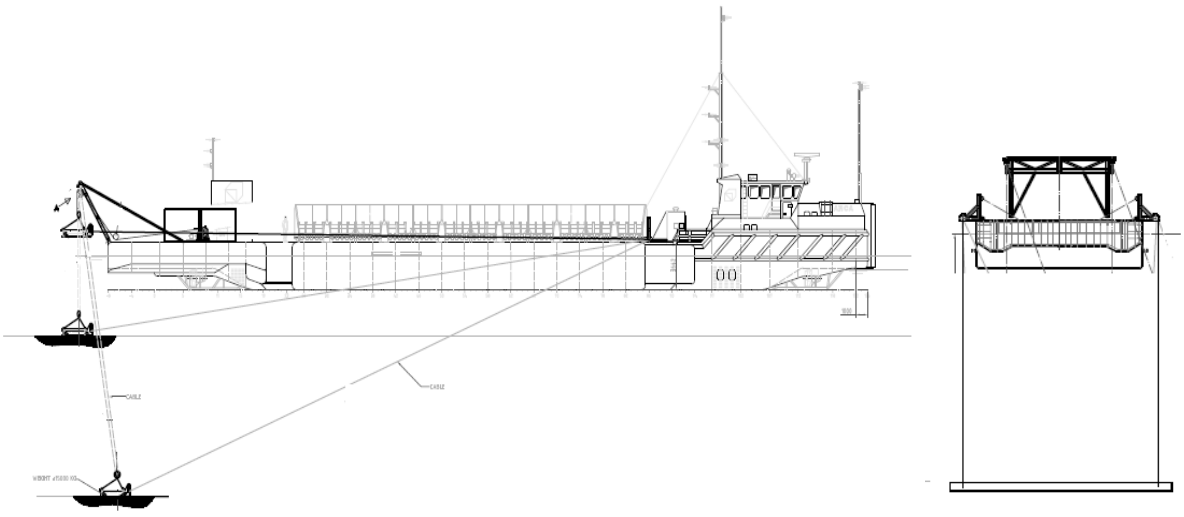

Figure 2.1 Plough suspension to the ship, two depth configurations

The progress of the revetment is depending on both the SSDV and the plough ship. The SSDV cannot deposit the next layer before the high spots have been removed. The estimated plough production is not achieved at the project. Some changes to the shape of the plough have been made to improve the production. These changes are based on perception and experience, the effect of changing the plough shape is not based on scientific research.

2.2 Problem analysis

The plough production is insufficient and is causing delay to other ships and the progress of the revetment. The reason that the estimated production is not met can depend on several causes which will be discussed in this chapter.

In order to determine the cause of the low production of the plough a good understanding of the plough process in coarse material is important. The different variables that influence the production must be determined in order to optimize the plough production. The following variables can be the reason for not meeting the estimated production, see also Appendix 1.

1 Ship dimensions
2 Plough design
3 Soil/ material properties
4 Measure and control system
5 Boundary conditions (flow, waves, wind, swell, water depth etc.)
6 Shipping crew
7 Bathymetry (roughness, slope, target depth)

Ad1 The dimensions of the ship determine the maximum bollard pull, the angle of the drag wires and the ship movements. A long vessel can provide a lower pulling angle, because the wires will reach the bow of the ship under a smaller slope angle. This results in a more horizontal pulling force on the plough. The roll, pitch and yaw movement of the ship will decrease with a larger ship size, resulting in a more steady plough suspension. On the other hand the flexibility in small plough areas or limited water depth is restricted for larger ships. The horizontal pulling force is depending on the maximum bollard pull (in tons) delivered by the propellers of the specific ship.

Ad2 The plough shape determines the cut and transport function. Every soil has its own properties and therefore needs its specific plough design. It is important to determine the shape variables responsible for the cutting and transporting properties of the plough.

Ad3 The soil properties determine the behaviour of the soil during ploughing. To understand the processes when cutting different soils is crucial. The friction forces, interlocking, water pressure forces, adhesion etc. determine the soil movement in front of the blade and cutting forces on the blade. The soil behaviour differs for each soil type.

Ad4 The quality of the measurement and control systems determine the accuracy of the operations. Survey beneath the water level is often carried out with a multibeam sonar. A good map of the bottom profile is necessary for a good work instruction. In this work instruction is given where soil has to be removed and where soil has to be supplemented. The control system for lowering and controlling the plough depth is determining the accuracy of the cutting depth. The ship movements has to be taken into account during wave and other ship motions. The control system has to predict the ship movement in order to control the plough depth..

Ad 5 Boundary conditions at sea determine the ship and plough motion, therefore a good knowledge in the effect of these sea conditions is relevant.

Ad 6 For good results the shipping crew must have experience in ploughing. The interpretation of the survey data and the proper plough depth adjustment determine the production.

Ad 7 The transport distance depends on the bathymetry of the dumped rockfill layers. Varying transport distances are not unusual, because the bed roughness is difficult to control with SSDVs. A soil balance determines where high spots need to be removed and where this soil can be stored within the area (chapter 3.5).

2.3 Research definition and research goals

From the production dependant variables mentioned in the previous paragraph the interaction between the plough and the soil will be examined in this thesis. The production can be increased due to a better understanding in the cutting and transport processes during ploughing.

From preliminary research follows that, unlike cutting fine material, knowledge of cutting and transporting coarse material is very limited. Knowledge of equalizing rockfill is mainly gained during dredging projects and is mostly based on experience. By changing the bar shape and analysing the results during operation gave insight in some of the effects during ploughing. In addition, several tests have been performed by dredging companies and Rijkswaterstaat. These tests were based on ploughing fine material, very little information is available on ploughing in grain sizes larger than medium coarse sand. More research in ploughing coarse material is important to really understand the plough process and optimise the variables that determine the plough process. This thesis will focus on gaining knowledge in equalizing coarse material, what brings us to the research question:

“What important processes are involved in equalizing rockfill with a plough (gravel, cobbles and boulders) and how to model these processes”.

The following sub research questions will be examined and used to answer the main question:

- Can cutting & transporting of coarse material be described with existing continuum cutting models. What are the limitations and what adjustments have to be made to these models?

- What is influencing the moving behaviour of the plough in the coarse material and how does this affect the transport distance of soil?
- What is the movement of the individual grains in front of and between both blades.

In order to give a good solution to the formulated research question the focus of the research is the soil behaviour in front of the plough(blade). So the research will focus on the grain movement and the forces needed to excavate and transport a certain volume of soil. The plough/grain interaction will be modeled with mathematical models and made visible with a physical scale model.

2.4 Research boundary

The research is performed within the following scope.

- The research is based on equalizing coarse material, the particles are large enough to neglect the effect of significant pore water under pressures .
- The grain-size distribution used in the scale experiment is based on distributions used at the Maasvlakte II project. The influence of varying the grain distribution is not examined.
- The shape of the scale model plough differs from the prototype used at the Maasvlakte II project, see Appendix 2. This decision is made by the availability of a model plough that is recently used in a scale model research by Rijkswaterstaat. Some variables like the height and width are fixed. The weight, blade angle and drag angle can be varied (see figure 2.2).
- The drag and suspension cables are assumed to be infinite stiff and the movement of the plough or ship due to wind and waves will not be taken into account.

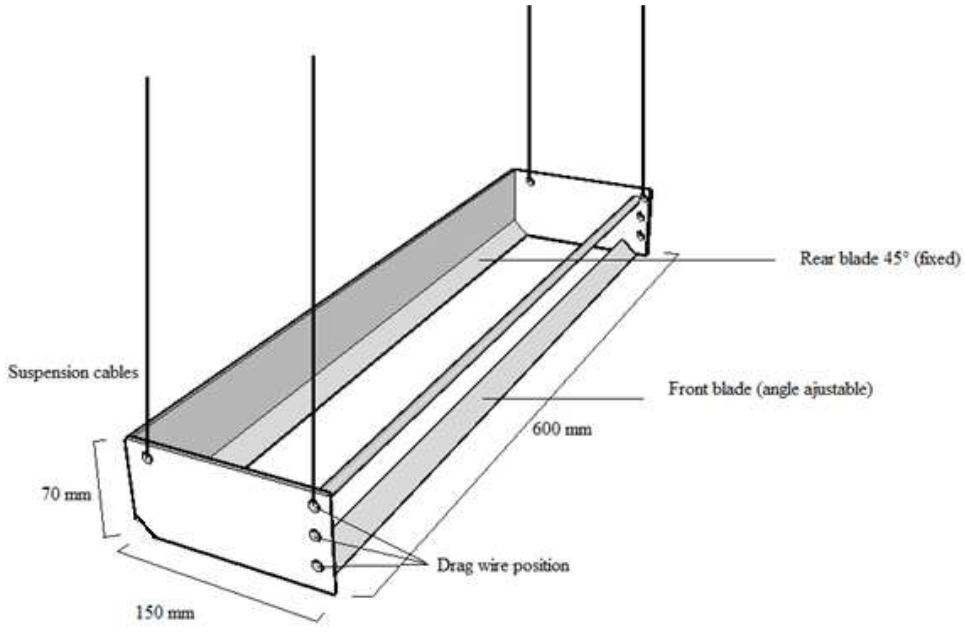

Figure 2.2 3D drawing of model plough used for physical scale modelling

I Literature study

Chapter 3 The principles of ploughing

3.1 Plough design

A plough consists of a cutting blade and a dozer blade with a storage area. These two parts deliver the two main functions: Cutting and transporting soil. The cutting blade is used to loosen the soil layer to be removed by penetrating into the grain structure. The material is than transported over the front blade and deposited behind this blade. The space between the cutting and the dozer blade is a buffer zone where the soil loosened by the front blade is accumulated. The rear blade transports the soil that is accumulated in the storage area and is therefore often higher than the front blade. Both blades are connected by side beams forming a stiff construction. The integral construction is called the plough. The shape of the plough depends on the soil that is equalized. Some examples of plough designs are given below.

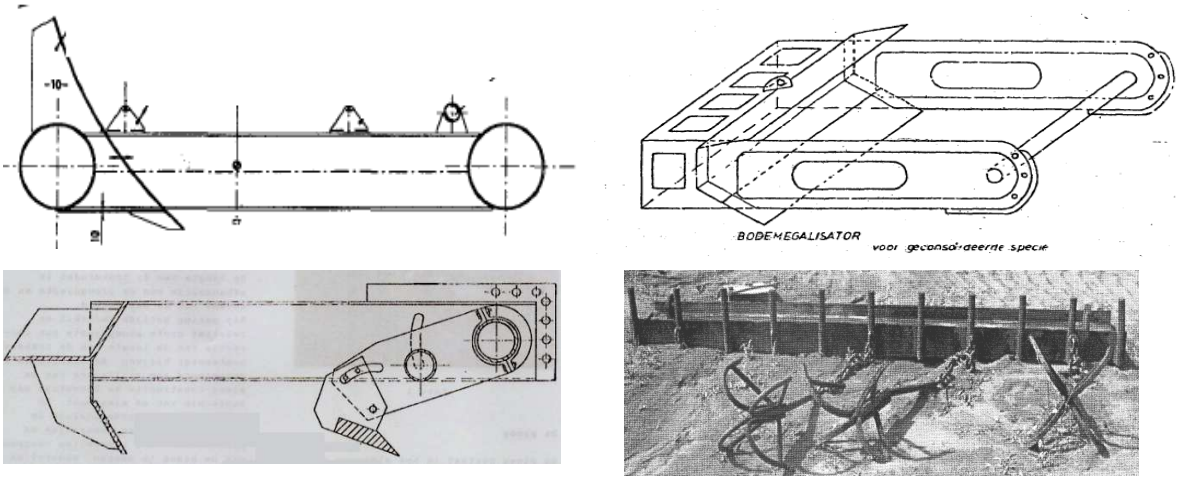

Figure 3.1 Plough designs used for different soil types

There are 3 main types of cutting tools that can be distinguished, straight blades, curved blades and ripper teeth, see figure 3.2. The choice for a cutting tool depends on the material that is cut. A ripper is in fact a narrow blade used for penetration into the soil. Straight blades are used for cutting and shoving material.

Figure 3.2 Types of cutting tools

The plough is suspended by one or more steel suspension cables at a fixed water depth. This suspensions prevents a free downward movement of the plough. The plough is not therefore entirely resting on the bed and cannot cut to an uncontrolled large cutting depth.

The cables are vertically connected to a steel frame welded to the back of the vessel, see figure 2.1. This steel frame has a suspension function but is also used to hoist the plough above the water level. Pulley blocks on the frame guide the cables to winches that are placed on deck of the ship.

To generate a pulling force another one or two wires are connected to the front of the plough. The first few meters often consists of a steel chains to create a lower pull angle due to the weight of the chain. Another function of these chains is to withstands the wear effects during ploughing. The wires are attached near the bow of the ship to create a low pulling angle, resulting in a horizontal force.

The plough is brought to a target depth beneath the water level during sailing. The plough suspension is adjusted by winches until it equals the desired target depth. The plough level is kept constant during wave motions with the help of an automated wire motion sensor. The sensor measures the ship motion and gives a signal to a computer that is controlling the winches.

3.2 Cutting process (basics of soil mechanics)

The force that is required to cut a layer of soil is depending on the soil properties and the dimensions of the cutting tool. The exerted force must be high enough to penetrate and cut loose the soil by failure of the grain structure. Due to deformation of the grain structure the grains move in relation to each other by sliding, rolling and shearing. From the literature follows that the strength of the grain structure depends on density, particle size (distribution), particle roughness, particle shape, porosity and saturation [5].

Reynolds (1985) [7] considered that in order to slide grains over each other a change in volume is necessary. The phenomenon of an increase of pore volume is called dilatancy. As a result of the increase in pore volume, water will flow in the deformation zone. This causes a decrease of the pore water pressure p_w and because the soil stress σ remains constant the grain stress σ' will increase. In fine sand this causes an additional shear force between the grains that will increase the cutting force. Terzaghi [7] formulated in Eq. (3.1) that a change in soil stress σ due to compression, deformation and shear, is a direct result of a change in effective stress σ':

$$\sigma = \sigma' + p_w \tag{3.1}$$

A bed consisting of large grains has large pores and a high permeability. This results in a negligible low decrease in water pressure p_w. The intergranular force sole depends on the contact forces between the rock particles due to dilatancy and shearing. The amount of dilatancy depends on the particle shape. With increasing irregularities more volume must be created between for the grains to roll or shear. Spherical particles shift primarily by rolling, while angular grains move by dilatation [1]. As shown in figure 3.4 the sand that passed the shear plane is fully dilated, the increase in pore volume Δn due to dilatancy can be calculated by the relation:

$$\Delta n = \frac{\Delta V}{V} = \frac{(n_{loose} - n_0)}{(1 - n_{loose})} \tag{3.2}$$

Where:

n_0 = Initial porosity of the soil [-]

n_{loose} = Porosity of the loosened soil [-]

Assuming the grains are perfectly spherical shaped, the increase in porosity is given in figure 3.3. When the soil package is very dense, so a low porosity, more energy is needed to create space in between the grains. In reality the grains have an angular irregular shape and the pore volume differs for different soil types. The initial porosity depends on the shape of the particles, the gradation curve and the compaction. In order to dilate irregular particles, more space must be created to move particles over each other. The extra dilation results in a higher and more fluctuating cutting force.

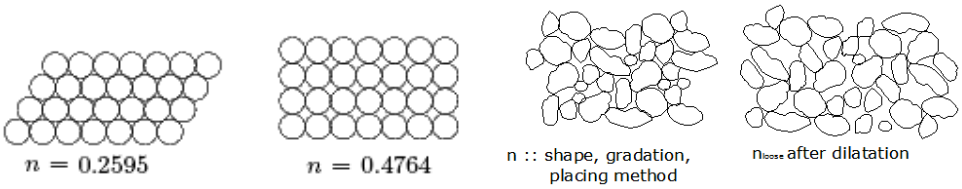

Figure 3.3 Dilatancy in spherical and angular shaped particles [7]

When the exerted shear force is reaching a critical value, a shear plane will cause the grain structure to fail. The shear plane starts at the blade tip and continues to the surface under an angle β. The thickness of the cutting layer and the angle β determine the length of the shear plane. Experimental research [2] has shown that the value for the shear angle β is determined by the lowest cutting energy. In sand this leads in practice to β of 25-35 degrees for blade angles α between 30 and 60 degree. The friction angle δ between steel and grains is examined by Miedema, 1987 [3] and is between 20-25 degrees in sand.

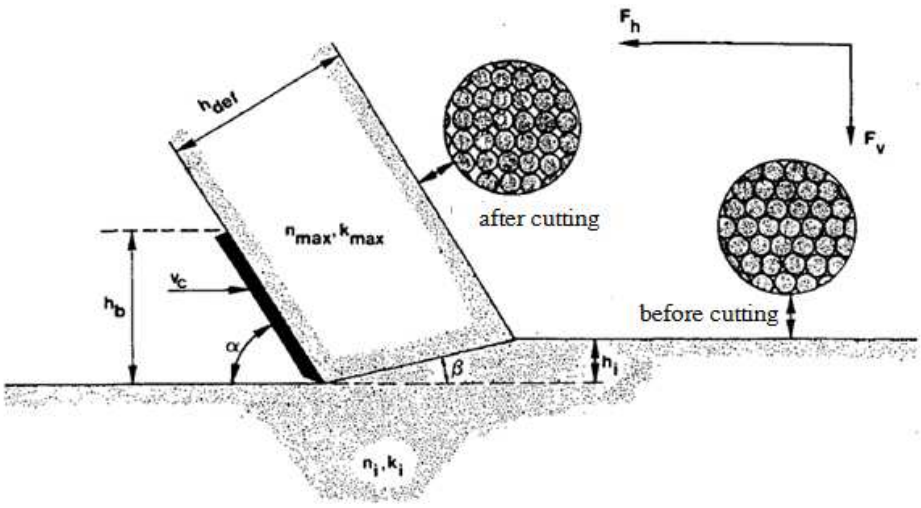

Figure 3.4 Dilatancy of the layer cut after passing the shear plane under angle β [3]

A more accurate shape of the shear plane is given by a logarithmic spiral from the blade point, see figure 3.5. The origin of the logarithmic spiral will be such that the total force on the blade is minimal. Terzaghi (1941) [18] examined that the basic models can be fairly simplified by assuming a straight shear line instead of a logarithmic slip line to calculate the cutting forces, see figure 3.5. To simplify the models in this research the shear plane will be assumed to have a straight line in front of the plough blade. From this follows that the length of the shear plane is proportional to the cutting depth of the plough

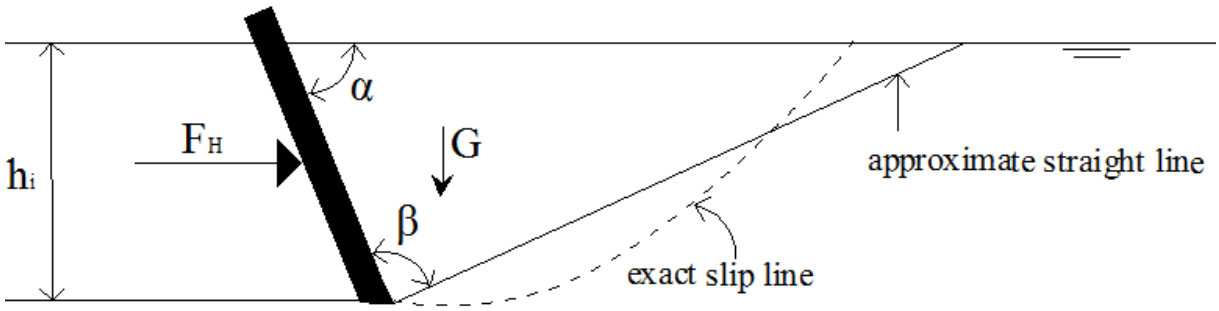

Figure 3.5 Simplification of the wedge theory of passive soil failure

Coulomb(1776) [7] described a linear relation between the normal stress σ_n and the shear stress τ_s on the shear plane. When the shear stress exceeds a critical value $\tau_{s,critical}$ the soil body will start sliding. Coulomb's Law of Friction notes that the friction factor is given by $\mu = \tan(\varphi)$ and is independent of the sliding velocity.

The Mohr-Coulomb criteria reads:

$$\tau_s = c + \sigma_n * \tan(\varphi) > \tau_{s,critical} \quad (3.3)$$

Where c = cohesion, σ_n = the normal stress and ϕ = internal friction angle of the material. In coarse material the cohesion is zero c = 0. The internal friction angle ϕ determine the friction between grains in the shear zone and is between 30-45 degree depending on the shape of the particles.

In 1914 (18), Mohr provided equations and a graphical method for finding stresses on different planes in a material at equilibrium, the Mohr circle. Mohr placed the normal stress σ_n in Eq. (3.3) at the horizontal axis and the shear stress τ_s on the vertical axis, see figure 3.6. The horizontal effective soil stress σ3´ and the vertical effective soil stress σ1´, are two points on the horizontal axis with midpoint σ2´ = (σ3´+σ1´)/2 . When a circle is drawn, the angle of the tangent to this circle gives the value for the internal friction angle ϕ. For stresses above this tangent the grain structure will fail. More complex cutting models using the Mohr-Coulomb criterion to describe the soil failure are extensively described in chapters 4.1 and 4.2.

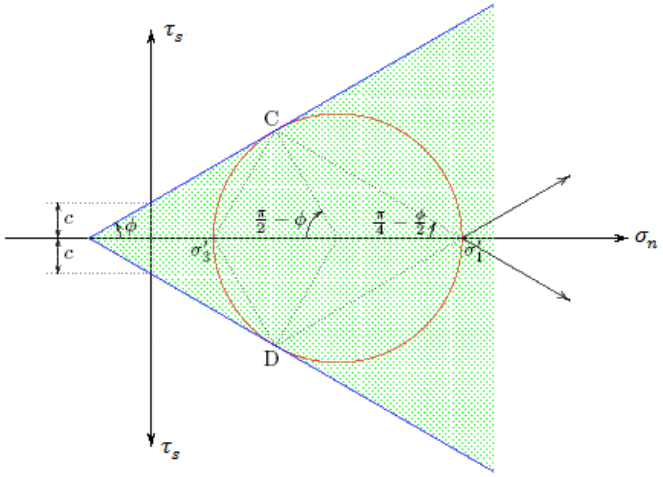

Figure 3.6 Mohr circle, visual presentation Mohr- Coulomb criterium

When ploughing a horizontal bed, not only the drag force but also the vertical penetration is important. The grain structure yields under the normal force of the plough blade tips on the subsoil. The origin of the normal force is exerted by the mass of the plough plus the mass of the soil that rests on the plough. Installing rippers will create room between the grains to facilitate dilatation. As a result of the decrease of the penetrating surface the pressure on the blade tip increases. The penetration model is described in chapter 4.3.

3.3 Soil accumulation in front of rear blade

The loosened material is deposited behind the cutting blade and accumulated in front of the rear blade. The way the material behaves in front of the blades is not clear and will be examined during this research.

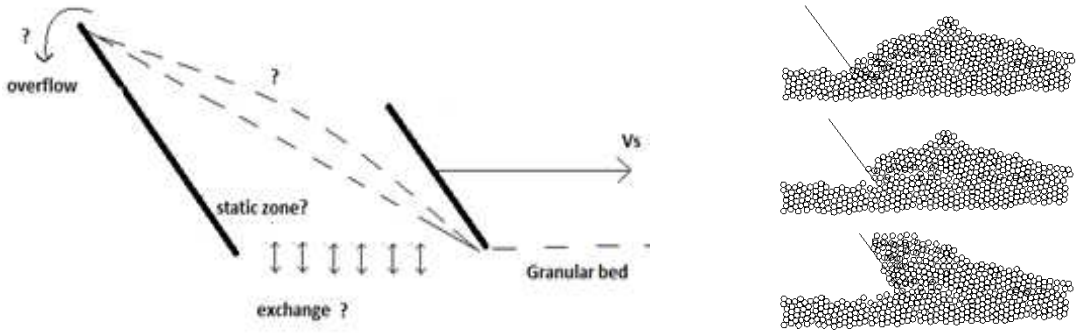

Figure 3.7 Soil accumulation in front of rear blade

With the current knowledge bulking starts at the plough surface and it continues to grow in front of the material that is already build up. The bar has a maximum transport capacity. This is the maximum volume of soil in front of the rear blade before material starts to overflow. The angle of repose of the soil in front of the blade can differ from the internal friction angle due to the motion of the blade. The shape of the transported soil volume in front of the rear blade and the exchange of material between this volume the subsoil will be examined during this research.

3.4 Transport behaviour

The soil that is accumulated in front of the rear blade is transported. During transport material is exchanged between the bulked volume and the bed. The soil volume in front of the blade depends on the amount of material deposited and picked up from the sub layer or high spots. There are different ways to describe the plough movement and the inflow and outflow of soil during equalizing. Figure 3.8 explains how to read the following schematizations describing this plough behaviour.

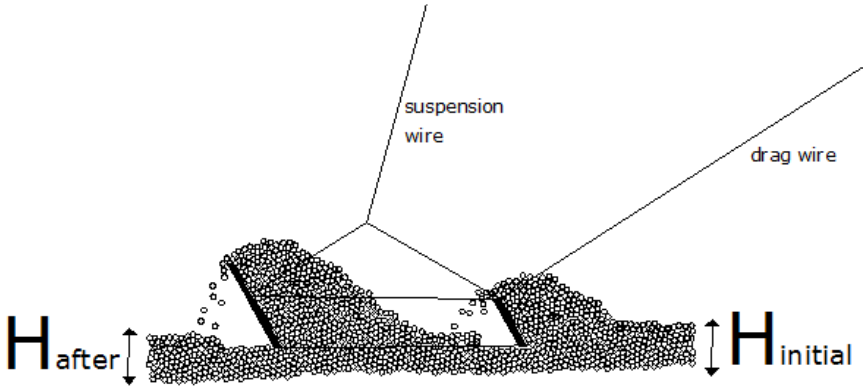

Figure 3.8 Equalizing with both blades, the blade has a straight movement trough the rock cover

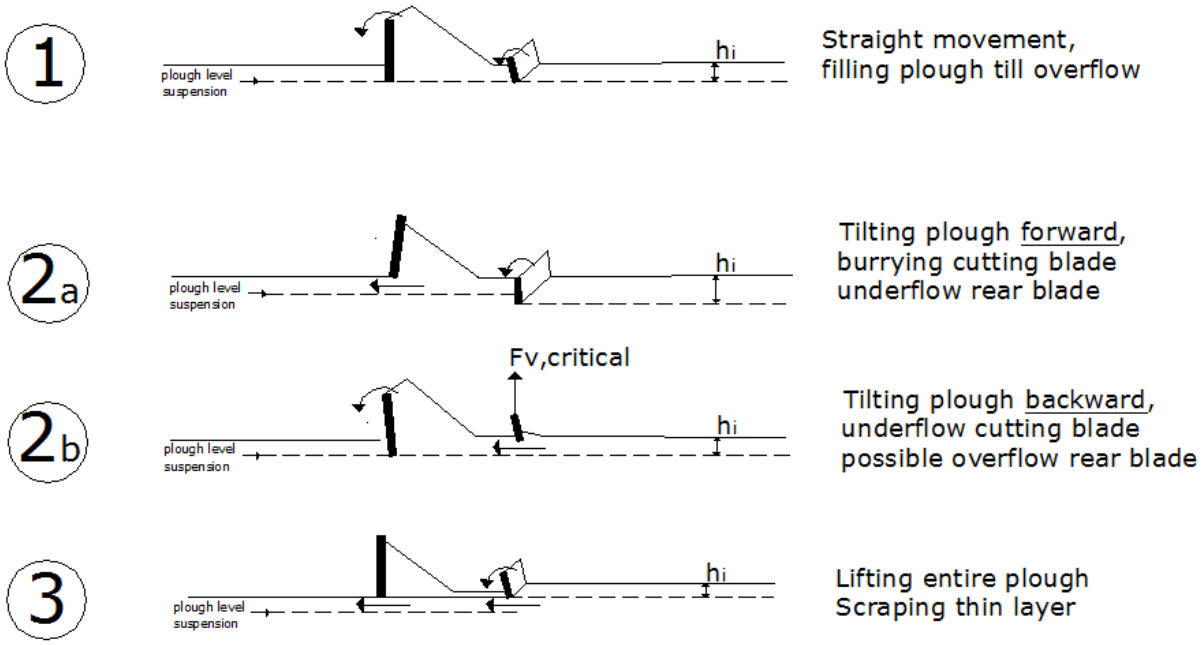

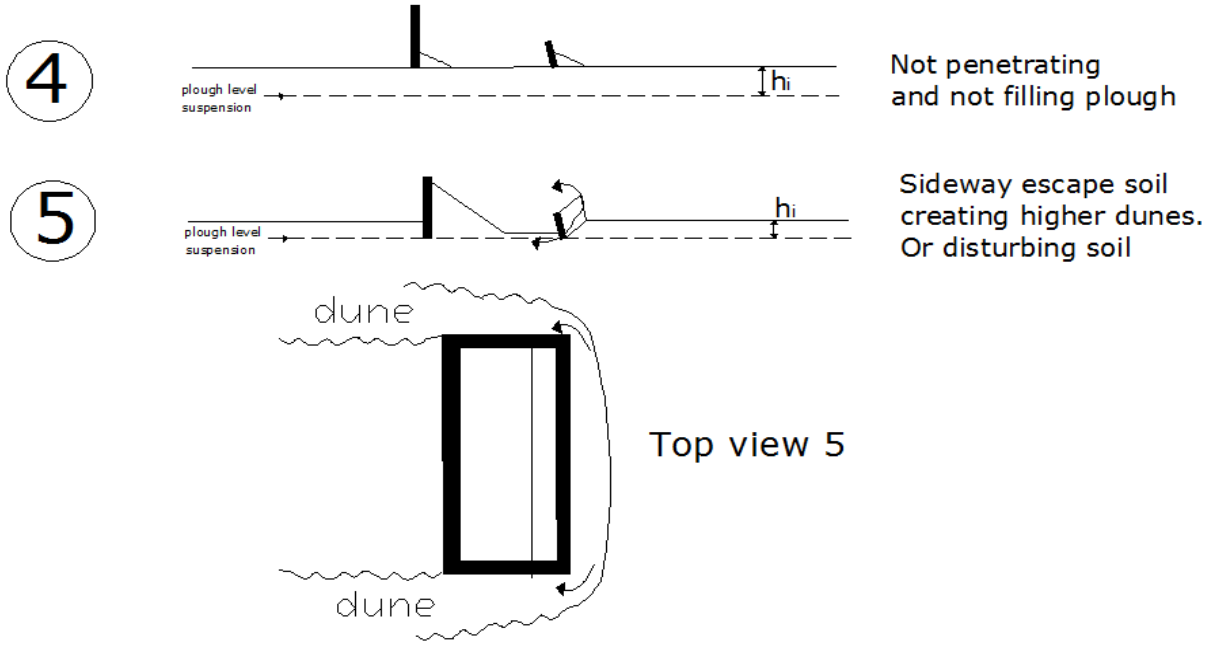

Figure 3.9 Schematizations of the plough movement when equalizing rockfill

Explanation figures:

1) The plough stays in a horizontal position and moves in a straight horizontal line, the cutting depth is constant. When the plough is completely filled material will overflow. This is the maximum production. When the plough is entirely filled the high spots will directly be deposited behind the plough.

2a) The plough is tilting because of a large resistance in front of the cutting blade. The resistance in front of the blade is caused by a high spot or a large cutting depth. When the force becomes too high the plough rotates around the front blade tip. The tilt movement will cause material to escape underneath the rear blade.

2b) The plough is lifted from the bed due to a high pulling force in a short period of time, for instance because of wave motion. The cutting blade is lifted from the soil that is allowing material to flow underneath the front blade. The rear blade will have an backward rotation, this facilitates overflow of the rear blade. The front blade can also be lifted in case of a high vertical cutting force. The rear blade is still penetrating due to a higher mass.

3) The plough finds an equilibrium at a cutting depth hi. This cutting depth is smaller than the initial plough suspension. This causes the plough to scrape a thin layer of the subsoil or the dune. The high spot will be lowered in layers, each time the plough is dragged across the high spot a thin layer is scraped of the top.

4) No material is transported, only set in motion over a very small distance. The plough bounces on the top of the sub layer and is not penetrating. The layer after ploughing equals the initial bed level.

5) Rocks are pulled out of the sub layer causing the bed roughness to increase. Also material can flow sideways of the blades, two dunes will be created on both sides of the plough.

It is desirable that the plough moves in a straight line through the rockfill. In this way an accurate cutting depth can be determined and the exact volume of soil that is removed. The filling distance is the distance in which the plough is entirely filled. This is an interesting parameter, since the plough preferably has to be completely filled just before it reaches a storage area.

3.5 Soil balance

To store the transported soil within the area the soil balance must be satisfied. The coordinates of the high spots are determined by survey using multibeam sonar. The high spots must be transported to a storage area where the material can be deposited. This storage area must be in the sailing direction of the ship with the criterion that the volume of the storage area is equal or larger than the volume of the high spot $V_{storage} \geq V_{dune}$. With a more complex bed configuration an accurate ocean floor survey and volume calculations can be carried out to determine the soil balance.

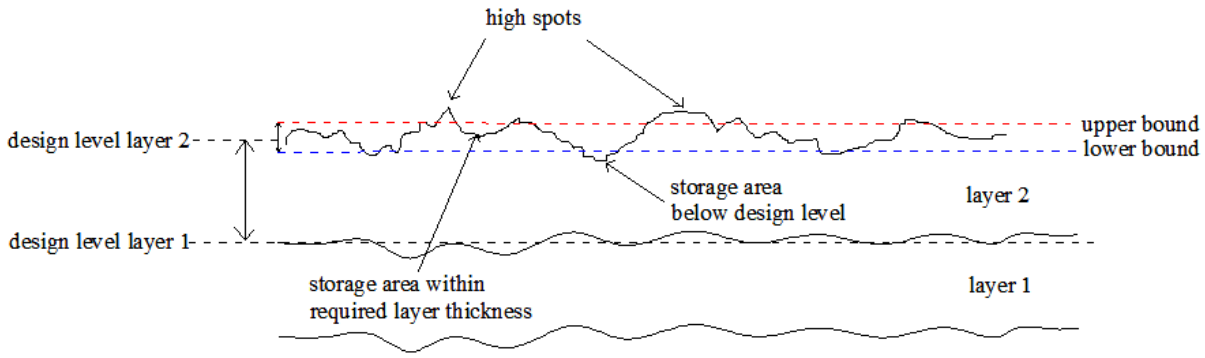

Figure 3.10 Bed configuration with high spots exceeding the upper bound of the design level

When the plough comes to an area where the bed level in below the plough suspension, the material can escape underneath the blades and the plough will unload itself. The transport distance differs by soil type and bar design. A consequence is that for some materials the distance to the storage area is to large. In case this storage area is below the design level (lower bound), additional material must be deposited to fill the storage area. High spots can also be removed by backhoe's or dredgers.

3.6 Equilibrium of forces

This thesis focuses on the cutting forces on the blades and the responding behaviour of the plough. In order to predict the movement of the plough the forces acting on the plough are drawn from figure 3.11. The horizontal pull force F_{bp} determines the required bollard pull and engine power of the ship. The lift forces $F_{lift1} + F_{lift2}$ in combination with the vertical blade forces determine the lift of the plough. The mass of the plough and the weight of the soil resting on the blades G_c an G_R are counteracting the vertical plough lift.

The horizontal and vertical forces on the blade are assumed to act on the tip of the blades. In reality the soil wedge in front of the blade is causing these forces to act at different heights on the blade, depending on the cutting depth. The downward weight of the soil is assumed to act on the middle of the blade and is also depending on the cutting depth and the grain movement along the blade surface.

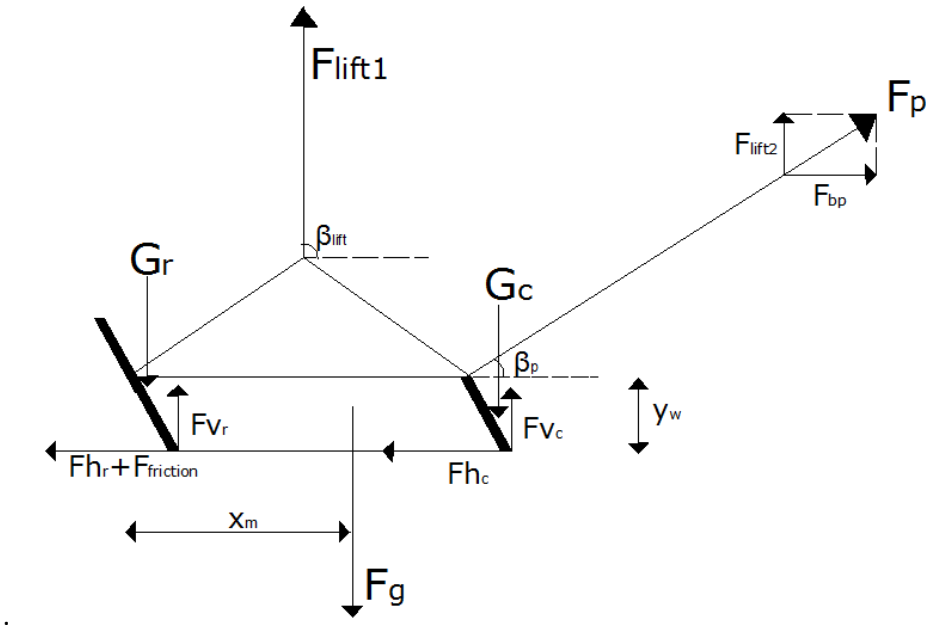

Figure 3.11 Forces acting on the plough

Fg	= Plough mass	[N]
X_m	= Horizontal distance to mass centre of the plough	[m]
$F_{friction}$	= Friction force between side beams and rockfill	[N]
$F_{v,r}$	= Vertical force on rear blade	[N]
$F_{H,r}$	= Horizontal force on rear blade	[N]
$F_{V,c}$	= Vertical force on cutting blade	[N]
$F_{H,c}$	= Horizontal force on cutting blade	[N]
y_w	= Vertical distance to wire attachment	[m]
β_{lift}	= Angle suspension wire with horizontal	[°]
β_d	= Angle drag wire with horizontal	[°]
F_p	= Pull force	[N]
F_{bp}	= Horizontal pull force, bollard pull	[N]
G_R	= Weight of soil on rear blade	[N]
G_C	= Weight of soil on cutting blade	[N]
F_{lift1}	= Suspension force rear wire(s)	[N]
F_{lift2}	= Suspension force front wire(s)	[N]

Horizontal equilibrium of forces:

$$\sum F_H = F_{Hc} + F_{Hr} + F_{friction} - F_p \cos(\beta_d) - F_{lift} \cos(\beta_s) = 0 \tag{3.4}$$

Vertical equilibrium of forces:

$$\sum F_V = F_g - F_{Vr} - F_{Vc} - F_p \sin(\beta_d) - F_{lift} \sin(\beta_s) + G_r + G_c = 0 \tag{3.5}$$

To move a volume of material the ship has to provide enough bollard pull to overcome the horizontal cutting and transporting forces $F_{bp} > \Sigma F_H$. Bollard pull is the horizontal force that can be delivered by a ship and is generated by the propellers F_e, but also by the inertia force needed to decelerate the ship F_i.

$$F_{bp} = F_i + F_e \tag{3.6}$$

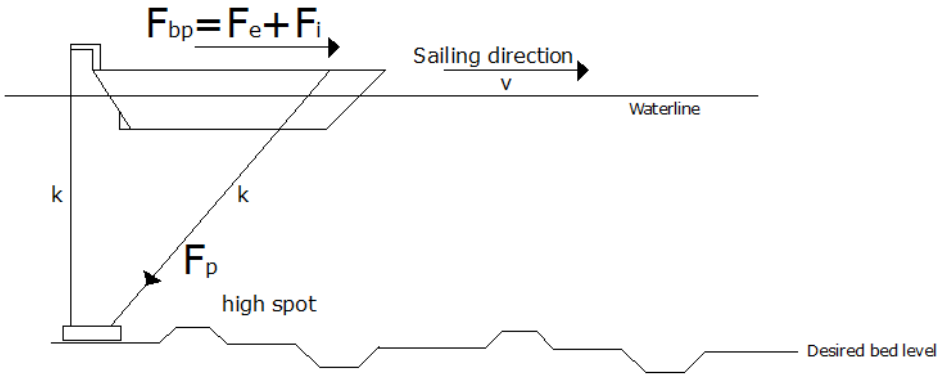

Figure 3.12 Ship forces during ploughing without contribution of waves, wind, current

The kinetic energy is depending on the sailing speed and the mass of the ship, see Eq. (3.7). C_m is a factor for the virtual mass of the surrounding water which is acting as an additional inertia force on the ship.

$$E_{kin} = 0,5 \cdot m \cdot v^2 \cdot C_m \tag{3.7}$$

$$F_i = \frac{E_{kin}}{s} \tag{3.8}$$

E_{kin}	= Kinetic energy ship	[KNm]
m	= Water displacement	[KN]
v	= Sailing speed	[m/s]
C_m	= Factor for virtual mass → 1+ 2*D/B (depth/with)	[-]
F_i	= Inertia Force by deceleration	[KN]
F_e	= Propeller force	[KN]
F_p	= Pulling force	[KN]
k	= Elasticity pulling wires	[m/KN]
s	= Cutting distance	[m]

From Eq (3.8) follows that in order to stop a ship over a short distance a very large force must be exerted due to the inertia of the ship. This force is used to pull the plough through high spots. When the ship is cutting and transporting for larger distances the kinetic energy is dissipating and the plough will start to act as an anchor, causing the ship to decelerate. The plough acts as an anchor if the cutting blade buries itself to deep into the subsoil and is exceeding the propeller force for a longer period of time. For short periods of time the inertia of the ship allows the drag force to be higher than the force generated by the propellers.

3.7 Conclusions based on preliminary research by contractors

The conclusions below are drawn from experience during operational phase. The conclusions are mainly observations done by the contractors and are not always based on scientific research.

- Every type of soil needs its own specific plough design to get to optimum results. (Rijkswaterstaat)
    - When ploughing sand spill the teeth of the plough should be placed almost vertically in order to disturb and penetrate into the soil.
    - When ploughing clay spill no teeth should be used at all but knives in order to cut and transport the clay.
    - In coarse material the plough does not make a continuous cut, but lifts itself out of the ground.
- Experiments have proved that de blade angle has to be determined very accurate considering the soil that is cut.
- Very dense sand results in high cutting forces.
- From tests performed by Rijkswaterstaat it was concluded that cutting soil using a blade with nozzles seemed an energetic unattractive solution. Besides that, the nozzles are very vulnerable.

Chapter 4 Mathematical models

In this chapter mathematical models will be derived for the processes discussed in chapter 3. A repetition of the recognized processes are: Cutting, penetrating, transporting and unloading. Each of the processes will be described with a separate model. The models are drawn from the literature (chapter 4.1) and where necessary adapted to make applicable for equalizing coarse material (chapter 4.2). First all the mathematical models will start with a continuum approach. Limitations of applying a continuum approach will be indicated and possible solutions to deal with these limitations will be introduced.

4.1 Cutting theories from literature

To get a first insight in the cutting forces during ploughing two dimensional cutting theories will be used from the literature. These models describe relations between normal force, shear forces and deformations of the grain structure.

Van Os (1977) describes the cutting of saturated soil due to deformation of the grain structure [3]. He notes that the cutting force is a function of the permeability of the grain structure. Equation (4.1) gives the relation between the cutting velocity v_C, the cutting depth h_i and the pore water under pressures due to deformation. The pore water pressures are considered as the dominant source for the cutting force. When looking at the formula it can be concluded that when the permeability k increases the pore water pressure influence decreases. As mentioned in chapter 3.2, when the pore water pressure decreases the effective grain stress increases. When cutting through very large grains the permeability is very large and therefore the increase in effective grain stresses due to water under pressures can be neglected.

$$Van\,Os[1977] \qquad p :: \frac{v_c \cdot h_i \cdot e}{k} \tag{4.1}$$

Miedema (1987) uses the deformation rate defined by Van Os and models it as a boundary condition in the shear zone [8]. He used the soil mechanical parameters relevant when cutting soil determined by Van Leussen and Nieuwenhuis [1984]. Miedema showed that for cutting velocities in a range from 0.5 to 5 m/s the cutting process is dominated by the phenomenon dilatation. When cutting sand this means that the contributions of gravitational, cohesive, adhesive and inertial forces can be neglected and the effect of pore water underpressure due to inflow of water is dominant.

$$Miedema[1987] \qquad F_{ci} :: \frac{\rho_w \cdot g \cdot v_c \cdot h_i^2 \cdot b \cdot e}{k_m} \tag{4.2}$$

Because pore water under pressure is not an issue in ploughing rockfill another model must be examined in which the force depends on the friction forces due to rolling and sliding of grains. The cutting process also depends on the weight of the grains. This is especially true in the case of cutting dry sand.

Because the increase in pore water pressures in cutting rockfill is considered negligibly low, a closer view is given on models for cutting dry soil. Reece (1965) [14, 15, 16, 18] made an analytical model for cutting dry soil by calculating the soil resistance on a tool, in this case a straight blade. Reece recognized that the mechanics of earthmoving are similar in many respects to the bearing capacity of shallow foundations as described by Terzaghi in 1943. Reece produced the following earthmoving equation for describing the force necessary for cutting soil:

$$\text{Re}\,ece[1965] \qquad P = (\gamma g d^2 N_\gamma + cdN_c + qdN_q)w \qquad (4.3)$$

Where P = Total cutting force, γ = soil density, g = gravitational acceleration, d = cutting depth, c = soil cohesion, q = vertical surcharge pressure on soil surface, w = blade width. The N factors are dimensionless passive coefficients depending on tool geometry and soil properties.

In case of a 2-dimensional case, Reece (1965) [18] used the method of stress characteristics to solve the stress distribution in a body of soil at state of failure. Reece [18] stated that in order to move a blade towards the passive zone, a force P is needed, with the assumption that the grain force is acting perpendicular to the blade. This is the case of a perfectly smooth blade unable to support shear forces parallel to its surface. The characteristics consist of constant stress lines under an angle β. This method of passive soil failure is also known as the sheet pile approach.

When the weight of soil is considered to be important, such as in case of soils with small cohesion strength, or deep soil cutting, the method used by Reece is no longer workable. In this case the calculations become of impossible complexity to integrate the stress equations along the logarithmic failure characteristic lines exactly. Sokolovski (1956) and Harr (1966) [18] have integrated the stresses and stress angles for the soil characteristics by use of numerical methods. The procedure involved a finite difference method to calculate changes along characteristic lines for small changes in x and z direction.

Hettiaratichi (1969) and Hettiaratichi and Reece (1974) [18] developed a set of charts for quick solution for particular problems using the method of Sokolovski. Equation (4.3) was again used with an additional term N_a for the adhesion between blade and soil. Calculations where done for wide range of cutting angles α , friction angles ϕ and N factors for smooth and rough blades. The procedure for calculating the passive soil resistance involves the interpolation of the soil resistance coefficients off these charts. Limitation of the passive soil pressure calculations by Hettiaratichi and Reece is that the soil surface must be horizontal. For this reason these models are not applicable for calculating the cutting forces on a soil volume under a slope.

According to Hettiaratichi and Reece (1975) [16], alternatively to the charts, a static analysis of soil forces acting on a soil wedge can be carried out. Miedema (1987) used the static analysis to predict the cutting forces on a layer cut. Miedema used the approximation of a straight shear plane and has created a cutting models for water saturated sand based on the horizontal and vertical equilibrium of forces. In 2004, Miedema [17] created a model for cutting saturated sand with large cutting angles based on papers from Hettiaratichi and Reece [14, 15,16, 18]. The static analysis of soil forces by Miedema will be used to create a model for coarse grains in this thesis.

4.1.1 Model Miedema (1987), cutting saturated sand for small blade angles [3]

A cutting model for saturated soil cutting is proposed by Miedema in 1987 [3]. This continuum cutting model is based on horizontal and vertical force balance equations. Because a plough consists of two straight blades in sequence the sheared layer may be considered as a 2 dimensional deformation. The forces on the blade can be determined by an equilibrium of forces on a layer cut. The forces acting on the blade and the layer cut with the contribution of water pressure is shown in figure 4.1.

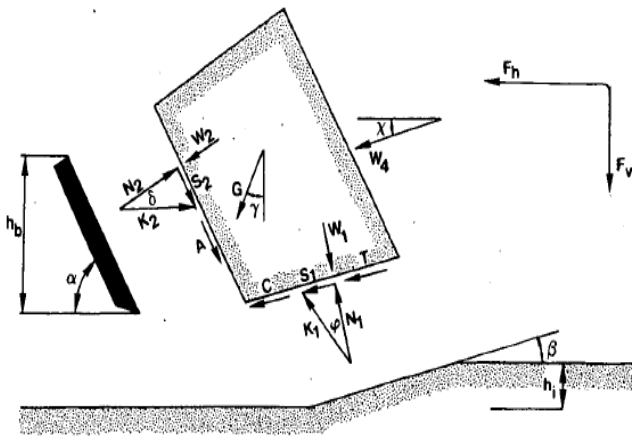

G = Mass soil wedge	[N]
β = Angle of the shear zone	[°]
T = inertia force	[N]
C = Cohesion force	[N]
S1 = Shear force in shear zone	[N]
A = Adhesion	[N]
S2 = Shear force between blade/grains	[N]
α = Blade angle	[°]
Hi = Cutting depth	[m]
Ki = Grain force	[N]
Ni = Normal force	[N]
Wi = Water pressure	[N]
ϕ = Internal friction angle soil	[°]
χ = Angle water resistance on wedge	[°]
δ = Angle of steel/soil friction	[°]
γ = Angle gravitational force with vertical	[°]

Figure 4.1 Two dimensional cutting forces on a straight blade [3]

To create a model for cutting soils consisting of coarse grains the water pressures, cohesion and adhesion forces will be neglected. In coarse grains these terms are very small compared to the rest of the forces. The cutting forces are solely depending on the gravitational, shear and inertial forces between grains. In the following force balance equations by Miedema [3] the forces due to water pressures, adhesion and cohesion are therefore given between brackets. In case of horizontal ploughing the angle of the gravitational force is zero γ=0.

The horizontal equilibrium of forces on the layer cut (to the right is negative):

$$K_1 \cdot \sin(\beta+\varphi) + T \cdot \cos(\beta) + G \cdot \sin(\gamma) - K_2 \cdot \sin(\alpha+\delta) + \left[W_4 \cdot \cos(\chi) - A\cos(\alpha) + W_2 \cdot \sin(\alpha) - W_1 \cdot \sin(\beta) + C \cdot \cos(\beta)\right] = 0 \quad (4.4)$$

The vertical equilibrium of forces on the layer cut (upward is negative):

$$-K_1 \cdot \cos(\beta+\varphi) + T \cdot \sin(\beta) + G \cdot \cos(\gamma) - K_2 \cdot \cos(\alpha+\delta) + \left[W_4 \cdot \sin(\chi) + A\sin(\alpha) + W_2 \cdot \cos(\alpha) + W_1 \cdot \cos(\beta) + C \cdot \sin(\beta)\right] = 0 \quad (4.5)$$

Without the contribution of the forces between brackets a new model is given, depending sole on the inertia and grain forces due to the soil weight. The shape of the layer cut in figure 4.2 is taken equal to the shape in figure 4.1. Without the contribution of pore water under pressure this shape is not realistic. The grains will not be held together and the layer cut will break up and the grains will roll and slide down under the angle of repose. This phenomena will be further discussed in chapter 4.2. First the layer cut is assumed to maintain the original shape and the contribution of pore water pressure is neglected.

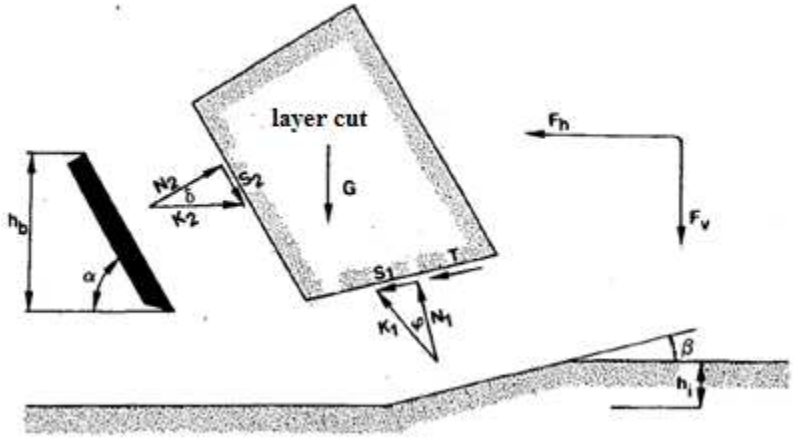

Figure 4.2 Forces on soil wedge without water and adhesion forces [3]

Eliminating the forces between brackets from Eq. (4.4) and Eq. (4.5) gives new relations for respectively the horizontal and vertical equilibrium of forces:

$$K_1 \cdot \sin(\beta+\varphi) + T \cdot \cos(\beta) + G \cdot \sin(\gamma) - K_2 \cdot \sin(\alpha+\delta) = 0 \tag{4.6}$$

$$-K_1 \cdot \cos(\beta+\varphi) + T \cdot \sin(\beta) + G \cdot \cos(\gamma) - K_2 \cdot \cos(\alpha+\delta) = 0 \tag{4.7}$$

The grain force K_1 can be eliminated by rewriting the last equations into Eq. (4.8) and Eq. (4.9) and sum both relations. The formula can now be written in terms of K_2, G and T in Eq. (4.10):

$$K_1 + \frac{T \cdot \cos(\beta)}{\sin(\beta+\varphi)} + \frac{G \cdot \sin(\gamma)}{\sin(\beta+\varphi)} - \frac{K_2 \cdot \sin(\alpha+\delta)}{\sin(\beta+\varphi)} = 0 \tag{4.8}$$

$$-K_1 + \frac{T \cdot \sin(\beta)}{\cos(\beta+\varphi)} + \frac{G \cdot \cos(\gamma)}{\cos(\beta+\varphi)} - \frac{K_2 \cdot \cos(\alpha+\delta)}{\cos(\beta+\varphi)} = 0 \tag{4.9}$$

$$+$$

$$K_2\left(\frac{\cos(\alpha+\delta)}{\cos(\beta+\varphi)} + \frac{\sin(\alpha+\delta)}{\sin(\beta+\varphi)}\right) = G\left(\frac{\cos(\gamma)}{\cos(\beta+\varphi)} + \frac{\sin(\gamma)}{\sin(\beta+\varphi)}\right) + T\left(\frac{\sin(\beta)}{\cos(\beta+\varphi)} + \frac{\cos(\beta)}{\sin(\beta+\varphi)}\right) \tag{4.10}$$

With γ=0, the grain force on the blade K_2 is expressed by:

$$K_2 = \frac{\dfrac{G}{\cos(\beta+\varphi)} + T\left(\dfrac{\sin(\beta)}{\cos(\beta+\varphi)} + \dfrac{\cos(\beta)}{\sin(\beta+\varphi)}\right)}{\left(\dfrac{\cos(\alpha+\delta)}{\cos(\beta+\varphi)} + \dfrac{\sin(\alpha+\delta)}{\sin(\beta+\varphi)}\right)} = \boxed{\frac{G\sin(\beta+\varphi) + T\cos(\varphi)}{\sin(\alpha+\beta+\varphi+\delta)}} \tag{4.11}$$

With the derived relation for the grain force on the blade for coarse grains, the horizontal and vertical force are given by Eq. (4.12) and Eq. (4.13). The horizontal force gives the required bollard pull of the vessel, the vertical force determines the lift force of the plough.

$$F_H = K_2 \cdot \sin(\alpha + \delta) \tag{4.12}$$

$$F_V = K_2 \cdot \cos(\alpha + \delta) \tag{4.13}$$

A force must be exerted to give the grains in front of the blade a velocity and a direction. The inertia force T in Eq. (4.14) is examined by (Wismer and Luth, 1972) [3] and is expressed in the next relation. Besides the inertia force of grains in the shear zone, the inertia of the particles at the surface is relevant to compare dry and saturated cutting. The inertia force reads:

$$T = \rho_g \cdot v_c^2 \frac{\sin(\alpha)}{\sin(\alpha + \beta)} h_i \cdot b \tag{4.14}$$

The gravitation force, which can be described as the force by the weight of the layer cut is determined by Miedema [3] and reads:

$$G = \gamma \cdot h_i \cdot b \cdot \frac{\sin(\alpha + \beta)}{\sin(\beta)} \cdot \left[\frac{h_b + h_i \cdot \sin(\alpha)}{\sin(\alpha)} + \frac{h_i \cdot \cos(\alpha + \beta)}{2 \cdot \sin(\beta)} \right] \tag{4.15}$$

Where $\gamma = (\rho_g - \rho_w) \cdot g \cdot (1 - n)$.

To calculate the gravitational force G, Miedema assumed that the top of the layer cut has an angle perpendicular to the blade and has an additional soil layer h_i protruding above the blade.
The shape of the wedge in dry soil will be different from the shape of the wedge shown in figure 4.2. The mass of the wedge will consequently change and will differ from Eq (4.15). The relation for the actual shape and mass of the wedge is derived in chapter 4.2.

The following equations give the relation between the normal force, grain force and shear force. The relation for the normal force Eq. (4.16) is used later to determine the horizontal force in the EDEM computer model:

$$S_2 = N_2 \cdot \tan(\delta) \tag{4.16}$$

$$N_2 = K_2 \cdot \cos(\delta) \tag{4.17}$$

The specific cutting energy in [N/m^2] is expressed by [2]:

$$E = \frac{F_H}{h_i \cdot b} \tag{4.18}$$

4.1.2 Model Miedema (2004), cutting saturated sand for large blade angles [16]

In case of large blade angles Eq. (4.11) and Eq. (4.12) for the horizontal cutting force derived in the previous chapter are no longer valid. Miedema stated [17]: "In the equations derived, the denominator contains the sine of the sum of the 4 angles involved, the cutting angle α, the shear angle β, the angle of internal friction ϕ and the soil interface friction angle δ. So when the sum of these 4 angles approaches 180° the sine will become zero and the cutting forces become infinite. When the sum of these 4 angles is greater than 180° the sine becomes negative and so do the cutting forces. Since this does not occur in reality, nature must have chosen a different mechanism for the case where the sum of these 4 angles approaches 180° ", this is shown in figure 4.3.

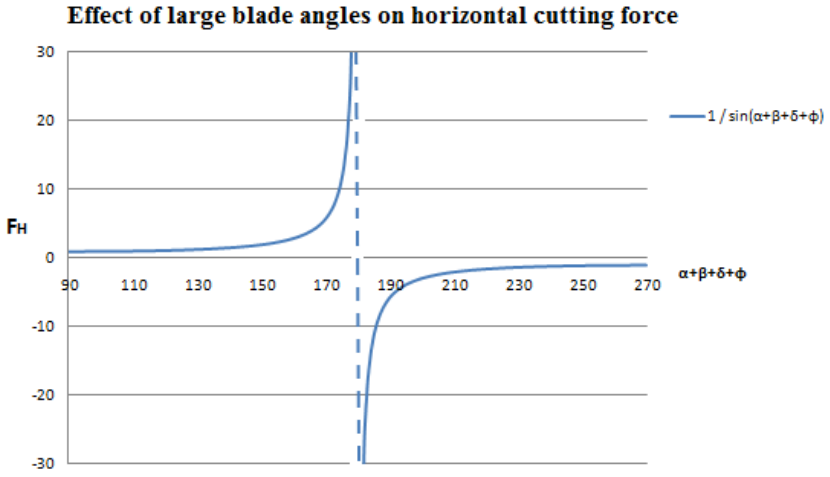

Figure 4.3 Effect of changing the paramters in the denominator of Eq (4.11)

Form research performed by Hettiaratchi and Reece (1975) [16] and Miedema (2006) [15] follows that for large cutting angles a triangular wedge of dead soil will form near the blade surface, a boundary wedge. This boundary wedge acts as a blade with a smaller blade angle α^* and has a soil-soil friction angle λ with the layer cut. Miedema graphically showed [15] in figure 4.5 that the wedge angle is around 55° for cutting water saturated sand and will barely change for increasing blade angles α.

He (1998) [17] proved experimentally that grains inside the boundary wedge have a decreasing speed towards the blade as shown in figure 4.4. He showed that the failure in front of large blade angles is different from that with small blade angles. At the interface between the boundary wedge and the layer cut the grains move relative to each other, the speed is no longer uniform. The layer cut is called a Rankine passive earth zone.

The upward grain velocity inside the Rankine zone are higher than the velocity of the grains inside the boundary wedge, causing an apparent shear plane to occur at the interface. The interface is in fact a transition zone from a constant velocity inside the Rankine zone to a decreasing varying speed inside the boundary wedge, see figure 4.4. The friction angle λ on the interface is depending on the speed distribution between the boundary wedge and the Rankine zone $0 < \lambda \leq \phi$. The change in speed is depending on the blade angle and the blade-soil friction angle δ. With an increasing blade

angle α the value for the blade soil friction δ will decrease below the critical value. If δ comes below the critical value the grains near the blade will stop moving and a dead wedge will form, the grains are not moving vertically relative to the blade. In case δ is higher than the critical value the grains are fully mobilized and the cutting model for low cutting angles α from chapter 4.1.1 can be applied.

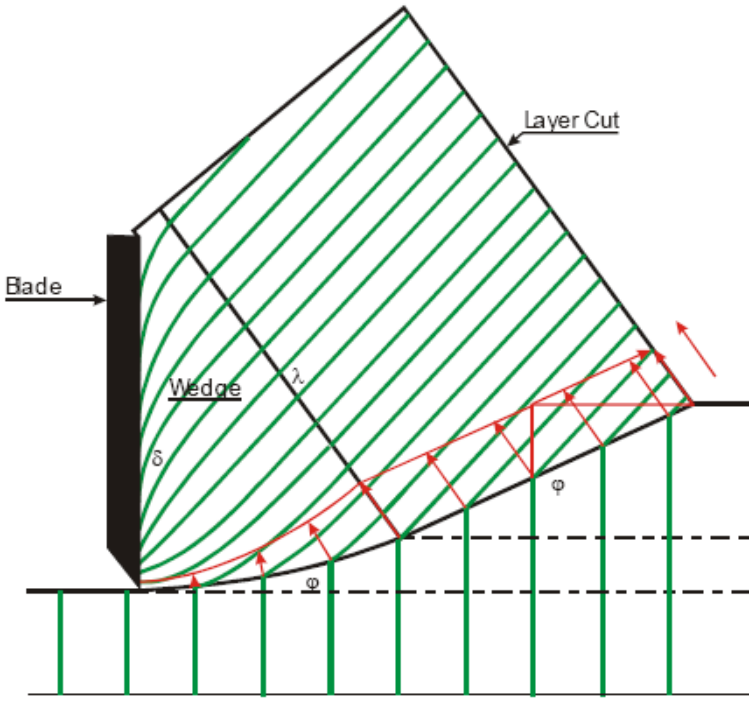

Figure 4.4 Velocity distribution in boundary wedge and Rankine zone, Miedema [17]

At very large cutting angles the blade-soil friction δ becomes negative, see figure 4.5. If the critical negative value - δ is reached it will result in a downward movement of the grains near the blade surface and an underflow of soil beneath the blade.

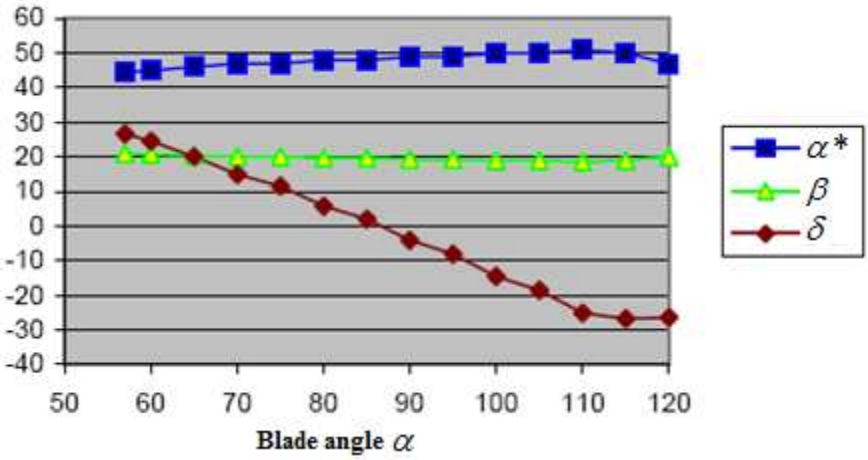

Figure 4.5 Relation blade angle α and α, β, δ in water saturated sand, Miedema [17]*

The velocity change inside the boundary wedge would indicate that the entire wedge is at a state of failure according to the Mohr-Coulomb criterion. And would indicate several shear planes parallel to the blade.

The main difficulty is finding a rigorous solution for the forces on the boundary wedge. The value for the steel-soil friction angle δ is between the positive and negative critical value for mobilization and also the friction angle λ between boundary wedge and Rankine zone can vary between $0 < \lambda \leq \phi$. In case the boundary wedge is consisting of fully dead soil zone the wedge can be considered as a blade with a roughness equal to the internal friction angle ϕ. In case the friction angles λ and δ are not fully mobilized the horizontal and vertical equilibrium of forces is not enough and the momentum balance needs to be considered to determine the extra unknown parameters [17].

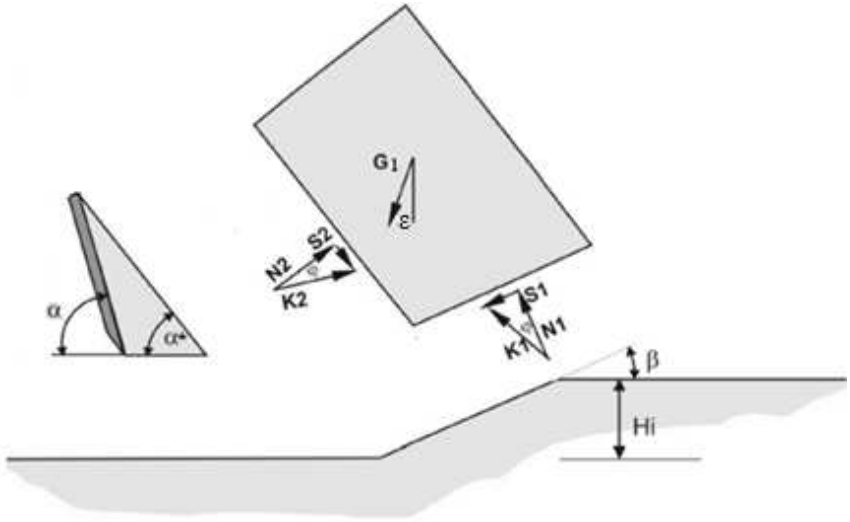

Figure 4.6 Forces acting on the passive Rankine zone [17]

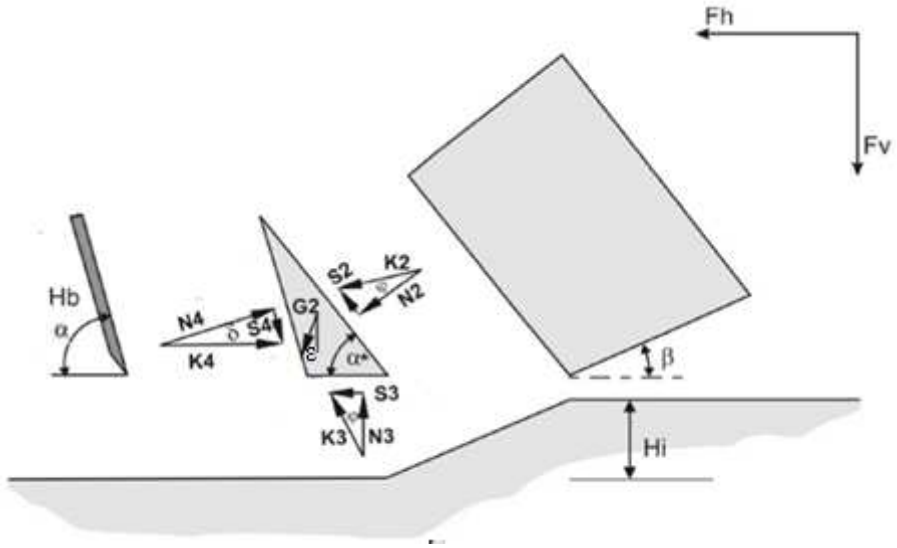

Figure 4.7 Forces acting on the boundary wedge (right) [17]

The grain force K_2 derived in Eq. (4.11) will differ from Eq. (4.19) with a boundary wedge. The blade-soil friction angle δ is replaced by the soil-soil friction angle λ at the interface between the boundary wedge and the passive Rankine zone. The blade angle is replaced by the angle of the boundary wedge α* with the horizontal. The grain force on the boundary wedge is now expressed by:

$$K_2^* = \frac{G_1 \sin(\beta+\varphi) + T\cos(\varphi)}{\sin(\alpha^*+\beta+\varphi+\lambda)} \tag{4.19}$$

If the boundary wedge is assumed to have a straight horizontal shear plane the grain force on the blade is given by to Eq. (4.20). For the derivation of this formula is referred to the paper of Zhao Yi & Miedema [19]. The pore water pressures and cohesion and adhesion forces are left out, like the derivation of the grain force for small blade angles in chapter 4.1.

$$K_4 = \frac{K_2 \sin(\alpha^*+\lambda+\varphi) + G_2 \sin(\varphi)}{\sin(\alpha+\delta+\varphi)} \tag{4.20}$$

$$F_H = K_4 \cdot \sin(\alpha+\delta) \tag{4.21}$$

$$F_H = K_4 \cdot \cos(\alpha+\delta) \tag{4.22}$$

Where G_1 = gravitational force of the Rankine zone, G_2 = gravitational force of the boundary wedge, T = inertia Force, α* = angle boundary wedge, λ = friction angle between boundary wedge and Rankine zone, δ = soil/steel friction angle, α = blade angle, γ = angle gravitational force, ϕ = internal friction angle.

Before calculations with or without a boundary wedge can be executed for coarse grains the shape of the passive Rankine zone has to be determined. The shape of the layer cut in coarse material will differ from the shape shown in figure 4.7. The relations for G_1 and G_2 are derived in chapter 4.2.

4.1.3 Effect of increasing the stone size on the cutting behaviour

When cutting granular soil with larger grain diameters some extra effects must be taken into account. With an increasing stone diameter the number of stones in front of the blade decreases. At the point the number of grains influenced by the blade gets lesser than the order of 10 stones [9] , the grains cannot be described as a continuum cutting model. This can result in a less clearly shear zone or no shear zone at all. The grain structure can have a different failure method like particle rolling instead of shearing.

The bed properties and particle shape also determine stable or unstable shearing. From research performed by the Rock Mechanics Department of Geosciences, Pennsylvania State University [1] was found that for unstable sliding regimes force chains are build and broken. The appearance of “rock columns” cause a stress drop, recurrence interval, preseismic slip, and dynamic slip. A difference was made between spherical and angular grains a smooth or rough moving boundary. During this experiment performed by Anthony, J. and Marone, C. (2005) [1] it was found that particle angularity and bounding surface roughness cause an increase of the frictional strength within

sheared layers. This will result in more fluctuations in the drag force due to unstable sliding. Larger stone diameters can create higher force chains by creating thicker “rock columns”.

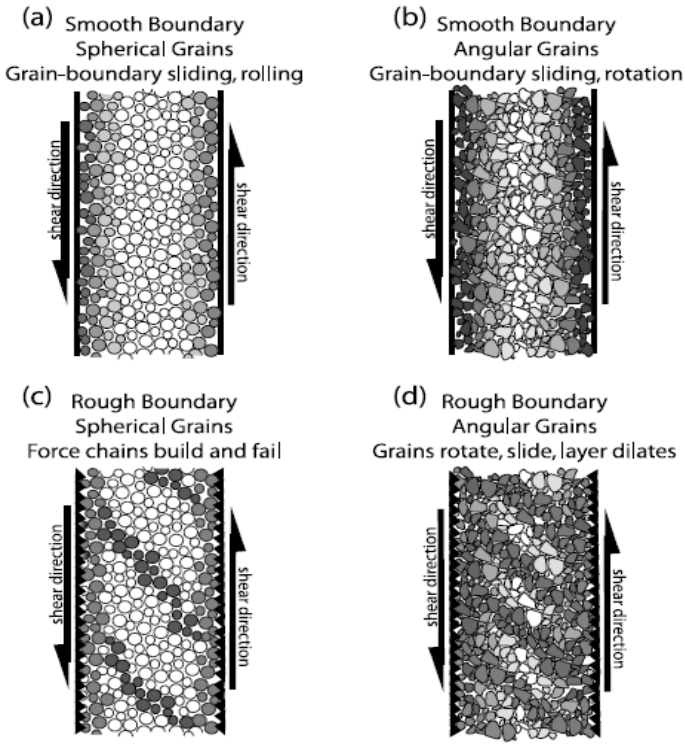

Figure 4.8 Forming of rock colums by research Rock Department Pennsylvania [1]

This can be also the case in cutting a granular rockfill consisting of large stones compared to the cutting tool. When several stones are aligned they will form a column consisting of rock particles. These “rock columns” increase the cutting forces and encourage a vertical lift of the blade, see figure 4.9. The strength of the columns might be determined by the buckling force of these columns [9].

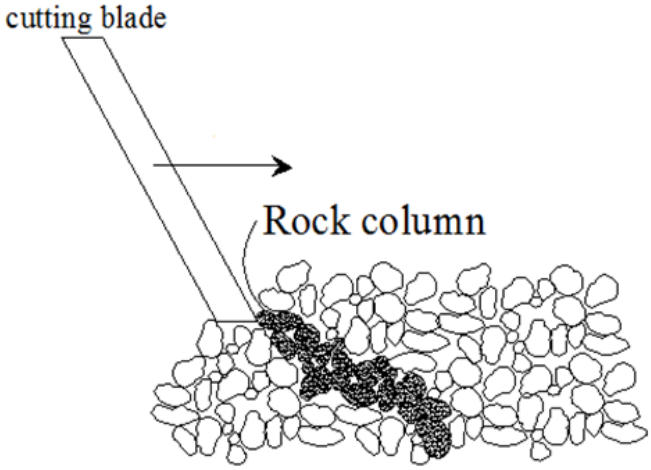

Figure 4.9 Forming of rock columns during cutting with a blade

4.2 Cutting & transport model for coarse material with limited surface slopes

The cutting and transport model for coarse material will be derived with a static analysis. This approach is similar to the model for cutting water saturated sand by Miedema in chapter 4.1. The vertical and horizontal equilibium of forces on a layer cut will be determined. The shape of the layer cut will differ from the situation with pore water underpressures. The layer cut in coarse grains will collapse and settle under the angle of repose η. Due to this limited surface slope a new relation has to be found for the shape of the layer cut and the corresponding gravitational force G acting on the shear zone. The horizontal cutting force is given by Eq. (4.12) or Eq. (4.21). Because the layer cut is no longer a fixed shape it will be called a sheared volume or a sheared zone.

In order to create a model that is applicable for coarse material a closer look on the grain movement is required. It is assumed that, similair to cutting soil consisting of fine grains, a shear plane under an angle β will occur for a critical value of F_H based on the Mohr-Coulomb failure mechanism. The shear line is assumed to be a straight shear line along the lowest slip line instead of a logarithmic slip line.

Grains pass the shear plane and are given an momentum upward. Because the entire cutting layer hi crosses the shear plane and the only expansion possibility is upward, the whole sheared volume will move upwards. The sheared volume moves along the shear plane, but the shape is also disturbed by the compressive force of the blade. Due to the disturbance and movement of the sheared volume along the shear plane the surface slope increases. For a critical surface slope, the angle of repose, grains will roll down. Underlying reach the surface at the room created by the grains rolling down. The grains that roll down the surface settle at the toe of the wedge and are passing the shear zone again. This circular movement is also known in front of bulldozer blades. To visualize this process the different stages of material build up in front of the blade will be discussed.

4.2.1 Different phases of material building up in front of the rear blade

To create an analytical model that is applicable for both cutting and transporting first the different phases of filling the plough will be considered. The arrows in the figures indicate the movement of the grains. In order to prevent to much information in the figures the front blade is assumed to cut according to the Miedema model. In fact the front blade will behave similair to the rear blade for coarse grains.

Filling phase (figure 4.10 and 4.11):

The front blade is cutting a layer thickness hi. The coarse material will accumulate in front of the cutting blade untill this blade starts to overflow with a flow rate Q [m^3/s]. The soil volume that is overflowing is deposited behind the blade creating a layer thickness h_Q equal to the cutting depth hi. The rear blade will start to cut this layer h_Q and transport this material upward according to figure 4.10. The inflow is depending on the overflow rate Q. Because the height of rear blade is larger than the cutting blade the layer cut will not overflow. The grains will roll down creating a slope with an angle η forming a triangular layer cut in front of the rear blade, see figure 4.11. As long as the inflow

of soil Q from the cutting blade is larger than zero the layer cut will continu to grow, causing a stationairy zone to form on top of h_Q. This stationary zone increases the layer thickness from h_Q to hi* and can be seen as an "imaginary cutting depth". The material is reintegrated into the system and the process will repeat itself with a larger shear plane. The soil beneath the shear zone can be seen as a stationary zone at the moment the wedge starts shearing.

The stone movement is presented in figure 4.11. As long as Q is larger than zero the cutting volume will continu to grow and hi* will increase.

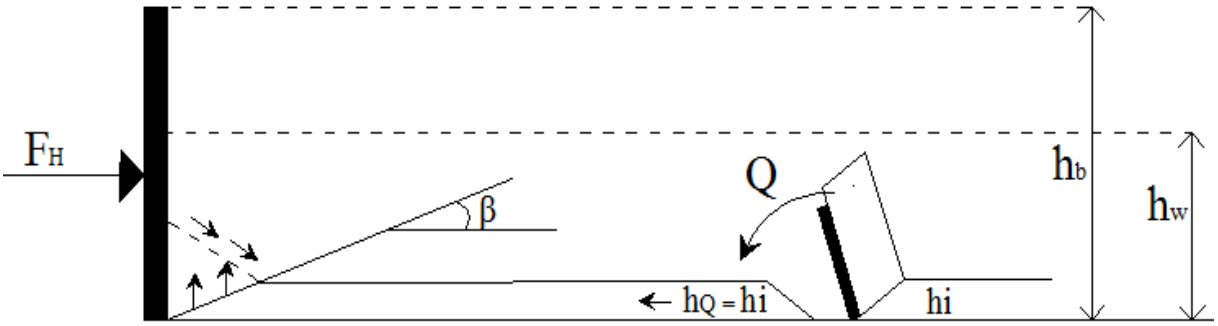

Figure 4.10 Oveflow of the front blade, creating a cutting layer $h_Q = hi$

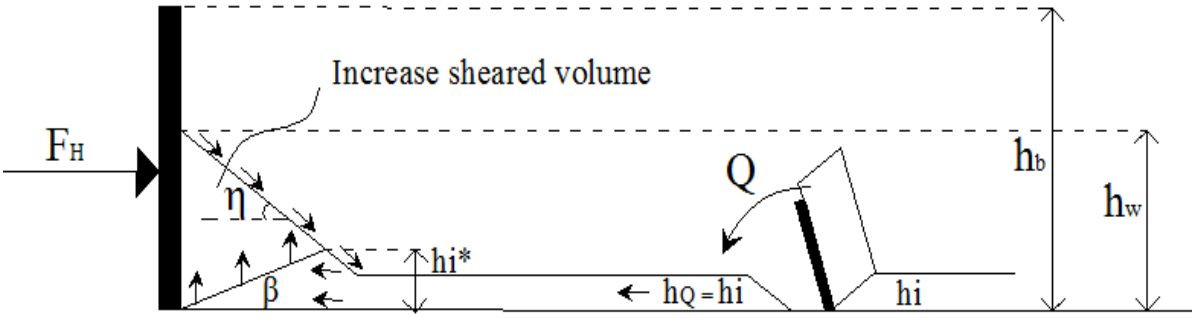

Figure 4.11 Increase of the sheared volume, grains roll down under angle of repose η

Overflow phase (figure 4.12 and 4.13):

The soil volume in front of the rear blade keeps growing untill it reaches the top of the blade, see figure 4.12.

When Q > 0 m^3/s the wedge will continue to grow and the rear blade will start to overflow with Q*. The volume Q* will be deposited behind the rear blade and form a layer thickness equal to the initial cutting layer hi. The overflow volume Q will pass the wedge and will directly outflow over the rear blade of the plough, see figure 4.13. The increase of the soil volume due to a larger inflow Q results in a larger mass acting on the shear plane and will result in higher cutting forces. On the front side of the sheared zone grians will continue to roll down the slope and follow the circular movement as discussed earlier. At the toe of the wedge grains that roll down and blend with grains that overflow from the cutting blade.

When the soil inflow from the front blade becomes zero Q = 0 m^3/s, the sheared volume will keep a stationairy shape with a possible maximum height as presented in figure 4.12. In this case h_Q is zero and the surface of the triangular soil shape is now extended to the bed level. The grains will move within the tiangular soil volume. The grains will follow a circualr motion: the stationary zone will be supplemented by the grains rolling down the slope and the blade will continue to cut this stationary zone. The shape of the soil volume is depending on the blade angle α, this will be discussed in the next chapter.

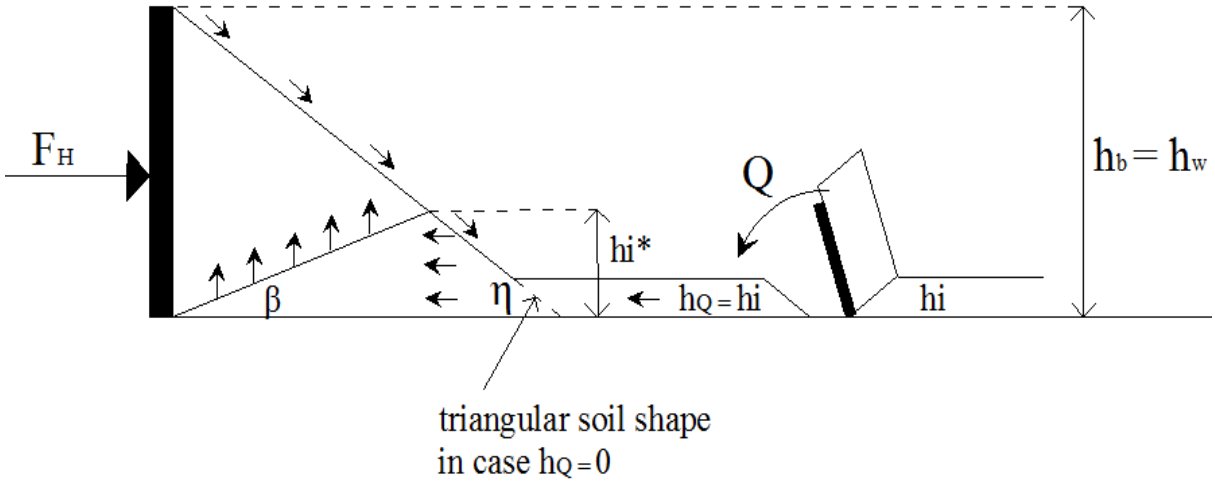

Figure 4.12 Transport model: Overflow phase or stationairy soil shape in case h_Q = 0 (dashed line)

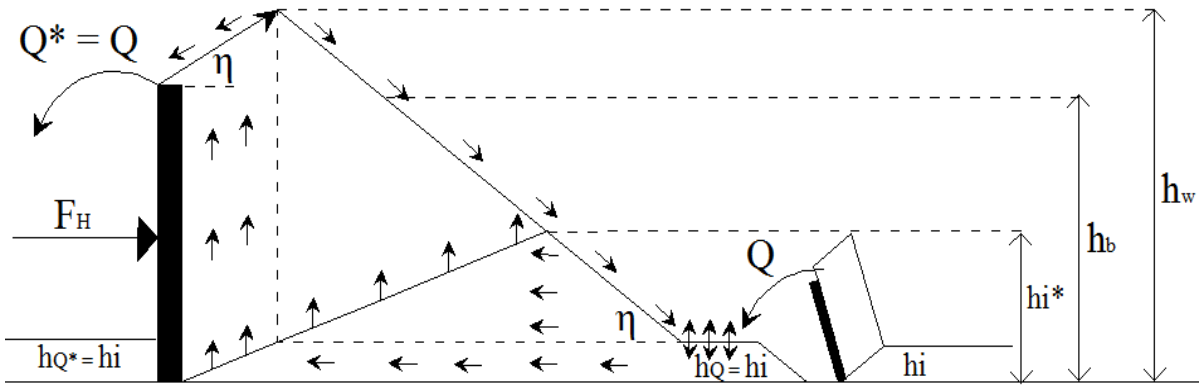

Figure 4.13 Cutting &Transport model: Additional growth of the soil volume depending on h_Q.

4.2.2 Analytical model for cutting and transporting soil with limited surface slopes

Figure 4.14 shows the stationairy final stage of filling. The shape of the soil volume is assumed to be constant, so there will be a constant inflow Q that is directly overflowing.
The analytical model will be devided in two stationairy situations: A model for sole transporting Q = 0 m^3/s and a model for cutting & transporting simultanuously Q > 0 m^3/s. The grain movement and the forces on the sheared zone for Q > 0 m^3/s are presented in the following figures. In case Q = 0 m^3/s the inflow and outflow is zero.

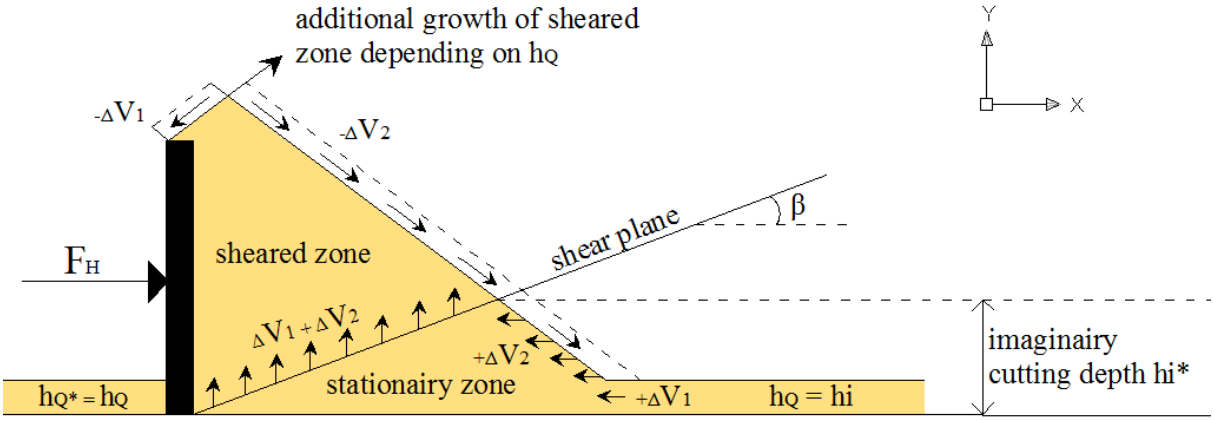

Figure 4.14 Stone movement for the cutting & transporting model

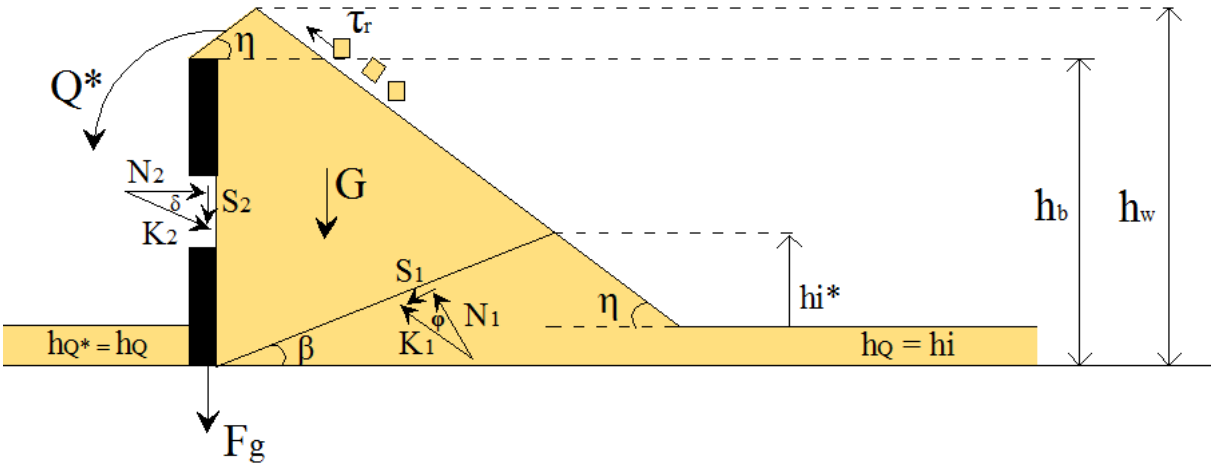

Figure 4.15 Forces acting on the sheared zone

The equation for the horizontal cutting force with of without a boundary wedge are derived earlier in Eq. (4.12) and Eq (4.21). Due to a limited surface slope the gravitational force of the sheared zone G is different from the cutting model for fine material and has to be recalculated.

The grain movement depends on the presence or absence of a boundary wedge as discussed in chapter 4.1.2. Therefore the models for transporting and cutting & transporting will be devided in a situation with or without a boundary wedge.

4.2.3 MODEL 1: Transporting without inflow of material (Q = 0 m³/s)

4.2.3.1 The shape and forces on the sheared zone for Q = 0 m³/s without a boundary wedge

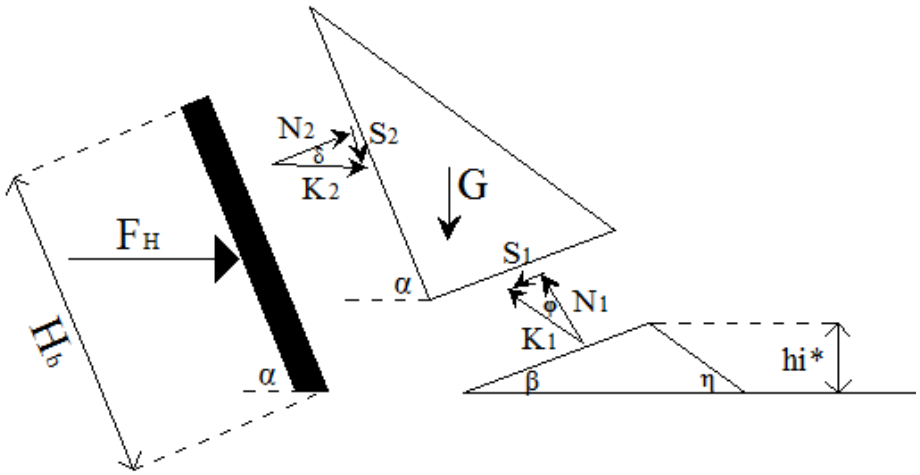

Figure 4.16 Forces on the sheared zone, for Q = 0 m³/s and no boundary wedge

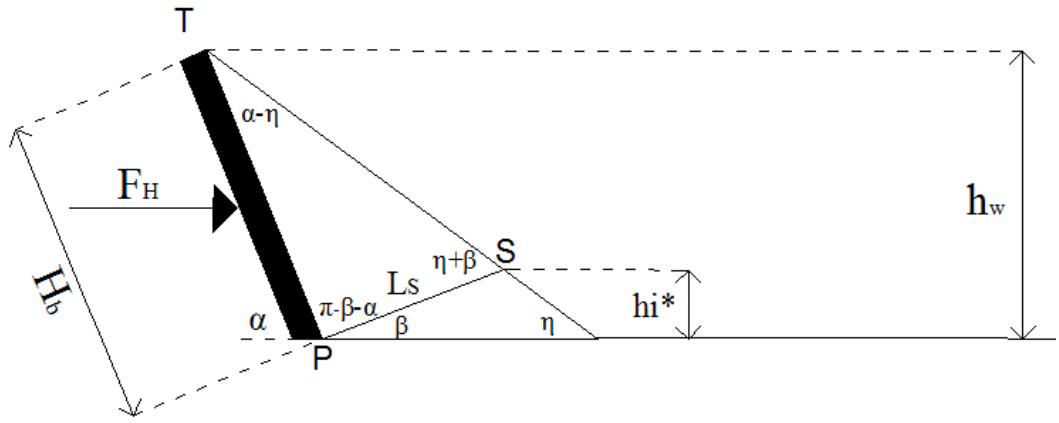

Figure 4.17 Shape of sheared volume for Q = 0 m³/s

From the sine rule [20] follows the length of the shear zone L_s by:

$$L_s = \frac{H_b \cdot \sin(\alpha - \eta)}{\sin(\eta + \beta)} \tag{4.23}$$

The imaginairy cutting depth:

$$h_i^* = L_s \cdot \sin(\beta) \tag{4.24}$$

The gravitational force of the sheared volume can now be calculated by [20]:

$$G = \frac{1}{2} \cdot L_s \cdot H_b \cdot \sin(\pi - \beta - \alpha) \cdot B_w \cdot \gamma \tag{4.25}$$

4.2.3.2 The shape and forces on the sheared zone for Q = 0 m³/s with a boundary wedge

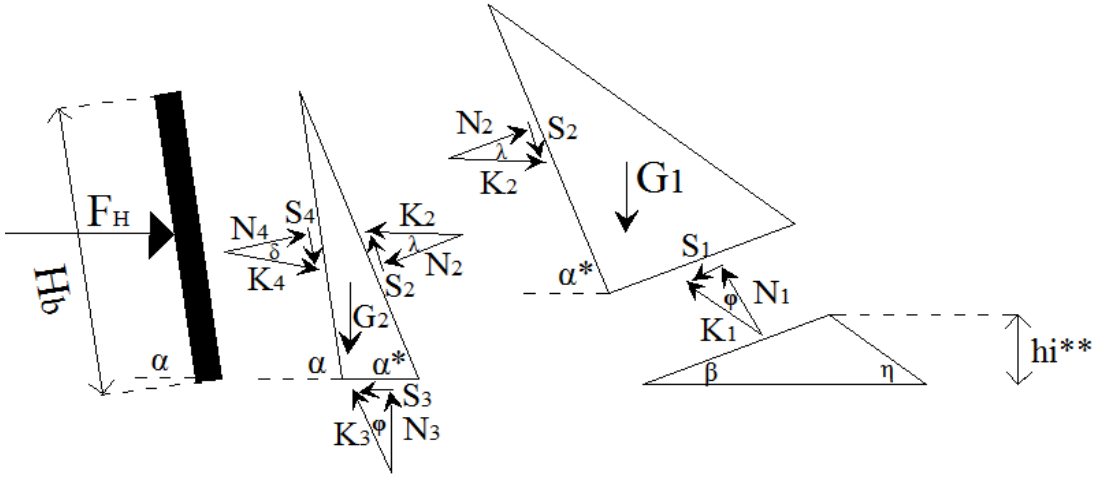

Figure 4.18 Forces on the sheared zone and boundary wedge for Q = 0 m³/s

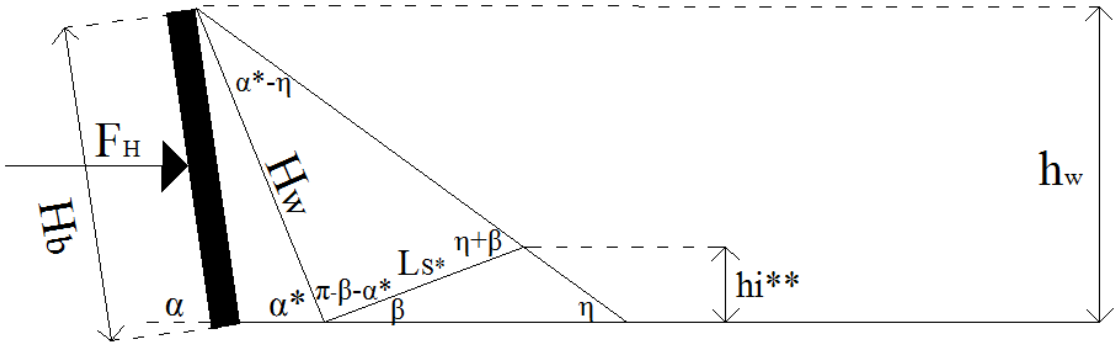

Figure 4.19 Shape of sheared volume and boundary wedge for Q = 0 m³/s

The height of the boundary wedge is calculated by:

$$H_W = \frac{H_b \cdot \sin(\alpha)}{\sin(\alpha^*)} \tag{4.26}$$

From the sine rule [20] follows the length of the shear zone L_s by:

$$L_s^* = \frac{H_W \cdot \sin(\alpha^* - \eta)}{\sin(\eta + \beta)} \tag{4.27}$$

The imaginairy cutting depth:

$$h_i^{**} = L_s^* \cdot \sin(\beta) \tag{4.28}$$

The gravitational force of the sheared volume can now be calculated by [20]:

$$G_1 = \frac{1}{2} \cdot L_s^* \cdot H_b \cdot \sin(\pi - \beta - \alpha^*) \cdot B_w \cdot \gamma \tag{4.29}$$

And the gravitational force of the boundary wedge:

$$G_2 = \frac{1}{2} \cdot H_w \cdot H_b \cdot \sin(\alpha - \alpha^*) \cdot B_w \cdot \gamma \tag{4.30}$$

4.2.4 MODEL 2: Cutting + transporting (Q > 0 m³/s)

4.2.4.1 The shape and forces on the sheared zone for Q > 0 m³/s without a boundary wedge

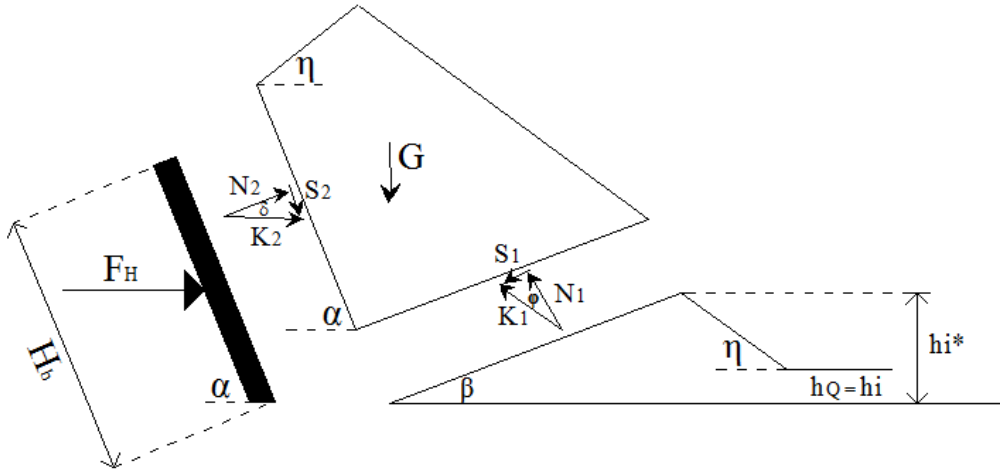

Figure 4.20 Forces on the sheared zone, for Q > 0 m³/s and no boundary wedge

To calculate the surface of the sheared zone an auxiliary triangle TT*T** is formulated. This allows us to reuse the equations from chapter 4.2.3.

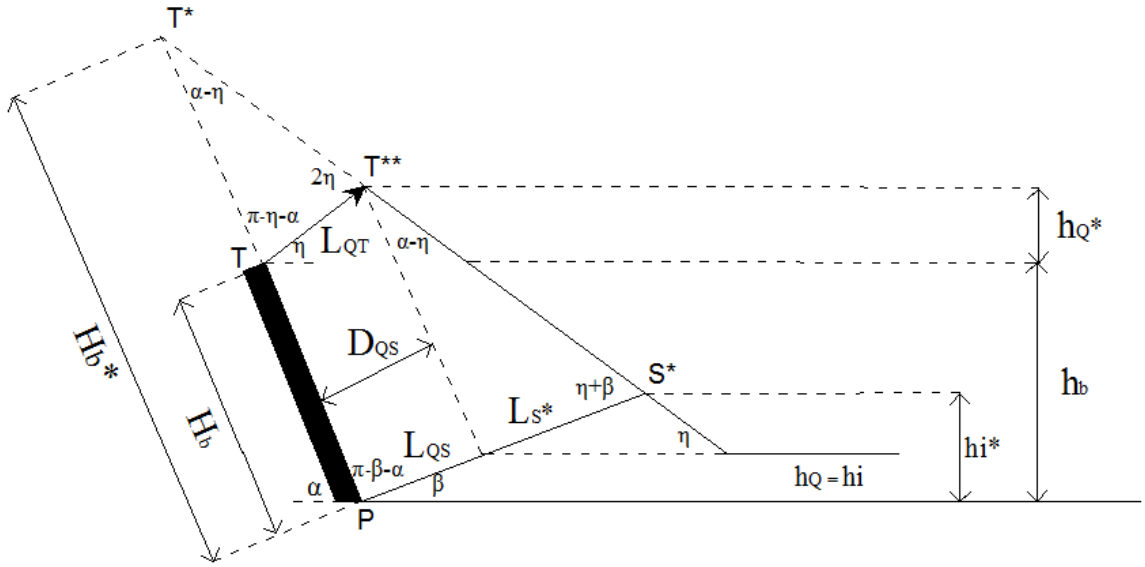

Figure 4.21 Shape of sheared volume for Q > 0 m³/s

The length of the shear zone L_{QS} ifollows from the layer thickness of the inflow of material h_Q. This material is directly deposited behind the rear blade by overflow so will be transported upward through the wedge:

$$L_{QS} = \frac{h_Q}{\sin(\beta)} \tag{4.31}$$

Thickness of the overflow layer perpendicular to blade surface:

$$D_{QS} = L_{QS} \cdot \cos(\frac{\pi}{2} - \alpha - \beta) \tag{4.32}$$

Length of the overflow layer protruding above the blade:

$$L_{QT} = \frac{D_{QS}}{\cos(\alpha - \frac{\pi}{2} + \eta)} \tag{4.33}$$

Height of the overflow layer protruding above the blade:

$$h_{Q*} = L_{QT} \cdot \sin(\eta) \tag{4.34}$$

Height of the auxiliary triangle:

$$TT^* = L_{QT} \cdot \frac{\sin(2\eta)}{\sin(\alpha - \eta)} \tag{4.35}$$

The joint height of the blade and auxiliary triangle:

$$H_b^* = TT^* + H_b \tag{4.36}$$

The length of the shear zone for the grains that are not overflowing, but rolling down the front side of the sheared zone:

$$L_S^* = \left(\frac{H_b^* \cdot \sin(\alpha - \eta)}{\sin(\eta + \beta)} \right) - L_{QS} \tag{4.37}$$

The imaginairy cutting depth:

$$h_i^* = (L_s^* + L_{QS}) \cdot \sin(\beta) \tag{4.38}$$

The gravitational force of the sheared volume can now be calculated by subtracting the surfaces of the large triangle PS*T* and the auxiliary triangle TT*T**:

$$G = (PS^*T^* - TT^*T^{**}) \cdot B_w \cdot \gamma \tag{4.40}$$

$$G = \left[\left(\frac{1}{2} \cdot H_b^* \cdot (L_s^* + L_{Qs}) \cdot \sin(\pi - \alpha - \beta) \right) - \left(\frac{1}{2} \cdot TT^* \cdot L_{QT} \cdot \sin(\pi - \alpha - \eta) \right) \right] \cdot B_w \cdot \gamma \tag{4.41}$$

4.2.4.2 *The shape and forces on the sheared zone for Q > 0 m³/s with a boundary wedge*

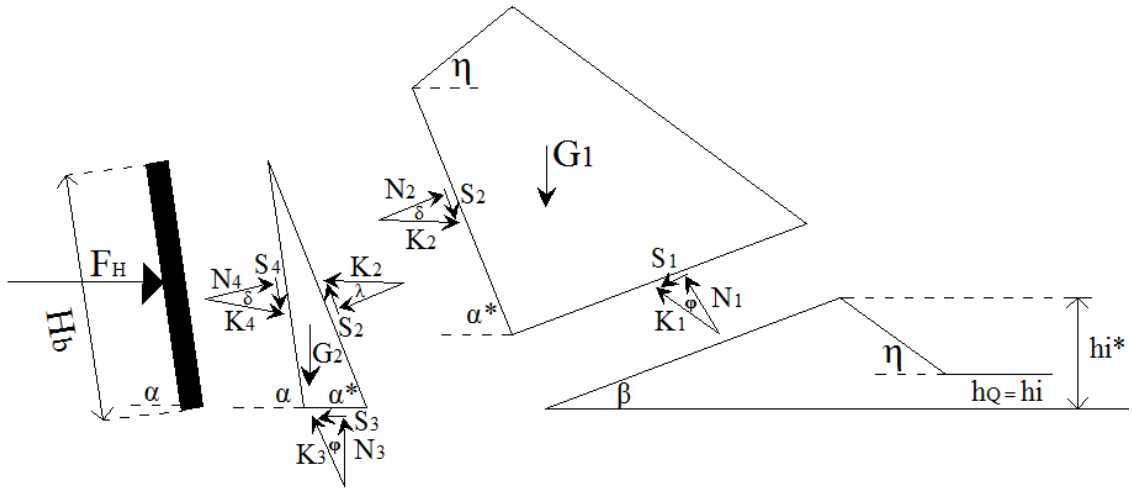

Figure 4.22 Forces on the sheared zone and boundary wedge for Q > 0 m³/s

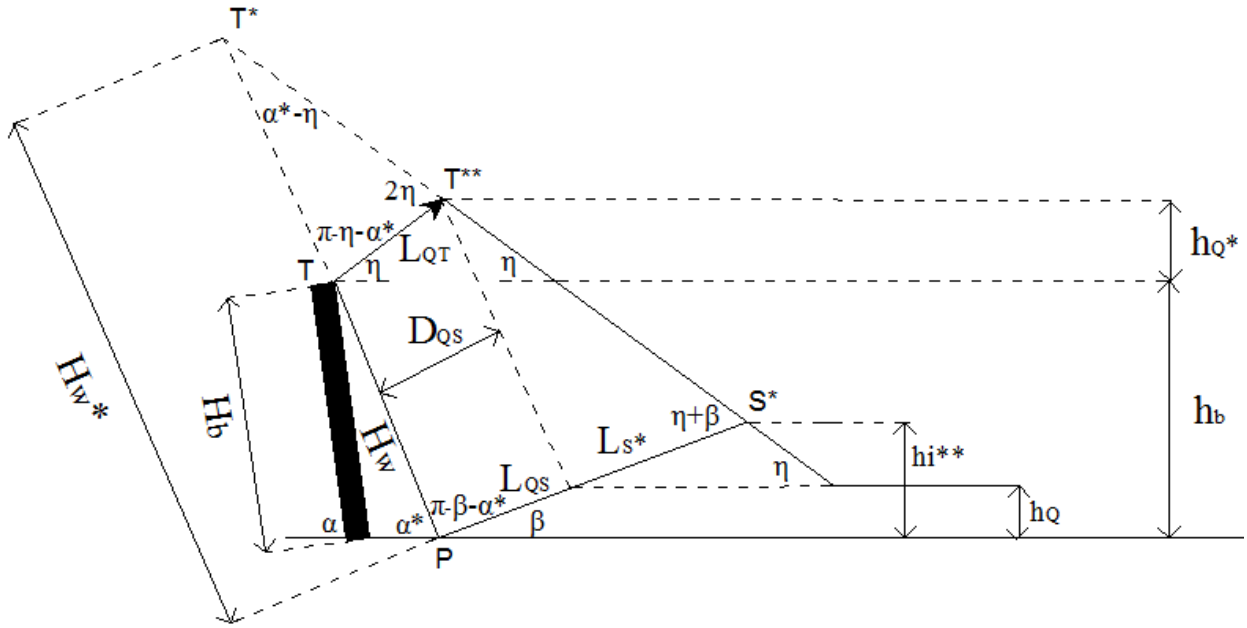

Figure 4.23 Shape of sheared volume and boundary wedge for Q > 0 m³/s

The length of the shear zone L_{QS} is equal to the situation without a boundary wedge:

$$L_{QS} = \frac{h_Q}{\sin(\beta)} \tag{4.42}$$

Thickness of the overflow layer perpendicular to the boundary wedge:

$$D_{QS} = L_{QS} \cdot \cos(\frac{\pi}{2} - \alpha^* - \beta) \tag{4.43}$$

Length of the overflow layer protruding above the blade:

$$L_{QT} = \frac{D_{QS}}{\cos(\alpha^* - \frac{\pi}{2} + \eta)} \tag{4.44}$$

Height of the overflow layer protruding above the blade:

$$h_{Q^*} = L_{QT} \cdot \sin(\eta) \tag{4.45}$$

Height of the auxiliary triangle:

$$TT^* = L_{QT} \cdot \frac{\sin(2\eta)}{\sin(\alpha^* - \eta)} \tag{4.46}$$

The height of the boundary wedge is calculated by:

$$H_W = \frac{H_b \cdot \sin(\alpha)}{\sin(\alpha^*)} \tag{4.47}$$

The joint height of the boundary wedge and auxiliary triangle:

$$H_w^* = TT^* + H_w \tag{4.48}$$

The lenght of the shear zone for the grains that are not overflowing, but rolling down the front side of the sheared zone:

$$L_S^* = \left(\frac{H_w^* \cdot \sin(\alpha^* - \eta)}{\sin(\eta + \beta)} \right) - L_{QS} \tag{4.49}$$

The imaginairy cutting depth:

$$h_i^{**} = (L_s^* + L_{QS}) \cdot \sin(\beta) \tag{4.50}$$

The gravitational force of the sheared volume can now be calculated by subtracting the surfaces of the large triangle PS*T* and the auxiliary triangle TT*T**:

$$G_1 = (PS^*T^* - TT^*T^{**}) \cdot B_w \cdot \gamma \tag{4.51}$$

$$G_1 = \left[\left(\frac{1}{2} \cdot H_w^* \cdot (L_s^* + L_{Qs}) \cdot \sin(\pi - \alpha^* - \beta) \right) - \left(\frac{1}{2} \cdot TT^* \cdot L_{QT} \cdot \sin(\pi - \alpha^* - \eta) \right) \right] \cdot B_w \cdot \gamma \tag{4.52}$$

And the gravitational force of the boundary wedge:

$$G_2 = \frac{1}{2} \cdot H_w \cdot H_b \cdot \sin(\alpha - \alpha^*) \cdot B_w \cdot \gamma \tag{4.53}$$

In fact Model 1 can be obtained from Model 2 by putting the inflow cutting depth h_Q on zero.

4.2.5 Example Calculation

Assumptions:

1. The boundary wedge is still consisting of upward moving particles at the blade surface. Under this assumption the steel-soil friction angle is fully mobilized and is equal to δ.
2. The friction angle λ between the boundary wedge and the Rankine zone is assumed to be also fully mobilized and equal to the internal friction angle ϕ.
3. The boundary wedge has horizontal slip line and an wedge angle α* = 55°.

With this assumptions in fact a rough blade is created with the angle of the boundary wedge α*. The particles are moving upward in front of the boundary wedge. The horizontal cutting force for a boundary wedge with friction angles δ and λ that are not fully mobilized is not treated in this thesis.

The horizontal cutting force without a boundary wedge by combining Eq. (4.11) and Eq. (4.12):

$$F_H = \left(\frac{G\sin(\beta+\varphi)+T\cos(\varphi)}{\sin(\alpha+\beta+\varphi+\delta)} \right) \cdot \sin(\alpha+\delta) \tag{4.54}$$

The horizontal cutting force with a boundary wedge by combining Eq. (4.20) and Eq. (4.21):

$$F_H = \left(\frac{K_2\sin(\alpha^*+\lambda+\varphi)+G_2\sin(\varphi)}{\sin(\alpha+\delta+\varphi)} \right) \cdot \sin(\alpha+\delta) \tag{4.55}$$

Where $K_2^* = \frac{G_1\sin(\beta+\varphi)+T\cos(\varphi)}{\sin(\alpha^*+\beta+\varphi+\lambda)}$

The calculation concerns a rockfill layer with D_{50} = 5,2 mm with an unknown internal friction angle ϕ. The soil-blade friction angle δ is equal to 20° for a fully mobilized case. The soil-interface friction angle λ is assumed to be equal to the internal friction angle ϕ = 30° of the material. The blade dimensions are a width of 0.6 m, a height of 0.02 m and a cutting angle α of 90°. A layer of rockfill of 0.01 m is cut with a cutting velocity of 0.1 m/s. The angle of the boundary wedge α* is equal to 55° and the angle of repose η = 30°.

The principle of minimum cutting energy is used to find the shear plane angle, this is equivalent to calculating the minimum horizontal cutting force.

The cutting depth is not zero so model 2 should be used to calculate gravitational force. The corresponding horizontal cutting forces are calculated by Eq. (4.54) and Eq. (4.55). The following table gives the results of the calculations. Figure 4.24 and Figure 4.25 give the cutting force as a function of β respectively without and with a boundary wegde.

Table 4.1 Horizontal cutting force [N] by the principle of minimum cutting energy

Model	Boundary wedge	Fh [N] for min β	β	sine nominator
Model 2	no	26.48	21	161
Model 2	yes	15.88	27	132

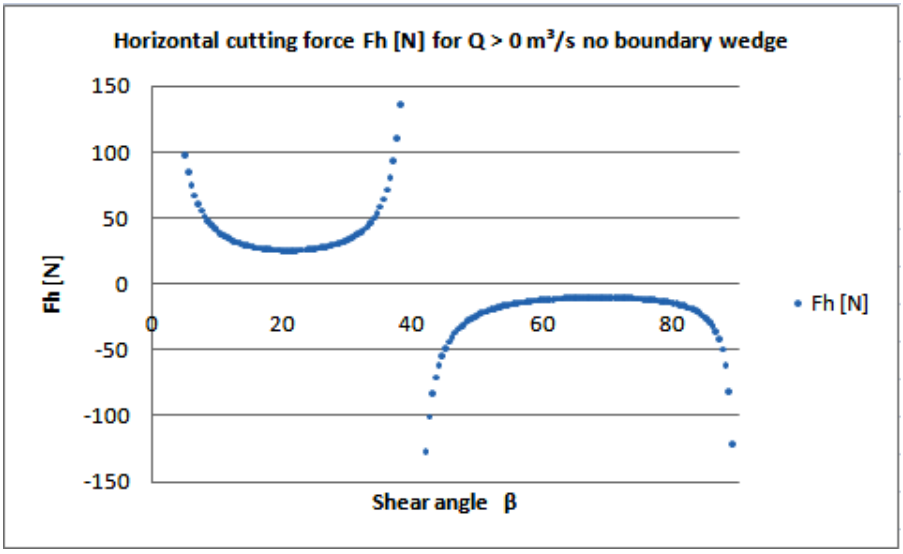

Figure 4.24 Principle of minimum cutting force [N] to determine β without a boundary wedge

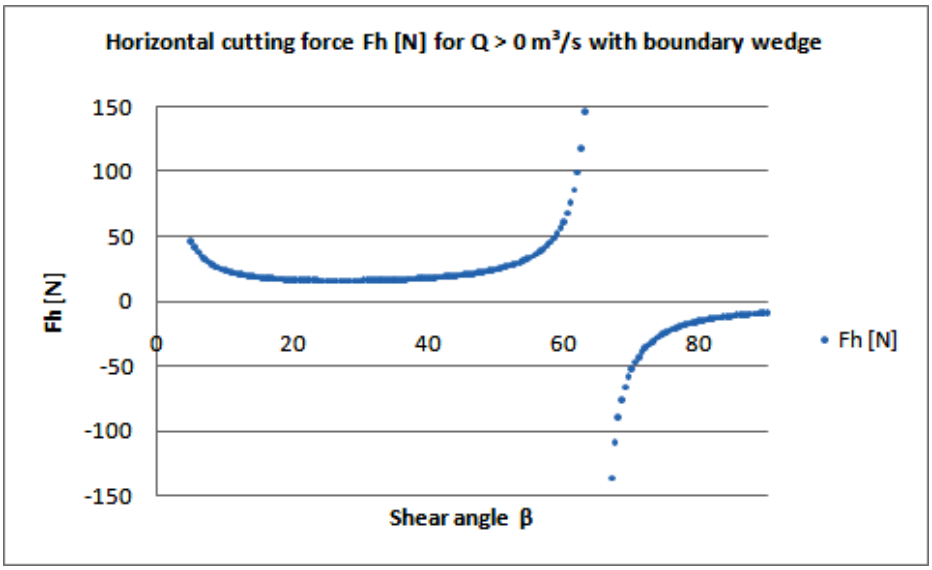

Figure 4.25 Principle of minimum cutting force [N] to determine β with a boundary wedge

4.3 Blade penetration in stationary bed (continuum approach)

When cutting a horizontal bed the bearing capacity of the bed determines the penetration of the blade into the subsoil. When the blade is not penetrating no material will be transported. Cutting a horizontal bed is different from cutting dunes where force can be delivered by the pulling wires. To create a trench or to equalize elongated high spots the vertical weight of the plough becomes main penetration force. The pull force from the wires is acting nearly perpendicular to the vertical penetration stress so the contribution to the penetration is very small.

To model the vertical penetration of a blade tip the bluntness of the blade will be considered as a strip foundation (shallow foundation) [7], see figure 4.26. The length of the strip L will be taken equal to the width of the blade and the width of the strip B equal to the bluntness or thickness of the blade.

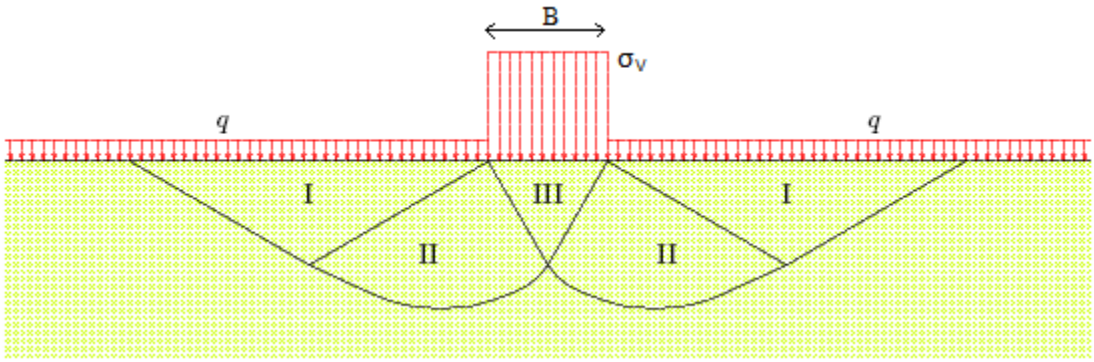

Figure 4.26 Force distribution under a strip foundation [7]

By K. Buisman, Caquot, Terzaghi and Brinch Hansen a relation is made between the area of the vertical strip footing and penetration resistance [7]. In section I the horizontal stress is larger than the vertical stress and can be seen as a passive Rankine zone. In Section III the vertical stress is equal the vertical stress generated by the strip footing σ_V. The vertical stress σ_V is in this case the vertical stress generated by the blade tip. The blade will penetrate the sub layer if the vertical penetration stress exceeds the bearing capacity of the material $\sigma_V > p_f$. Terzaghi [7] formulated a continuum relation for the bearing capacity p_f at the moment of failure:

$$p_f = q \cdot N_q \cdot s_q + \frac{1}{2} \cdot \gamma \cdot B \cdot N_\gamma \cdot s_\gamma \qquad (4.56)$$

Where p_f = the bearing capacity of an infinite soil layer [kPa], q = additional surface load [kPa], B = the width of the strip footing [m], γ = soil density [kg/m^3] and the coefficients Nq and Ny are dimensionless constants formulated by Prandtl. The factors for shape of the strip footing s_q and s_q are empirical determined by other researchers [7] and are given by Eq. (4.57) and Eq (4.58). These shape factors are equal to 1 in case of a long strip foundation:

$$s_q = 1 + \frac{B}{L} \cdot \sin\varphi \tag{4.57}$$

$$s_\gamma = 1 - 0.3 \cdot \frac{B}{L} \tag{4.58}$$

$$\gamma = (\rho_s - \rho_w) \cdot g \cdot (1 - n) \tag{4.59}$$

$$N_q = \frac{1 + \sin(\phi)}{1 - \sin(\phi)} \cdot \exp(\pi \cdot \tan\phi) \tag{4.60}$$

$$N_\gamma = 2 \cdot (N_q - 1) \cdot \tan\phi \tag{4.61}$$

In case the stress of the strip footing is not vertical but under an angle (figure 4.27), the bearing capacity p_f decreases. Inclination factors i_q and i_γ are used for a reduction of the load transverse to the strip footing.

$$i_q = \left(1 - \frac{\sigma_h}{\sigma_v \cdot \tan\varphi}\right)^2 \tag{4.62}$$

$$i_\gamma = \left(1 - \frac{\sigma_h}{\sigma_v \cdot \tan\varphi}\right)^3 \tag{4.63}$$

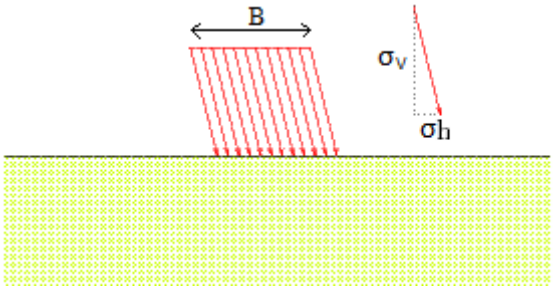

Figure 4.27 Force distribution under a strip foundation with a vertical stress under an angle [7]

The bearing capacity by Terzaghi for $s_q = s_q = 1$ and with the inclination factors i_q and i_γ gives:

$$p_f = q \cdot N_q \cdot i_q + \frac{1}{2} \cdot \gamma \cdot B \cdot N_\gamma \cdot i_\gamma \tag{4.64}$$

The left part of the Eq. (4.64) is the contribution of a surface load q [kPa] acting on the surface surrounding the blade. This surface load can be caused by an additional soil layer on the surrounding bed. The second term is the contribution of the natural weight of the soil underneath the strip, in which B is the blade thickness. The blade is assumed to penetrate in a horizontal soil surface. At the time op penetration no material is accumulated in front of the blade, so q = 0 kPa.

The coefficients N_q and N_γ are a function of the internal friction angle ϕ. Because the internal friction angle ϕ of the material is unknown this value can vary between 30° and 40°. The bearing capacity p_f by Terzaghi is therefore shown for ϕ different values of in the graph, in Figure 4.28. The strip dimensions based on the model plough, B_{blade} = 2 mm, L = 600 mm, q = 0 kPa and $i_q = i_\gamma = 1$.

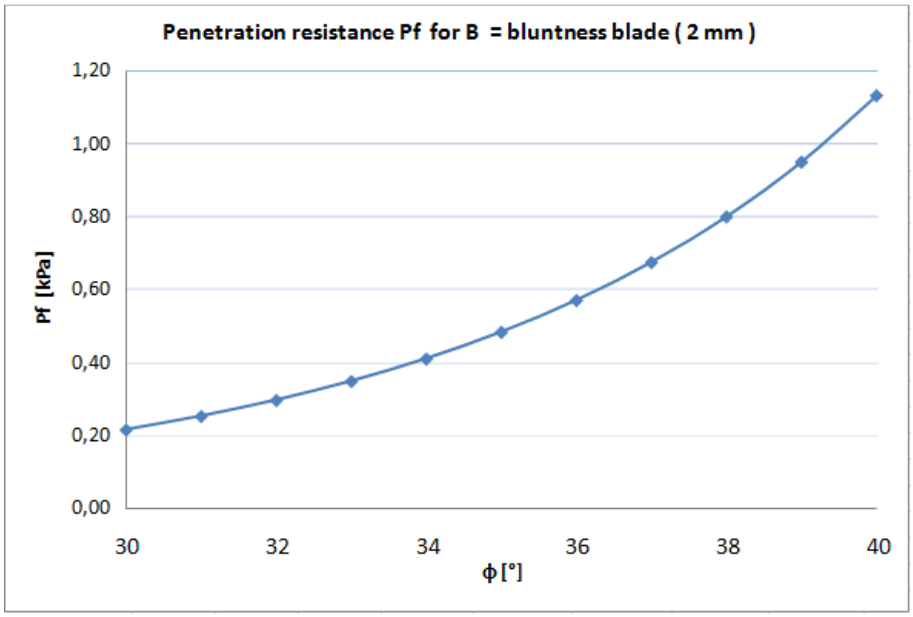

Figure 4.28 Blade penetration resistance pf for different values of φ: B=0.002,L = 0.6 m,q = 0

Effect of increasing the stone size on σ_v

The bearing capacity as formulated by Terzaghi is based on a continuum approach. In reality the layer thickness is not infinite and is influenced by the bottom of the physical scale model. With a limit number of particles in relation to the cutting tool, the behaviour is influenced by interaction between these grains. With a limit number of stones the soil layer will not behave as a continuum. The penetration resistance will be influenced by the appearance of rock columns like discussed in chapter 4.1.

When the stone diameter increases, the vertical penetration stress σ_V decreases due to an increase of strip surface. The load remains constant, but the width of the strip increases (figure 4.29). The relation of Terzaghi does not take the geometry of the particles in account. The strip surface in fine material is equal to the bluntness of the blade tip. In coarse rockfill the vertical stress decreases according to equation (4.63):

$$\sigma_{v,blade} = \frac{F}{A_{blade}} = \frac{F}{L_{blade} \cdot B_{blade}} \tag{4.65}$$

$$\sigma_{v,stone} = \frac{F}{A_{stones}} = \frac{F}{L_{blade} \cdot D_{stone}} \tag{4.66}$$

The spreading of the vertical penetration stress is in fact an increase of the bearing capacity of the soil. A soil consisting of larger particles has a higher bearing capacity. To model the bearing capacity of coarse material Eq. (4.64) will be modified by changing the width of the strip footing to the stone diameter B = D_{stone}.. The increase in bearing capacity will be predicted by two approximations. In the first approximation the width of the strip footing is increased from B to D_{stone}. For the second approximation the width of the strip footing is also increased from B to D_{stone}, but the first stone layer will also act as an additional surface load q. In this case the first stone actually becomes the blade and is therefore penetrating into the second soil layer according to figure 4.29.

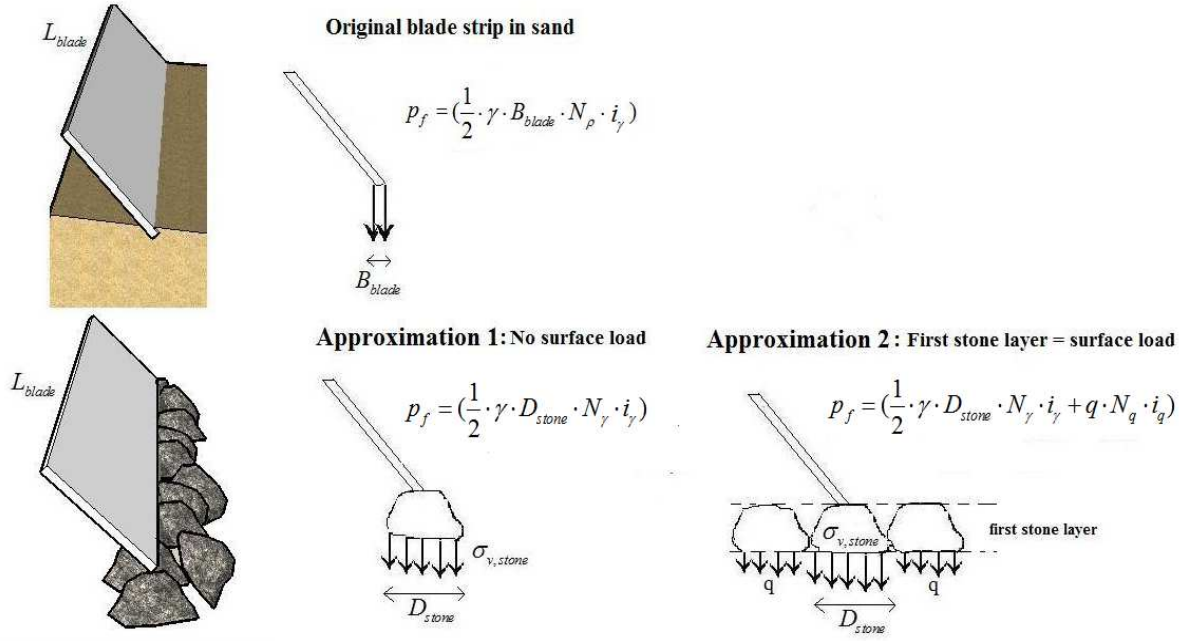

Figure 4.29 Influence particle size on surface load distribution

Approximation 1: The width of the strip is equal to the stone diameter.

$$p_f = (\frac{1}{2} \cdot \gamma \cdot D_{stone} \cdot N_\gamma \cdot i_\gamma) \quad (4.67)$$

The bearing capacity for values of ϕ between 30° and 40° is presented in figure 4.30. The calculations data is given in Appendix IV.1. The blade is first assumed to have only a vertical stress, so $i_q = i_\gamma = 1$. From the graph follows that the penetration resistance p_f increases rapidly by increasing of the width of the strip or by increasing the internal friction angle ϕ. The input parameters are B_{blade} = 2 mm, L = 600 mm, q = 0 kPa.

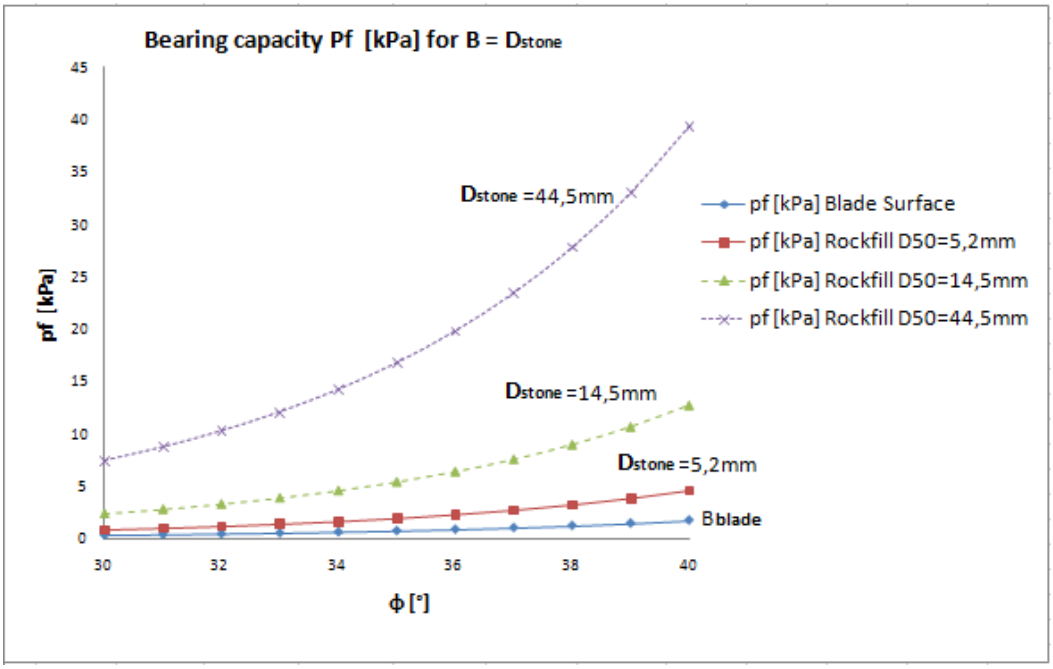

Figure 4.30 Penetration resistance with assumption that width strip is equal to stone diameter

Approximation 2: The width of the strip foundation is equal to the stone diameter, and a surface load q is added. The surface load is caused by the first layer of stones, assuming the blade to penetrate the second soil layer.

$$p_f = (\frac{1}{2} \cdot \gamma \cdot D_{stone} \cdot N_\gamma \cdot i_\gamma + q \cdot N_q \cdot i_q) \tag{4.68}$$

$$q = N_{stones} \cdot M_{stone} \cdot (1-n) \tag{4.69}$$

Where q = surface load of a soil layer N_{stone} = number of stones/m^2, M_{stone} = Mass of one stone [kN], n = porosity [-].

The bearing capacity for values of ϕ between 30° and 40° for approximation 2 is presented in figure 4.31. The input parameters are B_{blade} = 2 mm, L = 600 mm and $i_q = i_\gamma = 1$. The surface load q is calculated by Eq. (4.69) and differs for each material.

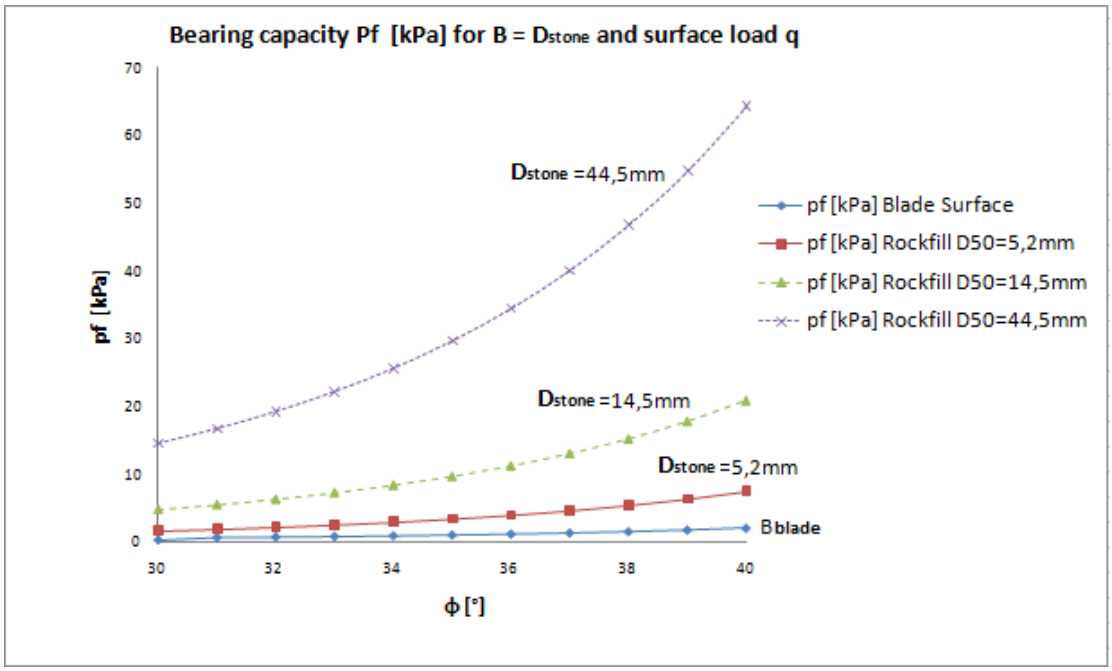

Figure 4.31 Penetration resistance with B = stone diameter and surface load

Example:

The penetration resistance p_f for dry rockfill with D_{50} = 14.5 mm, porosity n=0.4 and ϕ=30 degree and ρ_s = 2700 kg/m^3 the penetration resistance p_f becomes:

$$\gamma = (\rho_g - \rho_w) \cdot g \cdot (1-n) = 2700 \cdot 9{,}81 \cdot 0{,}6 = 16.86\, kN/m^3$$

$$N_\gamma = 2(N_q - 1)\tan\phi = 2\left(\left(\frac{1+\sin(30)}{1-\sin(30)}\exp(\pi \tan 30)\right) - 1\right)\tan 30 = 20{,}1$$

$$q = N_{stones} \cdot M_{stone} \cdot (1-n) = \frac{1000000}{14{,}5} \cdot \left(\frac{1}{6} \cdot \pi \cdot 14{,}5^3 \cdot \frac{2700}{1000}\right) \cdot (1-0.4) = 0{,}127\, kPa$$

Approximation 1:

$$p_f = \frac{1}{2} \cdot \gamma \cdot B \cdot N_\gamma \cdot i_\gamma = \frac{1}{2} \cdot 16{,}86 \cdot 14{,}5 \cdot 20{,}1 \cdot 1 = \boxed{2{,}41\ kPa}$$

Approximation 2:

$$p_f = \frac{1}{2} \cdot \gamma \cdot B \cdot N_\gamma \cdot i_\gamma + q \cdot N_q \cdot i_q = \frac{1}{2} \cdot 16{,}86 \cdot 14{,}5 \cdot 20{,}1 \cdot 1 + 0{,}127 \cdot 18{,}4 \cdot 1 = \boxed{4{,}76\ kPa}$$

Table 4.2 Penetration resistance pf for different strip stone diameters, ϕ=30 degree (no water)

	pf [kPa] for Blade bluntness B_{blade}=2mm	**Pf [kPa] for Rockfill D_{50}=5,2mm**	**Pf [kPa] for Rockfill D_{50}=14,4mm**	**pf[kPa] for Rockfill D_{50}=44,5mm**
Approximation 1	0.34	0.87	2.41	7.46
Approximation 2	0.34	1.71	4.76	14.61

If the vertical penetration stress of the blade σ_v is too low to penetrate the material, rippers are used to increase the vertical stress. These rippers have a smaller penetration surface which results in an increase of σ_v . The soil is moved upward and transported by the blade, but also the grain structure is restructured. This allows particles to move in between other grains and inside the space created by the rippers. Zelenin (1950) and Kostritsyn (1956) [18] divided the soil in front of the ripper in an area that moves upward and an area of soil in front of the blade that is compressed. Godwin (1974) [18] made a mechanical model for the movement of soil around very narrow cutting tools. This model can be used in case rippers are installed underneath the cutting blade, the vertical stress increases according to Eq. (4.62).

4.4 Model for unloading soil

The model for unloading the plough is almost similar to the model for transporting (chapter 4.2). The initial volume is decreasing because soil is deposited under the level of the blade. This material is not reintegrated in front of the plough. The triangular shaped soil volume in front of the blade will decrease according to figure 4.32.

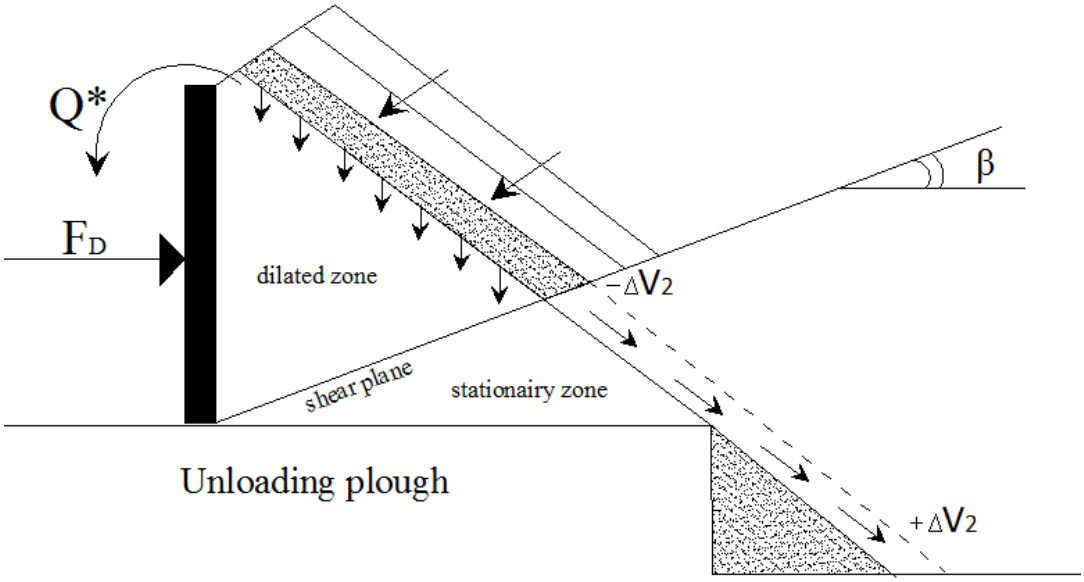

Figure 4.32 Model for unloading plough

4.5 Model for strength of individual grains (crack)

During cutting and penetrating high peak local stresses could cause failure of the grain (crack) due to a high point contact stress. There are ways to test the strength of rock in physical experiments like an Axial point load test, Schmidt hammer test or the Brazilian split test.

To determine whether a stone will break before it is moved, the next formula for the point load strength is used [12]:

$$I_{sd} = \frac{P}{D_e^2} \tag{4.70}$$

I_{Sd}	=	Point load strength	[kPa]
P	=	Failure Load (pressure x piston area)	[kN]
De	=	Equivalent core diameter	[m]

The stones used at the Maasvlakte have a point load strength of about 9,4 Mpa and a compressive strength 250 N/mm^2 (Mpa). If this value is exceeded crack formation will occur.

II Physical scale model

Chapter 5 Scale Model

5.1 Introduction

To verify the analytical model, a physical scale model is set up. The advantage of a scale model is a clear view of the processes in limited space. The effect of changing one parameter is examined by keeping the rest of the parameters constant. The actual situation is on full scale, the prototype. The aim is to achieve similarity between the corresponding dimensions and the physical processes of the model and the prototype [2]. Chapter 5.2 will give the derivation of the scaling rules used to build and interpret the scale model. In chapter 5.3 the test configuration is presented.

The goal of the physical experiment is divided in visual and quantitative goals. The visual goals are used to validate the geometrical set up of the models in chapter 4. The quantitative goals are used to verify the formulas corresponding with the models.

Visual Goals

1 What is the movement of the individual grains and the grain structure in front of the dozer and cutting blade?
2 What is the visual effect of varying the plough mass on:
   a. The dynamics of the plough, underflow and overflow.
   b. The blade penetration in the sub layer.

Quantitative goals

3 Do the following analytical models (in different sizes of rockfill) agree with the scale results :
   a. The modified Terzaghi penetration model derived in chapter 4.3.
   b. Transporting Model 1 for coarse grains without a soil inflow from the cutting blade Q = 0 derived in Chapter 4.2
   c. Cutting & Transporting Model 2 for coarse grains with a soil inflow from the cutting blade Q > 0 derived in Chapter 4.2.

5.2 Scaling rules

Before a scale model can be designed a good understanding in the scale rules is required. To get a realistic representation of the processes of the prototype, the scale effects must be minimized. The goal is to limit these scale effects by imitating the prototype as good as possible. As mentioned before the aim is to achieve similarity between the dimensions and the physical processes of the model and the prototype

The soil and geometrical shape parameters that have to be scaled are.

- Plough dimensions
- Stone dimensions
- Bed properties (dune height)

The processes that have to be scaled are:

- Cutting & Transporting
  - Forces in shear zone
  - Stone fall velocity
  - Pore water flow

5.2.1 Length Scaling

The length scale factor n_L is the ratio between the model and the prototype. This scaling factor is applied to the various parameters in the model to create geometrical similarity. This can be realised by scaling all the length dimensions of the prototype Xp by the same factor n_L=20.

$$\boldsymbol{n_L = \frac{X_p}{X_m} = 20} \tag{5.1}$$

For dynamic similarity all the velocities have to be scaled with the same velocity scale factor as well. For the movement of objects under water Froude scaling is used. Equating the Froude number of the model and the prototype ensures that the gravitational and inertial forces are scaled in the same proportion. The Froude number is defined as

$$\boldsymbol{Fr = \frac{v}{\sqrt{gL}}} \tag{5.2}$$

Where *v* is the velocity of the plough, *g* is the acceleration due to gravity, and *L* is the length of the plough. The acceleration due to gravity is equal to the prototype (n_g=1), the Froude number has to equal to the model as well for a good representation of the physical quantities of the prototype(n_{Fr}=1).

$$\boldsymbol{n_{Fr} = \frac{n_v}{\sqrt{n_L}} = 1} \tag{5.3}$$

$$\boldsymbol{n_v = \sqrt{n_L} = \sqrt{20} = 4.47} \tag{5.4}$$

$$\boldsymbol{n_v * n_t = n_L \rightarrow n_t = \sqrt{n_L} = 4.47} \tag{5.5}$$

5.2.2 Stone fall velocity in water

The equation of a falling stone under water is given by the next formula. Note that fall velocities in air are much larger, so this is only valid for stone velocities in water:

$$\boldsymbol{w = \beta \sqrt{\frac{4}{3}\frac{g\Delta D}{C_D}}} \tag{5.6}$$

Where: $\Delta = \frac{\rho_s - \rho_w}{\rho_w}$. Scaling all the parameters in equation (5.6) gives:

$$\boldsymbol{n_w = \sqrt{n_\Delta \cdot n_g \cdot n_D}} \tag{5.7}$$

The stone density and the gravitational force is equal to the prototype $n_\Delta = n_g = 1$.The stones dimensions are scaled with the length scale factor $n_L = n_D = 20$. Processing this in formula (5.6) gives Froude scaling:

$$\boldsymbol{n_w = \sqrt{n_L}} \tag{5.8}$$

This is in agreement with scale factor (5.4).

5.2.3 Cutting forces

Both the plough and the stones are scaled with the length scale factor $n_L = 20$ in x-y-z direction. The relation for the horizontal cutting force follows from Eq. (4.12) in Chapter 4.1:

$$\boldsymbol{F_H = \frac{Gsin(\beta + \varphi) + Tcos(\varphi)}{sin(\alpha + \beta + \varphi + \delta)} \cdot sin(\alpha + \delta)} \tag{5.9}$$

Scaling inertia force from Eq. (4.14) gives:

$$\boldsymbol{T :: \rho_g \cdot v_c^2 \cdot h \cdot b} \tag{5.10}$$

$$\boldsymbol{n_T = n_\rho \cdot n_v^2 \cdot n_L^2 = 1 \cdot \sqrt{n_v^2} \cdot n_L^2 = n_L^3} \tag{5.11}$$

Scaling the gravitational from Eq. (4.15) gives:

$$\boldsymbol{G :: \rho \cdot g \cdot l^3} \tag{5.12}$$

$$\boldsymbol{n_G = n_\rho \cdot n_g \cdot n_L^3 = 1 \cdot 1 \cdot n_L^3 = n_L^3} \tag{5.13}$$

Both the inertia force and the gravitational force are scale by $\boldsymbol{n_L^3}$. Scaling the cutting forces:

$$\boldsymbol{F_H = G \cdot constant + T \cdot constant}$$

$$\boldsymbol{n_F = n_G = n_T = n_L^3} \tag{5.14}$$

5.2.4 Stone and plough dimensions

The plough dimensions and the rockfill gradation curves and are scaled by the length scale factor n_L=20 and presented in respectively Appendix II and III. The gradation curves are based on the prototype rockfill used at the Maasvlate and are given between brackets: The stones vary in D_{50} from 0.38mm (filter material), 5.2mm (Cobbles), 14.5mm (5-70kg) and 44.5 (300-1200kg)

5.2.5 Dune and sub layer

The dune dimensions are also scaled by the length scale factor n_L=20. In reality the dune height can vary between 0,5m and 1m, corresponding to 25 and 50 mm in the model. To imitate this in the scale model the number of stones stacked on top of each other must agree with the prototype. To get a good view of the number of stones to create a realistic dune this is defined in table 5.1.

This table will also help to determine whether a process can be considered as a continuum or the number of particles are limited compared to the medium.

Table 5.1 Dune and Plough height expressed in number of stones stacked

D_{50} (mm) Scale Model	Dune height 25mm	50mm	Rear blade 70mm	Cutting blade 20mm	Sub layer 150mm
0,38	66	132	184	53	395
5,2	4,8	9,6	13	3,8	29
14,5	1,7	3,4	4,8	1,4	10
44,5	0,6	1,3	1,6	0,4	3,4

5.2.6 Scale and boundary effects

Stone crushing/crack: A scale effect during cutting is the stress at the contact points between stones. The surface of these points determine the stress at a contact point and the penetration/crack formation. A crushed zone will always occur between two stones an can be infinitely small, but the crushed zone grows with an increasing tension. Stones on a normal scale in the prototype tend to break more easily, so in the real situation more stones will break. Also the tensions are higher so crushed zones will be higher. This is explained in the point load index in Chapter 4.5.

Porosity: After each experiment the bed is brought back to a ”zero profile”. Reshaping the bed has effect on the porosity of the sub layer. The porosity is also affected by the vibrations of the plough moving on the bed. The error due to the change in porosity is not taken into account in this research.

Wall effect: On both sides of the plough 10 cm space is left between the plough and the glass wall. The wall can affect the sideway outflow of material. Also the grain stresses in y-direction could be influenced. Because in rockfill types with D_{50}=5,2 mm and D_{50}=14,5 mm this distance is more than 6 stone diameters the wall effect is assumed to be acceptable. For the biggest stone size of D_{50}=44,5 mm the wall effect should be taken into account.

Bottom effect: With an increase in stone diameters the layer will consist of less particles stacked on top of each other see table 5.1 last column. The number of stones determine the application of a continuum penetration approach or a discrete approach. The same assumption is made as by the wall effect.

5.3 Model set up

5.3.1 Location

The experiments are carried out in “de Speurwerkgoot” in the laboratory of Civil Engineering, TU Delft. The flume contains glass windows and is 30 meters long, 80 cm wide and has a depth of 1 meter. On top of the flume a rail is mounted on which a drag mechanism is installed. The pulling force of this drag mechanism is over 300 Newton and moves at a constant speed. The speed is independent of the resistance. The drag speed can be varied from 2 cm/s up to 1 m/s. The speed was set to 10 cm/s to get a good view of the stone movement in front of the plough. This is equal to 0,447m/s ≈ 1 knot with the prototype.

Figure 5.1 Speurwerkgoot: flume (left), drag mechanism (right top)

The flume is filled with 4 types of rockfill, varying in D_{50} from 0.38, 5.2, 14.4 and 44.5 mm. The gradation curves of these materials are given in Appendix III. The lanes are placed in an extended line with a length of 3 meter and a layer thickness 15 cm layer for each lane, see figure 5.1 (right bottom).

5.3.2 Model Plough

All laboratory experiments were performed using the plough given in figure 5.2 This plough consists of a steel body and a cutting blade with a adjustable blade angle. To increase the weight of the plough, weights of 1 kg could be added. The weights are held in place by the steel plates attached to both sides of the plough to prevent interaction with the sub layer.

Figure 5.2 Model plough

The suspension consists of 4 steel wires with a deformation of ± 2 mm by 5kg. The wires could be varied in length by turnbuckles (figure 5.7) to adjust the suspension height. Two additional wires are used for the drag force, these wires are attached to the front of the plough. The plough has three levels to attach the drag wires; low, middle or near the top of the plough (side view figure 5.3).

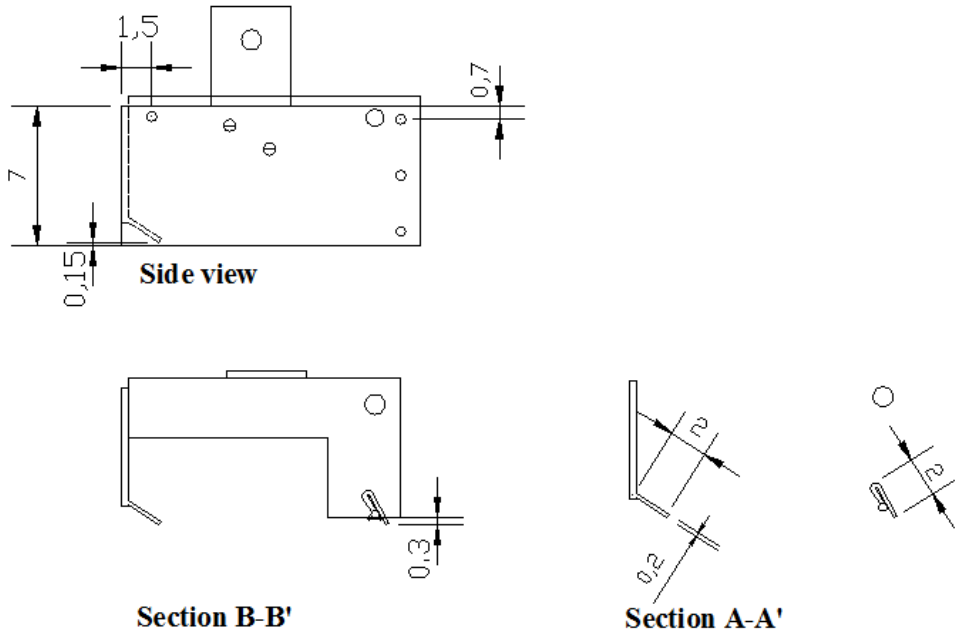

Figure 5.3 Drawing model plough: Side view

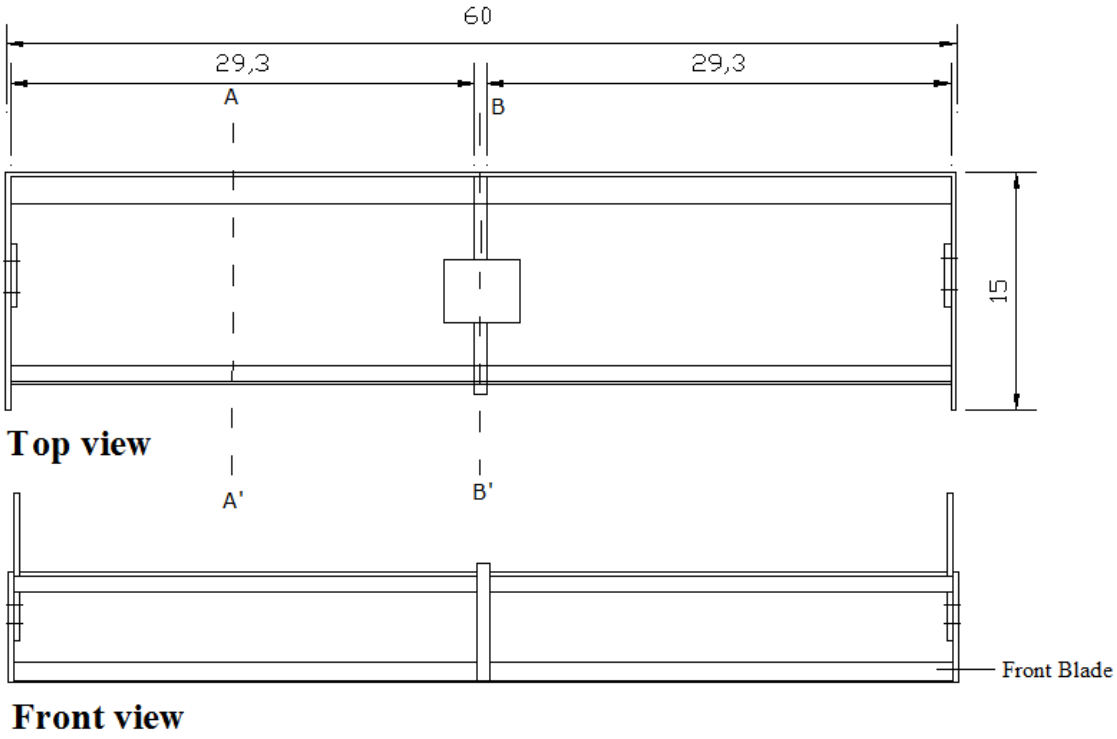

Figure 5.4 Drawing model plough: Top & Front view

5.3.3 Measurement tools

Measurement tools are used to record the drag force and the penetration of the plough. These tools are calibrated at the start of every test sequence. The penetration of the plough was measured using a single beam laser. The laser was calibrated by installing 3 blocks with different heights in the flume. The dimensions of these three blocks where measured with a ruler to calibrate the laser.

In front of every lane a brick was placed in the flume at a calibrated level of 15 cm. These bricks where also used to check the laser, bed level and plough suspension before every test.

The load cell is calibrated by loading it with weights of respectively 2, 4 and 8 kg. The output voltage was measured and the volt meter was set to match the force on the load cell. The load cell only measured perpendicular loading and was mounted in such a way that only the horizontal force is measured when the suspension wires are under an angle. This is the force that is relevant to the bollard pull of the ship so no additional calculation have to be performed to the output values. The load cell is placed in the middle of the flume and both drag wires are attached to the same load cell. This results in a total horizontal force, no force measurement is made for the left and right drag wire separately.


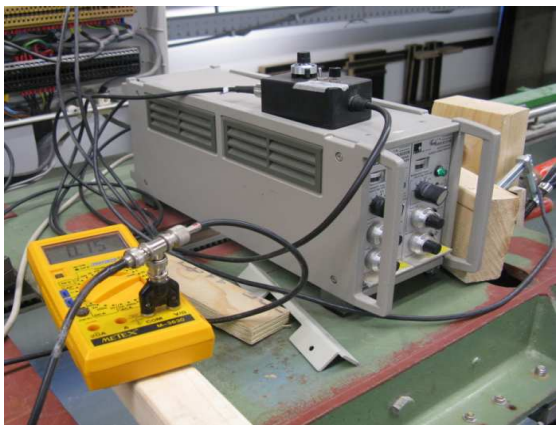

Figure 5.5 Force measurement tools: Load cell, Volt meter


Figure 5.6 Geometry measurement tools: Sinlge beam laser, distance "pulse ticker"


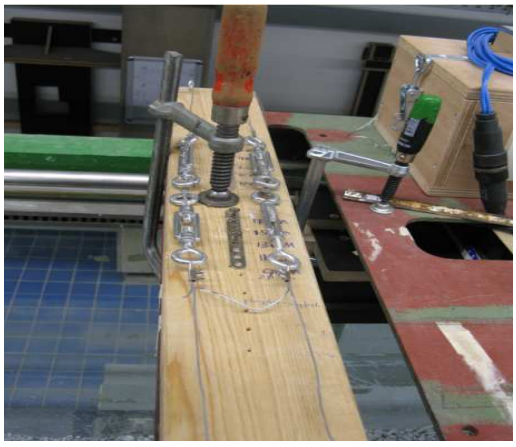

Figure 5.7 Suspension measurement tools: height caliberated bricks , turn buckels

5.4 Test description

The experiment is divided in three test lay outs: cutting, transporting and some additional test in equalizing dunes. The only parameters varied are the plough mass and the stone size. The load cell is fixed to a vertical beam to create a low drag angle. The drag wires are attached to the center fixation point at the half of the height of the plough. The suspension wires are also attached to the drag mechanism, so the entire plough construction has the same speed of 10 cm/s.

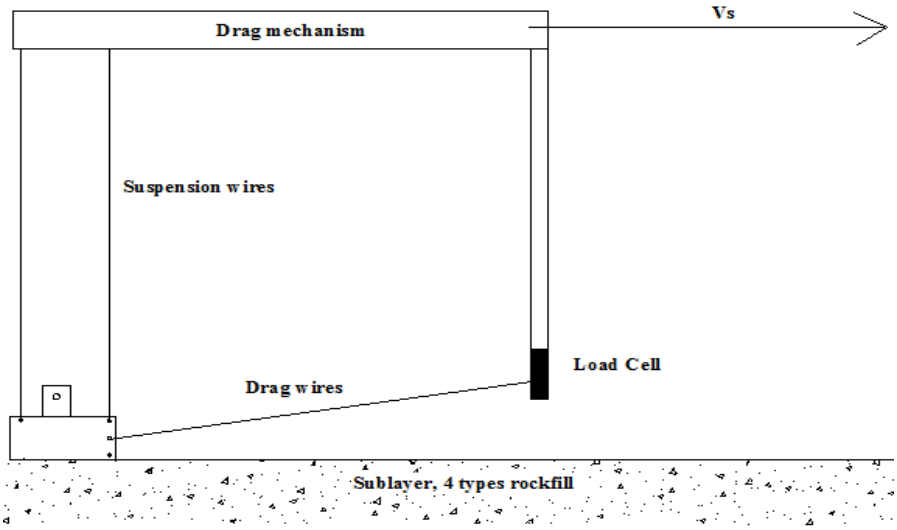

Figure 5.8 Test lay out Scheldegoot

At the start of every experiments a zero profile is made. This zero profile has a layer thickness of 15 cm over the entire length. The zero profile is made by suspending the plough at this level and dragging it across the surface until no material is transported. Afterward a laser measurement is executed to verify the layer thickness.

Each of the experiments has its own angle in which the plough is rotated. The three tests will be shortly discussed in the following paragraphs.

5.4.2 Transporting test

The plough is filled with an initial volume of 8 kg rockfill. The cutting blade is lifted 2 cm from the bottom to prevent contact with the sub-layer (figure 5.9). The drag force is solely depending on the rear blade and the soil in front of the blade. The initial stone volume is measured on a weighing platform to guarantee the same amount of soil with each experiment.

The effect of changing the plough mass is examined by adding additional weights, see also the test program in Appendix V. The goal is to determine the effect on drag force and the vertical lift of the plough. The position of the blade tip is measured by pointing a laser beam on the top plough surface and subtracting the plough height. The drag force will be related to the volume of material in front of the plough.

If the plough is lifted it will rotate around the front wire which is under tension. The rear wire is not supporting any weight, here the plough is supported by the rear blade. The vertical force distribution between the wire and the blade can be calculated by taking the momentum balance over the rear blade. The vertical blade force is presented in table 5.2. The dots in figure 5.9 represent the centre of mass of the different parts of the plough and the corresponding distances.

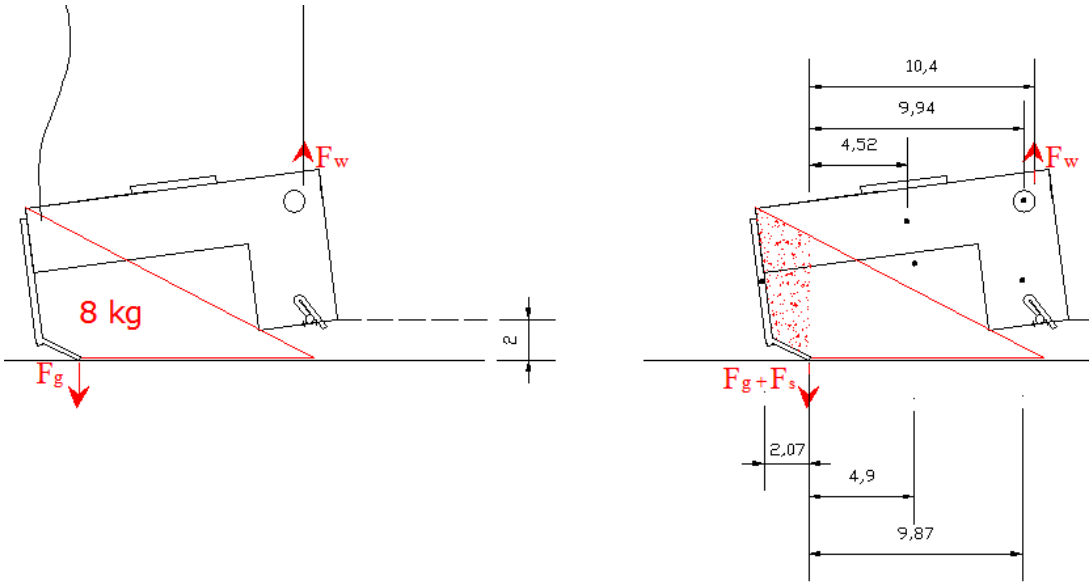

Figure 5.9 Penetration force: Momentum balance around cutting blade tip

As a result of the lift of the cutting blade the rear blade rotates. Due to the rotation the blade angles are different from the horizontal configuration. Because it is not clear what blade angle has to be used to calculate the horizontal cutting force three blade angles α_1, α_2, α_3 are given in figure 5.10.

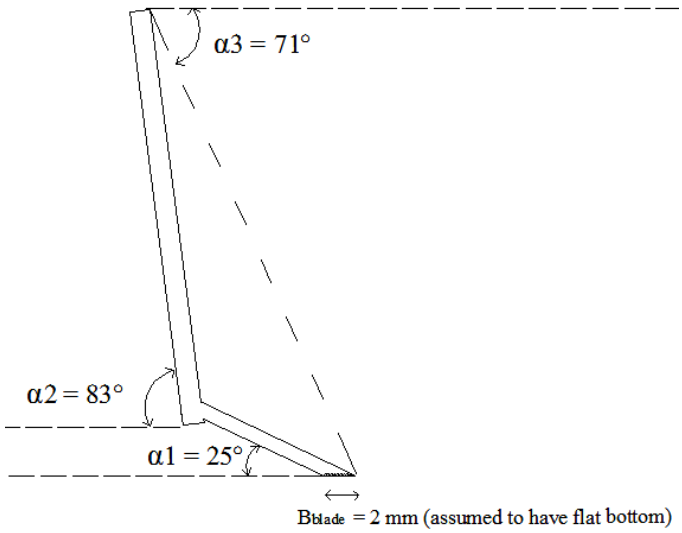

Figure 5.10 The different blade angles of the rear blade after lifting the front blade

To vertical penetration stress σ_v is calculated by Eq. (4.23) given below. The blade is assumed to have a flat bottom surface, as shown in figure 5.10. The penetration stress σ_v is given by:

$$\sigma_{v,blade} = \frac{F_g}{A_{blade}} = \frac{F_g}{L_{blade} \cdot B_{blade}} = \frac{F_g}{600 \cdot 2}$$

Where B_{blade} = thickness of the blade [m], L_{blade} = length of the blade [m] and F_g = plough mass [N] .In order to penetrate the sub layer the penetration stress of the blade must be higher than the penetration resistance p_f calculated in chapter 4.3 and Appendix IV.1. The mass of the initial plough is 2,4 kg. The plough mass is increased by adding 2 kg each time a new experiment is carried out. The maximum added mass is 10 kg.

Table 5.2 The vertical penetration stress **σ_v** of the rear blade without soil in front of the blade

Added mass [kg]	**Fg [N]** **Gravitational force on blade tip**	**σ_v [kPa]** **Vertical penetration stress by blade**
0 kg	18.8	15.7
2 kg	29.4	24.5
4 kg	40.0	33.3
6 kg	50.5	42.1
8 kg	61.1	50.9
10 kg	71.7	59.7

5.4.3 Cutting & penetration

The cutting experiment is almost similar to the transport experiment. The dozer blade (rear blade) is now lifted from the sub layer to prevent contact. Here also the wire force is calculated. Ones the wire force is known a vertical force balance is taken by subtracting the wire force from the total plough mass, determining the force on the blade tip.

The plough will start above a trench in the bed to determine the maximum cutting depth when the plough is fully suspended. This is the maximum cutting depth that is allowed by the wire, so if the blade is not lifted during the cutting experiment the penetration depth could lay deeper.

The cutting blade is pulled through the rockfill by the pulling wires and the cutting depth is measured with a single beam laser. This test is repeated in the different types of rockfill. During this tests both penetration and cutting force are measured. This way a relation between the cutting depth hi and the drag force can be made to compare the results with the analytical solution. Also a relation will be made between the penetration stress of the blade tip (table 5.3) and the penetration.

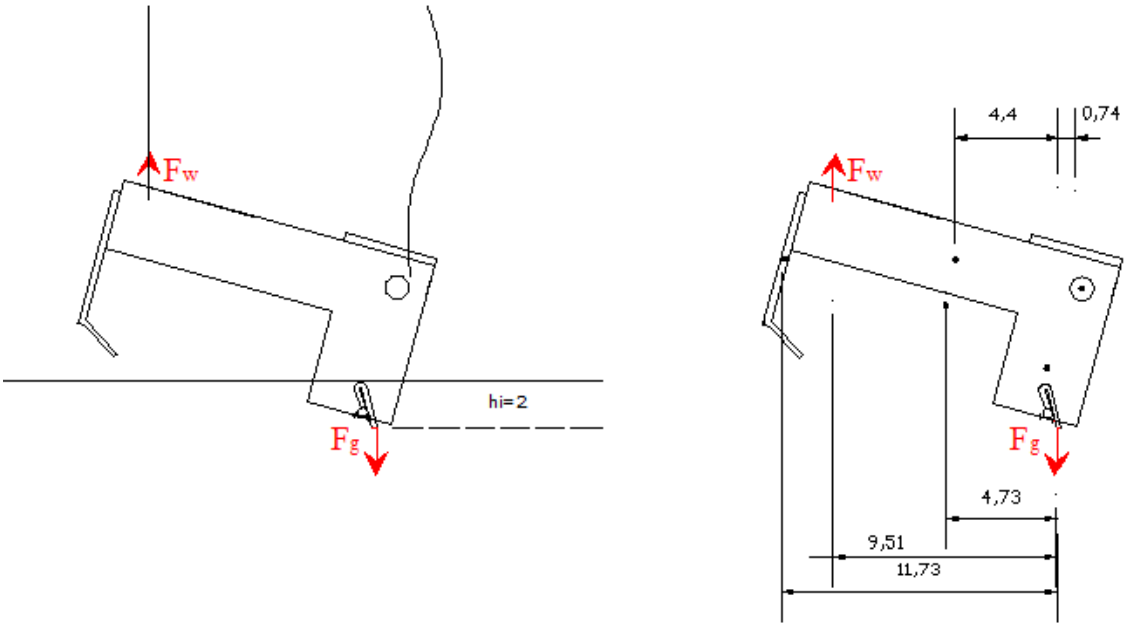

Figure 5.11 Momentum balance around cutting blade tip to calculate penetration force

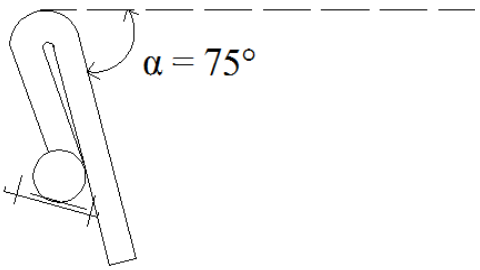

Figure 5.12 Angle of the cutting blade after lifting the rear blade

To vertical penetration stress σ_v of the cutting blade is also calculated by Eq. (4.23) and summarized in table 5.3.

Table 5.3 The vertical penetration stress σ_V of the cutting blade without soil in front of the blade

Added mass [kg]	Fg [N] Gravitational force of blade	σ_V [kPa] Vertical penetration stress by blade
0 kg	6.8	5.7
2 kg	16.9	14.1
4 kg	27.0	22.5
6 kg	37.0	30.8
8 kg	47.1	39.2
10 kg	57.1	47.6

The cutting depth laser measurement is performed by mounting a small steel plate on top of the plough, see figure 5.13. In this figure the two extreme situations are presented with a maximum penetration and penetration is zero. From the laser measurement the distance from the plate to the blade tip (7,75mm) was subtracted in Matlab to get the penetration at a certain time. The cutting depth was measured simultaneously with the force measurement. This way a good view is given of the drag force for a certain cutting depth hi. Due to a small rotation of the plough there was a small error in the order of 1% in the blade height between the two extreme plough configurations. This error was mediated.

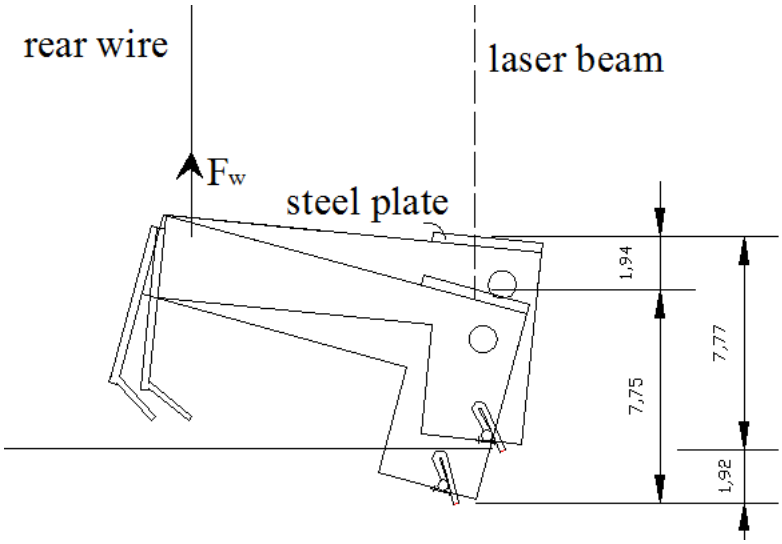

Figure 5.13 Sinlge laser beam measurment on a steel plate on top of the plough

5.4.4 Equalizing dunes

Some experiments are carried out by ploughing dunes. During these experiments some random bed configurations are made by just disturbing the layers with a shovel. At other experiments dunes are made with a known dune volume and different transport distances to the ridges L_{dr} (figure 5.14). The volume of the ridges is equal to the volume of the dune, 4 dm^3. The plough is suspended at the design level D.

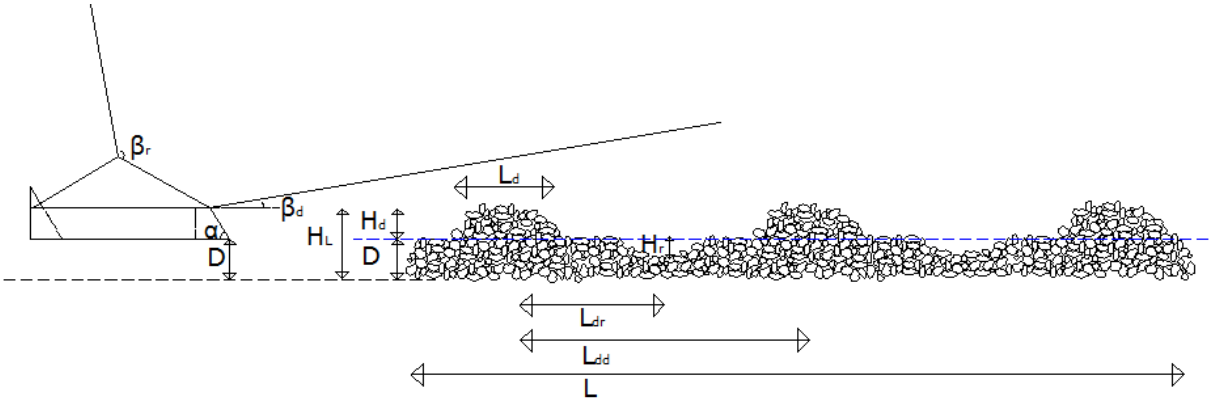

Figure 5.14 Test configuration ploughing dunes

To test different transport distances in one experiment the L_{dr} is varied between 20 cm and 80 cm. Three dunes are created with a mutual distance of L_{dd}=100 cm and height H_d=5 cm. Before and after the experiment a profile measurement is made to see the effect after each experiment. The profile will be reconstructed after 3 experiments.

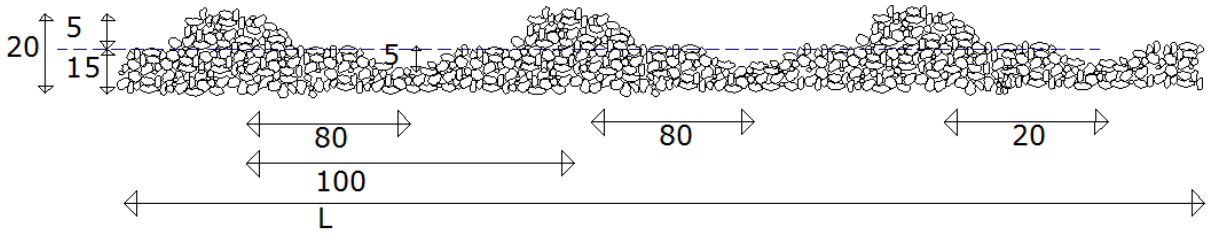

Figure 5.15 Dimensions profile equalizing dunes

Chapter 6 Experiment Results

6.1 Results from the transporting experiments (rear blade only)

The transporting experiments have been carried out according to the test lay out given in chapter 5.4.2. In front of the rear blade an initial volume of soil of 8 kg was placed at the start of each experiment. The cutting blade was lifted from the bed. The effect of increasing the plough mass is examined by adding additional weights. The horizontal cutting force and the plough elevation (lift) are measured for several added masses.

Figure 6.1 Plough suspension during a transporting experiment in cobbles(D_{50} = 5,2 mm)

6.1.2 Observations transporting experiments

During the transporting experiments the following processes where observed.

1. The rear blade was lifted during the experiments, resulting in an underflow of material. The plough was barely unloading by overflow.
2. The soil volume in front of the blade seemed to go an equilibrium triangular shape for high plough masses and was continuously decreasing for low plough masses. The outflow rate was depending on the material.
3. In rockfill consisting of large stones: D_{50} = 14,5 mm (prototype: 5-70 kg) and D_{50} = 44,5mm (prototype: 300-1200 kg), the rear blade was lifted significantly resulting in a high underflow. In D_{50} = 44,5mm the soil volume in front of the rear blade was instantly deposited by underflow for all plough masses. No material was transported for longer distances.
4. In fine material: D_{50} = 5,2mm (prototype: Cobbles) and D_{50} = 0,38mm (prototype: Filter) the plough makes a almost horizontal movement through the sub layer depending on the plough mass. This is shown in the graphs in chapter 6.1.3.

5 The experiment made visible that the grains move/dilate constantly in front of the blade. Grains are pushed to the surface and are following a circular movement when rolling down the slope, are being integrated in the grain body and reappear at the surface. This was also proven by adding some additional colored stones on top of the wedge and follow the track of these stones, this is shown in figure 6.2 and 6.3.

Figure 6.2 Testing stone movement by placing red stones on top of the soil volume

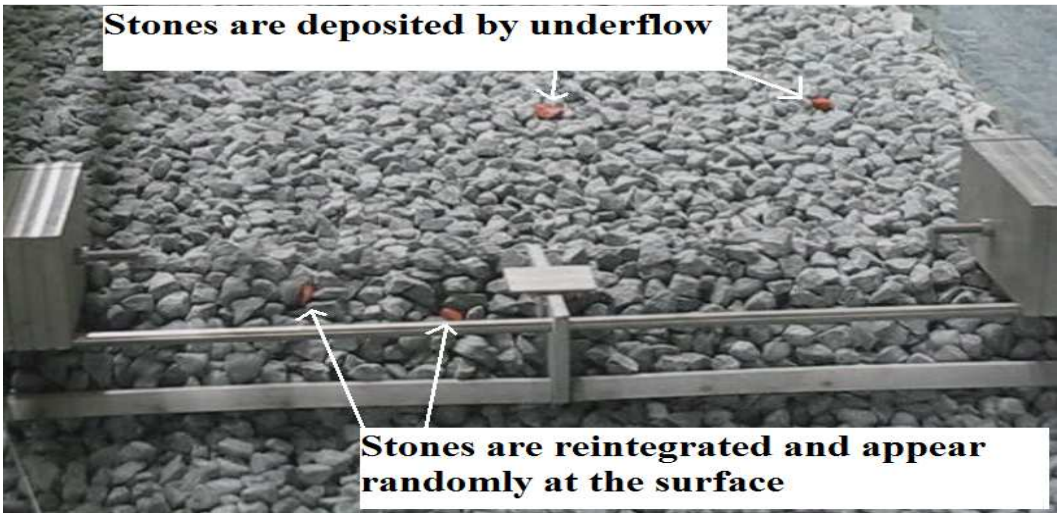

Figure 6.3 Position of the colored at the bed and in the soil volume stoned after 50 cm

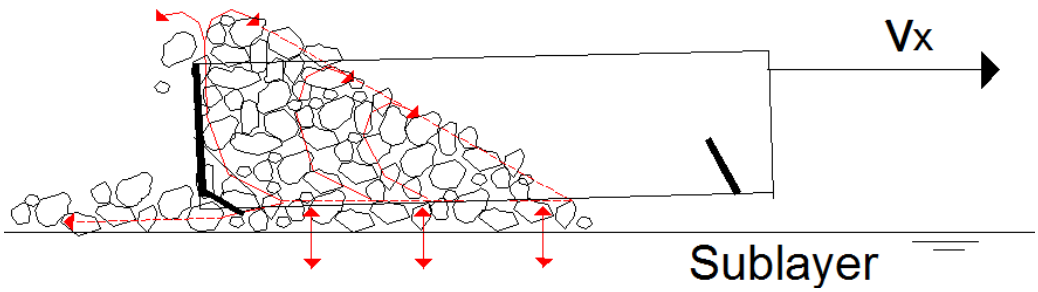

Figure 6.4 Visual presentation stone movement

6 Due to a water content in the “dry” filter material (coarse sand in scale model D_{50} = 0,38 mm) the soil showed barely individual grain movement and the soil volume was acting as one piece with a horizontal shear line.
7 The movement of the grains at the surface decreases when cutting in water. For Cobbles (D_{50} = 5,2 mm) there was a clear difference between the rate of particles pushed to the surface in dry or saturated cutting. For saturated cutting this was much less, while the behaviour for 5-70 kg rockfill (D_{50} = 14,5 mm) in dry and saturated cutting was almost similar. In cobbles a overflow was observed for high plough masses. Directly after the plough started moving the material was, unlike in the coarser materials, deposited by overflow.
8 In the scale experiments is was not possible to see a clear shear zone inside the wedge. The failure method of the grain structure was not visualized.
9 Another experiment with colored stones proved that an exchange of grains between the sub layer and the soil volume is present. The colored grains were placed on the bed and a transporting experiment was performed. Some stones where picked up from the bed and integrated into the soil volume. The stones appeared at the surface at random places.
10 Is the rear blade is placed on the bed without the initial volume of 8 kg the blade also starts cutting until a certain equilibrium volume is reached depending on the plough mass.

6.1.3 Processed measurement data from transport experiments

In this chapter the measurement data obtained from the transporting experiments are presented in graphs. A soil mass of 8kg is transported (rear blade only) with a cutting depth equal to zero. The numbers displayed in the graphs represent added mass to the plough, the mass of the initial plough is 2,4 kg. The plough mass is increased by adding 2 kg each time a new experiment is carried out. The maximum added mass is 10 kg. The forces and penetration are not made dimensionless and they are based on the forces measured in the scale model, this is still to be done.

D_{50} = 14,5 mm (prototype 5-70 kg)

The effect of increasing the plough mass on the horizontal cutting force in rockfill D_{50} = 14,5 mm is made visible in figure 6.5. The horizontal cutting force is shown on the vertical axis and the time [s] on the horizontal axis. The blade was moving with a constant speed of 10 cm/s, so in total 2 meters was traveled.

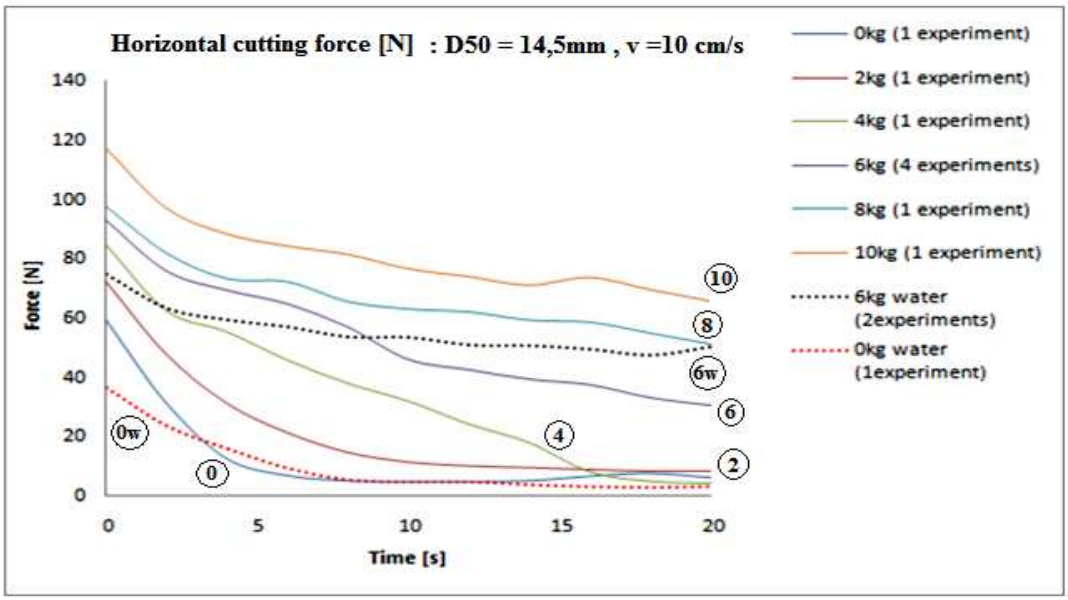

Figure 6.5 Horizontal force [N] for transporting 8kg rockfill (D_{50} = 14,5 mm) by increasing plough mass

During the experiments an outflow of material was observed underneath the rear blade. This follows also from the decrease of the horizontal cutting force F_H in figure 6.5. The outflow strongly depends on the plough mass. A plough with 0 kg added weight shows a rapid decrease of the horizontal cutting force by escape of the material, while a more heavy plough seem to go to an equilibrium situation where the horizontal cutting force F_H and thus the soil volume remains constant.

The vertical lift of the rear blade corresponding to the forces in figure 6.5 is presented in figure 6.6.

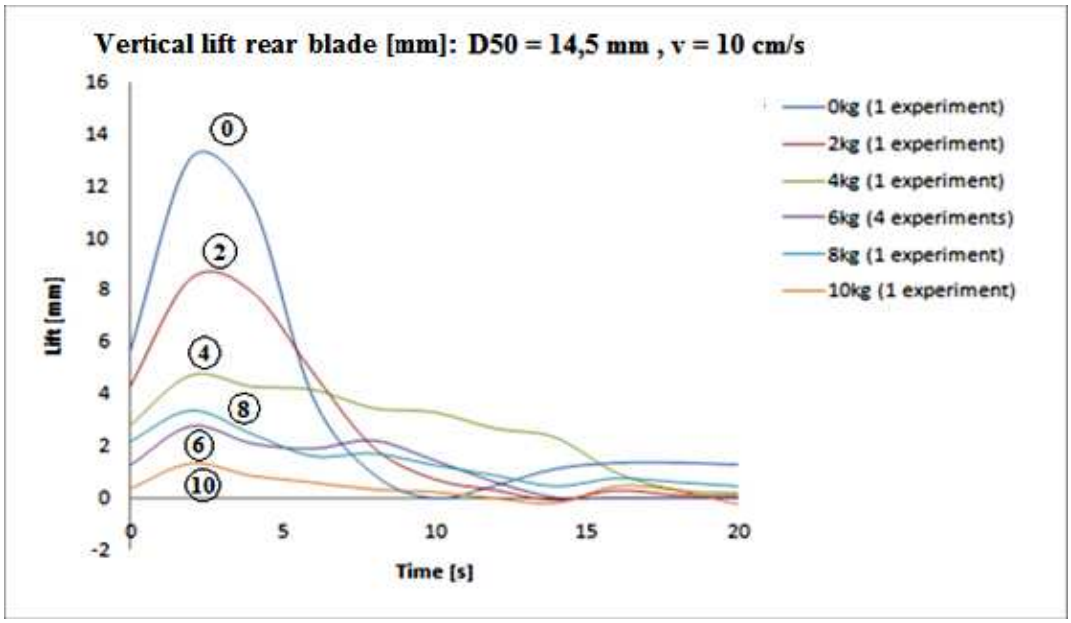

Figure 6.6 Vertical lift of the rear blade corresponding to the cutting forces of figure 6.5

When we look at the laser measurement of the figure 6.6 a clear view of the plough lift is given. A plough with 0 kg added weight shows an empty time of around 10 seconds (1 meter). At t = 20 s the plough lift is nearly zero at all the mass configurations. When the vertical lift is zero the plough is restsing on the sub layer and will barely empty by underflow. If the plough mass is high enough the blade will even start cutting and add material to the soil volume in front of the blade. An equilibrium soil volume is reached when the blade lift is zero and the blade is neither lifted nor cutting. The experiment with 0 kg added mass shows an additional lift after it is emptied at t = 10 seconds. This is the result of the plough bouncing over the top layer, the plough is not filled for the second time.

Experiments carried out in water showed that the equilibrium soil volume is reached in a earlier state and the outflow rate decreases. Unfortunately a laser measurement was not possible through the water surface, so no good comparison can be made between the lift of the plough and forces measured in water. The reason for an decrease of the outflow rate in water is the decrease in stone and plough mass according to Archimedes. The specific weight of the stones decrease from 27 kN/m^3 to 17 kN/m^3, this is a decrease of 37%. The plough consists of steel with a specific weight of 78 kN/m^3, the underwater weight becomes 68 kN/m^3. This is a decrease of 13%, so the stones become relatively much lighter than the plough. This is resulting in a larger transported volume, for a relative lower plough mass.

D_{50}=5,2mm (Cobbles)

In figure 6.8 is shown that in rockfill with D_{50} = 5,2mm (Cobbles) the plough is also lifted with an empty plough, but the vertical lift decreases rapidly with an increasing plough mass. When the results are compared with transporting D_{50} = 14,5 mm (5-70 kg) an equilibrium soil volume is reached for a lower plough mass. With an added mass of 4 - 6 kg the plough moves nearly in a straight line

with barely some underflow losses. Due to the small grain size the plough can easily penetrate the under flowing layer and find the equilibrium transport cutting depth.

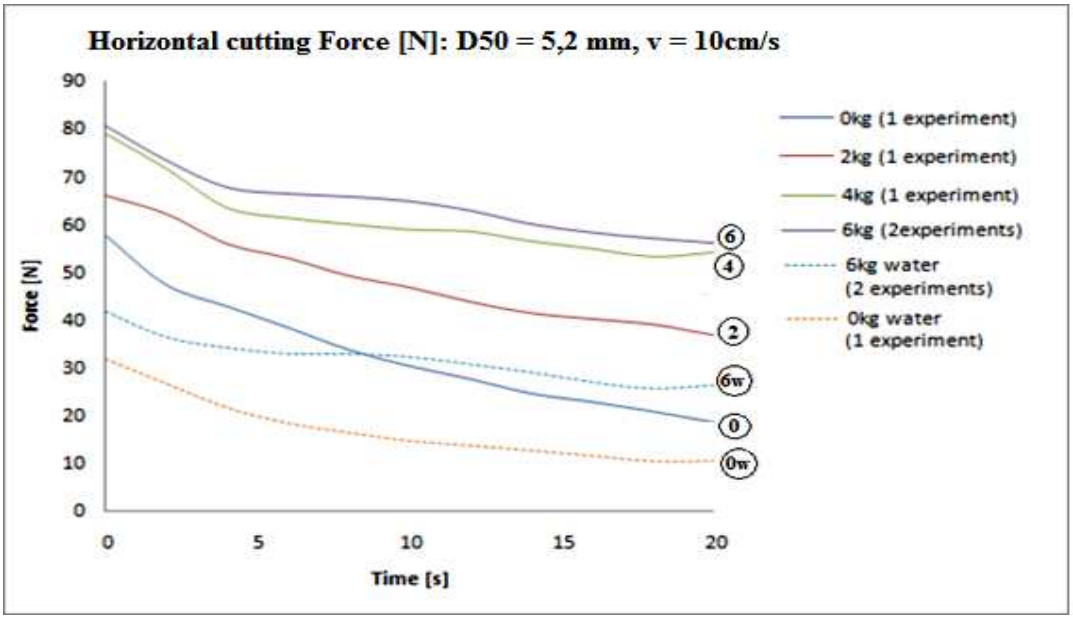

Figure 6.7 Horizontal force [N] for transporting 8kg Cobbles (D_{50} =5,2 mm) by increasing plough mass

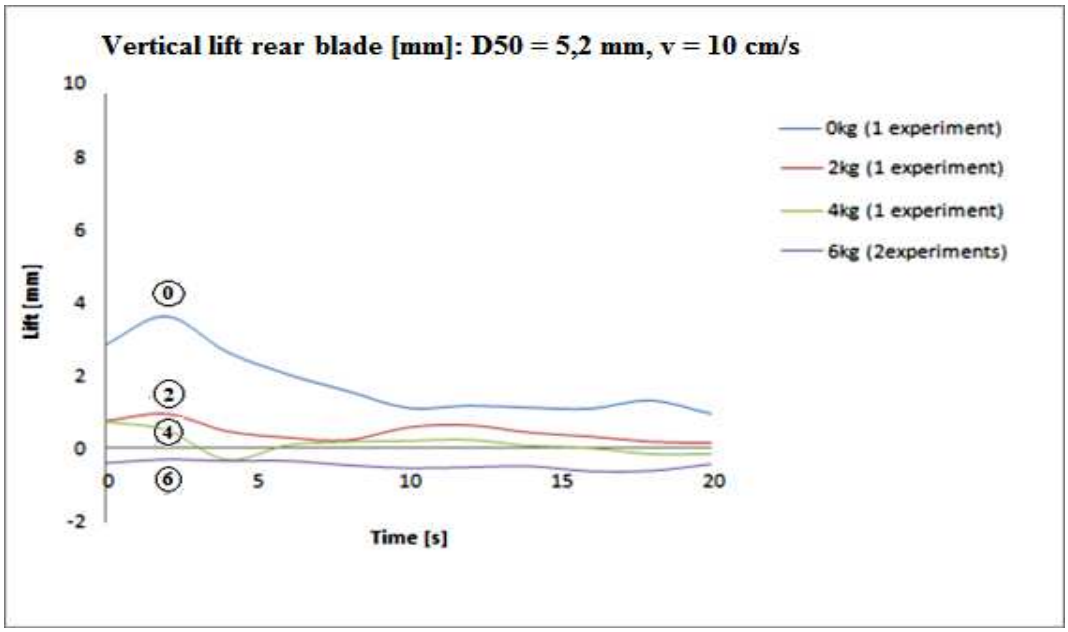

Figure 6.8 Vertical lift of the rear blade corresponding to the cutting forces of figure 6.7

In figure 6.8 the vertical lift shows that mass the initial plough is not sufficient to move in a straight line. A plough mass with 6 kg added weight shows a negative lift, so a penetration. This results in a cutting depth and an overflow of material, this was also observed in the experiment.

D_{50}=44,5mm (300-1200kg)

It seems not possible to transport rockfill with particles of D_{50} = 44,5 mm (300-1200 kg). Even with an added mass of 10 kg the plough emptied instantly. When the plough is empty it bounces across the surface, moving some stones over short distances. The stones that are moved are placed randomly on the bed, causing the bed roughness even to increase at some points.

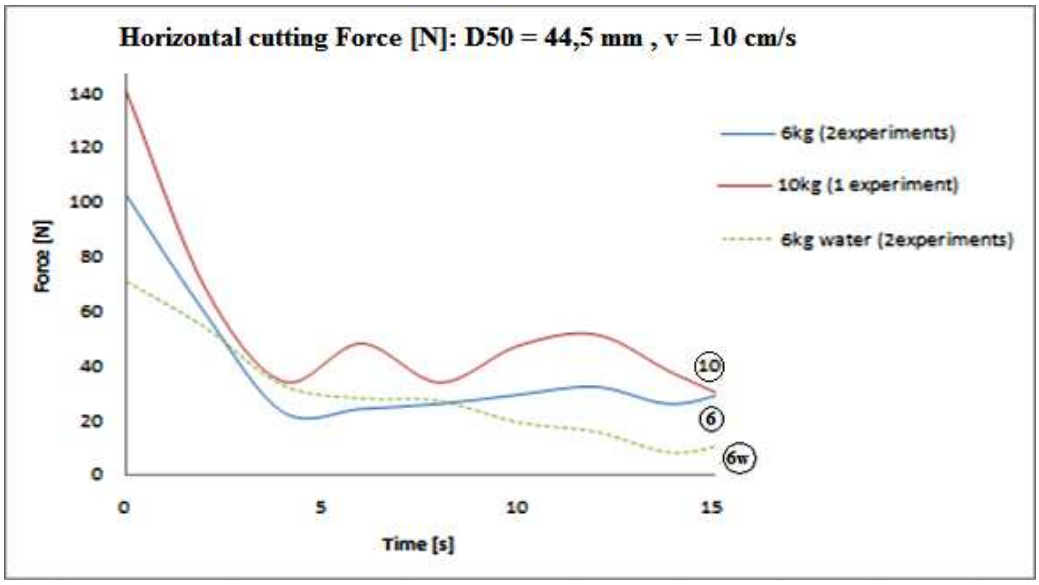

Figure 6.9 Horizontal force [N] for transporting 8kg boulders (D_{50} =44,5 mm) by increasing plough mass

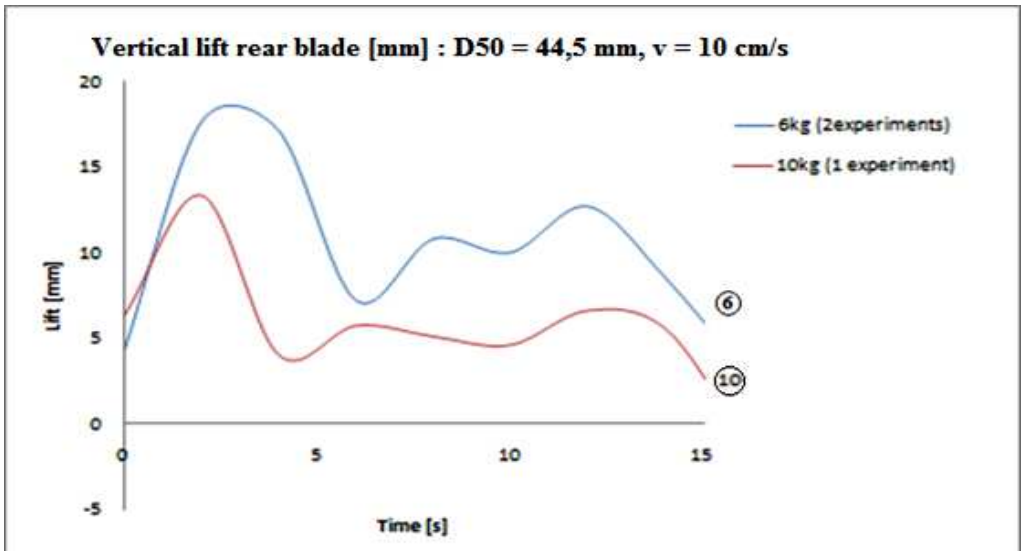

Figure 6.10 Vertical lift of the rear blade corresponding to the cutting forces of figure 6.8

D_{50}=0,38mm (Filter)

The filter material was not dry and therefore no reliable data could be taken from this experiments. To prevent wrong interpretation of the data no graphs are shown. Due to the water content the soil showed barely individual grain movement and was acting like with one piece a horizontal shear line.

6.2 Results cutting & penetration (front blade only)

The cutting experiments have been carried out according to the test lay out given in chapter 5.4.3. The rear blade was lifted from the bed to generate an experiment solely depending on cutting of the front blade. No initial soil volume was placed in front of the blade like in the transporting test. The effect of increasing the plough mass is examined by adding additional weights. The horizontal cutting force and the cutting depth (penetration) are measured for several added masses. At the start of each test the plough is suspended above a small ridge made in the bed. This way the plough is not resting on the bed at the start of each experiment and the maximum cutting depth is known. This maximum cutting depth is to prevent the plough from penetrating to very large depths. Is the maximum cutting depth is reached the suspension wires attached to the front of the plough are under tension. If the maximum depth is not reached there is slack in these wires and the plough is only suspending on the rear wires.

Figure 6.11 Maximum penetration during a cutting experiment in cobbles (D_{50} = 5,2 mm)

6.2.2 Observations cutting & transporting experiments

1 From the cutting experiments followed that the penetration of the blade into the sub layer seemed crucial. With a plough that is too light the blade will scrape and slide across the surface and will only move some stones on the top layer.
2 More force must be exerted to the blade tip to penetrate the blade tip in the sub layer when the rock size increases. This force must be created by the plough mass, the drag wires only create a horizontal cutting force.
3 When ploughing dunes are ploughed also clear view was given of the importance of the plough mass. When dunes are lowered, the angle between dune slope and the pulling wires angle becomes too small and the penetration force becomes dominant.

4 For stones with D_{50}= 14,5 mm (5-70kg prototype) the initial plough mass seems insufficient to penetrate into the sub layer. More mass had to be added to start penetrating and cutting. The blade is not able to cut half stone diameter so the blade penetrates the first layer between half and a whole stone diameter, see figure 6.12. This also follows also from the actual measurements shown in the graph of figure 6.14. Dunes in D_{50}= 14,5 mm are only spread over short distances with the initial plough mass, no material is actually transported.

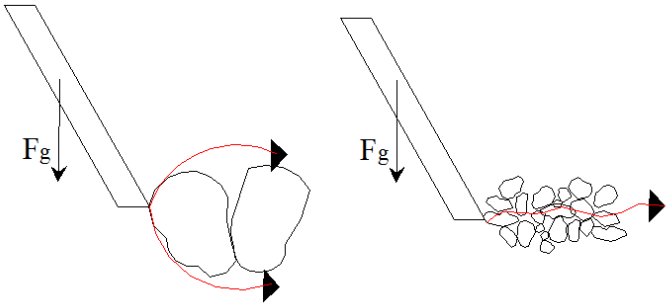

Figure 6.12 Plough movement in D50=14,5mm and D50=5,2mm

5 Cutting in D_{50} = 44,5 mm showed no results, the plough was not penetrating into the sub layer, even with the heaviest plough mass. The interlocking forces in D_{50} = 44,5 mm were causing the plough to have a significant movement across the surface. The plough is bouncing across the surface with sometimes elevations around 15mm.

6 For cobbles was shown that the present plough mass is enough to make a moderate straight line through the sub layer and dunes, but also a small lift of the plough through the sub layer was observed.

6.2.3 Processed measurement data from cutting & transporting experiments

In this chapter the measurement data obtained from the simultaneously cutting & transporting experiments are presented in graphs. The plough mass is increased by adding 2 kg each time a new experiment is carried out.

D_{50}=14,5mm (prototype 5-70 kg)

The effect of increasing the plough mass on the horizontal cutting force in rockfill D_{50} = 14,5 mm is presented in figure 6.13. The experiment results are divided in a penetration time and a stationary cutting period. In the stationary cutting period the blade is fully saturated with soil and is overflowing with a constant volume per time unit.

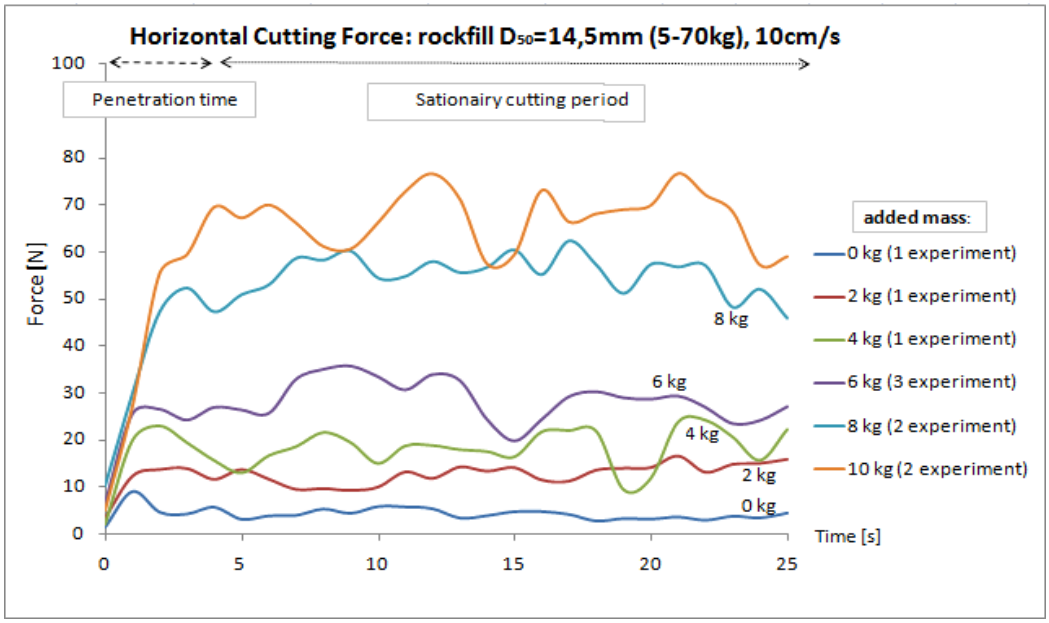

Figure 6.13 Cutting experiments in D_{50}=14,5mm with a penetration time and a stationairy cutting period

The horizontal cutting force increases is the plough mass is increased, but from figure 6.13 and observations follows that the blade is not cutting for every plough mass. If the added plough mass is below 8 kg the cutting blade is not penetrating into the sub layer. For 6 kg added mass the plough is randomly penetrating and breaking out. By increasing the added mass to 8 kg the bearing capacity of the boulders is reached, resulting in a penetration of the first stone layer. This is directly resulting in a higher horizontal cutting force in figure 6.13.

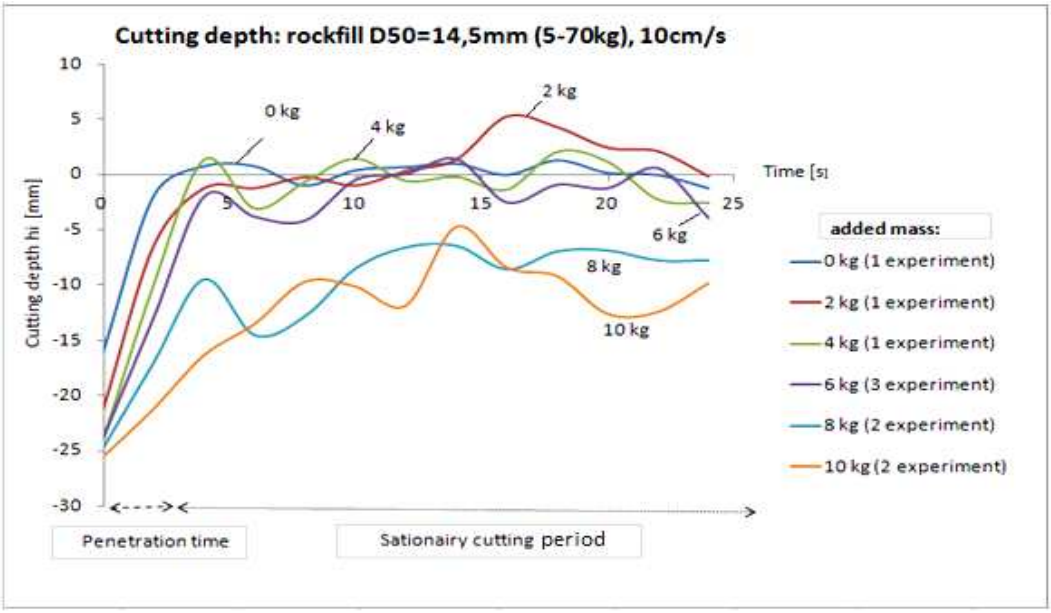

Figure 6.14 Cutting depth of the front blade corresponding to the cutting forces of figure 6.13

To visualize the relation between horizontal cutting force and cutting depth the data is combined in figure 6.15. From the figure 6.13 and 6.14 only the data for the stationary cutting period used to calculate an average cutting force and cutting depth. The standard deviation presented by a vertical branch to the average value. The standard deviation is increasing for a higher plough mass. Higher cutting depths show a higher standard deviation of the cutting because of stick and slip behaviour. The standard deviation for the cutting depth is higher for 6 kg than for 8 kg. This is caused by the randomly penetration and outbreak of the blade for 6 kg, while for 8 the blade has penetrated the first grain layer and is moving in a more horizontal line through the rockfill.

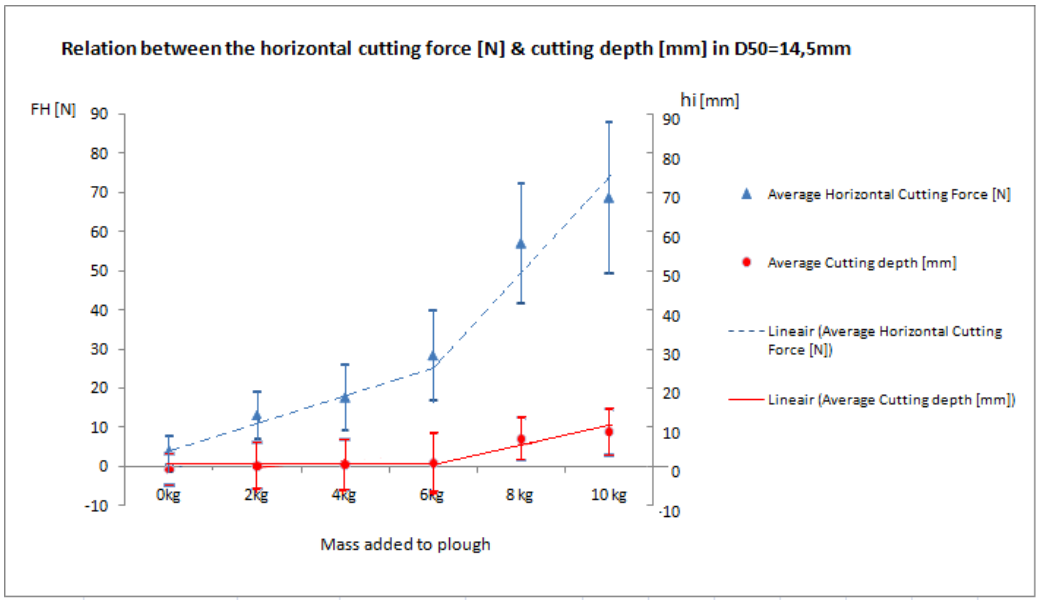

Figure 6.15 Average Horizontal cutting force[N] and penetration [mm] in D_{50}=14,5mm

Linear trendlines are assumed for the cutting force and the cutting depth. If this should be straight lines is a point of discussion. The trendline for the cutting depth starts at 6 kg, for lower masses the trendline is taken horizontal. The trendline for the horizontal cutting force starts under a low angle, this is the friction between the blade and the grains in case the plough is not penetrating. The angle of the trendline increases for higher plough masses when the blade starts cutting. The penetration could easily decrease if the second grain layer is reached. Another critical value for vertical penetration force might be necessary to penetrate the second grain layer.

D_{50}=5,2mm (Cobbles)

The effect of increasing the plough mass on the horizontal cutting force in rockfill D_{50} = 5,2 mm is presented in figure 6.16. These experiment results are also divided in a penetration time and a stationary cutting period. In the stationary cutting period the blade is fully saturated with soil and is overflowing with a constant volume per time unit. The forces are less fluctuating than the experiments in D_{50} = 14,5 mm. The plough was penetrating the sub layer until it reached an equilibrium cutting depth. From this depth the plough followed a moderate horizontal line through the sub layer. Because a continuous cutting process was observed, the forces measured in cutting cobbles are used later on to validate the analytical model.

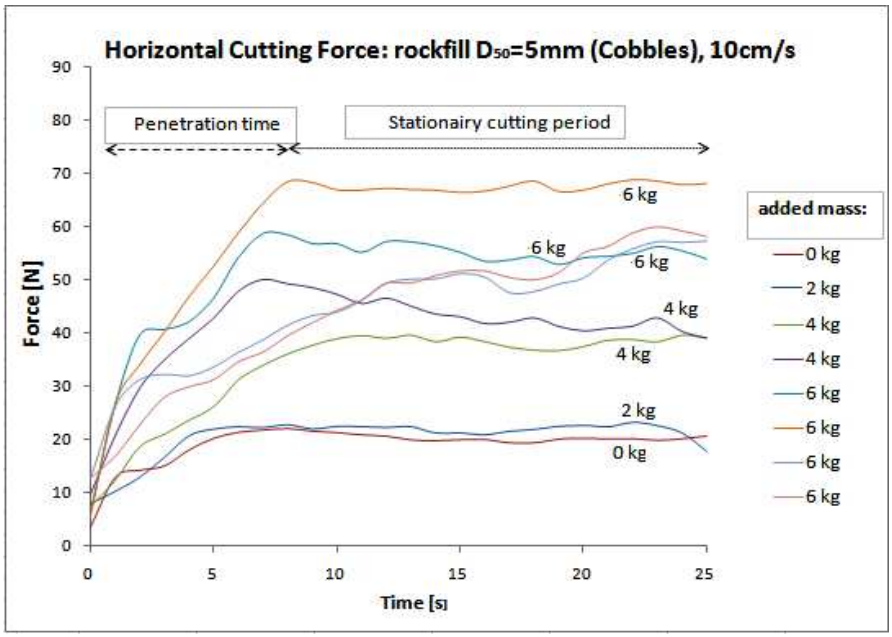

Figure 6.16 Cutting experiments in D_{50}=5,2 mm with a penetration time and a stationairy cutting period

In figure 6.17 the corresponding cutting depth is shown. From this figure follows that for a plough with 4 kg added weights the maximum cutting depth is reached. Note that the real maximum cutting depth could lay deeper, because the front suspension wire prevents a deeper penetration. The cutting depth of an “empty” plough is 15 cm. With the elevation of 0 kg added mass is shown that the plough is initially lifted, but will penetrate again till it reaches the equilibrium penetration depth.

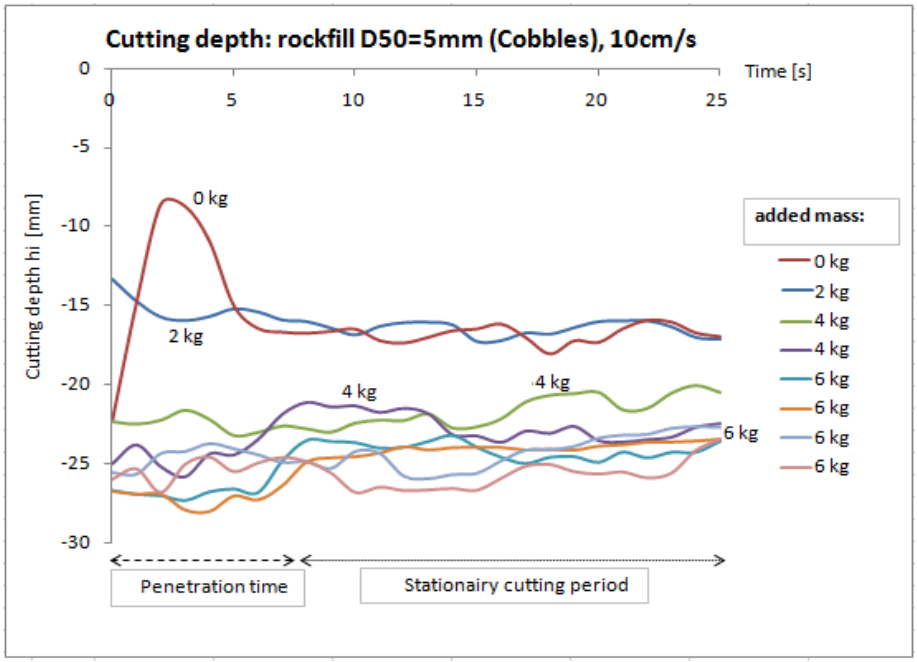

Figure 6.17 Cutting depth of the front blade corresponding to the cutting forces of figure 6.16

In figure 6.18 a summarization is given for the average cutting forces and the corresponding average cutting depth. The standard deviation for the cutting depth is very small. This proves that the blade is moving in a moderately horizontal line trough the sub layer. For cobbles the initial plough mass is high enough to penetrate the bed, so the bearing capacity of the material is already exceeded. Linear trendlines are drawn for both cutting depth and cutting force. The critical penetration mass lays between 0 and 2 kg (not added mass).

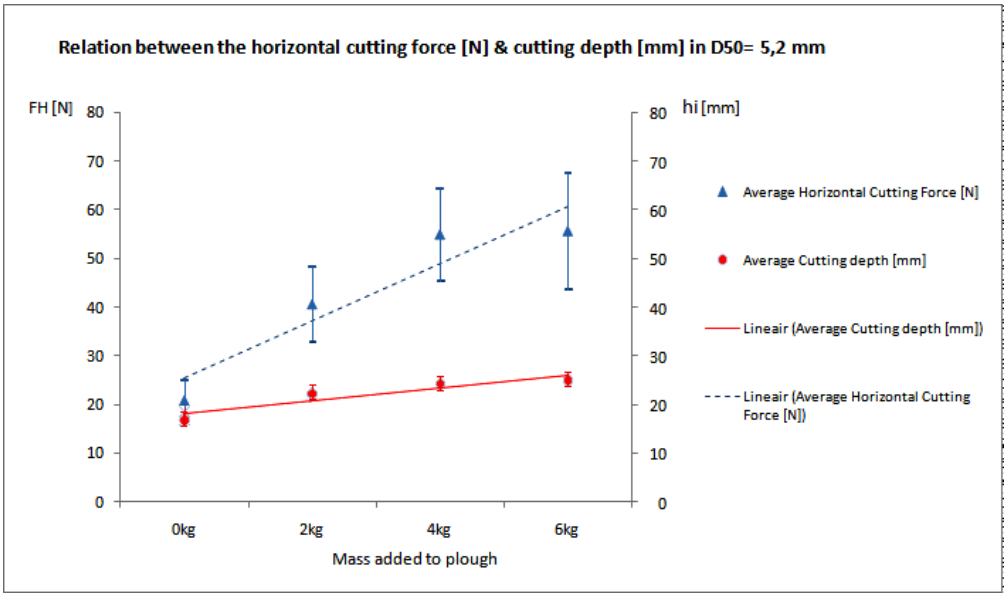

Figure 6.18 Average Horizontal cutting force[N] and penetration [mm] in D_{50}=5,2mm

6.2.4 Vertical blade penetration

In the graphs in the previous chapters the cutting depth was a plotted for the added plough mass. The cutting depth as a function of the vertical blade stress $\sigma_{v,blade}$ is given in figure 6.19. The vertical penetration stress $\sigma_{v,blade}$ is caused by the weight on the blade tip as calculated in chapter 5.4.2. So the penetration is not plotted as a function of the bearing resistance p_f. The blade penetrates is the vertical blade stress $\sigma_{v,blade}$ exceeds the bearing capacity of the soil. The bearing capacity of the soil increases if the stone diameter increases, so $\sigma_{v,blade}$ has to be higher. A repetition of the relation for $\sigma_{v,blade}$.

$$\sigma_{v,blade} = \frac{F_g}{A_{blade}} = \frac{F_g}{L_{blade} \cdot B_{blade}} = \frac{F_g}{0,6 \cdot 0,002}$$

Where F_g is the plough mass [N], B_{blade} the thickness of the blade [m] and L_{blade} the length of the blade.

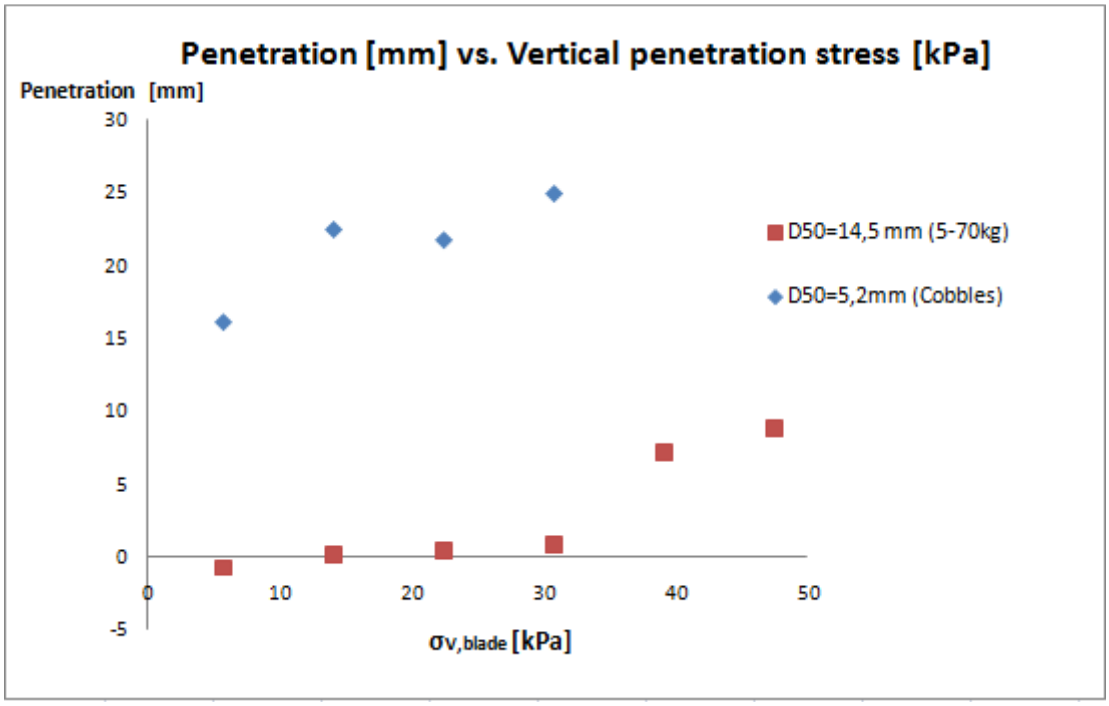

Figure 6.19 Penetration depth as a function of blade penetration stress for D_{50}=5,2mm and D_{50}=14,5mm

6.3 Results cutting & transporting both blades

6.3.1 Cutting and transporting both blades

When both cutting and dozer blade are resting on the sub layer the actual ploughing operation is imitated. Now both cutting and transporting forces are combined, but also the filling process of the plough becomes clear. In fine material the plough fills according to figure 6.20.

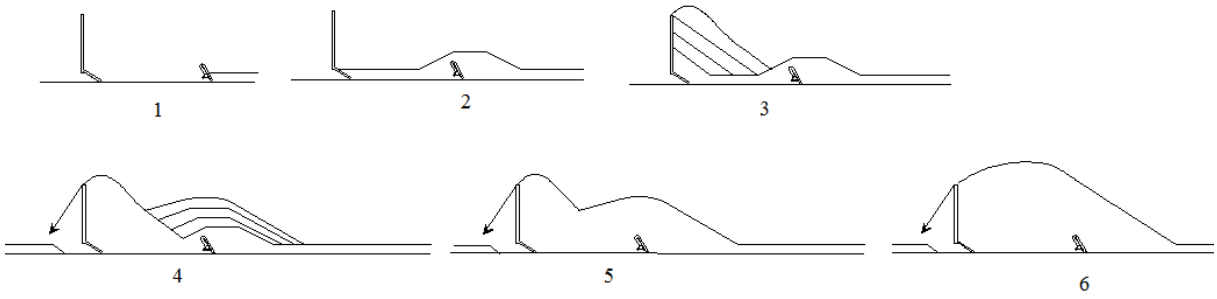

Figure 6.20 Six stages of plough filling

The filling process consists of different phases depending on the cutting depth and the amount of material supply. At the first phase the plough has a cutting depth hi which is causing the cutting blade to overflow. At this time there will accumulate a layer of material in front of the rear blade with layer thickness hi, see phase 2. The rear blade starts cutting too and a triangular soil wedge will build up in front of the dozer blade. The cutting blade also reaches a constant transport volume and overflow rate, phase 3. When the rear blade is entirely filled also here material will start to overflow. The shape of the wedge is not perfectly triangular as assumed in the models in chapter 4.2 but has a curved shape. The plough will continue to fill, but now by building up the area in front of the wedge, phase 4,5 and 6. This is contrary to the models in chapter 4.2 where the entire inflowing volume from the cutting blade is directly overflowing the rear blade. It seems that at some stage the soil volume in front of the rear blade for water saturated cutting starts acting as one piece. The surface friction of this wedge is too high for the grains to move upward , so this inflowing soil is accumulated at the toe of the soil wedge and a second soil volume starts building up in front of this wedge.

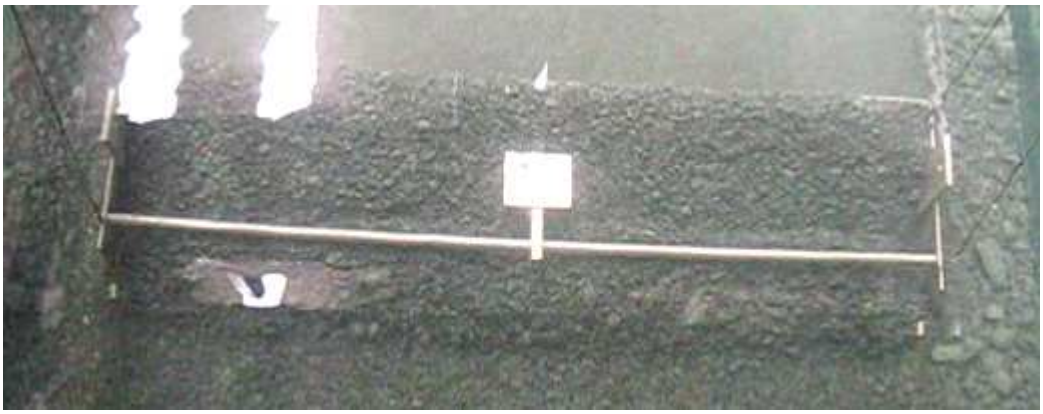

Figure 6.21 Picture of Stage 4 in scale experiment, formation of a second soil volume in front the wedge

6.3.2 Ploughing dunes of high spots

The experiments in ploughing dunes both blades are resting on the layer surface. The dune configuration is the same at each experiment like discussed in chapter 5.4.4. The bed lay out is after placement validated by a laser measurement at the centre of both blades. An example is given in figure 6.22 where the black line is the bed level across the flume at the centre of the left blade and the red line gives the bed level at the centre of the right blade. This is the initial bed lay after placement consisting of D_{50}= 14,5 mm grains (cobbles). The right picture is the bed level after 2 experiments with a plough with 0 kg added mass. The dunes are very well equalized as follows from the figures, only the ridges are still present. This is due to an underflow of the material caused a very small lift of the blade. The dunes are spread over the 80 cm transport distance. When the plough reaches the ridge all the material is deposited. To transport the entire volume the plough mass has to be higher. After one or two runs the dunes are to flat to equalize any further. The angle between the pulling wires and the dune slope has become so low that the blade is no longer pulled into the dune and therefore the transport volume solely depends on the penetration and thus the plough mass.

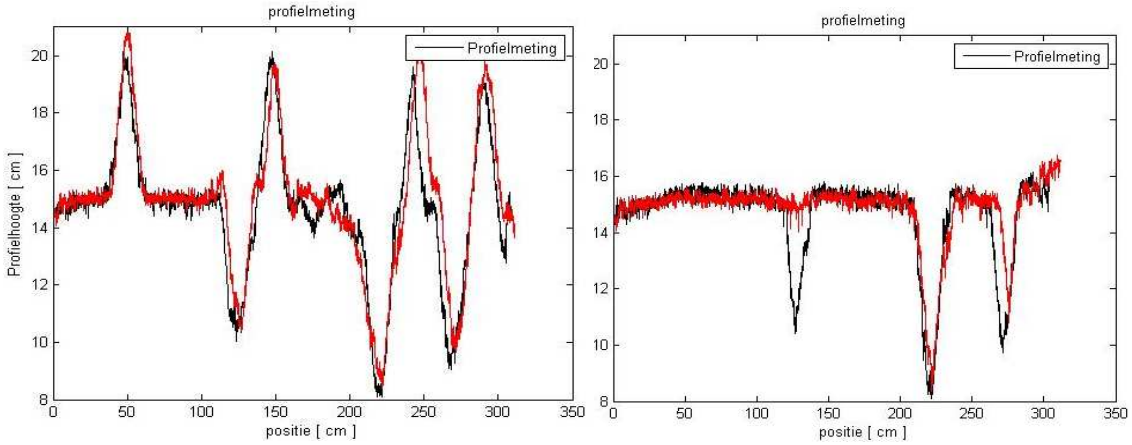

Figure 6.22 Initial dune configuration (left) and dunes after 2 experiments (right)

Dunes in D_{50}= 14,5 mm could only be moved over short very distances. The plough was removing the high spots by spreading the stones just behind the high spot creating and elongated dune. Another experiment at this elongated dune resulted in negligible transport and is therefore useless. The angle between horizontal pulling force and the dune surface becomes too small to generate a penetration force. The behaviour of the plough shows a good comparison if the experiments from the blades separately are combined.

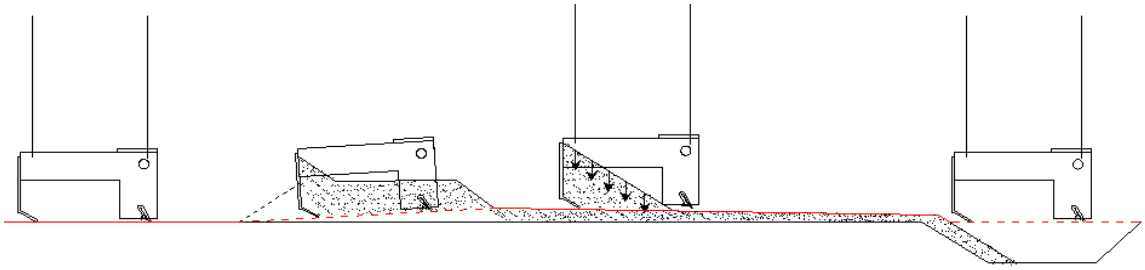

Figure 6.23 Visualization equalizing dunes in Cobbles 0kg added masss, explanation figure 6.22.

6.4 Feedback Scale model to Analytical model

In order to validate the analytical models for cutting coarse material derived in chapter 4.2, the horizontal cutting force is compared with cutting and transporting forces measured in the scale experiments. Only the experiment data for cutting and transporting rockfill D_{50} = 5,2 mm (Cobbles) is used. The experiment showed that, in comparison with the other materials, cobbles are behaving the most like a continuum. The following steps are followed to calculate the cutting force with the analytical model:

Step 1 A choice has to be made if the problem concerns a model or with inflow (model 2) of without inflow (model 1), to determine the gravitational force on the shear plane.
Step 2 The horizontal cutting forces is calculated by Eq. (4.12) without a boundary wedge or by Eq. (4.21) with a boundary wedge.
Step 3 The principle of minimum cutting energy is used to find the shear angle β and the corresponding minimum cutting force.
Step 4 The internal friction angle is varied to find the horizontal cutting force matching the forces from the experiments .

The horizontal cutting forces are based on cutting dry material.

Input parameters: Blade dimension and soil properties:
The blade dimensions of the cutting blade: H_b = 20 mm, B = 600 mm, α = 75°.
The dimensions of the rear blade: H_b = 70 mm, B = 600 mm, α = 83°.
The soil properties: density of the solids ρ_s = 2780 kg/m^3 , porosity n = 0.4, steel-grains friction angle δ = 20°, angle of repose η = 30°.
The cutting depth is equal to the cutting depth measured in the experiments for a given horizontal cutting force.

6.4.1 Validation Model 1: Transport model

In order to validate analytical Model 1 (inflow is zero), the horizontal cutting forces are compared with the transporting experiments in Cobbles. The horizontal cutting forces measured in the experiments are presented in table 6.1. The equilibrium cutting volume was nearly reached between 15-20 seconds. Tests with an added mass of 4 and 6 kg a nice triangular wedge was formed in front of the blade and the outflow was nearly zero.

Table 6.1 The horizontal cutting forces in Cobbles measured in the scale experiments

	FORCE [N]		Plough elevation [mm]	
Added mass	**Max**	**Mean 15 < t < 20**	**Max**	**End 15 < t < 20**
0 kg	80.44	20.83	5.14	1.26
2 kg	91.48	38.99	2.35	0.24
4 kg	93.88	53.69	1.62	-0.10
6 kg	107.76	52.71	2.06	-0.72
6 kg	101.04	61.53	1.25	-0.61

A nearly stationary wedge was formed in front of the blade for an added mass of 4- 6 kg. This is also drawn from the graph in figure 6.7 where the horizontal asymptote for F_H lays around 50 N for an added mass of 4-6kg. For this horizontal asymptote F_H the shape of the triangular soil volume is stationary, see figure 6.24.

Figure 6.24 Triangular soil volume in front of rear blade for a stationary cutting situation with hi = 0

The calculation with Model 1 is made for different values of ϕ to find the corresponding cutting force of 50 N that is measured in the experiment. The result of the calculations is presented in figure 6.25. For the blade angle of the model plough α = 83° an internal friction angle of 45° is found. This is quite high for rockfill but not overwhelming. If the blade angle is increased to α = 90° the cutting force of 50 N corresponds with an internal friction angle of 40°. Based on the principle of minimum cutting energy the shear angle β is equal to zero for all values of ϕ.

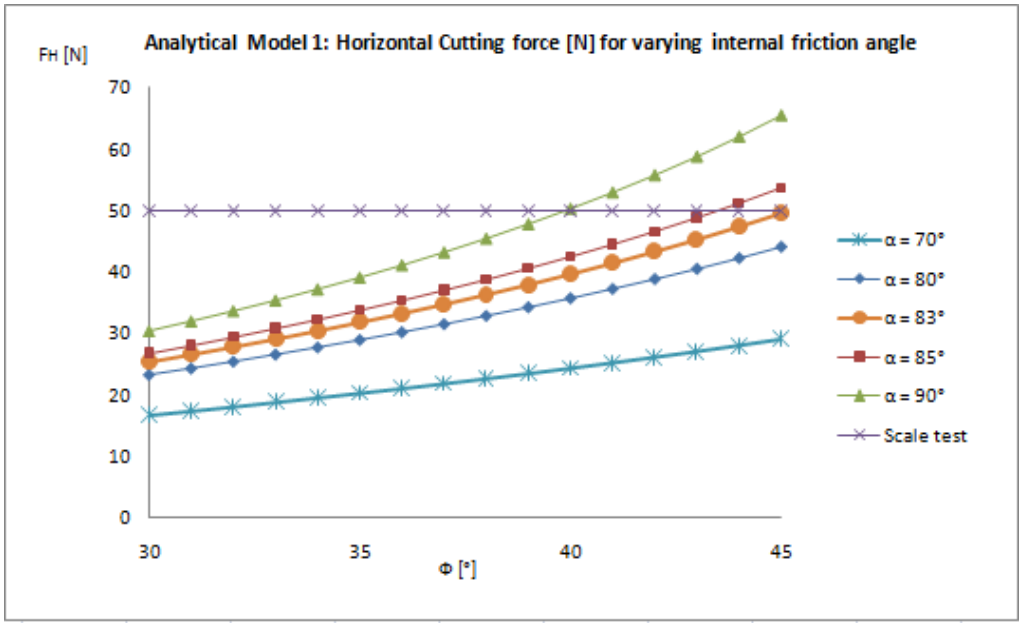

Figure 6.25 Result of calculations for transporting cobbles with Model 1 for different blade angles

The cutting force for α = 83° as a function of β is show in figure 6.26. Based on the principle of minimum cutting energy the shear plane angle is always zero for transporting material with Q = 0. This is strange compared to the scale model where particles are pushed to the surface. With a horizontal shear plane the wedge should move as a solid wedge across the surface. In coarse grains this is not possible because the grains are moving by rolling and dilating. If the surface slope becomes too steep the particles roll down. This will result in a cutting layer that is never exactly equal to zero in coarse material. In case of a boundary wedge the forces are equal to the forces without a boundary wedge because of the horizontal shear line.

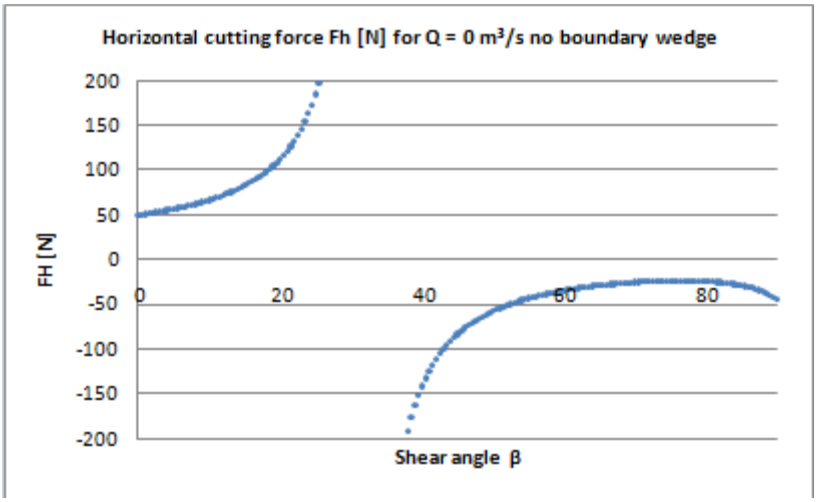

Figure 6.26 Cutting force as a fuction of β for α = 83°

6.4.2 Validation Analytical Cutting & Transporting model

The model for cutting & transporting coarse material will be validated by the cutting & transporting experiments performed in rockfill with D_{50} = 5,2 mm, see figure 6.27. The dimensions for blade angle α, the angle of repose η and the soil-steel friction angle δ are presented in figure 6.28: α = 75°, η = 30° and δ=20°. The shear angle β is based on the minimum cutting energy for each cutting depth. The internal friction angle ϕ is varied to find the cutting force that corresponds with the cutting forces measured in the experiments. Note that β is also changing for each new value of ϕ, so this is a iterative process. The calculation data for every value of ϕ is given in Appendix IV.2. The values for the cutting forces measured in the physical scale experiments are presented in table 6.2.

Figure 6.27 Cutting & Transporting experiments in D_{50} = 5,2 mm (Cobbles) for validation Model 2

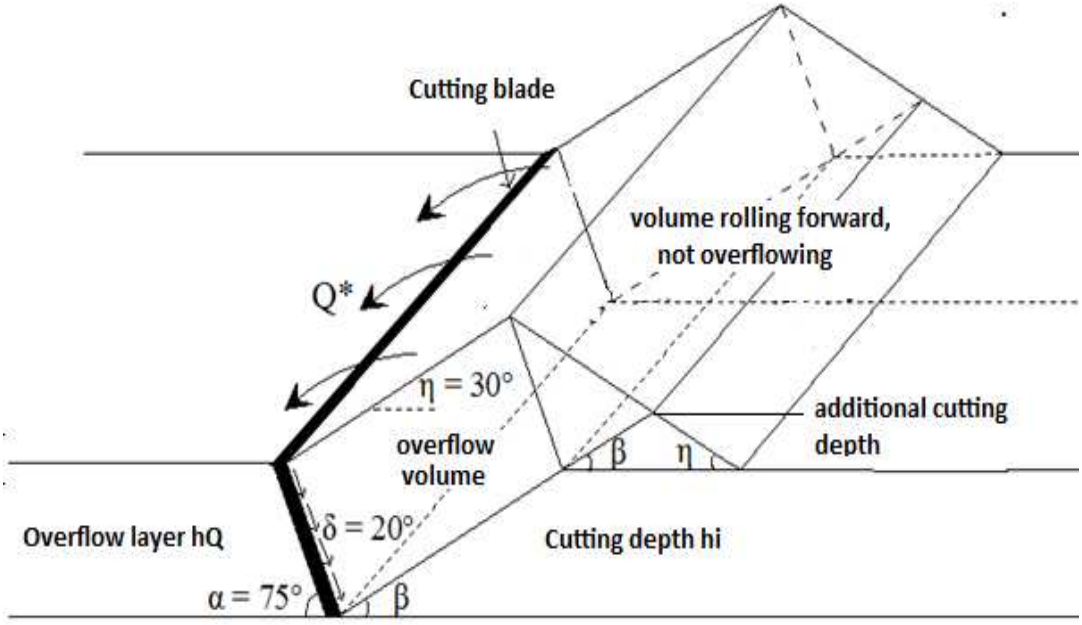

Figure 6.28 Visualisation Model 2 without boundary wedge

Table 6.2 The horizontal cutting force and corresponding values for ϕ and β without boundary wedge

Scale Model			Analytical Model		
Added Mass	Cutting depth [mm]	Horizontal Cutting Force [N]	Horizontal Cutting Force [N]	value β for min cutting energy	Corresponding ϕ
0 kg	16.50	21.97	21.80	30	31
0 kg	17.03	20.01	20.49	31	29
2 kg	21.68	38.10	36.42	29	37
2 kg	22.72	43.14	42.37	28	39
4 kg	24.25	54.84	53.80	26.5	42
6 kg	24.05	66.88	64.92	25	45
6 kg	24.74	49.12	48.46	28	40
6 kg	26.04	50.64	47.79	29	39

From this table follows that in order to match the analytical model to the scale model the average internal friction angle ϕ is 37°, based on the principle of minimum cutting energy. The shear plane angle β is depending on the internal friction angle but gives a value between 25° and 30°. These values are very common for sand and rockfill, so the models seems to agree. In reality the shape of the soil volume in front of the blade is somewhat curved instead of triangular shapes. This could be fine tuned in following research.

It is also possible a boundary wedge is formed in front of the blade due to the friction force between blade and grains. Table 6.3 gives a comparison between the scale experiment values and the analytical values with boundary wedge.

Table 6.3 The horizontal cutting force and corresponding values for ϕ and β with boundary wedge

Scale Model			Analytical Model		
Added Mass	Cutting depth [mm]	Horizontal Cutting Force [N]	Horizontal Cutting Force [N]	value β for min cutting energy	Corresponding ϕ
0 kg	16.50	21.97	21.6	28	33
0 kg	17.03	20.01	19.9	30	31
2 kg	21.68	38.10	37,6	25	37
2 kg	22.72	43.14	42,2	24	38
4 kg	24.25	54.84	52,4	23	40
6 kg	24.05	66.88	67,0	20	43
6 kg	24.74	49.12	49,4	24	39
6 kg	26.04	50.64	48,1	25	38

In the calculations with a boundary wedge can be clearly seen that the cutting force increases more rapidly with an increasing value of ϕ. This follows from the friction angle λ between the boundary wedge and the upward moving Rankine zone. This value was assumed to be equal to the internal friction angle. With an increasing internal friction particles have more trouble moving upwards to the boundary wedge, causing the cutting force to increase. Also with a boundary wedge shows realistic values, average internal friction angle ϕ of 37°, and a shear plane angle β between 20° and 30°.

6.4.3 Validation penetration model

Validation of the penetration model in Chapter 4.3 will be done for D_{50} = 14,5 mm grains. For D_{50} = 5,2 mm grains the bearing capacity is already reaches for the initial plough mass (without added weight) and can therefore not be determined. The bearing capacity of D_{50} = 14,5 mm grains can be drawn from the experiment results. In figure 6.29 the penetration depth is given for an increasing vertical blade stress σ_v. From the graph follows that the blade starts penetrating in D_{50} = 14,5 mm grains if the vertical penetration stress is between 30 and 40 kPa.

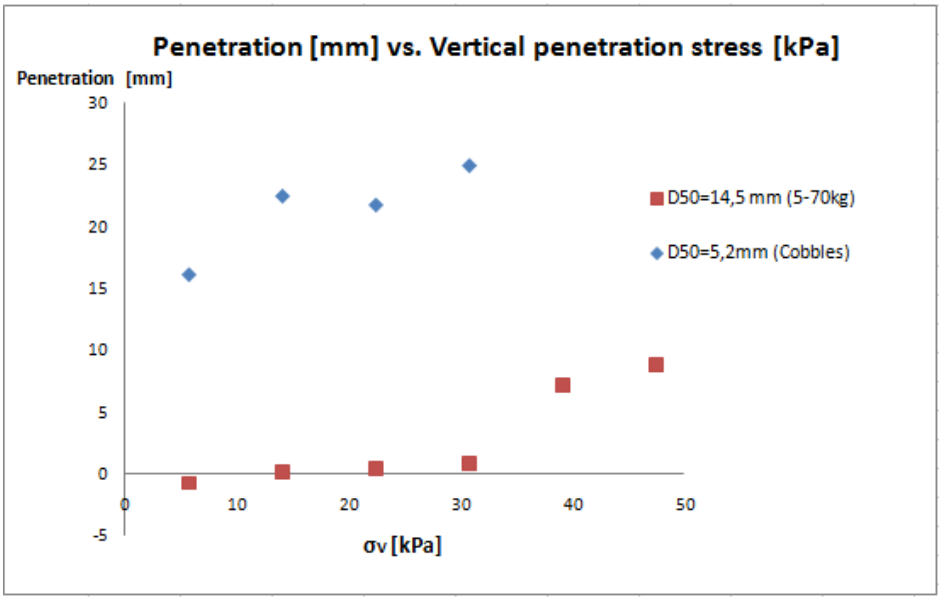

Figure 6.29 The vertical penetration depth of the cutting blade depending on the penetration stress

This does not agree with the value found in the value found with the modified Terzaghi penetration model given in chapter 4.2. Both approximations give a bearing capacity lower than this value and these values are not even for an inclined load, which gives even smaller bearing capacity. The following values are found from the calculations in Appendix IV.1:

Table 6.4 The analytical calculated bearing capacity for rockfill with D_{50} = 14,5 mm grains

Φ [°]	pf [kPa] Approximation 1	pf [kPa] Approximation 2
40	12.74	20.95

The modified penetration model still seem to give an underestimation of the bearing capacity of rockfill consisting of larger particles.

For the transporting tests the blade penetration was also important. Due to increase of stress in front of the plough a vertical force is created. The force is causing a vertical lift of the plough and an escape of material underneath the rear blade, figure 6.30. The weight of the plough and the friction force between plough and grains in front of the plough is counteracting this uplift force.

At a certain height h_{lift} an equilibrium is reached and the plough continues in a horizontal movement above the sub layer where $G_r + F_g \geq F_\delta$. When the volume in front of the plough decreases consequently the vertical upward force decreases $F_\delta = F_H * \tan(\delta)$, causing the plough to lower again. By increasing the plough mass, the force F_g increases. The equilibrium of vertical forces is than reached at a lower height above the sub layer.

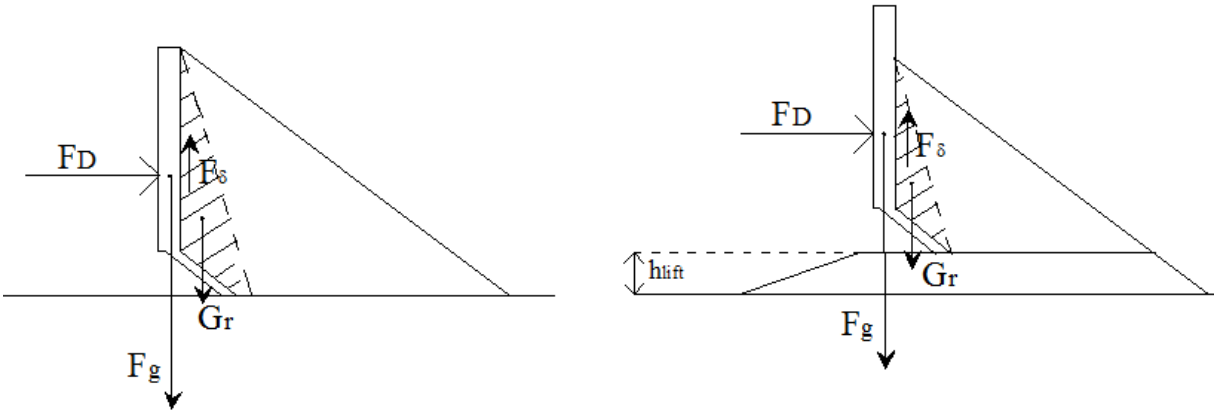

Figure 6.30 Lift of plough during transporting experiment

Ones the plough is lifted the penetration force becomes important. With an increasing stone size the penetration become more difficult because of the load spreading effect of the stones beneath the blade. Besides that, there is still an upward force F_δ from the upward moving grains in front of the blade, so not the entire plough mass is contributing to the penetration stress.

To prevent the plough from lifting a downward force has to be created. This force can be generated by increasing the weight of the plough, but also the weight of the granular body in front of the blade can be used. The angle and length of the plough blade can be adjusted to use the downward pressure of the soil body.

6.5 Conclusions Scale Model/ feedback to analytical models

Visual Goals

1 What is the movement of the individual grains and the entire grain structure in front of the dozer and cutting blade?
2 What is the visual effect of varying the plough mass on:
    a. The dynamics of the plough, underflow and overflow.
    b. The blade penetration in the sub layer.

1 Stone movement

The visual observations from the physical scale model showed a good agreement with the transport model made in chapter 4.2 for the movement of grains in front of the rear blade. The stones make a circular motion in front of both blades: the stones are rolling down the slope, are being reintegrated in the soil volume and appear at the surface. In the scale experiments this was made visible by adding some red stones on top of the soil volume. It was impossible to see a clear shear zone inside the wedge. This will be examined during the computer model with EDEM.

Only a little amount of overflow was observed, most of the material was lost by underflow. This is caused by lifting of the plough due to the upward movement of the stone mass in front of the blade. This upward movement results in a shear force between the grains and the steel blade. The blade is also lifted by stones at the blade tip. Ones the plough is lifted, it is difficult for the plough to lower again because penetration resistance of the bed becomes relevant, this is more extensively described in point 2B.

Filling the plough consists of different phases which are described in the transport model in chapter 4.2. The soil will start to build up in front of the rear blade due to an overflow of the cutting blade. The soil volume will continue to grow due an continuous inflow of material. When the triangular soil volume reaches the top of the rear blade, the rear blade will also start to overflow if the inflow from the cutting blade is larger than zero.

With water in the flume, the cobble volume started to act as a solid wedge with a horizontal shear line and a decrease in particle movement was observed. The inflow of soil from the cutting blade is not integrated in the soil volume in time and the grains tend to move upward across the surface of the wedge. Because the surface friction of this wedge is too high for the grains to move upward, the inflowing soil is accumulated at the toe of the soil wedge. A second soil volume starts building up causing the entire “buffer zone” to be filled.

2A. The dynamics of the plough, underflow and overflow.

The experiments have been performed with a straight blade. With this high and hardly backward shaped blade configuration the overflow rate is very small at all plough masses and nearly all the material loss is by underflow. With an increasing rockfill size the plough is bouncing across the surface and the movement of the plough becomes more extreme, sometimes with elevations around 15 mm. In stones with D_{50}= 44,5mm (prototype: 300-1200kg) the plough is tilting back and forward, stick and slip behaviour due to interlocking of the particles is observed. No material is transported

and the plough bounces across the surface. In stones with D_{50}= 14,5 mm (5-70kg prototype) the plough cuts into the subsoil and breaks out randomly. A significant mass of 6-8 kg had to be added to make a moderately straight line through the rockfill, this is a penetration stress of 30 – 40 kPa. Stones with smaller diameters can be equalized with the initial plough mass, the plough is only lifted under a small angle through the sub layer.

2B. Penetration

From the cutting experiment follows that the penetration of the blade is crucial. More force must be exerted to the blade tip to penetrate the blade tip in the sub layer when the rock size increases. This force must be created by the plough mass, the drag wires only create a horizontal cutting force. Also when dunes are ploughed a clear view was given of the importance of the plough mass. When dunes are lowered, the angle between dune slope and the drag wires angle becomes too small and the penetration force becomes dominant. For stones with D_{50}= 14,5 mm (5-70kg prototype) the plough mass seems insufficient to penetrate into the sub layer. Dunes in D_{50}= 14,5 mm are only spread over short distances with the initial plough mass, no material is actually transported. It is therefore useless to keep equalizing long stretched dunes with the present plough mass, so one or two runs is sufficient in D_{50}= 14,5 mm. For cobbles was shown that the present plough mass is enough to make a moderate straight line through the sub layer and dunes, but also a lift of the plough was observed. This plough elevation causes emptying of a part the soil volume before it reaches a trench.

Quantitative goals

3 Do the following analytical models (in different sizes of rockfill) agree with the scale results :
   a. The modified Terzaghi penetration model derived in chapter 4.3.
   b. Transporting Model 1 for coarse grains without a soil inflow from the cutting blade Q = 0 derived in Chapter 4.2
   c. Cutting & Transporting Model 2 for coarse grains with a soil inflow from the cutting blade Q > 0 derived in Chapter 4.2.

3A. The modified Terzaghi penetration model derived in chapter 4.3.

With a physical scale model the cutting depth of the blade is measured at different plough masses with a single laser beam. For every plough mass the cutting depth is plotted with the vertical blade stress σ_v to validate the analytical “modified Terzaghi bearing equations” in chapter 4.2. These equations determine at what penetration stress the bearing capacity of the soil is reached and the blade starts penetrating. Two approximations were made to predict the bearing resistance for rockfill consisting of large stones. In approximation 1 the blade penetration surface was replaced by the surface of the stones beneath the blade. The analytical calculations are shown in Appendix IV.1. In the second approximation the blade actually becomes the first stone, so the stone is penetrating in the 2nd soil layer. The first layer acts as an additional load on surface around the blade, because this first layer has to be pushed upward as well. From the test data is obtained that the critical penetration stress σ_v is between 30-40 kPa in D_{50}=14,5 mm rockfill (prototype 5-70 kg). This does not

agree with the values for the bearing capacity p_f of 13-21 kPa following from the analytical model, which still gives an underestimation of the bearing capacity for large stones. For D_{50}=5,2 mm the blade already penetrated with a plough mass with 0kg added weights. The bearing capacity could therefore not be determined, because the bearing capacity pf of the soil was already exceeded. To determine the real bearing capacity of different types of rockfill some additional experiment should be performed with a straight blade penetrating in different types of rockfill.

3B. Transporting Model 1 for coarse grains without a soil inflow from the cutting blade Q = 0 derived in Chapter 4.2

Model 1 is a transporting model for cutting coarse material with limited surface slopes. The inflow of material is zero and the grains are solely moving inside the soil body as described in conclusion 1. The friction angles of the material used for the scale model are unknown. In order to give an indication of the validness of the model the internal friction angle ϕ is varied and the horizontal cutting force F_H and shear angle β are calculated based on the principle of minimum cutting energy.

Comparing the model with the data obtained from the physical scale experiments gives an internal friction angle ϕ of the material of 45° and a shear angle β = 0. This indicates a horizontal shear line and a quite high value for the internal friction angle. Based on the principle of minimum cutting energy the shear plane angle is always zero for transporting material with Q = 0. This is strange compared to the scale model where particles are pushed to the surface. With a horizontal shear plane the wedge should move as a solid wedge across the surface. In coarse grains this is not possible because the grains are moving by rolling and dilating. If the surface slope becomes too steep the particles roll down. This will result in a cutting layer that is never exact equal to zero in coarse material. In case of a boundary wedge the forces are equal to the forces without a boundary wedge because of the horizontal shear line. Model 1 for transporting soil can be obtained from Model 2 by setting the cutting depth to zero.

3C. Cutting & Transporting Model 2 for coarse grains with a soil inflow from the cutting blade Q > 0 derived in Chapter 4.2.

Model 2 is a model for cutting & transporting coarse material with limited surface slopes. The inflow of material is not zero. The cutting layer of the bed is directly cut or is created by an overflow of the front blade.

From the calculations follows that in order to match the analytical model to the scale model the average internal friction angle ϕ is 37°, based on the principle of minimum cutting energy. The shear angle is depending on the internal friction angle but gives a value between 25° and 30°. These values are very common for sand and rockfill, so the models seems to give realistic values. The shape of the soil volume can be fine tuned and is now consisting of triangular shapes. Also the friction force between the blade surface and the sub layer can be taken into account as an extra force. The model could be validated further by an experiment in which the internal friction angle of the material is known and the blade angle can be determined very accurate.

III Discrete element computer model

Chapter 7 Introduction EDEM Research

7.1 Introduction

The observations done in the physical scale experiment and the analytical models are used to attempt to create a computer model to compute a straight blade moving through a granular layer. The discrete element computer model (EDEM) is carried out after the analytical models of Chapter 4 are made, so the model is not used to compose these analytical models. The EDEM computer model is validated by observations and data obtained from the physical scale experiments and the analytical models of chapter 4. In the EDEM research a uniform particle distribution is used consisting of grain particles with a D_{50}= 14,5mm. To create a smaller particle the simulation time increased to unworkable heights. Therefore to simulate these particles the blade height was increased.

EDEM is a discrete element simulation model. The computer model consists of a collection of spherical particles created in an area (for instance a square box). Each of the particles has its own initial speed and interaction with other particles (exchange of momentum). The DEM modelling is based on the behaviour between grains. The behaviour of the granular structure depends on the individual grains and their interaction. The contact between grains in EDEM are described by the Herz Mindlin contact model. The equations describing this contact model are presented in Appendix VI.

The contact mechanics of two grains according to the Herz Mindlin contact model can be seen as a "spring-dashpot" configuration consisting of springs and dampers [11], see figure 7.1. The normal and tangential force are calculated by the overlap between particles when particles collide.

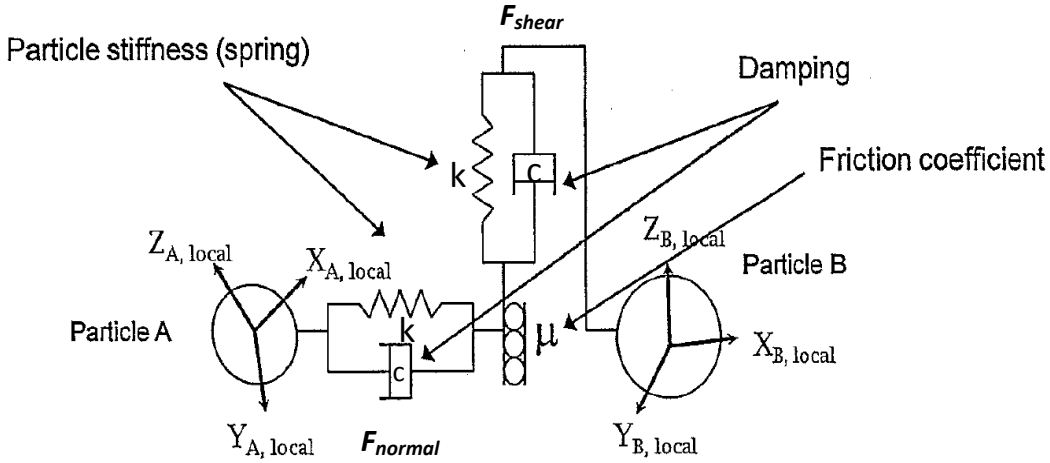

Figure 7.1 Herz Mindlin Contact model

The shape, internal friction, damping, density and other input parameters can be varied and will be applied to all the particles. Note that the properties are not applied to a soil layer but to individual particles. To model the plough processes with EDEM a good understanding in the limitations of using EDEM is required. Because the knowledge of EDEM is still in a developing state the computer model is not used to validate the scale and analytical models, but vice versa the computer model is validated by the previous chapters. Still useful insight and understanding in the grain movement inside the wedge can be obtained, but has to be handled with care.

7.2 Goal

EDEM will be used to calculate the forces on the blade when cutting threw a granular rock layer. The interest will be on the particle movement and the appearance of a shear zone inside the wedge. A comparison is made between the horizontal blade force in DEM and the horizontal force from the analytical calculations and the physical model. The points of interest are shown in figure 7.2.

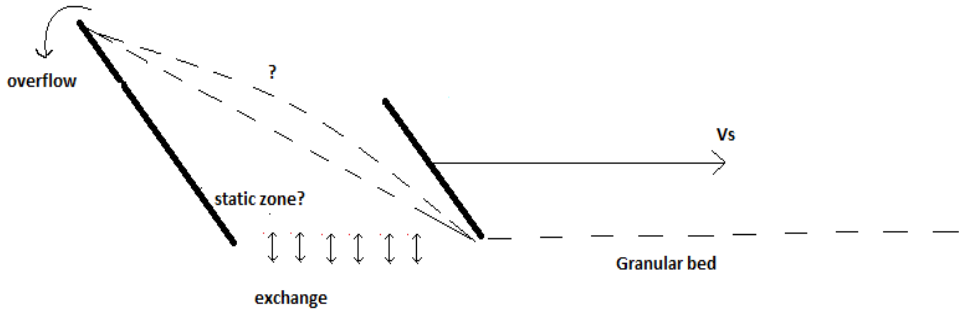

Figure 7.2 Fields of interest during the EDEM research

The desired goals:

- Creating a realistic rockfill material in EDEM, with particles behaving like actual rock particles
- Visualizing movement of inflowing layer from cutting blade.
- Visualizing the occurrence of a shear plane in front of the blades.
- Comparing the grain movement with the models derived in chapter 4.2.
- Comparing the horizontal cutting force from the scale model, analytical model and EDEM.

7.3 Limitations computer model EDEM

To simulate a plough cutting trough a rock bed EDEM has some limitation which will be discussed below.

7.3.1 Horizontal movement

In the computer model the blade is given a certain horizontal velocity. This is the speed in X-direction at a given cutting depth h_i (see figure 7.3). Unlike the reality, the blade in EDEM cannot move in vertical direction and will follow a straight line, even when the vertical forces increase. This can be compared with an infinite rigid plough suspension. Consequently a simulation of dynamic behaviour of the plough is not possible with EDEM, and therefore, the simulation should be interpreted on a different way.

To solve this problem the cutting depth h_i can be varied. The vertical and horizontal force on the blade is solved by EDEM for every time step t_i. When the vertical upward force on the blade is larger than the mass of the plough the plough is lifted in reality. The same problem occurs in case of and the upward force exceeds the vertical downward force when transporting material. Normally the plough will deposit material when the load in front of the dozer blade is too large. The plough will be lifted and material will escape underneath the plough.

Because the model is not capable of doing so, the h_i can be manually decreased and the simulation continued. This can be repeated until an equilibrium cutting depth is reached. The equilibrium depth is the depth where the downward force of the plough mass is equal of larger than to the uplift force.

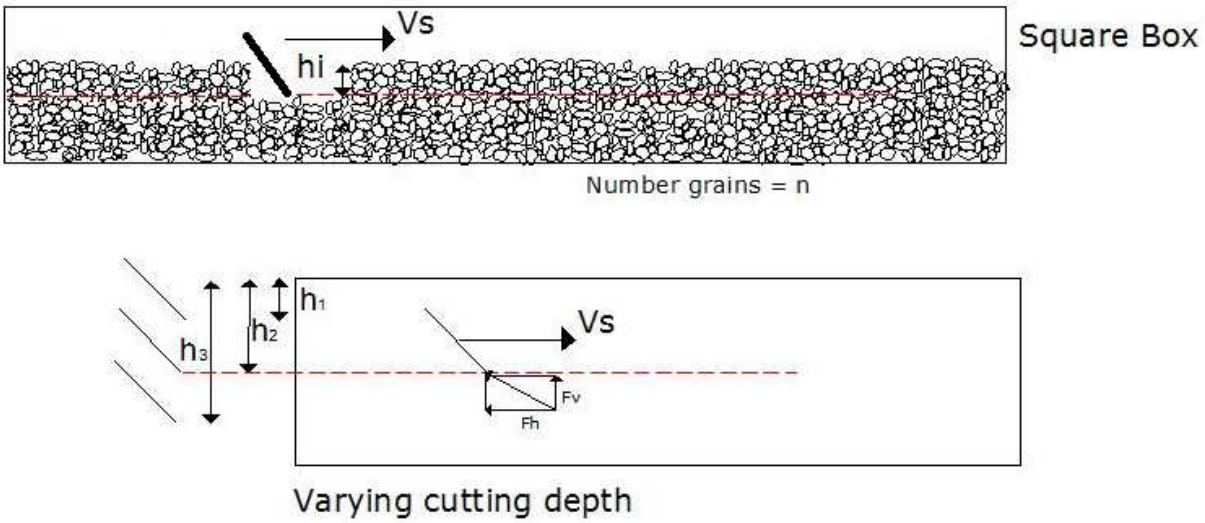

Figure 7.3 Varying plough depth configurations in EDEM

7.3.2 Particle shape

Particle dimensions

The shape of the grains must be approached, because EDEM is only simulating spherical particles. From previous research followed that a better behaviour of the soil was realized by changing the shape of the particles, especially to create a clear shear plane (M. Abdeli, 2009) [11]. With spherical particles the grain structure fails by rolling of the particles. To create a shear plane the grain structure must fail by shearing of the particles in the shear zone, so spherical particles are not presenting a realistic soil behaviour. The shape can be changed by connecting several spheres as drawn in figure 7.4. More spheres might create a better comparison with the real soil behavior, the disadvantages is more contact points are creating a longer simulation time.

From recent research in EDEM the effect of increasing the number of spheres within one particle was examined (X. Chen, 2011).

- 1 sphere will cause the grain structure to act as a fluid.
- 2 spheres create a shear plane, but particles will start to aim to one direction causing the phenomena of anisotropy to appear.
- 3 spheres show the same behaviour as two spheres
- 4 spheres create a pyramid shaped particle. The grains will form crystal shaped structures with an unrealistic behaviour.
- 5 spheres gives a realistic 3D distribution and minimum simulation time.

A particle is created based on the research of Chen, see figure 7.4. The dimensions of the particles used in the EDEM research is presented in Appendix VII.

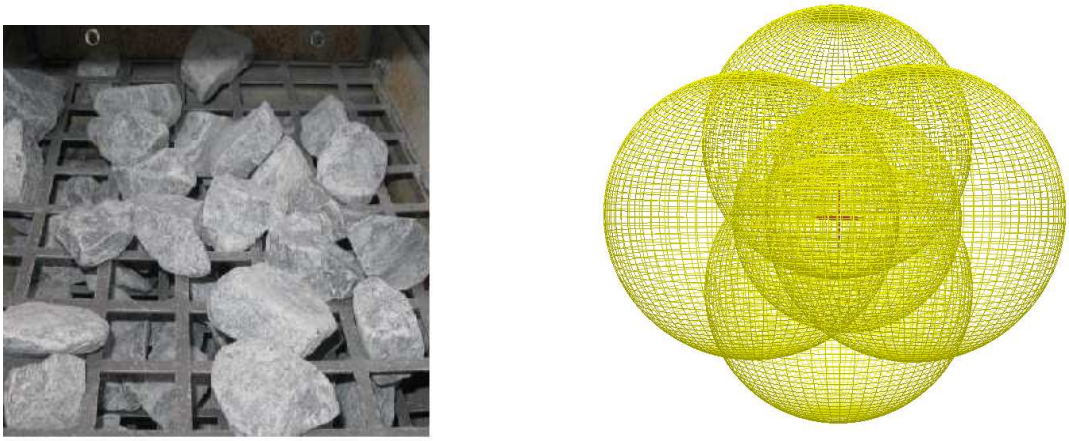

Figure 7.4 Particle shape approach in EDEM

7.4 Micro parameters and macro behaviour

As mentioned earlier the properties of the soil will not be applied to the soil layer as a whole, but to the individual grains. This means that properties that are normally applied to a soil package, like the internal friction angle, must be applied to an individual grain. So before the real simulation can be performed, the grain properties must be well assigned and compared with the actual physical behaviour of a soil layer. The micro behaviour of the individual grains must result in a realistic macro behaviour to agree with the prototype. The EDEM model can be considered as a black box model and the results depend on the input parameters. For the formulas used by the model to describe the relation between this particles is referred to the report of (M.Abdeli,2009) [11] and Appendix VI.

The input parameters are:

- Particle dimensions
- Particle density ρ_{EDEM}
- Static Friction coefficient μ_s
- Rolling friction coefficient μ_r
- Shear modulus G_{EDEM}

From previous research performed (M. Abdeli, 2009) was shown that the most important micro parameters are the static and rolling friction coefficients and the particle density. The other parameters have a little influence on the macro behaviour of the soil. The shear modulus determines the deformation of the particle due to shear stress and is negligible. With particles consisting of multiple spheres the rolling friction can be set to zero. In this case of multiple spheres the rolling friction is determined by the shape of the particle. In the report of Abdeli was faulty stated that the rolling friction coefficient is no longer influencing the behaviour of the particles.

7.4.1 Validation particle macro behaviour macro by initial tests

The EDEM software is a black box model. The input parameters strongly determine the output. To validate the macro behaviour of the material some initial tests are performed before a valid run of the real plough model can be made. The micro parameters have to be consistent with the macro parameters and behaviour of the prototype. Three tests are performed to validate the material behaviour:

Test 1 The bulk density check, determining porosity.

Test 2 The angle of natural repose test.

Test 3 Passive soil failure (sheet pile approach), occurrence of shear plane.

In this tests are performed with particles consisting of 5 spheres (Appendix VII), a rolling friction coefficient $\mu_r = 0$, a static friction or Coulomb friction coefficient $\mu_s = \tan(30) = 0{,}57$ and a particle density of 2650kg/m^3.

TEST 1 Bulk density check and determining porosity

A loose packing is created above a square box by dropping the stones from a height into the box. If all the grains are settled inside the box, the grains occupy a certain volume. The number of generated particles is given by EDEM and the volume can be measured. From this data the bulk density can be determined.

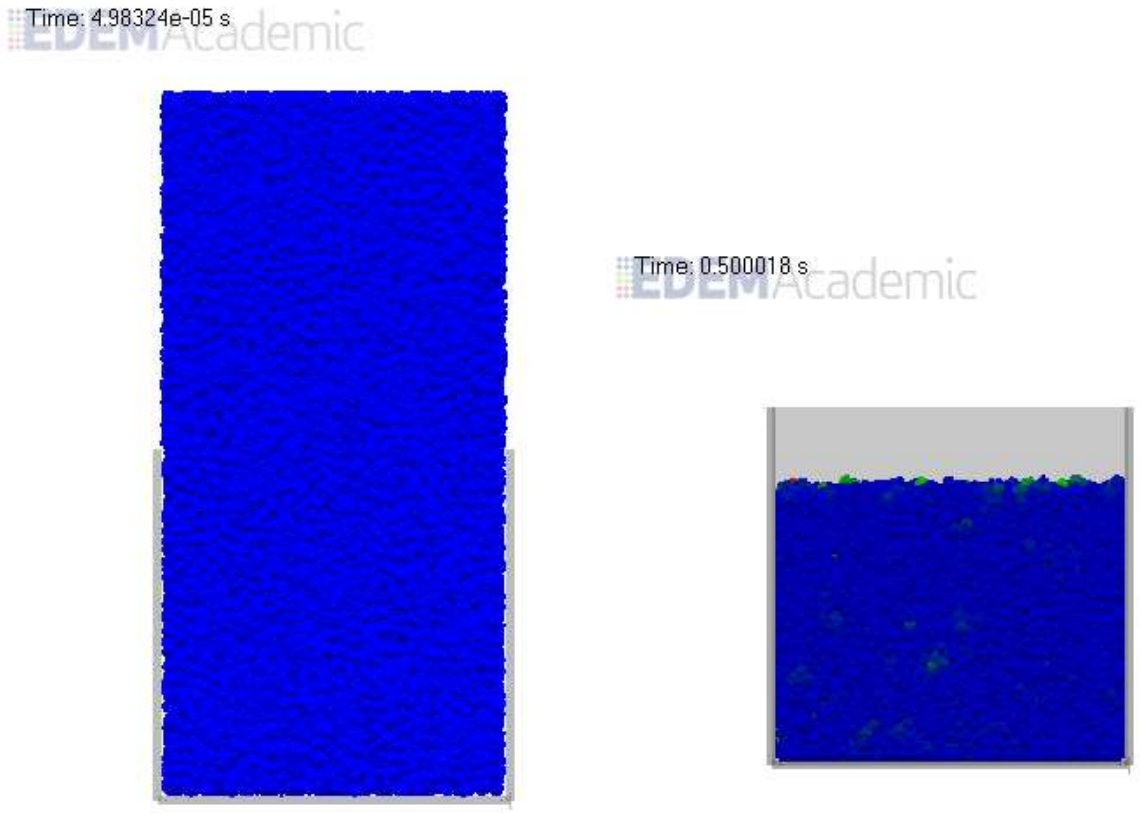

Figure 7.5 Left: Particle generation above a square box, Right: Settled grains with bulk density γ

The relation for the bulk density reads:

$$\gamma = (1 - \frac{V_{particles}}{V_{box}}) \cdot \rho_{particle} \tag{7.1}$$

Bottom plate	$l \cdot b = 390 \cdot 390$
Walls	$b \cdot h = 390 \cdot 390$
Inner volume box	$l \cdot b \cdot h = 390 \cdot 390 \cdot 390 = 59,32\, dm^3$
Volume particles	$l \cdot b \cdot h = 390 \cdot 390 \cdot 345 = 52,47\, dm^3$
Number of particles	24917 (given by EDEM)
Volume 1 particle	$1226\, mm^3$ (given by EDEM)

Porosity $$1-\frac{V_{particles}}{V_{box}}=1-\frac{24917\cdot 1226}{52,47\cdot 10^{6}}=0,4178$$

From the calculation follows a realistic porosity for sand and rockfill, the bulk density equals:

$$\gamma=(1-n)\cdot\rho_s\cdot g=(1-0,4178)\cdot 2650\cdot 9,81=15,1kN/m^3$$

TEST 2 Angle of natural repose test

One wall from test 1 is moved upward to allowing the particles to freely roll down. The grains start sliding and rolling and settle at the bottom of the box.

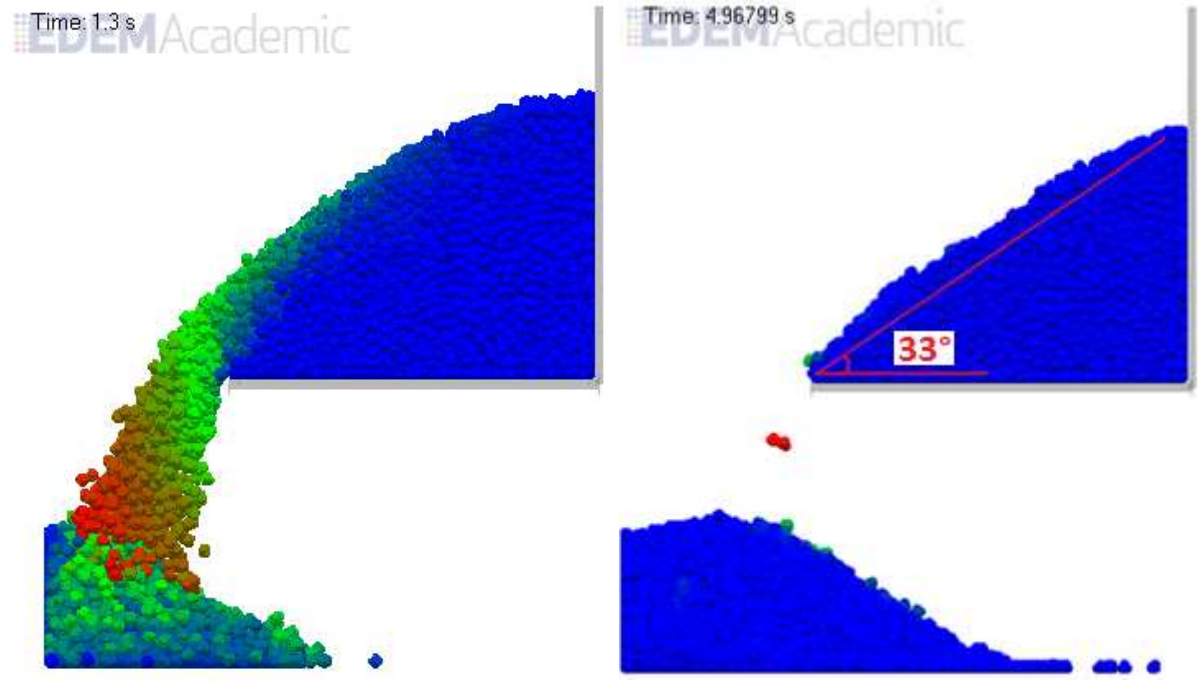

Figure 7.6 Particles rolling down and settling under the angle of repose of 33 -35°

In this test the walls and bottom are given the same friction coefficient as the particles. If the walls have no friction the soil volume starts sliding sideways by the gravitational force. The rolling friction between the particles is set to zero and is solely depending on the shape of the particles. The grains settle under an angle between 33-35° which is a realistic value for rockfill.

Table 7.1 Input parameters of the angle of natural repose test.

Coefficient of Static friction steel/grain	μ_{steel}	0.57	-
Coefficient of Static friction grain/grain	μ_{soil}	0.57	-
Coefficient of Rolling friction grain/grain	$\mu_{r,soil}$	0	-

TEST 3 Passive soil failure (sheet pile approach), occurrence of shear plane.

To test the appearance of a shear plane a test is carried out based on the sheet pile approach. The steel grain friction angle is set to zero. The compressive force on the blade is now only based on the horizontal grain force. The friction angle between grains and the bottom set to the internal friction angle between grains μs = tan(30) = 0,57 and the friction between the walls and the particles is also set to zero.

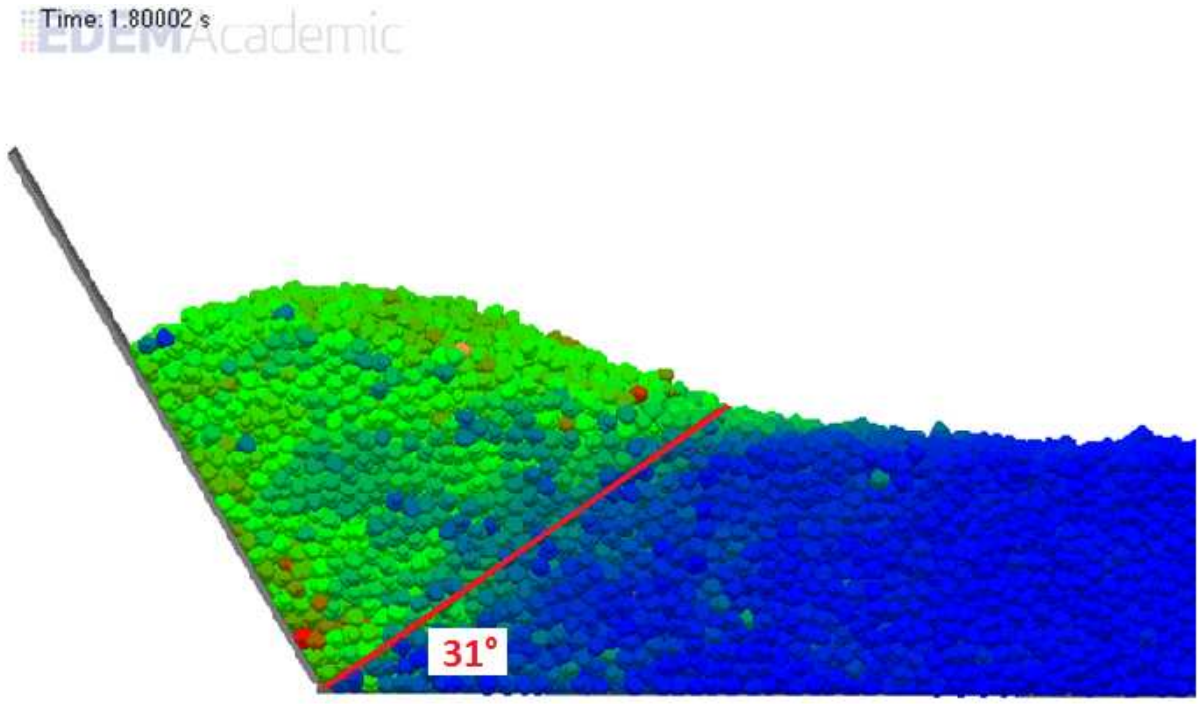

Figure 7.7 Sheet pile approach of passive soil failure in EDEM with a blade-soil friction angle of zero

First the cutting depth is determined based on the porosity calculated in Test 2.

Number of particles 32682 (given by EDEM)

Volume 1 particle $1226\,mm^3$ (given by EDEM)

Porosity $0,4178$ (given by EDEM)

Volume particles total $$\frac{Number\ particles \cdot Volume\ particle}{(1-porosity)} = \frac{32682 \cdot 1226}{1-0,4178} = 68821937\text{mm}^3$$

Box volume $$l \cdot b \cdot h = 2000 \cdot 200 \cdot h$$

Determining h: $$h = \frac{68821937}{2000 \cdot 200} = 172mm$$

At t = 0,5 s the blade starts moving towards the soil volume with 20 cm/s. From this point the compressive force on the blade increases and the grains start shearing. A clear shear zone is seen in figure 7.7. The material starts moving up the blade. No shear force is acting to the blade, because the blade friction is set to zero. The horizontal force that will be compared with the analytical sheet pile approach is the first moments a clear shear zone is observed. This was at T= 0.7 s, this is visible by a decrease of the force figure 7.8. After this time the sheared soil volume starts to move upward resulting in a higher cutting depth. The force at the time of shearing is compared with a theoretical sheet pile approach.

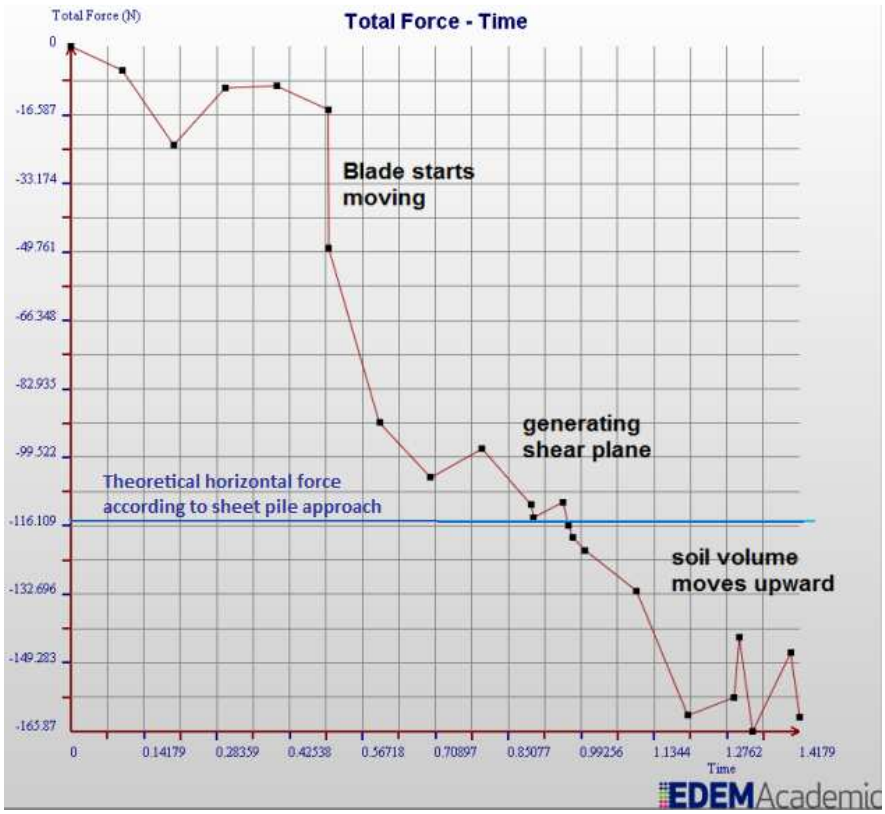

Figure 7.8 Compressive force in the first 0, s the blade starts moving towarsd a passive soil volume

The horizontal force resulting from passive earth failure according to the sheet pile approach [7] is given by:

$$K_p = \frac{1+\sin(\varphi)}{1-\sin(\varphi)} \tag{7.2}$$

$$Q = \frac{1}{2} \cdot \gamma \cdot h^2 \cdot K_p \cdot B \tag{7.3}$$

$$Q_H = Q \cdot \sin(\alpha) \tag{7.4}$$

Where Q_H = horizontal force on the blade [kN], K_p = Coefficient of passive earth pressure, γ = bulk density [kN/m^3], h = cutting depth (m) and α = blade angle [°].

Calculating the theoretical horizontal force on the blade gives:

$$K_p = \frac{1+\sin(30)}{1-\sin(30)} = 3$$

$$Q = \frac{1}{2} \cdot 15{,}1 \cdot 0{,}172^2 \cdot 3 \cdot 0{,}2 = 134N$$

$$Q_h = Q \cdot \sin(\alpha) = 134 \cdot \sin(60) = 116N$$

From figure 7.8 follows a horizontal force at which the passive soil body starts shearing between 104 and 111 N. This is a close value to the sheet pile approach.

Conclusions

From the initial tests follows that the grain particles consisting of 5 spheres shows a behaviour similar to real rockfill. The effect of the particle shape showed that it was allowed to set the rolling friction coefficient to zero. By increasing the rolling friction the particles settle under a higher angle and the shear plane angle increases. Material without the rolling friction coefficient will be used to simulate the following cutting and transporting test with a plough.

7.5 Cutting and transporting tests with EDEM

7.5.1 Input data micro parameters and plough geometry

The calculations are performed with a standard coefficient for the static friction μ_s = 0.57 which equals the Coulomb friction coefficient of tan(30°). From the analytical models followed that the internal friction angle was equal around 37°, but the EDEM simulation were performed during the elaboration of the analytical model so a value for ϕ was chosen. The rolling friction is set to zero, but to observe the effect of the rolling friction on the grain behaviour in front of the plough some additional simulations will be run with the rolling friction coefficient μ_r = 0.4 to Input parameters in the first set of EDEM simulations μ_r = 0

Table 7.2 Input parameters of the ploughing tests

Parameter	Symbol	Value	Dimension
Particle diameter	D_{edem}	14,5	mm
Poisson's ratio	v_{edem}	0.2	-
Shear Modulus	G_{edem}	$5 \cdot 10^7$	Pa
Density	ρ_{edem}	2700	kg/m^3
Coefficient of Restitution	ψ_{edem}	0.0001	-
Coefficient of Static friction	$\mu_{s,soil}$	0.57	-
Coefficient of Rolling friction	$\mu_{r,soil}$	0	-

At first the plough dimensions are taken equal to the physical scale model. The length of the blades (width of the plough) is taken 200 mm to decrease the simulation time. This is one third of the plough width used in the physical scale experiments. The dimensions are presented in figure 7.9.

Only a few tests are performed with this blade shape in order to visualize the possible stone movement in front of the scale model plough. The rest of the simulations and force data will be obtained from simulations with straight blades with different blade angles.

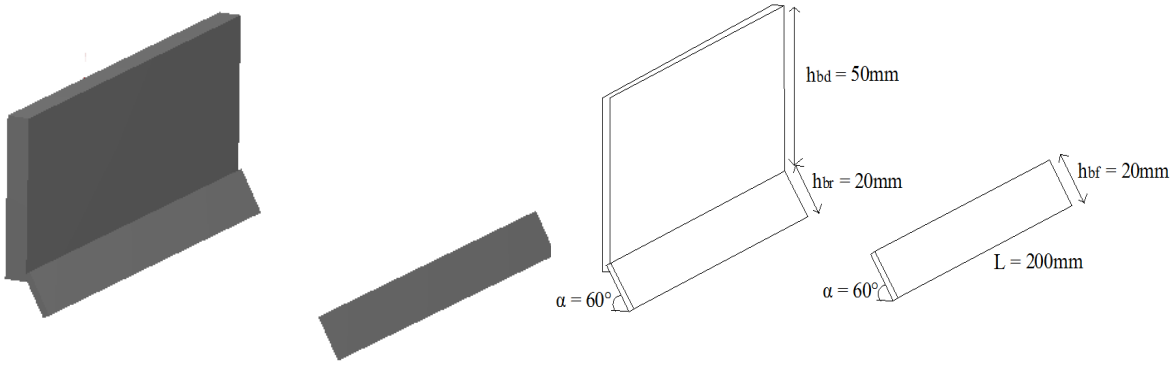

Figure 7.9 Plough dimensions used in EDEM

7.5.2 Output of simulations with scale model blades

7.5.2.1 Grain movement

To get a view of the grain movement in EDEM the movement of the grains is presented by colors. Blue presents a very low particle speed, green a medium speed and red a high speed. Only particles rolling down the slope are having a large speed, but the interest is inside the soil layer. This way it is possible to see a share plane within the layers. In front of both blades a shear plane is made visual in the pictures in figure 7.10. The particles at the surface have the highest velocity. In front of the dozer blade a shear zone can be seen on top of a stationary zone with no movement.

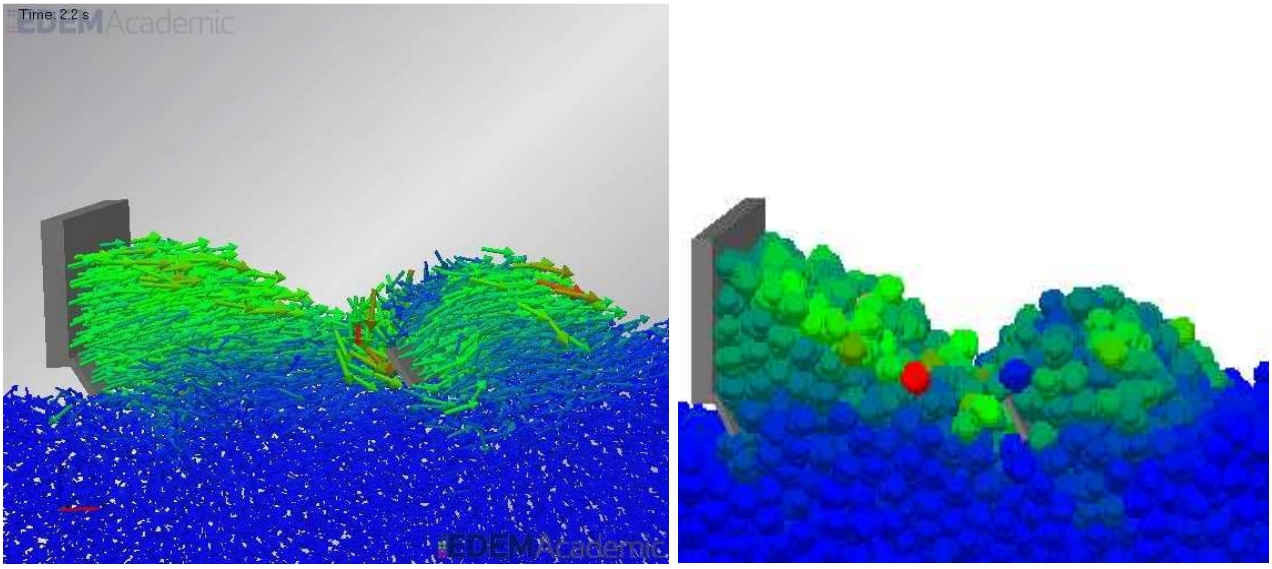

Figure 7.10 Stone velocity in front of rear blade, green and red particles present a higher velocity

With this presentation it is not possible to see the direction of the particles. To get a view of the direction the particles are displayed as vectors in figure 7.10 (left picture). Again two shear planes are shown and the particles above the shear plane have an upward movement. Due to the movement of the plough in x-direction the vectors are orientated in this direction and no good presentation of the particles within the volume is shown. It is not possible in this version of EDEM to show the vectors respectively to the plough movement. The grain movement is examined differently with straight blades (chapter 7.5.3).

7.5.2.2 Build up chain force columns

If not the grain movement but the compressive force is displayed by colors becomes clear that at some moments during cutting rock columns are formed. This phenomena was described earlier in by the theoretical explanations in chapter 4.2. Figure 7.11 shows that an entire row of particles is aligned. Dark blue indicates a high values for the compressive force and light blue small values. These rock columns and irregular shearing of the shear plane causes larger fluctuating in the cutting forces when cutting large particles.

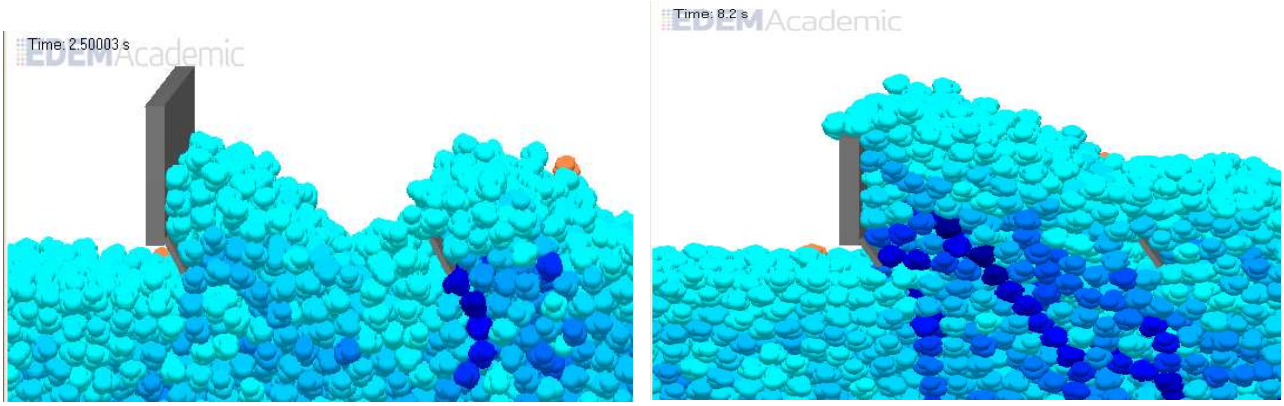

Figure 7.11 Formation of rock collumns in EDEM

7.5.2.3 Effect of increasing the rolling friction coefficient to $\mu_r = 0.4$

When the rolling friction coefficient is increased the movement of the particles at the surface and inside the soil volume decrease. This is resulting in a slower circular motion of the particles. The inflow volume is equal to the situation without the rolling friction coefficient, but the particles are not integrated inside the wedge fast enough. The soil volume starts to act as a boundary wedge with a solid triangular shape. The inflowing particles have to keep moving due to the continuous inflow of particle pushing them further. This is resulting an upward flow of particles across the surface of the formed wedge. In the right picture of 7.12 is also showed that the surface slope increases to almost a vertical position.

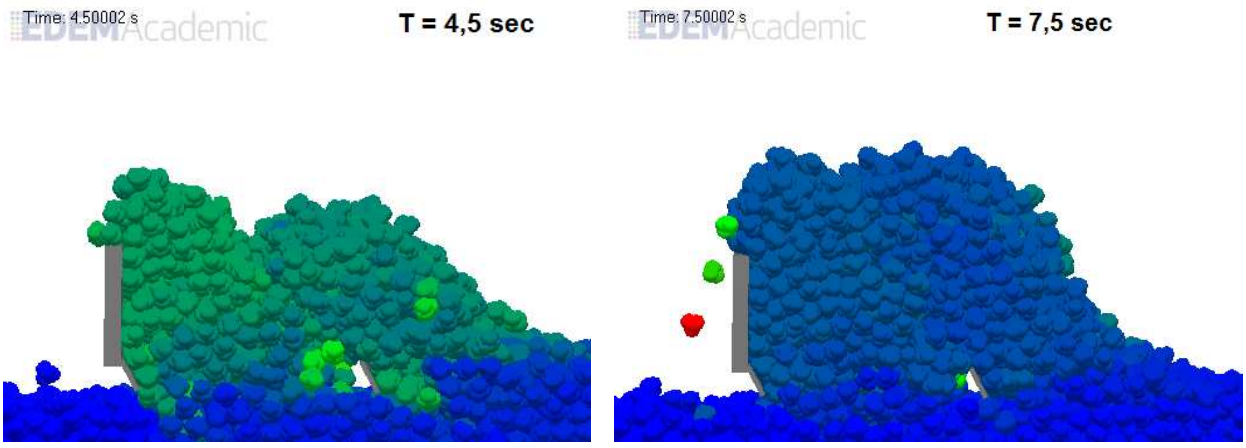

Figure 7.12 Effect of increasing the rolling friction coefficient to $\mu_r = 0.4$, formation boundary wedge

7.6 EDEM simulations with straight blades

In this simulations the blades will consist of straight blades under a blade angle α. The height of the is increased (doubled) compared to the physical scale experiment. This is done to increase the number of particles in front of the blade to get a more continuum behaviour and a clear shear plane.

Table 7.3 Input parameters of simulations with straight blades

Parameter	Symbol	Value	Dimension
Particle diameter	D_{edem}	14,5	mm
Blade speed	U_{edem}	0.2	m/s
Height rear blade	$H_{r,edem}$	140	mm
Height front blade	$H_{f,edem}$	40	mm
Angle front blade	$\alpha_{f,edem}$	60	degree
Width blades	B_{EDEM}	200	mm
Shear Modulus	G_{edem}	5 . 107	Pa
Density	ρ_{edem}	2650	kg/m3
Coefficient of Restitution	ψ_{edem}	0.0001	-
Coefficient of Static soil friction	$\mu_{s,soil}$	0.57	-
Coefficient of Rolling soil friction	$\mu_{r,soil}$	0	-
Coefficient of Static blade friction	$\mu_{s,blade}$	0.364	-

7.6.2 Straight blades configuration with a a rear blade angle α = 90°

7.6.2.1 Grain movement in front of a straight rear blade with α = 90°

To get a good view of the path of the inflowing soil volume and the movement of the particles in front of the blade the entire soil volume is colored orange at T = 1,6 sec. This way the inflowing soil volume which is blue can be distinguished from the soil volume that is already present in front of the rear blade. Figure 7.13 gives the starting and end situation. In Appendix VIII al the intermediate steps are presented and also the separate shape of the upward moving orange particles at every time step.

From the pictures in Appendix VIII follows:
The inflowing layer flows underneath the soil volume until it reaches the rear blade. The layer is cut by rear blade and moves upward. This layer seems initially to roll down already inside the soil volume and form an triangular shape. Most of the particles a clearly moving further upward near the blade and there can be clearly seen that particles at the blade interface are moving with a lower upward speed. Particles that reach the surface roll down and are reintegrated in the soil volume just above the inflowing soil layer. A few particles are mixed with the inflowing layer and are following this path.

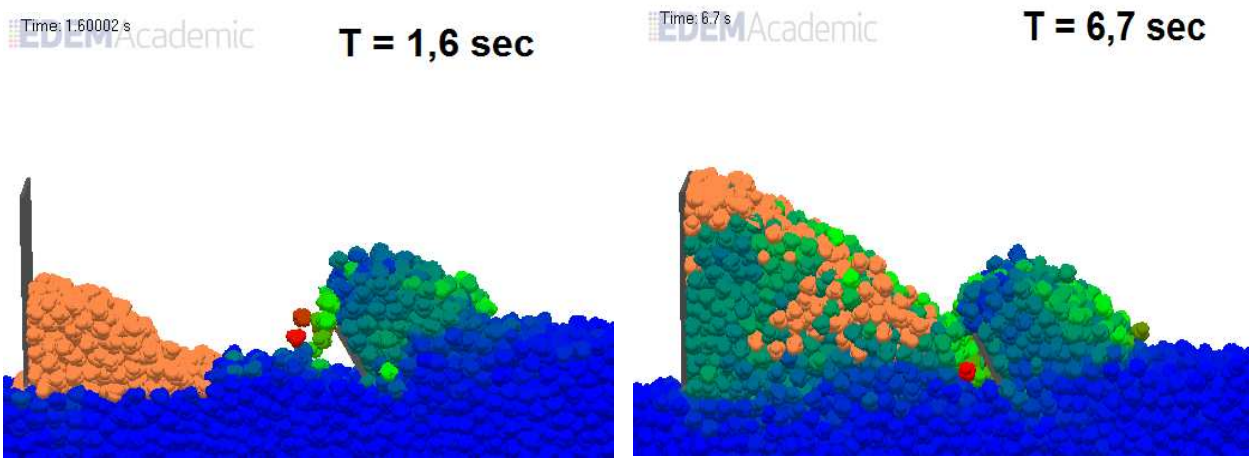

Figure 7.13 Grain movement captured by coloring the soil volume at T =1,6 s and follow the grain path

7.6.2.2 Horizontal cutting force on a straight rear blade with α = 90°

The horizontal force acting on respectively the rear and the front blade is presented in figure 7.14 and 7.15. The forces in the graph have a negative value because the forces are acting in the negative x –direction in EDEM.

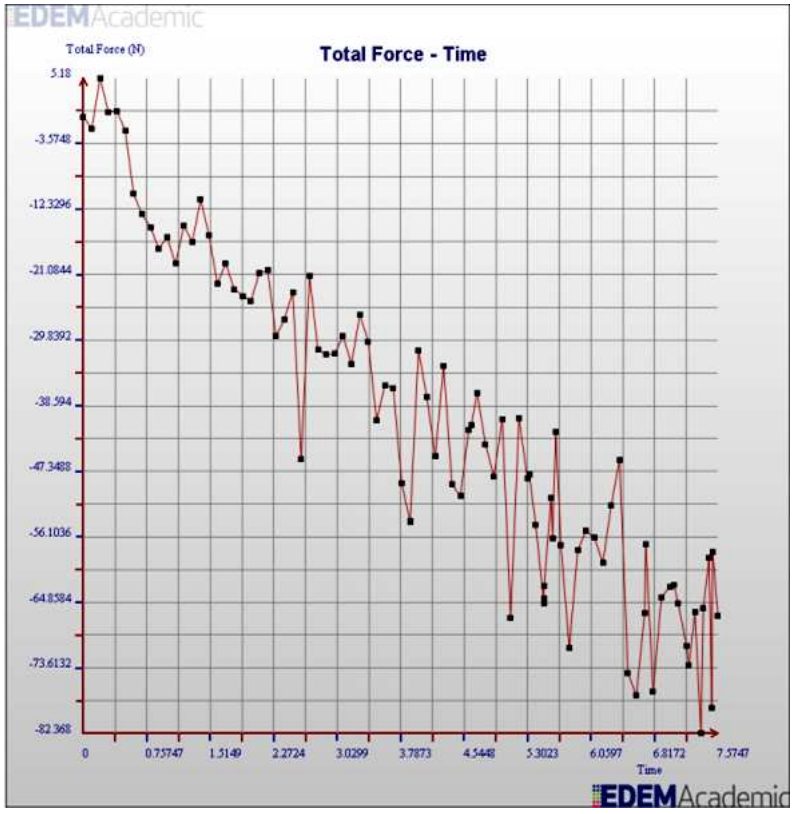

Figure 7.14 Horizontal force (rear blade) in EDEM: H_{blade}=40mm, Bblade=200 mm, φ=30°, δ=20°, α=70°

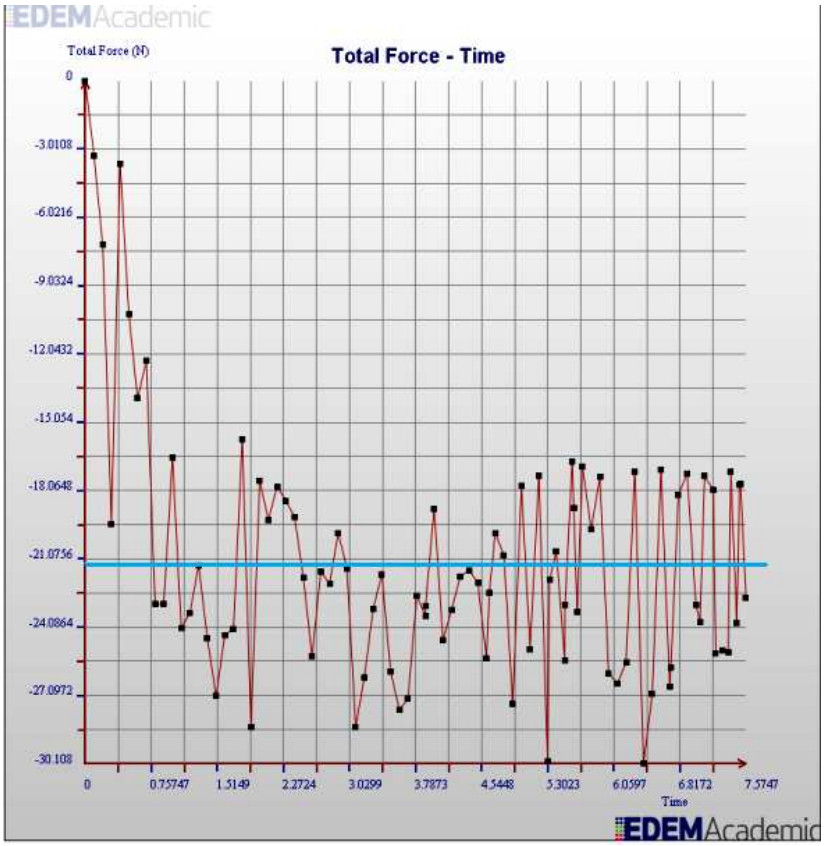

Figure 7.15 Horizontal force (front blade) in EDEM: H_{blade}=40mm, Bblade=200 mm, φ=30°, δ=20°, α=70°

From figure 7.14 follows that the horizontal force on the rear blade is increasing nearly constant, due to the constant inflow of the front blade. The force increases to around 80 N, when the blade starts overflowing. In figure 7.16 the grain volume and the shear plane angles belonging to this force is presented. The front blade is overflowing within 1-2 sec, resulting in an average force around 22 N.

In table 7.4 the forces are compared with the analytical model with inflow (Model 2). The cutting depth is equal to hi=172 mm.

Table 7.4 Comparing analytical model 2 with the EDEM output for α_{rear} = 90°

	Boundary wedge	Force EDEM [N]	β (EDEM)	Force Model 2 [N]	β (Model 2)
FH1 (rear)	no	80	15	129	16.5
FH2 (rear)	yes	80	15	94	20.5
FH1 (front)	no	22	22	9	33
FH2 (front)	yes	22	22	10	28

The analytical model gives a higher values for the values for the front blade. It seems that in of the front blade material is building up above the blade level. In the analytical model the shape of the soil volume in front of the blade is rolling down under the angle of repose without an extra height. In EDEM large particles are used which are protruding above the blade and contributing to the volume, see figure 7.16.

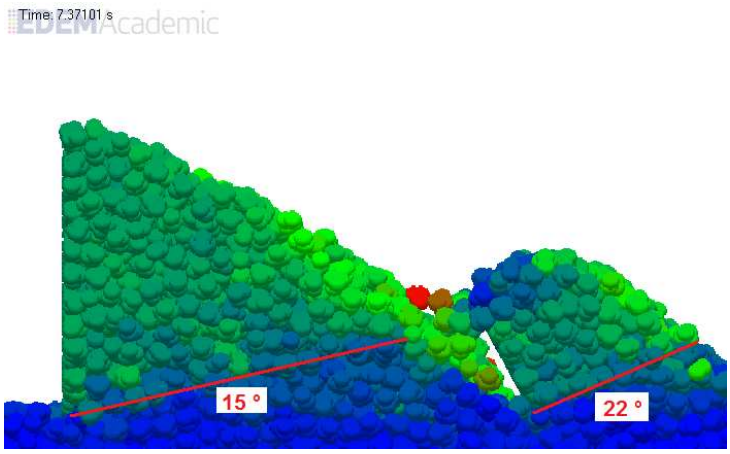

Figure 7.16 Shear plane angles β for a rear blade angle of α=90°

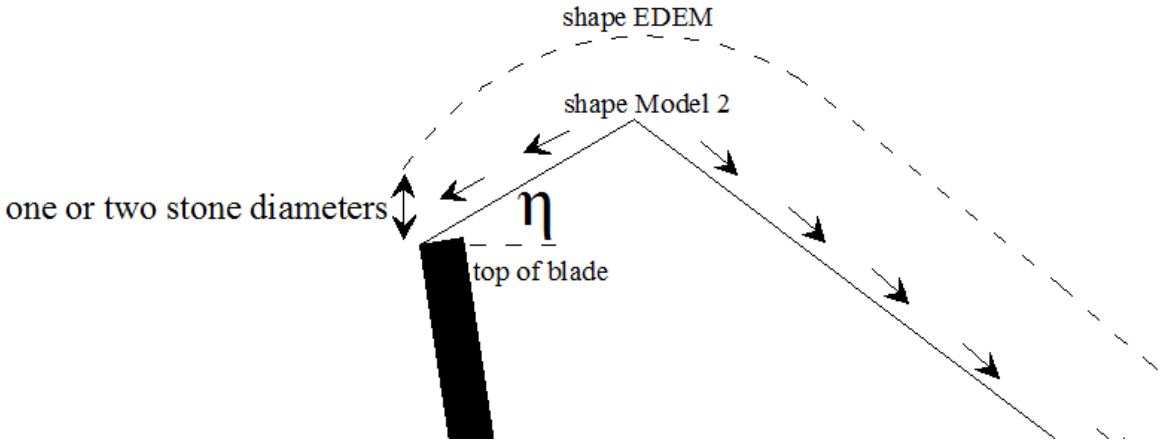

Figure 7.17 Different shapes of material build up in front of blade in EDEM and analytical model 2

7.6.3 Straight blades configuration with a a rear blade angle α = 70°

7.6.3.1 Grain movement in front of a straight rear blade with α = 70°

For this blade angle again the grain movement is visualized, but this time the inflowing layer is followed instead of the orange volume. The figures are also presented in Appendix VIII.

7.6.3.2 Horizontal cutting force on a straight rear blade with α = 70°

The horizontal force of the rear blade for α_{rear} = 70° is presented in figure 7.18. The front blade configuration is kept equal and the forces are therefore equal to the previous simulation.

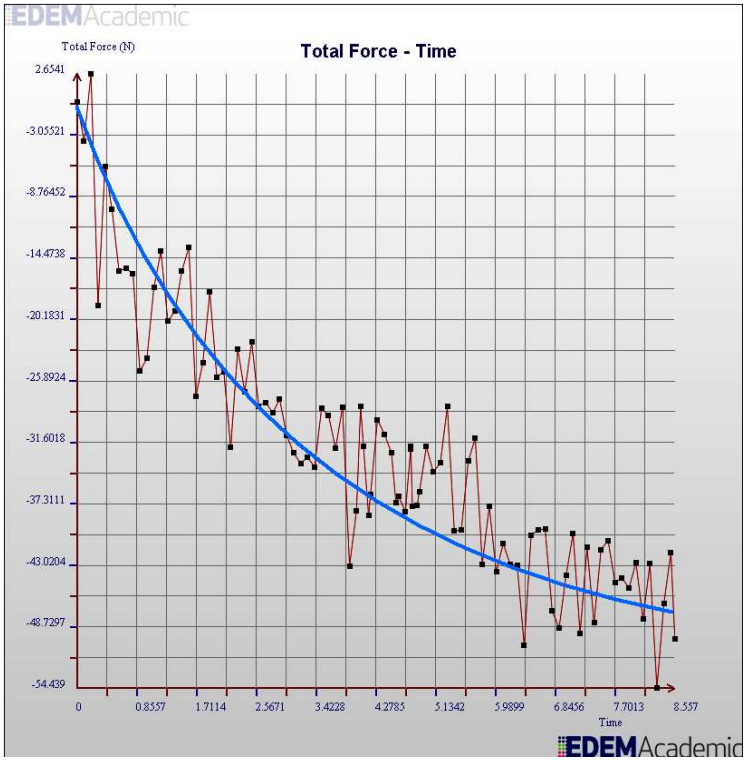

Figure 7.18 Horizontal cutting force in EDEM for H_{blade}=140 mm, Bblade=200 mm, φ=30°, δ=20°, α=70°

The horizontal cutting force that following from EDEM is equal to 50 N at the moment the rear blade starts overflowing. Figure 7.19 shows the grain volume and the shear plane angles belonging to this force.

Table 7.5 Comparing analytical model 2 with the EDEM output for α_{rear} = 90°

	Boundary wedge	Force EDEM [N]	β (EDEM)	Force Model 2 [N]	β (Model 2)
FH1 (rear)	no	50	16	64.0	22.0
FH2 (rear)	yes	50	15	61.6	20.5

The analytical calculations show a slightly bigger force compared to the force output from EDEM. When we look at figure 7.19 the inflowing layer is not equal to the overflowing layer, what can cause this lower value. The additional height of the particles protruding above the blade are in this case nearly contributing to the force, because the volume increase is very small compared to the rest of the volume in front of the blade.

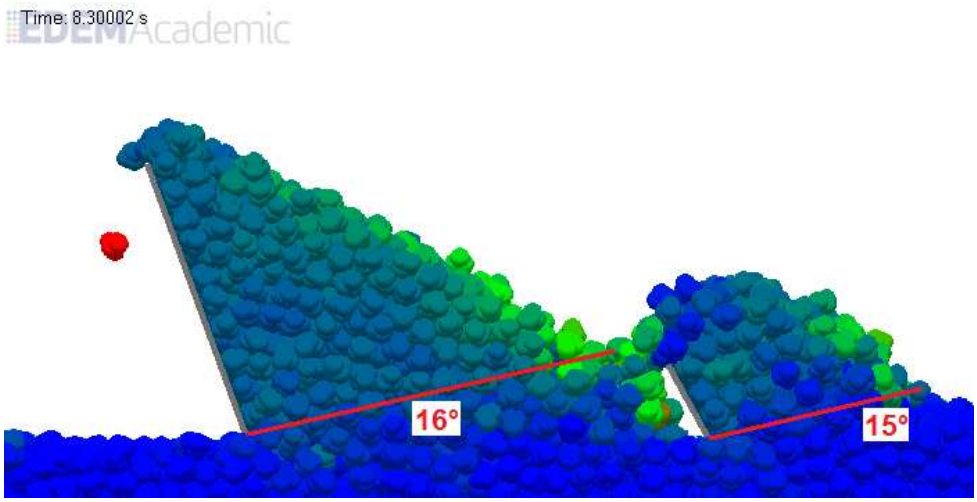

Figure 7.19 Shear plane angles β for a rear blade angle of α=70°

7.7 Conclusions EDEM/ feedback to physical model and analytical models

EDEM seems a good tool to describe the cutting process of granular materials. The grain movement in front of the blades agrees with analytical models for coarse cutting and transporting coarse material derived in chapter 4.2. EDEM seems useful to visualize the movement of grains for cutting simulations. Interesting is that EDEM shows that some particles are already rolling down inside the wedge before they reach the surface. The main volume of the inflowing layer however was cut and moved upward near the blade. Particles near the blade moved slower due to the friction of the blade.

The EDEM model also gave insight in the shape of the total soil volume in front of the blade. The soil volume is curved with some particles protruding above the blade, this was also observed in the scale experiments. The analytical model is still based on a continuum approach with very small particles. With larger particles the stones that protrude above the blade when are contributing to the soil cutting force, this is not taken into account in the analytical model. The output data still has to be handled with care until the effect of changing micro parameters on the macro behaviour is fully examined.

Chapter 8 Conclusions & Recommendations

The research question was formulated as follows:

"What important processes are involved in equalizing rockfill with a plough (gravel, cobbles and boulders) and how to model these processes".

In this master thesis three different types of models are used to answer this question: An analytical model, a physical scale model and a computer model using discrete element modeling.

The conclusions based on the validation of the analytical models with the scale experiments are already discussed in chapter 6.5. The conclusions based on combining the analytical, scale and EDEM model are discussed here.

8.1 Conclusions

In this report analytical models are derived for the main processes involved in equalizing coarse material; Cutting, penetrating, transporting and unloading soil. The analytical models are obtained by modifying continuum models from the literature. A physical scale experiments is carried out to validate the analytical models. EDEM is thereafter used to visualize the grain movement inside the soil volume.

8.1.1 Analytical model for cutting & transporting coarse

The observations during the scale experiments and the EDEM simulations confirmed the grain movement derived in the analytical models for cutting and transporting coarse material. The analytical models derived in chapter 4.2, have showed realistic values for ϕ and β after comparing the horizontal cutting forces with the physical scale model. The values for the shear plane angle β and horizontal cutting force F_H were based on the principle of minimum cutting energy. The model for sole transporting, so without an inflow of soil from the cutting blade resulted in a analytical slip line of $\beta = 0$ (horizontal). This is contrary to the observations done in the scale experiments where an upward movement of grains was observed. Apparently the cutting layer is never exactly zero due to the grains settling at the toe of the wedge. At low plough masses the blade was emptying by underflow of material. With the initial plough mass only Cobbles can be transported, larger particles are deposited by underflow due to a vertical lift of the blade. EDEM showed a good agreement concerning the grain movement in front of the blades and the exchange of material between the cutting blade and the rear blade. In the scale experiments it was impossible to see a shear plane but in EDEM a clear shear plane was observed inside the soil volume.

These models can be considered as tools to calculate the vertical and horizontal blade forces when equalizing rockfill and the effect of the forces by varying the blade angle α or the soil friction angle ϕ.

8.1.2 Analytical model for vertical blade penetration

The penetration model gives an underestimation of the bearing capacity of the soil. Larger grains result in a significant increase in bearing capacity of the sub layer. A high penetration stress must be exerted in order to penetrate the sub layer. This penetration resistance seems crucial for not only penetrating the sub layer, but also equalizing dunes and transporting material. Once plough is lifted the plough is not easily lowered, what is resulting in an underflow of material. From the experiments follows that cobbles can be very well equalized, the plough is only lifted under a small angle through the bed or dune. Rockfill dunes of consisting of 5-70 kg rockfill are shoved over very short distances and in order to penetrate and cut the sub layer the vertical blade stress has to be increased about 3 times. Equalizing 300-1200kg rockfill is impossible, the grains are to large compared to the cutting tool.

8.2 Recommendations

- To visualize the appearance of a shear plane inside the soil volume and the formation of an apparent boundary wedge tests could be performed in front of a glass wall. The blade should be placed against the smooth glass wall to visualize the upward grain movements. Layers with colored stoned can be placed to visualize slip line and the velocity of the particles.
- Some additional test should be performed to determine the exact penetration stress for a vertical and inclined blade configuration. The tests showed that the vertical penetration is very important for both cutting and transporting.
- Test could be performed with known values for the internal friction angle and the angle of repose of a material. This way the calculation can be executed with less unknown variables. A way to test the forces for different blade angles is pushing a straight blade through a rock rover with the help of a cylinder. The tests should be performed on a larger scale to determine an exact blade angle. The forces should be are measured by the cylinder.
- The analytical model can be fine tuned by exactly determine the shape of the transported soil volume and taking into account the friction between the plough bottom and the bed.
- EDEM is a very useful tool to visualize and simulate cutting processes. More research on the effect of the micro parameters on the macro behaviour is desirable.

Chapter 9 Bibliography

[1] Anthony, J.L., Marone, C. “Influence of particle characteristics on granular friction”. *Journal of geophysical research* B08409, 2005, Pennsylvania, pp. 1-14

[2] Van der Schrieck, G.L.M. “Dredging Technology”. *Lecture notes,* Delft, 2009, the Netherlands, pp. 4-21–4-31, 13-1–13-16

[3] Miedema, S.A., "The Calculation of the Cutting Forces when Cutting Water Saturated Sand, Basic Theory and Applications for 3-Dimensional Blade Movements" (in Dutch). Ph.D. thesis, Delft, 1987, the Netherlands.

[4] Baars, S. van. (1995) “Communications on Hydraulic and Geotechnical Engineering: Discrete Element Analysis of Granular Materials”. Ph.D. thesis, Delft, Septembe 1996, the Netherlands.

[5] Tyler G. Hicks, P.E.: “Civil Engineering Formulas” ISBN: 978-0-07-161470-2

[6] Sun, Xiaoshan. “Small and medium scale direct shear test of the Bremanger sandstone rockfill”. *Master Thesis, 2010, Delft*

[7] Verruijt, A. (2001)” GRONDMECHANICA” (in Dutch). *Lecture notes,* Technische Universiteit Delft, the Nederlands

[8] Miedema, S.A. “On the Snow-Plough Effect when Cutting Water Saturated Sand with Inclined Straight Blades”. *Journal, Technische Universiteit Delft, the Nederlands*

[9] Kesteren, W.G.M. “Penetratieweerstand bucket elevator”. *Research document Deltares, Delft, the Netherlands*

[10] Koolen, A.J, Kuipers, H (1983). “Agricultural soil mechanics, Advanced series in Agricultural Science 13”. ISBN 3-540-12257-5. Springer-Verlag, Berlin, Heidelberg, New York Tokyo

[11] Abdeli, M. ”Discrete modelling of sand/rock cutting”. *Master thesis, Delft, 2009, Netherlands*

[12] Ruznak, J. Mark, C. “Using the point load test to determine the uniaxial compressive strength of coal measured rock”. *Journal Geology, Rock mechanics, Pittsburgh*

[12] Miedema, S.A. & Frijters, D.D.J., "The wedge mechanism for cutting of water saturated sand at large cutting angles". WODCON XVII, September 2004, Hamburg Germany.

[13] Hettiaratchi, D.R.P. & Witney, B.D. & Reece, A.R., "The calculation of passive pressure in two dimensional soil failure". *Journal Agric. Engng*. Res. 11 (2), pp. 89-107, 1966.

[14] Hettiaratchi, D.R.P. and Reece, A.R., "Symmetrical three-dimensional Soil Failure". J. Terramech. 1967, pp. 45-67.

[15] Hettiaratchi, D.R.P. & Reece, A.R., "The calculation of passive soil resistance". Geotechnique 24, No. 3, pp. 289-310, 1974.

[16] Hettiaratchi, D.R.P. and Reece, A.R., "Boundary Wedges in Two Dimensional Passive Soil Failure". Geotechnique 25,No 2,pp. 197-220, 1975.

[17] Miedema, S.A. "The cutting of water saturated sand, the solution". CEDA African Section; Dedging days 2006 – Protection of the coastline, dredging sustainable development, Nov 1-3, Tangiers, Morocco

[18] McKeyes, E. (1985) “Soil cutting and tillage: Development in agricultural engineering 7”. Department of Agricultural Engineering, McDonald College of McGill University, Ste-Anne de Bellevue, Quebec, Canada, p20-59, p 75-76

[19] Zhao Yi & Miedema, S.A. “Finite Element Calculations To Pore Pressure When cutiing Water Saturated Sand At Large Cutting Angles”. CEDA Dredging Day 2001, November 2001, Amsterdam, The Netherlands.

[20] Gieck, K. “Technische Formelsamlung”. Deutsche auflage 1981, D-7100 Heilbron/N, West Duitsland

Appendix I Research boundary

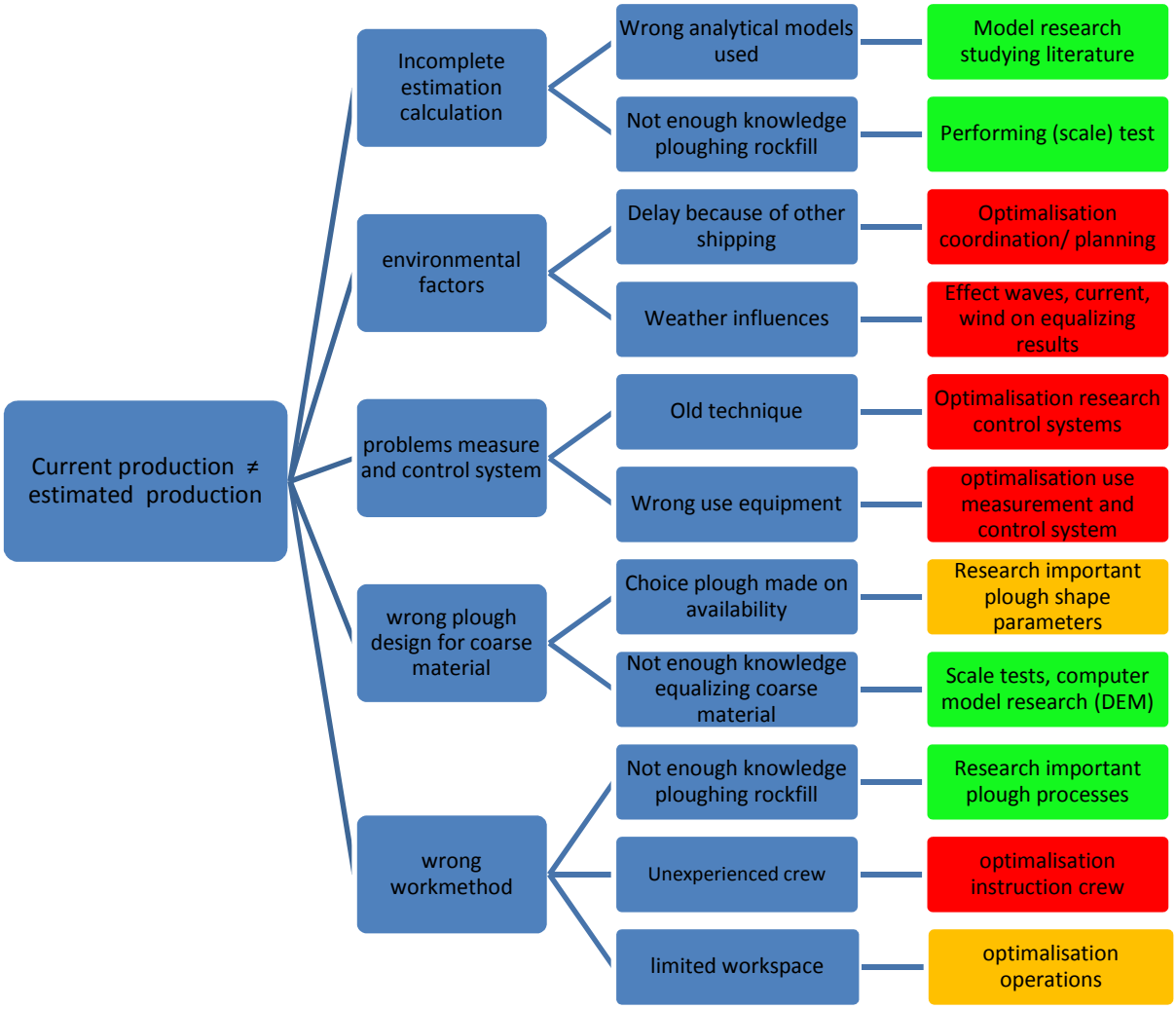

Research goal
Not part of research
Recommendation

Appendix II Prototype plough

Prototype plough

H dozer blade	0,7	m
H rear plough	0,7	m
H cutting blade	0,5	m
Whith plough	13	m
Mass plough	17	Ton
Blade angle	60	°

Arca ship

Length ship	55	m
Drag wire attachment position	44	m
Plough depth from	6	m
Plough depth to	18	m
Slope	1:7	
Slope	8,24	°
Angle drag wires deep water	22,2	°
Angle drag wires shallow water	7,8	°

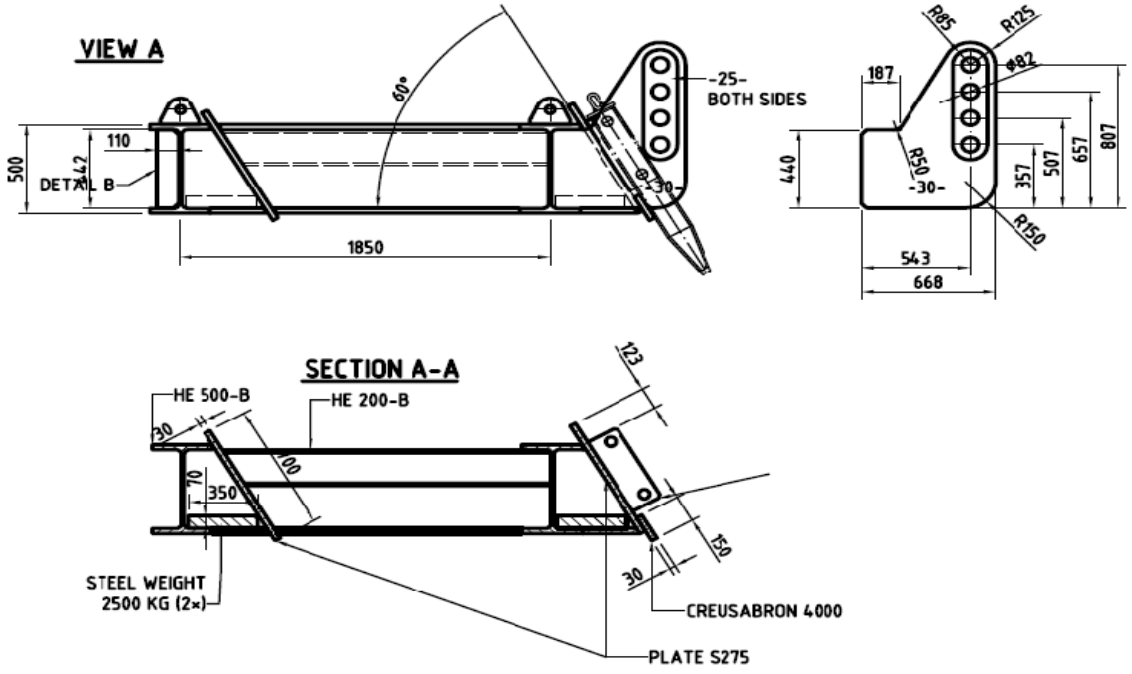

The plough dimensions are based on a design used for previous research by Rijkswaterstaat. The dimensions are not according to the prototype. The deviation is shown in the table where the model is scaled back to full scale with a scale factor of $n_L = 20$. The biggest difference is in the weight and the rear blade, this means that the production with the model plough can be a lot bigger than the real maximum production with a fully loaded plough.

Prototype Arca plough				**ARCA model n_L=20**	
H dozer blade	0,7	m		35	mm
H rear plough	0,7	m		35	mm
H cutting blade	0,5	m	→	25	mm
Whith plough	13	m		650	mm
Mass plough	17	ton		2125	gram
Mass/m'	1,31	ton/m'		33	g/cm'

Upscaling the Rijkswaterstaat plough back to full scale dimensions:

Prototype RWS plough				**Model plough**	**RWS**
H dozer blade	0,3	m		15	mm
H dozer	1,4	m		70	mm
H cutting blade	0,3	m		15	mm
Whith plough	12	m	←	600	mm
Mass plough	19,2	ton		2400	gram
Mass/m'	1,6	ton/m'		40	gram/cm'

Appendix III Material properties

The rockfill gradings used for the scale model are based on the grading used for the Maasvlakte 2 project. The rockfill types are all scales with a length scale of n_L=20 from the actual prototype gradings. In this appendix the sieve curves of the model gradings are presented.

Filter material (n_l=20)

Gradation PUMA

D%	Lower bound (mm)	Upper bound (mm)	Mean (mm)
5	0,002	0,015	0,0085
15	0,015	0,075	0,045
50	0,25	0,5	0,375
90	0,75	1,75	1,25
98	1	2,25	1,625

Gradation used for scale model

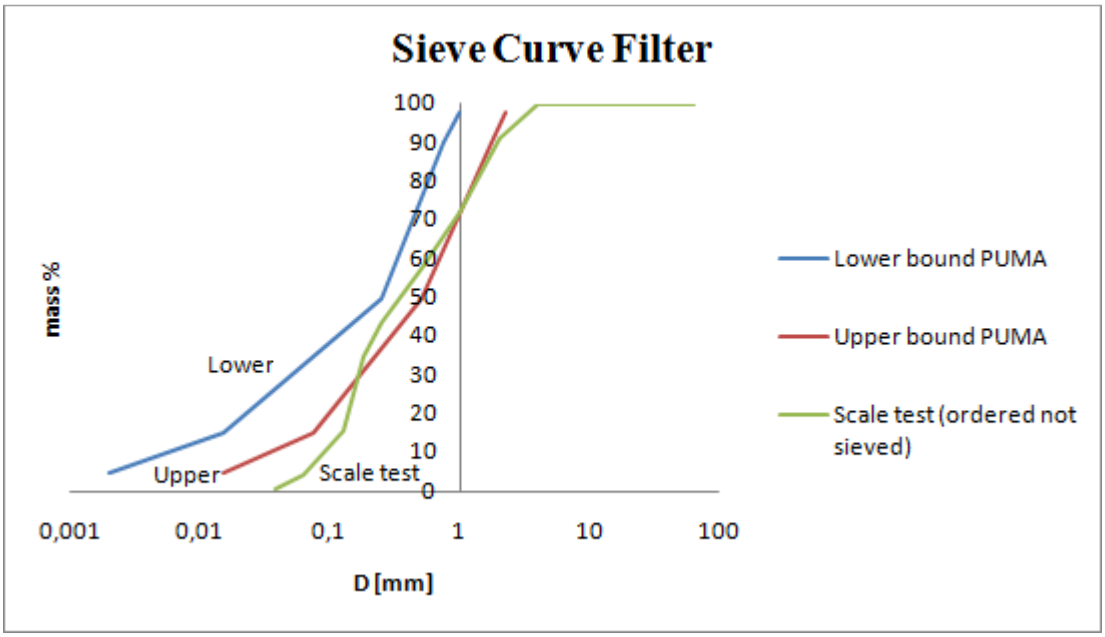

D (mm)	%
4	100
2	91
1	71.8
0.5	57.4
0.38	**50**
0.25	43.6
0.18	34.8
0.125	15.6
0.063	4.4
0.038	0.8
0	0

Cobbles (n_L=20)

Grading PUMA n_L =20

D%	Lower bound (mm)	Upper bound (mm)	Mean (mm)
5	0,5	1,25	0,875
15	1	2	1,5
50	3	5	4
90	5,25	6,75	6
98	6	9	7,5

Grading scale model

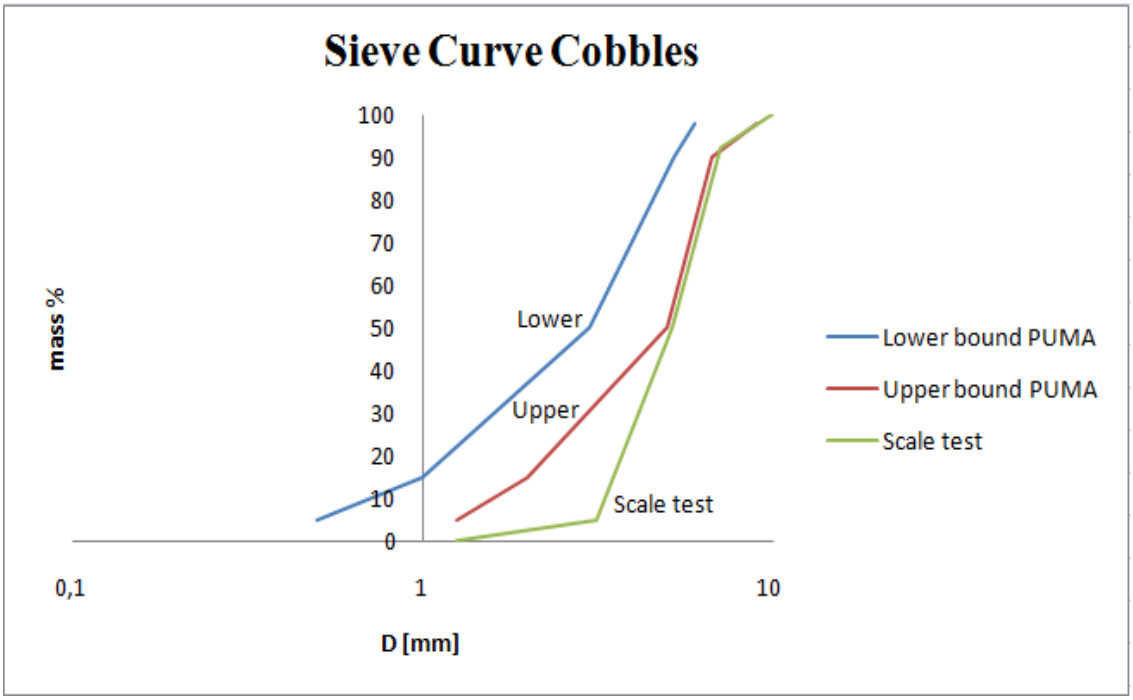

D (mm)	%
12,5	100
10	100
7,1	92
5,2	**50**
3,15	5
1,25	0

Boulders 5-70 kg (n_L=20)

Grading PUMA n_L =20

D%	Lower bound (mm)	Upper bound (mm)	Mean (mm)
2	5,42	7,80	6,61
10	7,36	10,61	8,98
50	11,68	15,30	13,49
85	15,85	17,73	16,79
100	17,73	21,22	19,47

Grading scale model

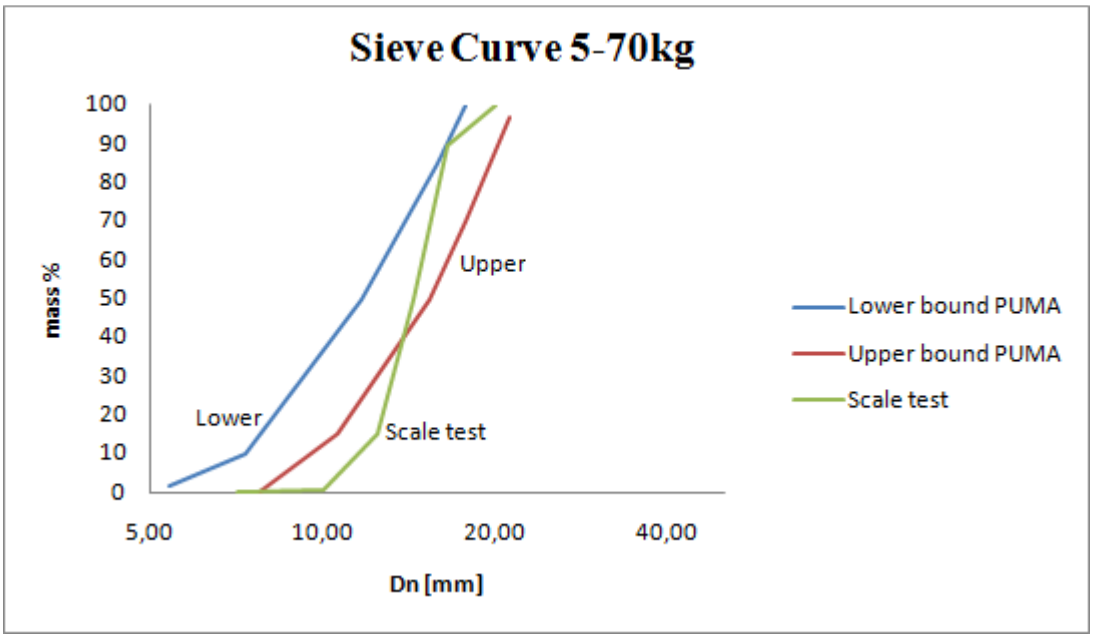

D [mm]	%
20	100
16,5	90
14,4	**50**
12,5	15
10	1
7,1	0

Boulders 300-1200 kg (n_L=20)

Grading PUMA n_L =20

D%	ondergrens (mm)	bovengrens (mm)	gemiddeld (mm)
5	19,97	22,85	21,41
10	22,85	28,79	25,82
50	31,69	36,28	33,99
85	38,19	39,93	39,06
100	39,93	46,34	43,13

Gradering Bontrup

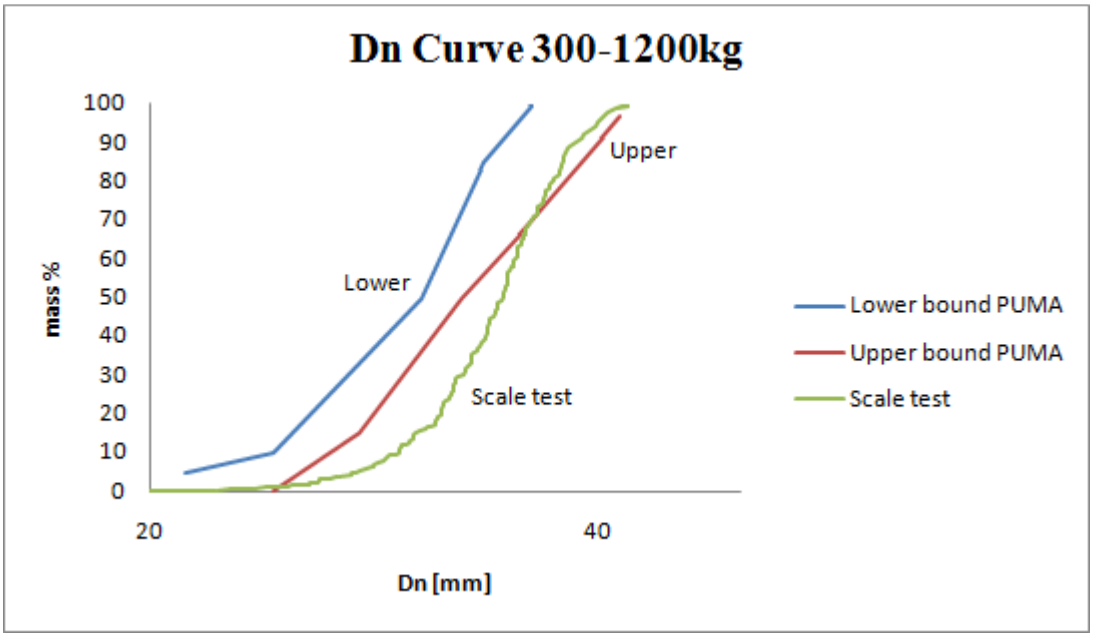

The curve for 300-1200kg is based on weighing 140 stones and determine the nominal diameter with the relation Dn = $\sqrt[3]{M_{stone}}$ and the stone diameter with D = Dn / 0,84 (rock manual).

D [mm]	%
63	100
50	73
44,5	**50**
40	31
31,5	3
20	0

Appendix IV Analytical calculations

IV.1 Calculation Penetration resistance figures 4.30, 4.31 and 4.32 (chapter 4.3)

The penetration resistance pf that is formulated by Terzaghi is modified to predict the penetration resistance of coarse material. in this Appendix two approximations are given to calculate the penetration resistance for rockfill consisting of large grains. The stones are still considered to behave as a continuum. In approximation 1 the bluntness of the blade B_{blade} is replaced by the stone diameter D_{stone}. For approximation 2 the first stone layer is assumed to act as a surface load q [kPa] on the surrounding soil surface, the bluntness of the blade is also taken equal to the stone diameter.

The internal friction angle is varied between ϕ = 30 in sand to 40 degree for sharp-edged rockfill [9]. A calculation is made for all the intermediate values of ϕ. For all models there is no water included and the width of the blade B_{blade}= 2mm, the blade length L_{blade}= 600mm and density of the solids ρ_s = 2780kg/m^3.

The relation for the penetration resistance p_f is given by Eq. (4.64) in Chapter 4.2 and reads:

$$p_f = q \cdot N_q \cdot i_q + (\frac{1}{2} \cdot \gamma \cdot B_{blade} \cdot N_\gamma \cdot i_\gamma)$$

Approximation 1: The width of the strip is duplicated with a factor for the stone diameter.

$$p_f = (\frac{1}{2} \cdot \gamma \cdot D_{stone} \cdot N_\rho \cdot s_\rho)$$

	Width strip/ Stone diameter (mm)
Blade	2
Cobbles	5.2
5-70 kg	14.4
300-1200 kg	44.5

Table 10.1 Penetration resistance pf with the assumption that the B_{strip}=D_{stone}.

ϕ	pf [kPa] Blade Surface	pf [kPa] Rockfill D50=5,2mm	pf [kPa] Rockfill D50=14,4mm	pf [kPa] Rockfill D50=44,5mm
30	0.34	0.87	2.41	7.46
31	0.39	1.02	2.83	8.76
32	0.46	1.20	3.33	10.29
33	0.54	1.41	3.91	12.10
34	0.64	1.66	4.61	14.24
35	0.75	1.96	5.43	16.79
36	0.89	2.32	6.41	19.82
37	1.05	2.74	7.59	23.45
38	1.25	3.25	9.00	27.80
39	1.48	3.86	10.69	33.03
40	1.77	4.60	12.74	39.36

Approximation 2: The width of the strip foundation is equal to the stone diameter, and a surface load is added. The surface load is caused by the first layer of stones, assuming the blade to penetrate the second soil layer. The first stone becomes the blade tip.

$$p_f = (\frac{1}{2} \cdot \gamma \cdot D_{stone} \cdot N_\gamma \cdot i_\gamma + q \cdot N_q \cdot s_q)$$

$$q = N_{stones} \cdot M_{stone} \cdot (1-n)$$

Where q = surface load of a soil layer N_{stone} = number of stones/m^2 , M_{stone} = Mass of one stone [kN], n = porosity [-].

Table 10.2 Calculation surface load for various rockfill type

	Width strip (mm)	Number of stones/ m²	Mass 1 stone (N)	Surface load q (kPa)
Filter	2	150000	1.16E-07	0.017
Cobbles	5.2	22189	2.05E-06	0.045
5-70 kg	14.4	2894	4.35E-05	0.125
300-1200 kg	44.5	303	1.28E-03	0.388

Table 10.3 Penetration resistance pf for B_{strip}=D_{stone} and an additional surface load q

Φ [°]	pf [kPa] Blade Surface	pf [kPa] Rockfill D50=5,2mm	pf [kPa] Rockfill D50=14,5mm	pf [kPa] Rockfill D50=44,5mm
30	0.34	1.71	4.76	14.61
31	0.71	1.96	5.47	16.77
32	0.78	2.25	6.29	19.29
33	0.87	2.60	7.25	22.24
34	0.96	3.00	8.37	25.68
35	1.08	3.47	9.69	29.73
36	1.21	4.03	11.24	34.49
37	1.38	4.69	13.08	40.13
38	1.57	5.47	15.25	46.81
39	1.81	6.40	17.85	54.78
40	2.09	7.51	20.95	64.31

IV.2 Horizontal cutting force for analytical model for cutting and transporting

To validate the analytical models derived in chapter 4.2 calculations have been carried out with the input parameters equal to the scale model experiments. The cutting models that are derived are:

1 Model 1: Transporting without inflow of material (Q = 0 m^3/s)
2 Model 2: Cutting and Transporting with inflow of material (Q > 0 m^3/s)

The scale experiments were divided in the same two categories to simulate the models. The transporting experiments were consisting of an initial soil volume of 8kg in front of the blade and without inflow. The cutting experiments were performed by cutting of the front blade only, whereby cutting & transporting of material was generated. The cutting experiments showed indeed a transported soil volume tests and an overflow of material.

The analytical models are calculated with the following equations. For the equations describing the gravitational force of the transported soil volume G is referred to chapters 4.2.3 and 4.2.4.

The horizontal cutting force without a boundary wedge by combining Eq. (4.11) and Eq. (4.12):

$$F_H = \left(\frac{G\sin(\beta+\varphi)+T\cos(\varphi)}{\sin(\alpha+\beta+\varphi+\delta)} \right) \cdot \sin(\alpha+\delta)$$

The horizontal cutting force with a boundary wedge by combining Eq. (4.20) and Eq. (4.21):

$$F_H = \left(\frac{K_2^* \sin(\alpha^*+\lambda+\varphi)+G_2\sin(\varphi)}{\sin(\alpha+\delta+\varphi)} \right) \cdot \sin(\alpha+\delta)$$

Where $K_2^* = \frac{G_1\sin(\beta+\varphi)+T\cos(\varphi)}{\sin(\alpha^*+\beta+\varphi+\lambda)}$ *and* $T = \rho_g \cdot v_c^2 \frac{\sin(\alpha)}{\sin(\alpha+\beta)} h_i \cdot b$

Calculation Model 1: Transporting without inflow of material (Q = 0 m^3/s)

Model 1 is calculated for several values for the blade angle α to check the sensitivity of the blade angle on the cutting force. The results are discussed in chapter 6.4.1.

	ϕ [°]															
hi	**30**	**31**	**32**	**33**	**34**	**35**	**36**	**37**	**38**	**39**	**40**	**41**	**42**	**43**	**44**	**45**
α = 70°	16.78	17.46	18.16	18.87	19.60	20.35	21.11	21.90	22.70	23.53	24.38	25.26	26.16	27.10	28.06	29.06
α = 80°	23.33	24.39	25.49	26.62	27.78	28.99	30.24	31.54	32.89	34.28	35.74	37.26	38.85	40.50	42.24	44.06
α = 83°	25.40	26.60	27.85	29.13	30.47	31.85	33.29	34.79	36.35	37.98	39.69	41.47	43.35	45.32	47.39	49.58
α = 85°	26.81	28.11	29.46	30.86	32.32	33.84	35.42	37.07	38.79	40.60	42.50	44.49	46.59	48.80	51.14	53.63
α = 90°	30.45	32.04	33.70	35.43	37.25	39.15	41.15	43.26	45.48	47.84	50.33	52.98	55.80	58.81	62.04	65.50
Scale test	50	50	50	50	50	50	50	50	50	50	50	50	50	50	50	50

Calculation Model 2: Cutting and Transporting with inflow of material (Q > 0 m^3/s)

Several parameters, like β, ϕ, δ and η where unknown during the scale experiments. Therefore some assumptions had to be made for the analytical model calculations. The steel soil friction angle δ was set to 20° and the angle of repose η equal to 30°. An iteration of the minimum cutting force is made for different values of the internal friction angle ϕ. The soil-soil friction angle λ between boundary wedge and Rankine zone is changing with the same value for ϕ.

The cutting depth taken equal to the cutting depths measured in the scale model. The blade dimensions of the cutting blade Hb = 20 mm , B = 600 mm, α= 75°. The density of the solids ρ_s = 2780 kg/m^3 and a porosity n = 0.4. The horizontal forces are based on dry cutting.

The results of calculating the horizontal blade force F_H with Model 2 is presented in table 10.4 and 10.5. The horizontal cutting forces are based on the principle of minimum cutting energy with the corresponding shear angle β. Table 10.4 is the horizontal cutting force without boundary wedge and table 10.5 the horizontal cutting force with a boundary wedge. The values that are matched to the scale model experiments are highlighted in tables. The results are discussed in chapter 6.4.1.

Table 10.4 F_H [N] based on minimum cutting energy for various ϕ [°] without a boundary wedge

	hi							
ϕ (°)	**16.5**	**17.0**	**21.7**	**22.7**	**24.3**	**24.1**	**24.7**	**26.0**
30	20.9	21.4	25.7	26.7	28.0	27.8	28.4	29.5
β	30	31	32	33	33	33	34	34
31	21.8	22.3	26.9	27.9	29.4	29.2	29.8	31.0
β	30	30	32	32	33	33	33	33
32	22.8	23.4	28.3	29.3	30.8	30.6	31.3	32.6
β	30	30	32	32	32	32	33	33
33	23.9	24.5	29.7	30.8	32.4	32.2	32.9	34.3
β	29	29	31	31	32	32	32	32
34	25.0	25.6	31.2	32.4	34.1	33.9	34.7	36.1
β	29	29	31	31	31	31	31	32
35	26.2	26.9	32.8	34.1	35.9	35.7	36.5	38.1
β	28	29	30	30	31	31	31	31
36	27.5	28.2	34.5	35.9	37.9	37.7	38.6	40.2
β	28	28	30	30	30	30	30	31
37	28.9	29.7	36.4	37.9	40.1	39.8	40.7	42.6
β	27	28	29	29	30	30	30	30
38	30.4	31.2	38.5	40.0	42.4	42.1	43.1	45.1
β	27	27	28	29	29	29	29	30
39	32.0	32.9	40.7	42.4	44.9	44.6	45.7	47.8
β	26	27	28	28	29	29	29	29
40	33.8	34.7	43.1	44.9	47.6	47.3	48.5	50.8
β	26	26	27	28	28	28	28	28
41	35.7	36.7	45.6	47.6	50.6	50.2	51.5	54.0
β	26	26	27	27	27	27	28	28
42	37.8	38.9	48.5	50.6	53.8	53.4	54.8	57.5
β	25	25	26	27	27	27	27	27
43	40.0	41.2	51.6	53.9	57.3	56.9	58.4	61.4
β	25	25	26	26	26	26	26	27
44	42.5	43.7	54.9	57.5	61.2	60.7	62.4	65.6
β	24	24	25	25	26	26	26	26
45	45.1	46.5	58.6	61.4	65.5	64.9	66.8	70.3
β	24	24	25	25	25	25	25	25

Table 10.5 F_H [N] based on minimum cutting energy for various ϕ [°] with a boundary wedge

	hi							
ϕ (°)	**16.5**	**17.0**	**21.7**	**22.7**	**24.3**	**24.1**	**24.7**	**26.0**
30	18.3	18.8	22.9	23.7	25.0	24.8	25.4	26.5
β	31	31	33	34	34	34	35	35
31	19.4	19.9	24.2	25.2	26.5	26.4	27.0	28.1
β	30	30	32	33	33	33	33	33
32	20.4	21.0	25.7	26.7	28.2	28.0	28.7	29.9
β	29	29	31	31	32	32	32	33
33	21.6	22.2	27.3	28.4	30.0	29.8	30.5	31.9
β	28	28	30	30	31	31	31	32
34	22.9	23.5	29.0	30.2	31.9	31.7	32.5	34.0
β	27	28	29	29	30	30	30	30
35	24.3	25.0	30.9	32.2	34.1	33.8	34.7	36.3
β	26	27	28	28	29	29	29	29
36	25.8	26.5	32.9	34.3	36.4	36.1	37.1	38.8
β	26	26	27	27	28	28	28	28
37	27.5	28.3	35.2	36.7	39.0	38.7	39.7	41.6
β	25	25	26	26	27	27	27	27
38	29.3	30.2	37.6	39.3	41.8	41.5	42.6	44.7
β	24	24	25	25	26	26	26	26
39	31.3	32.3	40.4	42.2	45.0	44.6	45.8	48.1
β	23	23	24	24	25	25	25	25
40	33.6	34.6	43.5	45.5	48.5	48.1	49.4	52.0
β	22	22	23	23	24	24	24	24
41	36.1	37.2	46.9	49.1	52.4	52.0	53.4	56.3
β	21	21	22	22	23	23	23	23
42	38.9	40.1	50.8	53.2	56.8	56.3	58.0	61.1
β	20	21	21	22	22	22	22	22
43	42.0	43.4	55.2	57.9	61.9	61.3	63.1	66.6
β	20	20	20	21	21	21	21	21
44	45.6	47.1	60.2	63.2	67.6	67.0	69.1	72.9
β	19	19	20	20	20	20	20	20
45	49.8	51.4	65.9	69.3	74.3	73.6	75.9	80.2
β	18	18	19	19	19	19	19	19

Appendix V Output data from scale experiments

V.1 Test program & output data: Transporting

Table 10.6 Test program transporting

Test code	material		water	bed properties		plough		Plough suspension		
	name	d50 (mm)		L (cm)	D (cm)	αr (°)	Mass (kg)	Hr (cm)	Hf (cm)	v (cm/s)
tr.5-70 kg3	5-70 kg	14,5	no	320	15	25	2.4	15	17	10
tr.5-70 kg4	5-70 kg	14,5	no	320	15	25	4,4	15	17	10
tr.5-70 kg5	5-70 kg	14,5	no	320	15	25	6,4	15	17	10
tr.5-70 kg1	5-70 kg	14,5	no	320	15	25	8,4	15	17	10
tr.5-70 kg1n	5-70 kg	14,5	no	320	15	25	8,4	15	17	10
tr.5-70 kg6	5-70 kg	14,5	no	320	15	25	8,4	15	17	10
tr.5-70 kg7	5-70 kg	14,5	no	320	15	25	10,4	15	17	10
tr.5-70 kg8	5-70 kg	14,5	no	320	15	25	12,4	15	17	10
wtr.5-70 kg3	5-70 kg	14,5	yes	320	15	25	2,4	15	17	10
wtr.5-70 kg1	5-70 kg	14,5	yes	320	15	25	8,4	15	17	10
wtr.5-70 kg2	5-70 kg	14,5	yes	320	15	25	8,4	15	17	10
tr.Cobbles3	Cobbles	5,2	no	320	15	25	2.4	15	17	10
tr.Cobbles4	Cobbles	5,2	no	320	15	25	4,4	15	17	10
tr.Cobbles5	Cobbles	5,2	no	320	15	25	6,4	15	17	10
tr.Cobbles1	Cobbles	5,2	no	320	15	25	8,4	15	17	10
tr.Cobbles2	Cobbles	5,2	no	320	15	25	8,4	15	17	10
wtr.Cobbles3	Cobbles	5,2	yes	320	15	25	2,4	15	17	10
wtr.Cobbles1	Cobbles	5,2	yes	320	15	25	8,4	15	17	10
wtr.Cobbles2	Cobbles	5,2	yes	320	15	25	8,4	15	17	10
tr.300-1200kg1	300-1200kg	44,5	no	320	15	25	8,4	15	17	10
tr.300-1200kg2	300-1200kg	44,5	no	320	15	25	8,4	15	17	10
tr.300-1200kg8	300-1200kg	44,5	yes	320	15	25	12,4	15	17	10
wtr.300-1200kg1	300-1200kg	44,5	yes	320	15	25	8,4	15	17	10
wtr.300-1200kg2	300-1200kg	44,5	yes	320	15	25	8,4	15	17	10
tr.Filter3	Filter	0,38	no	320	15	25	2,4	15	17	10
tr.Filter1	Filter	0,38	no	320	15	25	8,4	15	17	10
wtr.Filter3	Filter	0,38	yes	320	15	25	2,4	15	17	10
wtr.Filter1	Filter	0,38	yes	320	15	25	8,4	15	17	10

Table 10.7 Output data transporting: Horizontal cutting force [N] and plough elevation [mm]

	FORCE [N]		Plough elevation [mm]	
Code	**Max**	**Mean 15 < t < 20**	**Max**	**End 15 < t < 20**
tr.5-70kg3	95.40	6.85	18.89	0.10
tr.5-70kg4	111.37	8.29	12.27	0.19
tr.5-70kg5	112.50	4.69	7.13	0.38
tr.5-70kg1	112.84	41.21	5.58	-0.92
tr.5-70kg1n	130.69	44.01	7.28	-0.81
tr.5-70kg6	120.66	34.10	5.14	0.06
tr.5-70kg7	124.37	55.73	5.73	0.70
tr.5-70kg8	138.49	69.71	4.92	0.23
wtr.5-70kg3	74.09	2.57	no data	no data
wtr.5-70kg1	112.77	46.57	no data	no data
wtr.5-70kg2	116.15	50.37	no data	no data
tr.Cobbles 3	80.44	20.83	5.14	1.26
tr.Cobbles 4	91.48	38.99	2.35	0.24
tr.Cobbles 5	93.88	53.69	1.62	-0.10
tr.Cobbles 1	107.76	52.71	2.06	-0.72
tr.Cobbles 2	101.04	61.53	1.25	-0.61
wtr.Cobbles 3	58.76	10.49	no data	no data
wtr.Cobbles 1	90.91	27.28	no data	no data
wtr.Cobbles 2	88.90	24.84	no data	no data
tr.300-1200kg 1	140.23	74.14	37.34	0.00
tr.300-1200kg 2	127.26	6.55	30.72	0.00
tr.300-1200kg 8	171.65	26.90	31.09	0.00
wtr.300-1200kg 1	117.25	34.34	no data	no data
wtr.300-1200kg 2	114.14	1.99	no data	no data
tr.Filter 3	79.04	46.50	1.25	-1.05
tr.Filter 1	102.20	54.04	0.07	-1.29
wtr.Filter 3	93.27	7.20	no data	no data
wtr.Filter 1	154.56	5.13	no data	no data

V.2 Test program & output data: Cutting & transporting

Table 10.8 Test program cutting

Test code	material		water	bed properties		plough		Plough suspension		
	soort	d50 (mm)		L (cm)	D (cm)	αf (°)	Mass (kg)	Hr (cm)	Hf (cm)	v (cm/s)
st.5-70kg3	5-70 kg	14,5	no	320	15	60	2.4	17	15	10
st.5-70kg4	5-70 kg	14,5	no	320	15	60	4,4	17	15	10
st.5-70kg5	5-70 kg	14,5	no	320	15	60	6,4	17	15	10
st.5-70kg1	5-70 kg	14,5	no	320	15	60	8,4	17	15	10
st.5-70kg2	5-70 kg	14,5	no	320	15	60	8,4	17	15	10
st.5-70kg6	5-70 kg	14,5	no	320	15	60	8,4	17	15	10
st.5-70kg7	5-70 kg	14,5	no	320	15	60	10,4	17	15	10
st.5-70kg7n	5-70 kg	14,5	no	320	15	60	10,4	17	15	10
st.5-70kg8	5-70 kg	14,5	no	320	15	60	12,4	17	15	10
st.5-70kg8n	5-70 kg	14,5	no	320	15	60	12,4	17	15	10
wst.5-70kg3	5-70 kg	14,5	yes	320	15	60	2.4	17	15	10
wst.5-70kg1	5-70 kg	14,5	yes	320	15	60	8,4	17	15	10
wst.5-70kg2	5-70 kg	14,5	yes	320	15	60	8,4	17	15	10
st.Cobbles 3	Cobbles	5,2	no	320	15	60	2.4	17	15	10
st.Cobbles 3n	Cobbles	5,2	no	320	15	60	2,4	17	15	10
st.Cobbles 4	Cobbles	5,2	no	320	15	60	4,4	17	15	10
st.Cobbles 4n	Cobbles	5,2	no	320	15	60	4,4	17	15	10
st.Cobbles5	Cobbles	5,2	no	320	15	60	6,4	17	15	10
st.Cobbles 6	Cobbles	5,2	no	320	15	60	8,4	17	15	10
st.Cobbles 1	Cobbles	5,2	no	320	15	60	8,4	17	15	10
st.Cobbles 2	Cobbles	5,2	no	320	15	60	8,4	17	15	10
wst.Cobbles3	Cobbles	5,2	yes	320	15	60	2,4	17	15	10
wst.Cobbles1	Cobbles	5,2	yes	320	15	60	8,4	17	15	10
wst.Cobbles2	Cobbles	5,2	yes	320	15	60	8,4	17	15	10
st.Filter3	Filter	0,38	no	320	15	60	8,4	17	15	10
st.Filter1	Filter	0,38	no	320	15	60	8,4	17	15	10
wst.Filter1	Filter	0,38	yes	320	15	60	8,4	17	15	10
wst.Filter3	Filter	0,38	yes	320	15	60	8,4	17	15	10
wst.300-1200kg1	300-1200kg	44,5	yes	320	15	25	8,4	17	15	10
wst.300-1200kg2	300-1200kg	44,5	yes	320	15	25	8,4	17	15	10

Table 10.9 Output data transporting: Horizontal cutting force [N] and plough elevation [mm]

	FORCE [N]				CUTTING DEPTH [mm]			
Code	**Max**	**Min**	**average**	**st deviation**	**Max**	**Start**	**average**	**st deviation**
st.5-70kg3	23.00	-1.79	4.07	3.64	9.73	-17.83	0.75	4.00
st.5-70kg4	41.59	-1.28	13.09	6.12	16.72	-21.72	-0.20	5.93
st.5-70kg5	50.89	-4.59	17.61	8.46	10.84	-23.78	-0.42	6.41
st.5-70kg1	66.86	-5.49	28.09	11.47	10.84	-23.12	-0.04	6.88
st.5-70kg2	70.88	-5.54	30.85	11.29	7.90	-24.37	-2.79	7.10
st.5-70kg6	69.80	-4.59	26.09	11.80	11.87	-24.81	0.26	8.01
st.5-70kg7	104.65	-5.03	57.70	15.09	4.52	-24.37	-7.16	6.03
st.5-70kg7n	96.65	-6.25	56.17	15.55	3.34	-24.37	-7.06	4.97
st.5-70kg8	117.38	-8.39	66.00	18.57	0.47	-27.09	-8.31	5.56
st.5-70kg8n	121.45	-8.73	71.10	20.19	4.00	-25.77	-9.33	6.42
wst.5-70kg3	20.87	-12.48	4.06	2.64	no data	no data	no data	no data
wst.5-70kg1	90.72	1.91	37.24	10.15	no data	no data	no data	no data
wst.5-70kg2	67.79	3.85	35.28	9.56	no data	no data	no data	no data
st.Cobbles3	27.96	-12.39	21.97	4.22	-12.02	-12.24	-16.50	0.82
st.Cobbles3n	30.51	-0.98	20.01	3.64	-6.51	-24.08	-17.03	2.74
st.Cobbles4	45.89	0.76	38.10	8.01	-16.95	-22.24	-21.68	1.12
st.Cobbles4n	56.48	-0.91	43.14	7.50	-18.49	-26.72	-22.72	1.31
st.Cobbles5	71.56	-2.45	54.84	9.57	-21.72	-26.43	-24.25	1.31
st.Cobbles6	80.66	-3.31	66.88	13.56	-21.14	-26.87	-24.05	1.53
st.Cobbles1	65.19	1.86	49.12	10.13	-21.65	-24.81	-24.74	1.27
st.Cobbles2	69.28	6.97	50.64	12.35	-22.53	-26.21	-26.04	1.14
wst.Cobbles3	24.48	-6.01	16.39	4.15	no data	no data	no data	no data
wst.Cobbles1	28.23	4.02	19.18	2.62	no data	no data	no data	no data
wst.Cobbles2	40.98	1.18	17.13	3.03	no data	no data	no data	no data
st.Filter3	24.97	2.62	15.31	2.36	-22.38	-22.41	-22.79	0.09
st.Filter1	114.61	1.10	93.96	14.61	-21.67	-21.94	-21.97	0.14
wst.Filter1	74.63	2.23	40.79	12.84	no data	no data	no data	no data
wst.Filter3	23.35	-19.99	6.24	3.90	no data	no data	no data	no data
wst.300-1200kg1	96.75	-3.26	32.17	19.58	no data	no data	no data	no data
wst.300-1200kg2	100.55	-4.73	30.68	19.38	no data	no data	no data	no data

Appendix VI Hertz-Mindlin (no slip) [11]

The contact between grains in EDEM are described by the Herz-Mindlin contact model. The normal is the shear forces are as follows:

$$F_n = \frac{4}{3} \cdot Y^* \cdot \sqrt{R^*} \delta_n^{\frac{3}{2}}$$

$$\frac{E^*}{E_a} = n\frac{A_a}{A_{tot}} + \frac{E_b}{E_a}\left[1 - \left(\frac{nA_a}{A_{tot}}\right)\right]$$

Where, Y^* is the equivalent Young's Modulus (it this thesis the equivalent Young's modulus is the same as relative Young's Modulus, because all particles have the same material properties, R^* is the equivalent radius and δ_n is the normal overlap. Additionally there is a damping force, given by:

$$F_n^d = -2\sqrt{\frac{5}{6}} \cdot \beta \cdot \sqrt{S_n \cdot m^*} \cdot v_n^{\overline{rel}}$$

$$\beta = \frac{\ln e}{\sqrt{\ln^2 e + \pi^2}}$$

$$S_n = 2 \cdot Y^* \cdot \sqrt{R^* \cdot \delta_n}$$

Where, m^* is the equivalent mass, $v_n^{\overline{rel}}$ is the normal component of the relative velocity, e is the coefficient of restitution and S_n is the normal stiffness. The shear force, F_s, depends on the tangential overlap δ_t and the tangential stiffness S_t.

$$F_s = -S_t \cdot \delta_t$$

$$S_t = 8 \cdot G^* \cdot \sqrt{R^* \cdot \delta_n}$$

Where, G^* is the equivalent shear modulus. In the tangential direction there is also a damping force, give by:

$$F_t^d = -2\sqrt{\frac{5}{6}} \cdot \beta \cdot \sqrt{S_t \cdot m^*} \cdot v_t^{\overline{rel}}$$

Where, $v_t^{\overline{rel}}$ is the relative tangential velocity. The tangential force is limited by Coulomb friction $\mu_s \cdot F_n$ where μ_s is the coefficient of static friction.

For simulation in which the rolling friction is important, it will be calculated by applying a torque to the contacting surfaces.

$$\tau_i = -\mu_r \cdot F_n \cdot R_i \cdot \omega_i$$

Where, μ_r is the coefficient of rolling friction, R_i is the distance of the contact point from the center of mass and ω_i is the unit angular velocity vector of the object at the contact point.

Appendix VII Particle shape EDEM

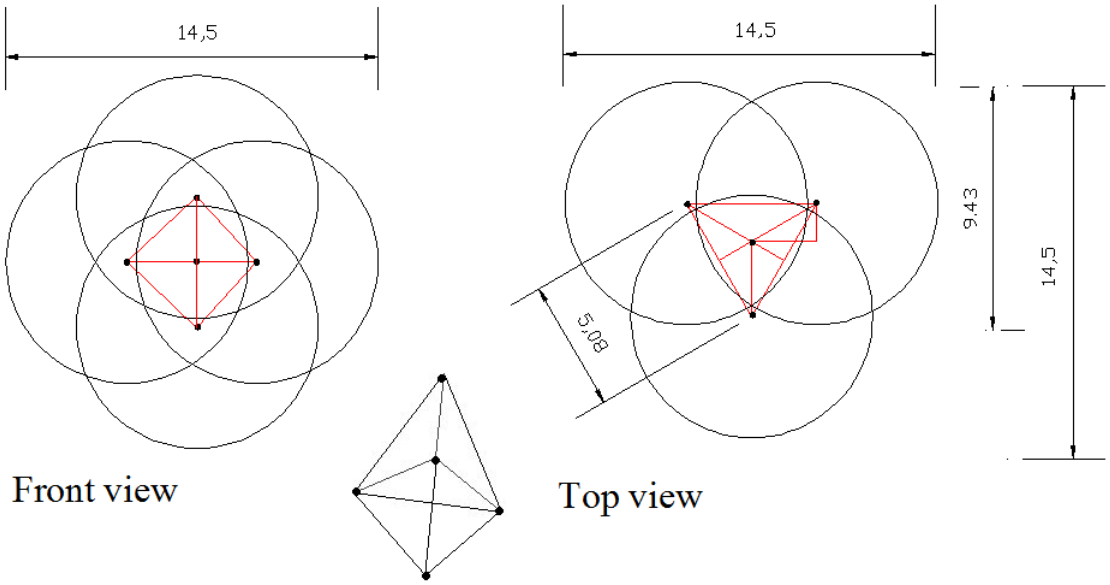

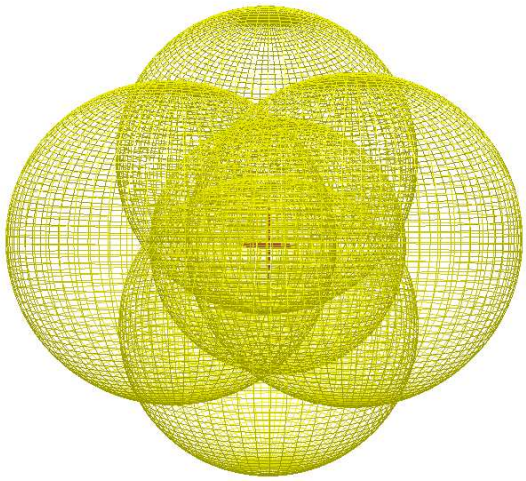

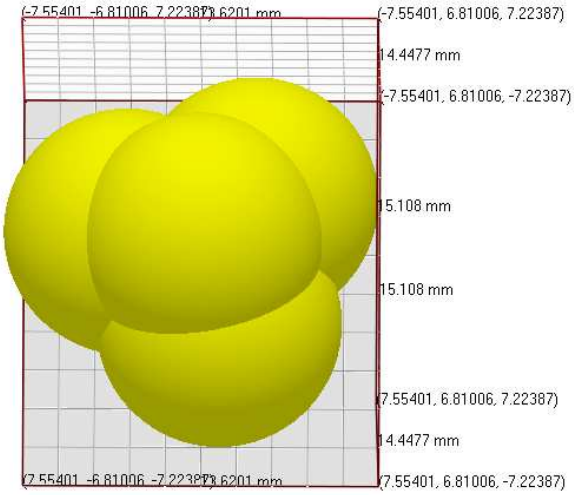

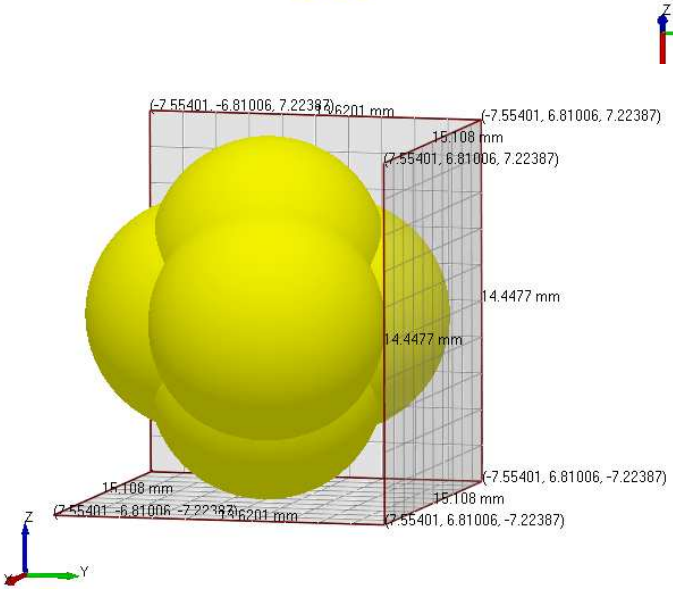

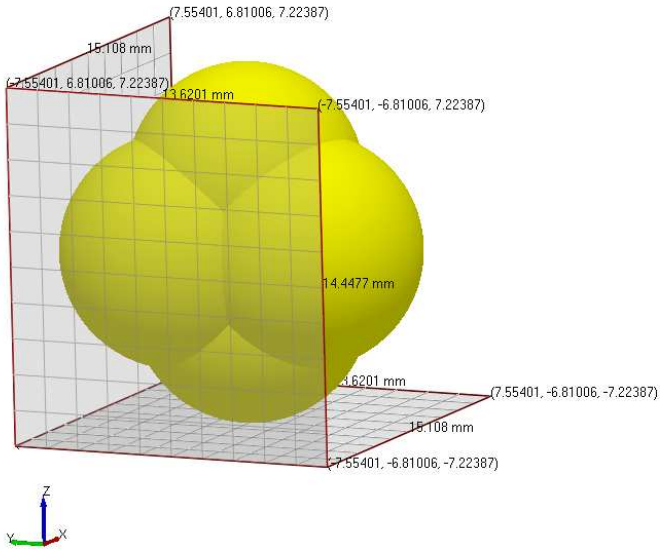

Appendix VIII Seven stages of soil accumulation in front of rear blade with Q>0m/s³ in EDEM

Stone movement for rear blade angle α =90°

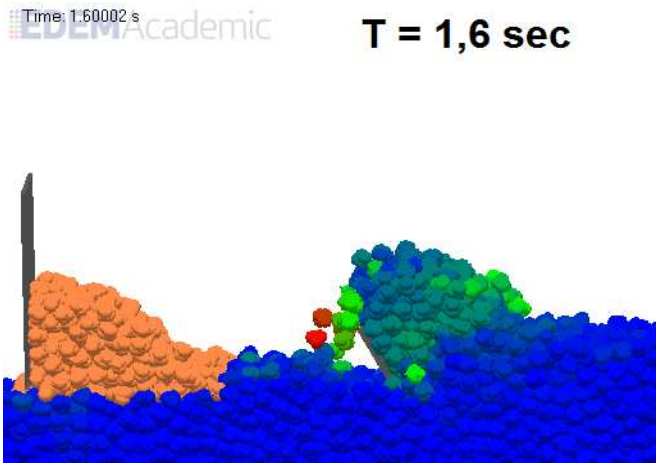

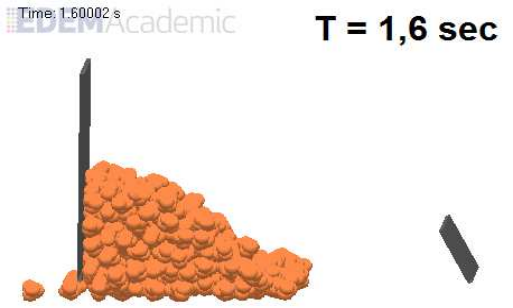

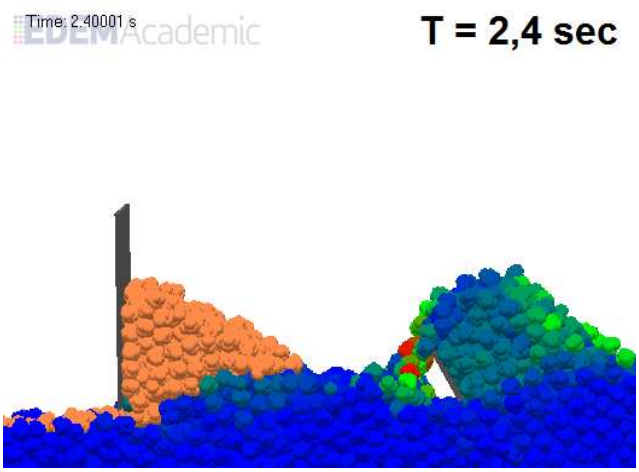

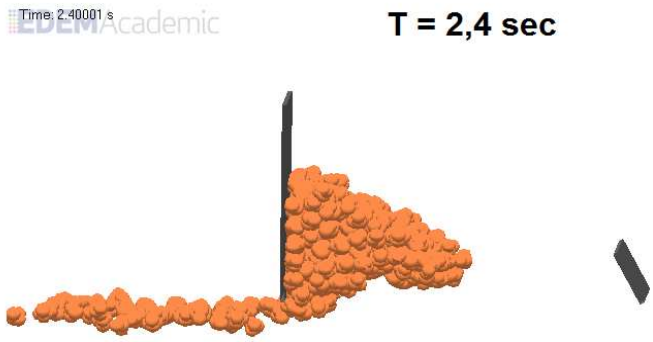

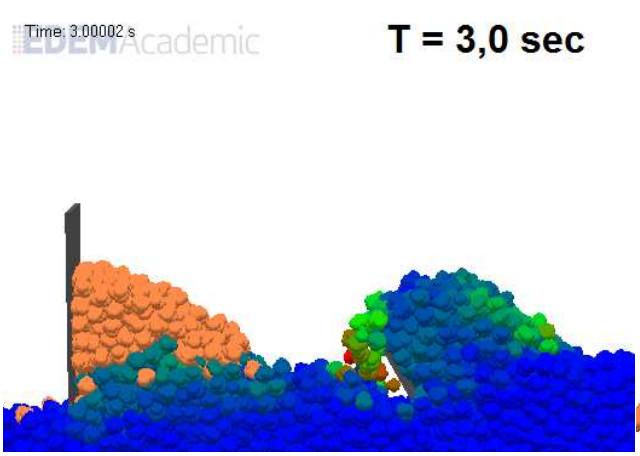

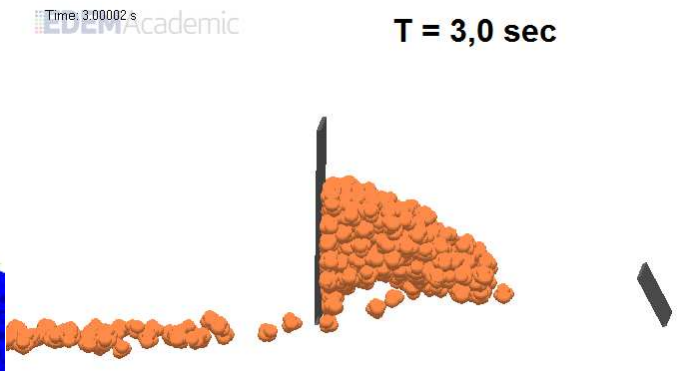

Time: 3.80002 s

T = 3,8 sec

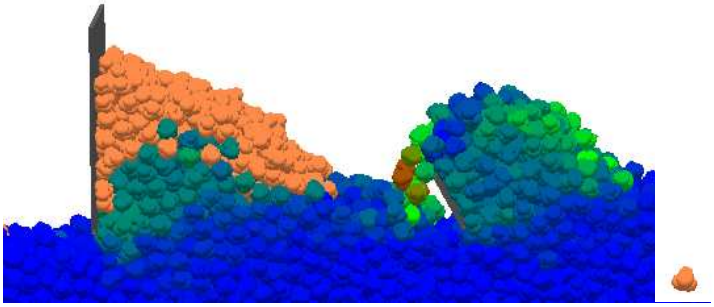

Time: 3.80002 s

T = 3,8 sec

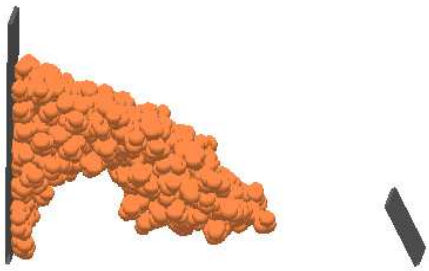

Time: 4.63234 s

T = 4,6 sec

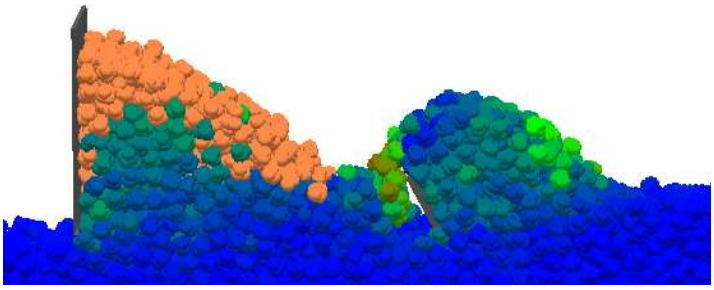

Time: 4.63234 s

T = 4,6 sec

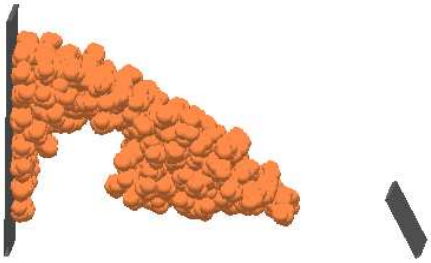

Time: 5.32311 s

T = 5,3 sec

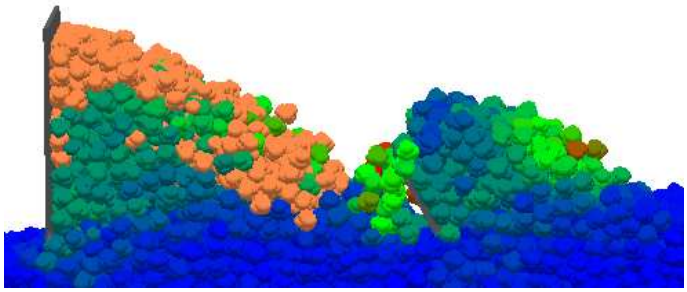

Time: 5.32311 s

T = 5,3 sec

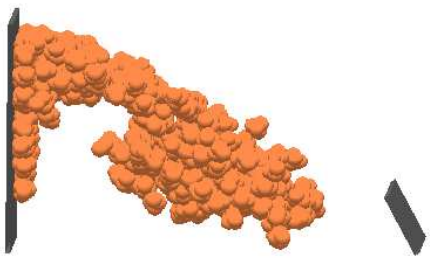

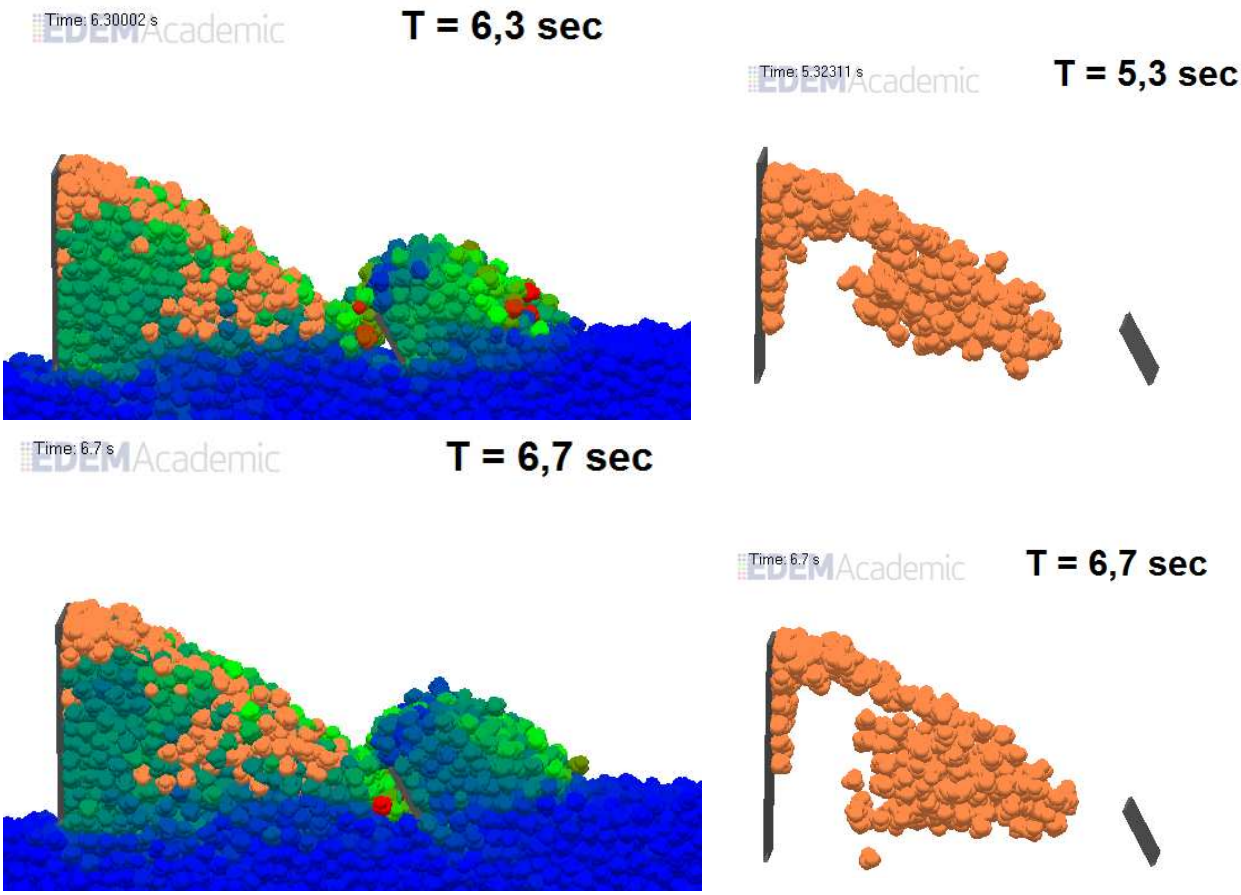

Explanation figures:

1. The start posiotn is at T = 1,6 sec where the soil volume in front of the rear blade is colored orange. The goal is to to view the movement of this volume and the movement of the incoming soil layer by overflow of the front blade. Blue = very small movement, Green = medium movement, Red = large movement.
2. The inflowing soil layer (by the front blade) is colored blue and is therefore laying still at bed. The layer flows underneath the soil volume until it reaches the rear blade at T = 3,0 sec.
3. The layer is cut by rear blade and moves upward, this is more clearly presented in the right figures where the empty space presents the upward moving layer cut. This layer seems initially to roll down already inside the soil volume and form an triangular shape. Later on, at T = 4,6 a soil layer is clearly moving further upward near the blade (empty space). Here can also be seen that particles at the blade interface are moving with a lower upward speed.
4. Particles that reach the surface roll down and are reintegrated in the soil volume just above the inflowing soil layer. A few particles are mixed with the inflowing layer and are following this path.
5. The line from the blade tip to the lower left bound of the orange particles (right picture T = 6,7 sec) gives the shear plane with the corresponding shear angle.

Stone movement for rear blade α =70°

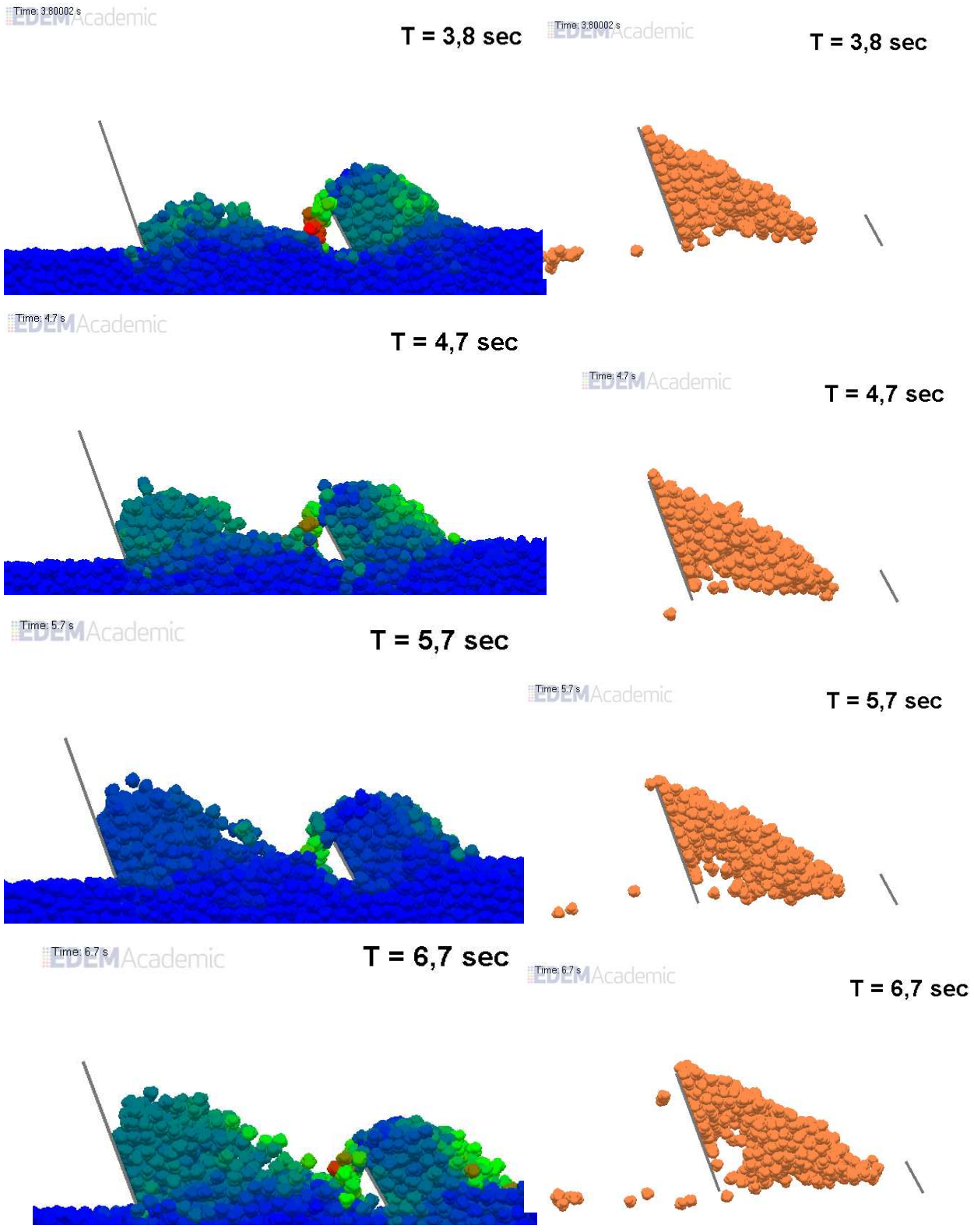

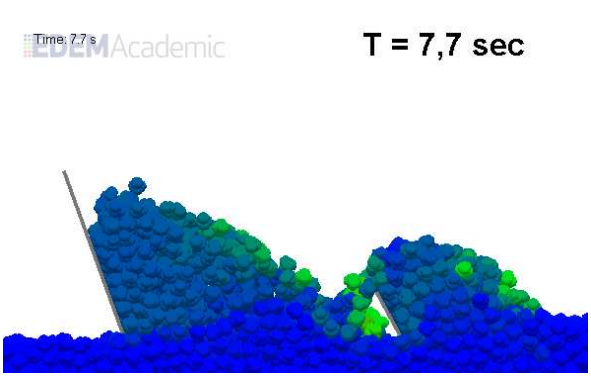

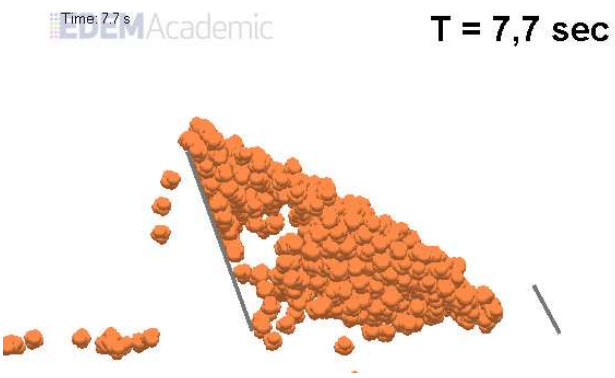

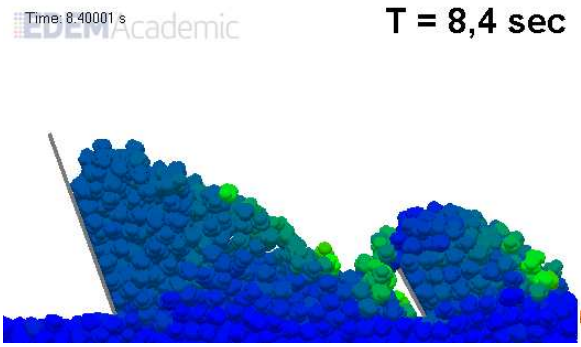

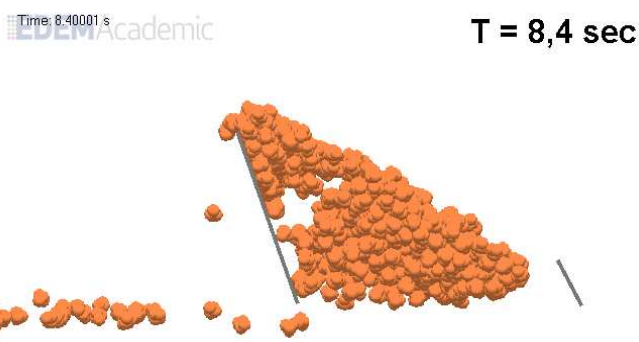

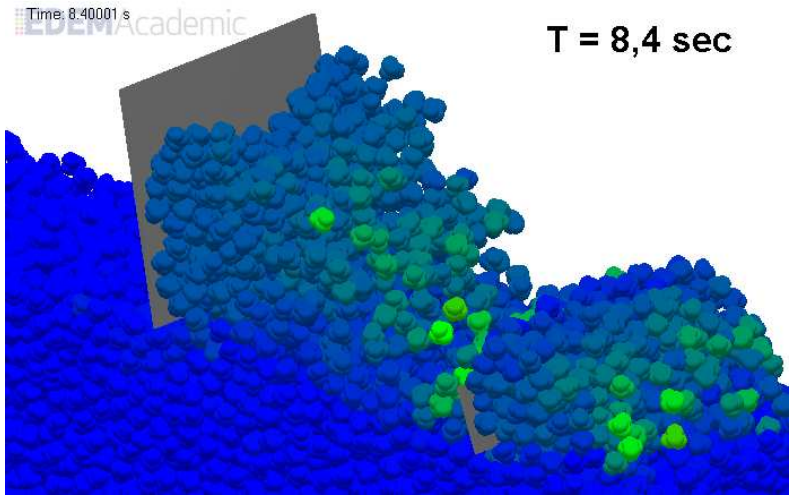

Explanation figures:

The incoming soil layer is indeed building up in a triangular shape, so particles are already rolling down inside the soil volume. The last picture shows on the other hand that the density of the bleu particles is increasing towards the blade and the particles that roll down inside the soil volume are mixed with orange particles.

Appendix IX Graphs Scale model: Transporting

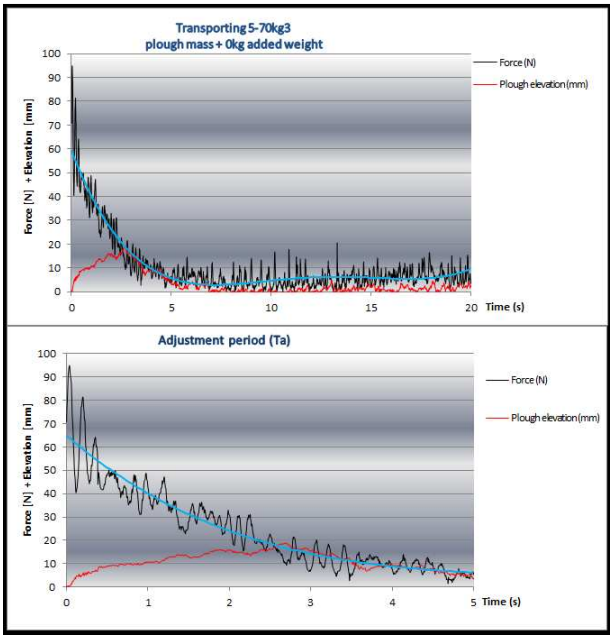

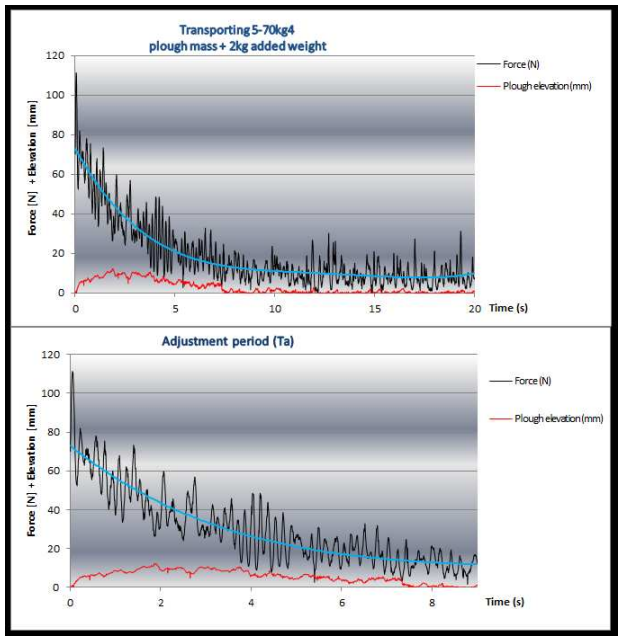

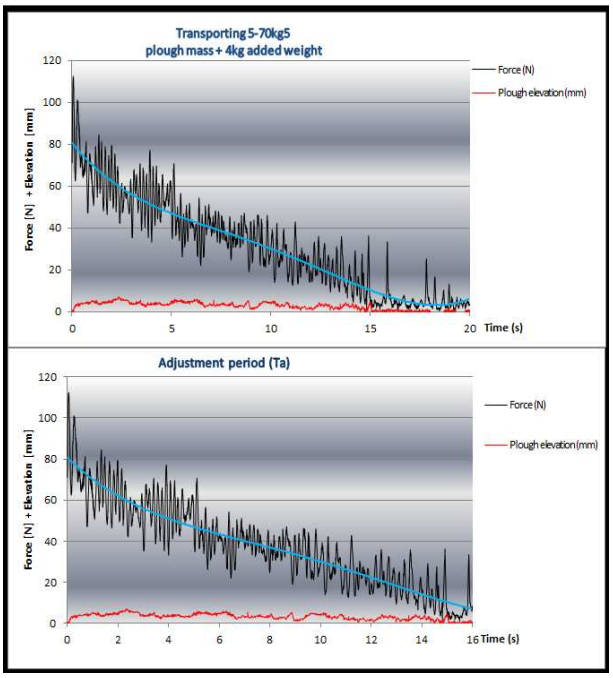

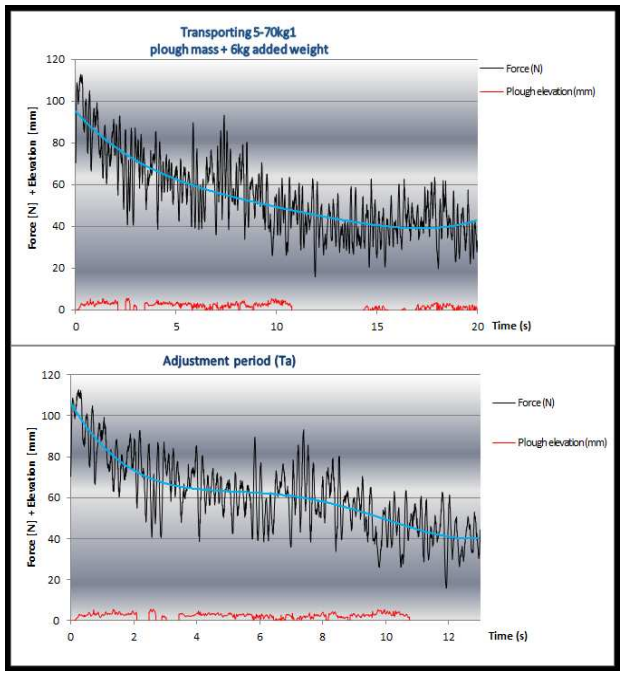

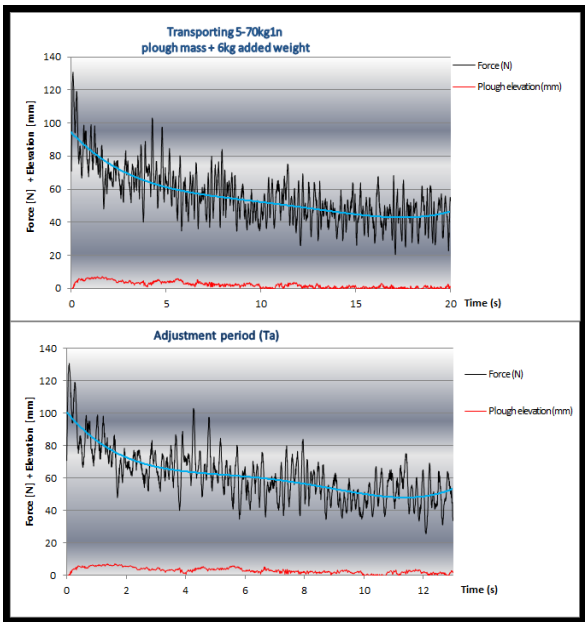
Transporting 5-70kg1n
plough mass + 6kg added weight
Force [N] + Elevation [mm]
Time (s)
Force (N)
Plough elevation (mm)
Adjustment period (Ta)
Force [N] + Elevation [mm]
Time (s)
Force (N)
Plough elevation (mm)

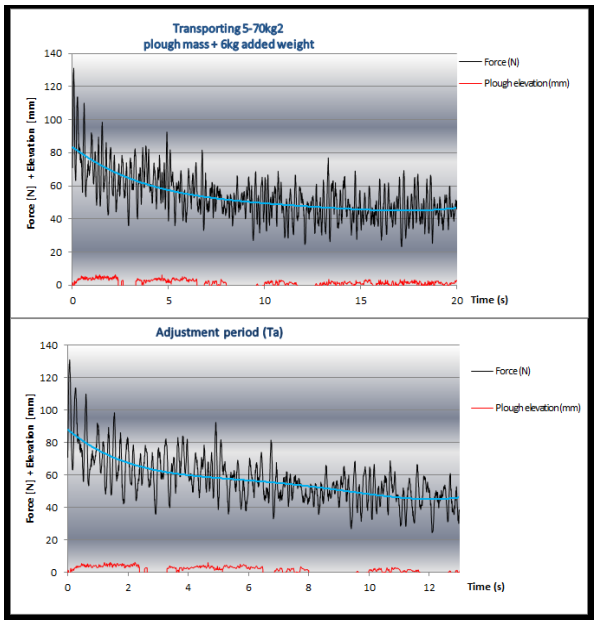
Transporting 5-70kg2
plough mass + 6kg added weight
Force [N] + Elevation [mm]
Time (s)
Force (N)
Plough elevation (mm)
Adjustment period (Ta)
Force [N] + Elevation [mm]
Time (s)
Force (N)
Plough elevation (mm)

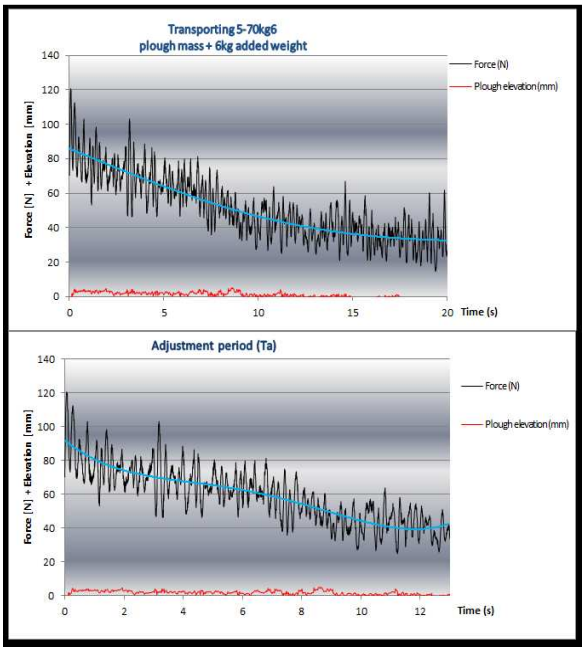
Transporting 5-70kg6
plough mass + 6kg added weight
Force [N] + Elevation [mm]
Time (s)
Force (N)
Plough elevation (mm)
Adjustment period (Ta)
Force [N] + Elevation [mm]
Time (s)
Force (N)
Plough elevation (mm)

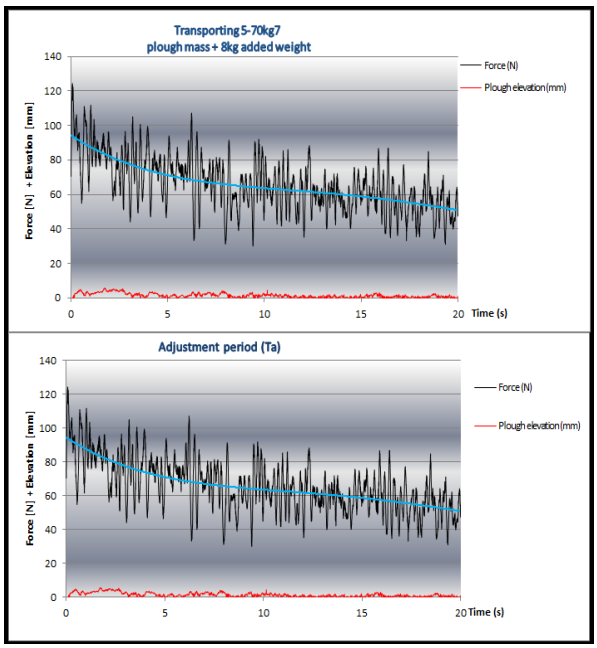
Transporting 5-70kg7
plough mass + 8kg added weight
Force [N] + Elevation [mm]
Time (s)
Force (N)
Plough elevation (mm)
Adjustment period (Ta)
Force [N] + Elevation [mm]
Time (s)
Force (N)
Plough elevation (mm)

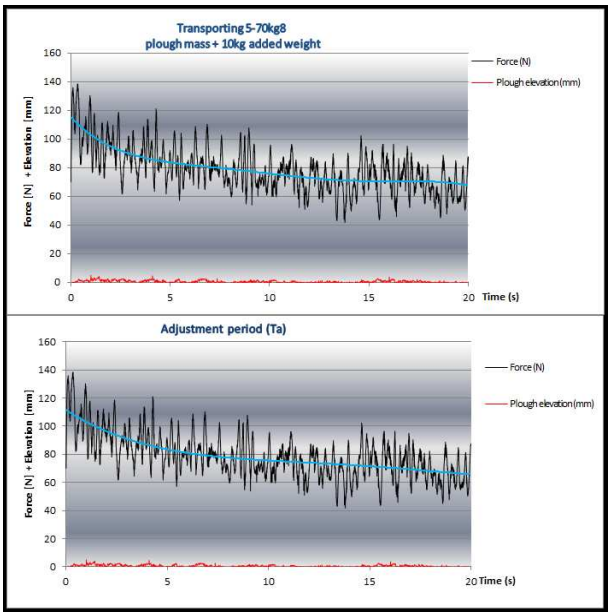
Transporting 5-70kg8
plough mass + 10kg added weight
Force (N)
Plough elevation (mm)
Force [N] + Elevation [mm]
Time (s)
Adjustment period (Ta)
Force (N)
Plough elevation (mm)
Force [N] + Elevation [mm]
Time (s)

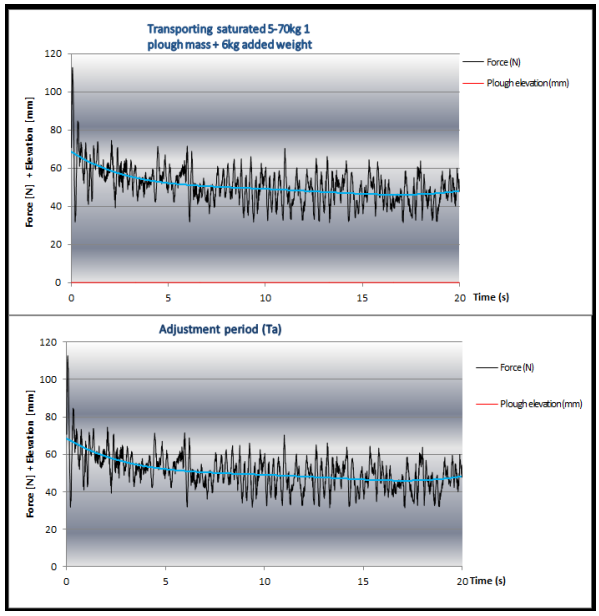
Transporting saturated 5-70kg 1
plough mass + 6kg added weight
Force (N)
Plough elevation (mm)
Force [N] + Elevation [mm]
Time (s)
Adjustment period (Ta)
Force (N)
Plough elevation (mm)
Force [N] + Elevation [mm]
Time (s)

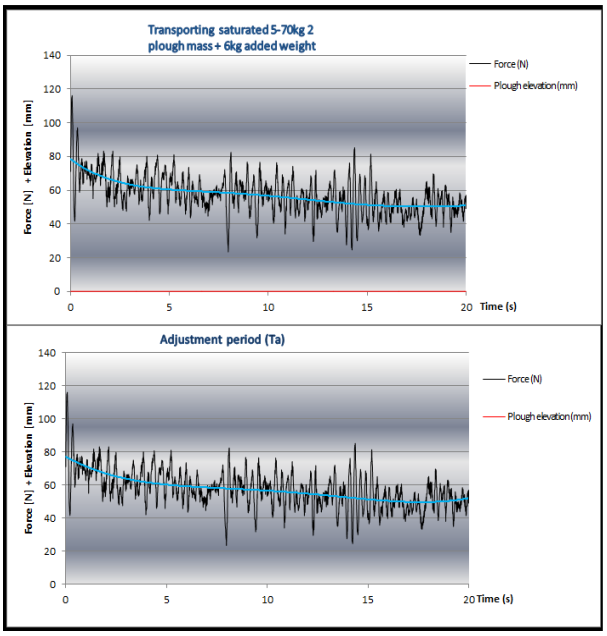
Transporting saturated 5-70kg 2
plough mass + 6kg added weight
Force (N)
Plough elevation (mm)
Force [N] + Elevation [mm]
Time (s)
Adjustment period (Ta)
Force (N)
Plough elevation (mm)
Force [N] + Elevation [mm]
Time (s)

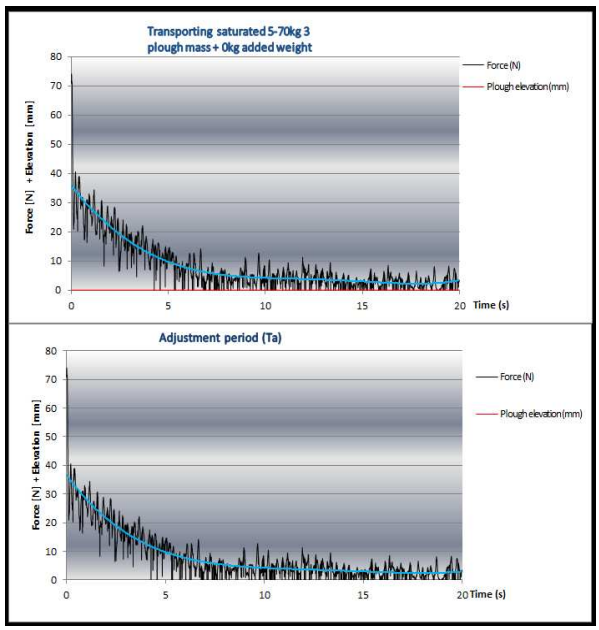
Transporting saturated 5-70kg 3
plough mass + 0kg added weight
Force (N)
Plough elevation (mm)
Force [N] + Elevation [mm]
Time (s)
Adjustment period (Ta)
Force (N)
Plough elevation (mm)
Force [N] + Elevation [mm]
Time (s)

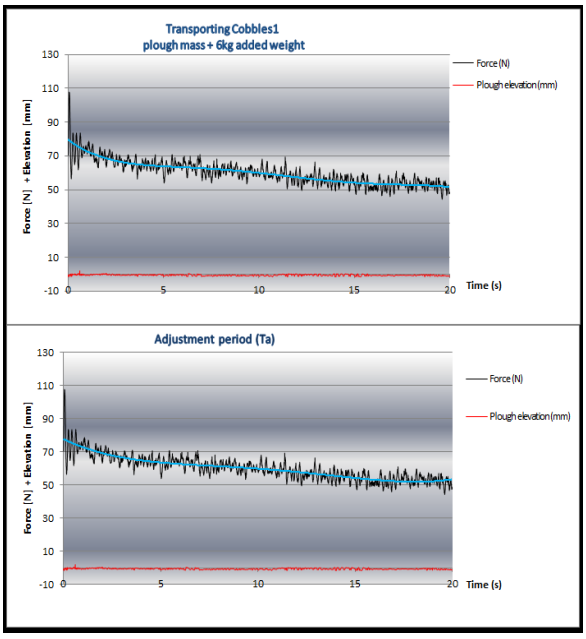
Transporting Cobbles1
plough mass + 6kg added weight
Force (N)
Plough elevation (mm)
Force [N] + Elevation [mm]
Time (s)
Adjustment period (Ta)
Force (N)
Plough elevation (mm)
Force [N] + Elevation [mm]
Time (s)

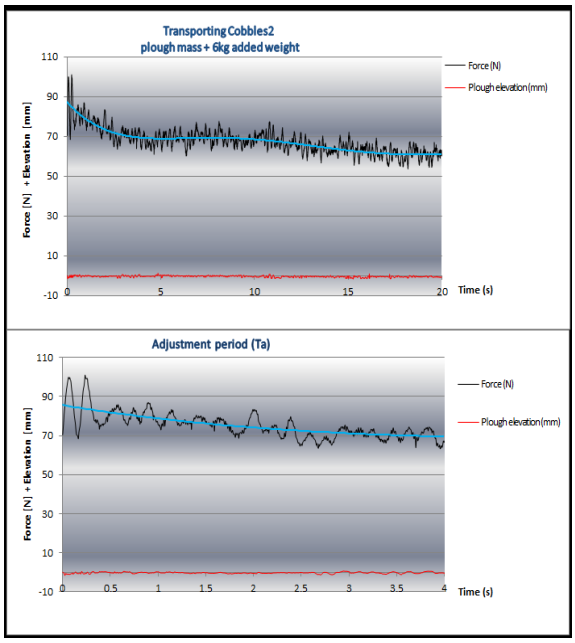
Transporting Cobbles2
plough mass + 6kg added weight
Force (N)
Plough elevation (mm)
Force [N] + Elevation [mm]
Time (s)
Adjustment period (Ta)
Force (N)
Plough elevation (mm)
Force [N] + Elevation [mm]
Time (s)

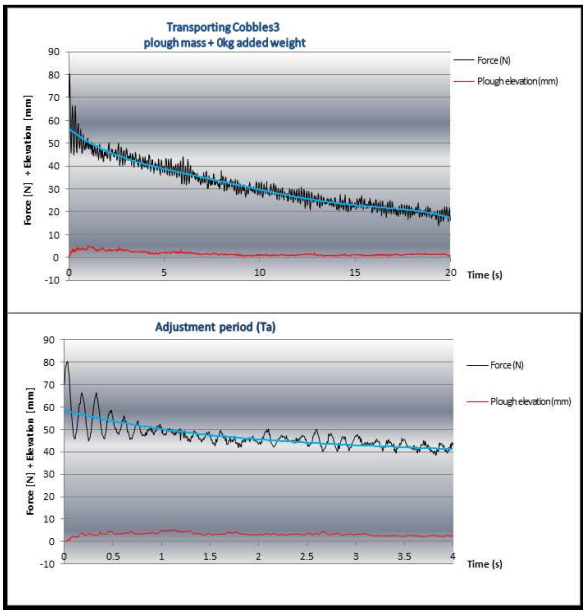
Transporting Cobbles3
plough mass + 0kg added weight
Force (N)
Plough elevation (mm)
Force [N] + Elevation [mm]
Time (s)
Adjustment period (Ta)
Force (N)
Plough elevation (mm)
Force [N] + Elevation [mm]
Time (s)

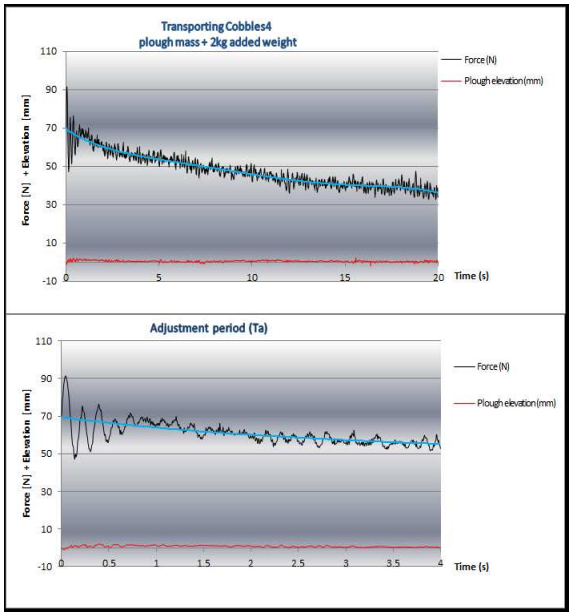
Transporting Cobbles4
plough mass + 2kg added weight
Force (N)
Plough elevation (mm)
Force [N] + Elevation [mm]
Time (s)
Adjustment period (Ta)
Force (N)
Plough elevation (mm)
Force [N] + Elevation [mm]
Time (s)

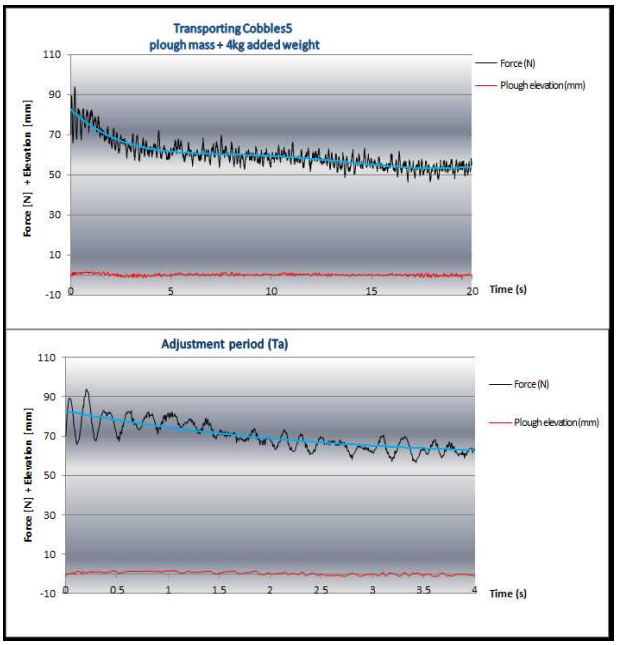
Transporting Cobbles5
plough mass + 4kg added weight
Force [N] + Elevation [mm]
Time (s)
Force (N)
Plough elevation (mm)
Adjustment period (Ta)
Force [N] + Elevation [mm]
Time (s)
Force (N)
Plough elevation (mm)

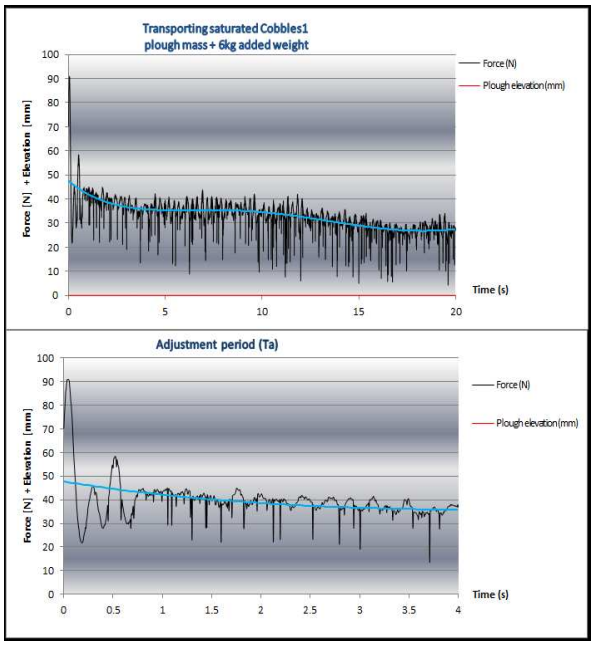
Transporting saturated Cobbles1
plough mass + 6kg added weight
Force [N] + Elevation [mm]
Time (s)
Force (N)
Plough elevation (mm)
Adjustment period (Ta)
Force [N] + Elevation [mm]
Time (s)
Force (N)
Plough elevation (mm)

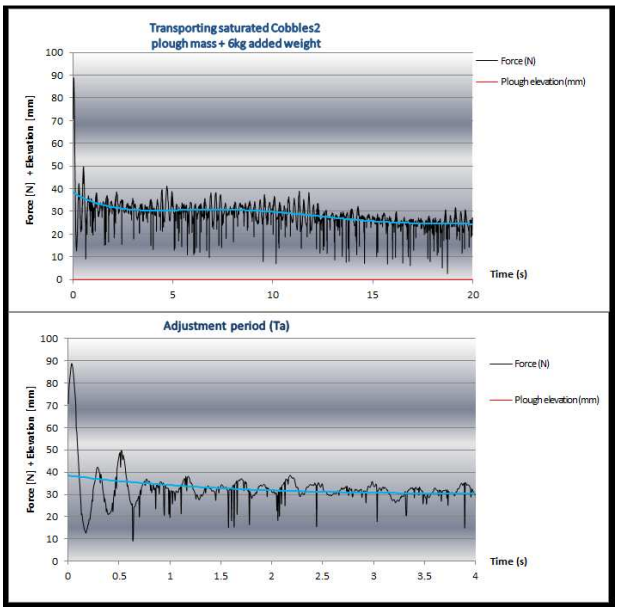
Transporting saturated Cobbles2
plough mass + 6kg added weight
Force [N] + Elevation [mm]
Time (s)
Force (N)
Plough elevation (mm)
Adjustment period (Ta)
Force [N] + Elevation [mm]
Time (s)
Force (N)
Plough elevation (mm)

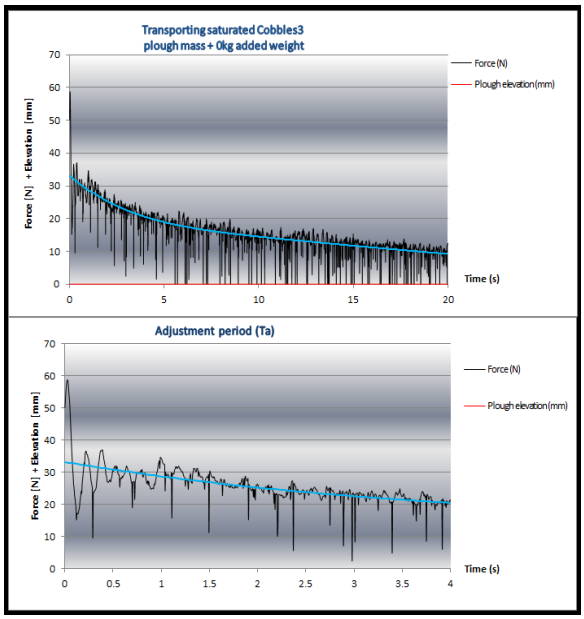
Transporting saturated Cobbles3
plough mass + 0kg added weight
Force [N] + Elevation [mm]
Time (s)
Force (N)
Plough elevation (mm)
Adjustment period (Ta)
Force [N] + Elevation [mm]
Time (s)
Force (N)
Plough elevation (mm)

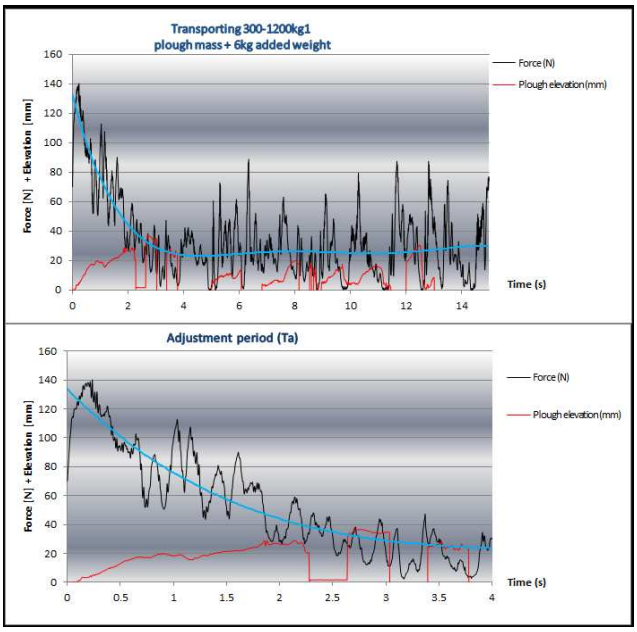
Transporting 300-1200kg1
plough mass + 6kg added weight
Force [N] + Elevation [mm]
Force (N)
Plough elevation (mm)
Time (s)
Adjustment period (Ta)
Force [N] + Elevation [mm]
Force (N)
Plough elevation (mm)
Time (s)

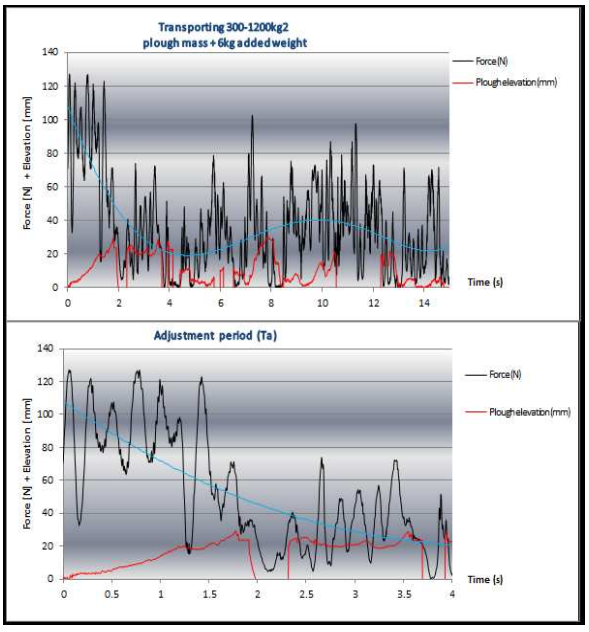
Transporting 300-1200kg2
plough mass + 6kg added weight
Force [N] + Elevation [mm]
Force (N)
Plough elevation (mm)
Time (s)
Adjustment period (Ta)
Force [N] + Elevation [mm]
Force (N)
Plough elevation (mm)
Time (s)

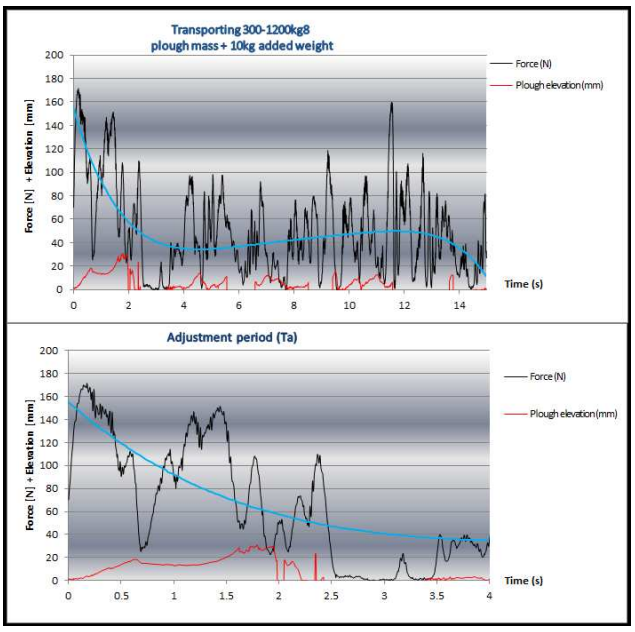
Transporting 300-1200kg8
plough mass + 10kg added weight
Force [N] + Elevation [mm]
Force (N)
Plough elevation (mm)
Time (s)
Adjustment period (Ta)
Force [N] + Elevation [mm]
Force (N)
Plough elevation (mm)
Time (s)

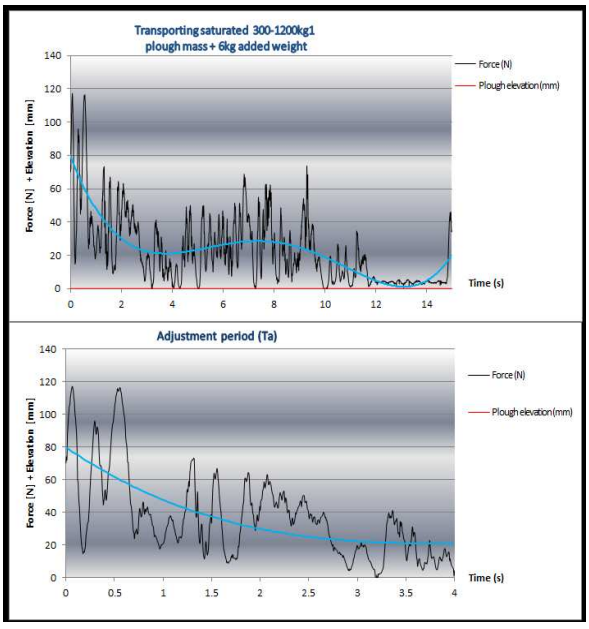
Transporting saturated 300-1200kg1
plough mass + 6kg added weight
Force [N] + Elevation [mm]
Force (N)
Plough elevation (mm)
Time (s)
Adjustment period (Ta)
Force [N] + Elevation [mm]
Force (N)
Plough elevation (mm)
Time (s)

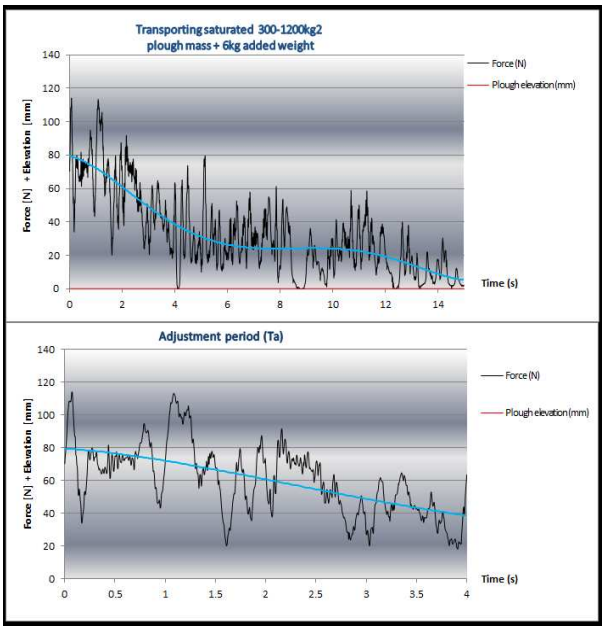
Transporting saturated 300-1200kg2
plough mass + 6kg added weight
Force (N)
Plough elevation (mm)
Force [N] + Elevation [mm]
Time (s)
Adjustment period (Ta)
Force (N)
Plough elevation (mm)
Force [N] + Elevation [mm]
Time (s)

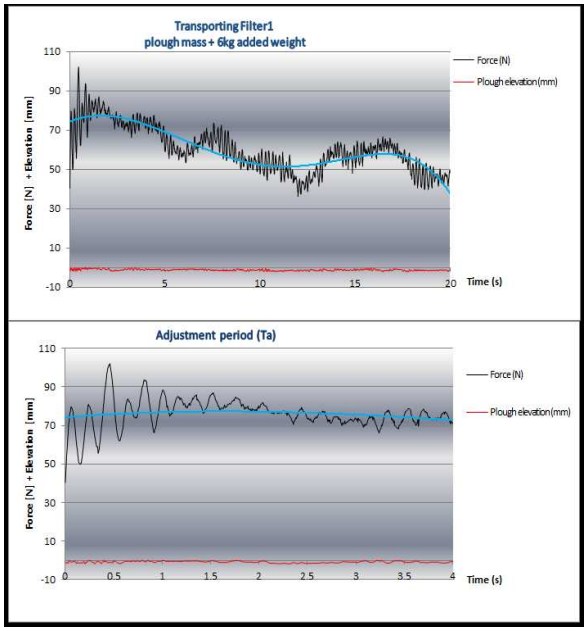
Transporting Filter1
plough mass + 6kg added weight
Force (N)
Plough elevation (mm)
Force [N] + Elevation [mm]
Time (s)
Adjustment period (Ta)
Force (N)
Plough elevation (mm)
Force [N] + Elevation [mm]
Time (s)

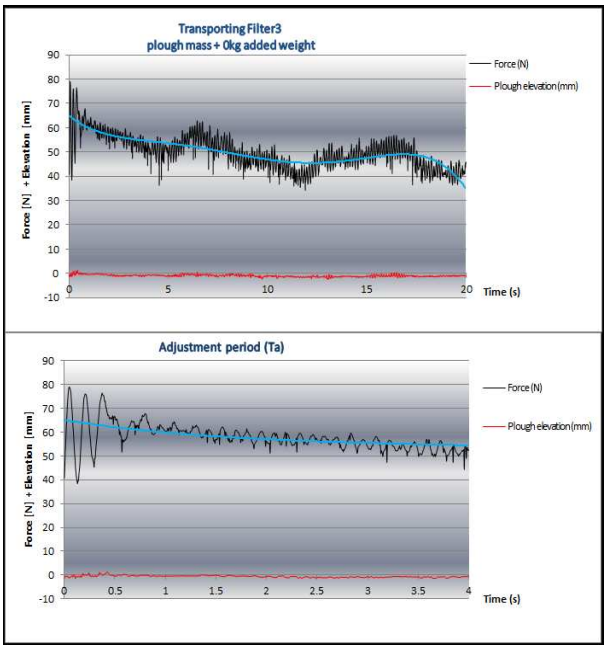
Transporting Filter3
plough mass + 0kg added weight
Force (N)
Plough elevation (mm)
Force [N] + Elevation [mm]
Time (s)
Adjustment period (Ta)
Force (N)
Plough elevation (mm)
Force [N] + Elevation [mm]
Time (s)

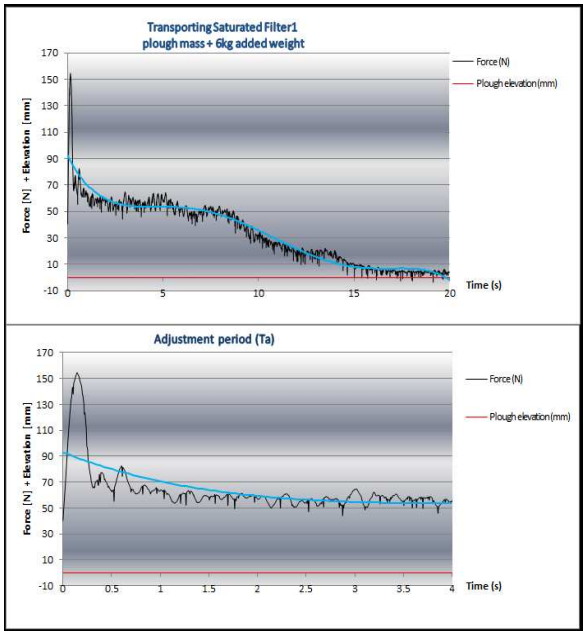
Transporting Saturated Filter1
plough mass + 6kg added weight
Force (N)
Plough elevation (mm)
Force [N] + Elevation [mm]
Time (s)
Adjustment period (Ta)
Force (N)
Plough elevation (mm)
Force [N] + Elevation [mm]
Time (s)

Appendix X Graphs Scale model: Cutting & Transporting

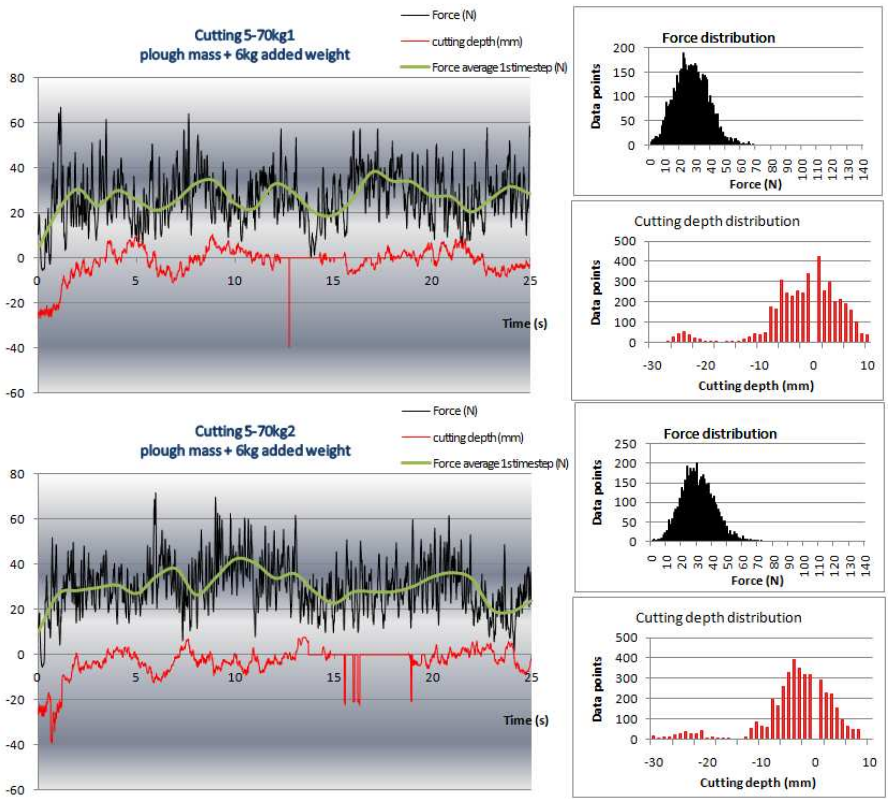

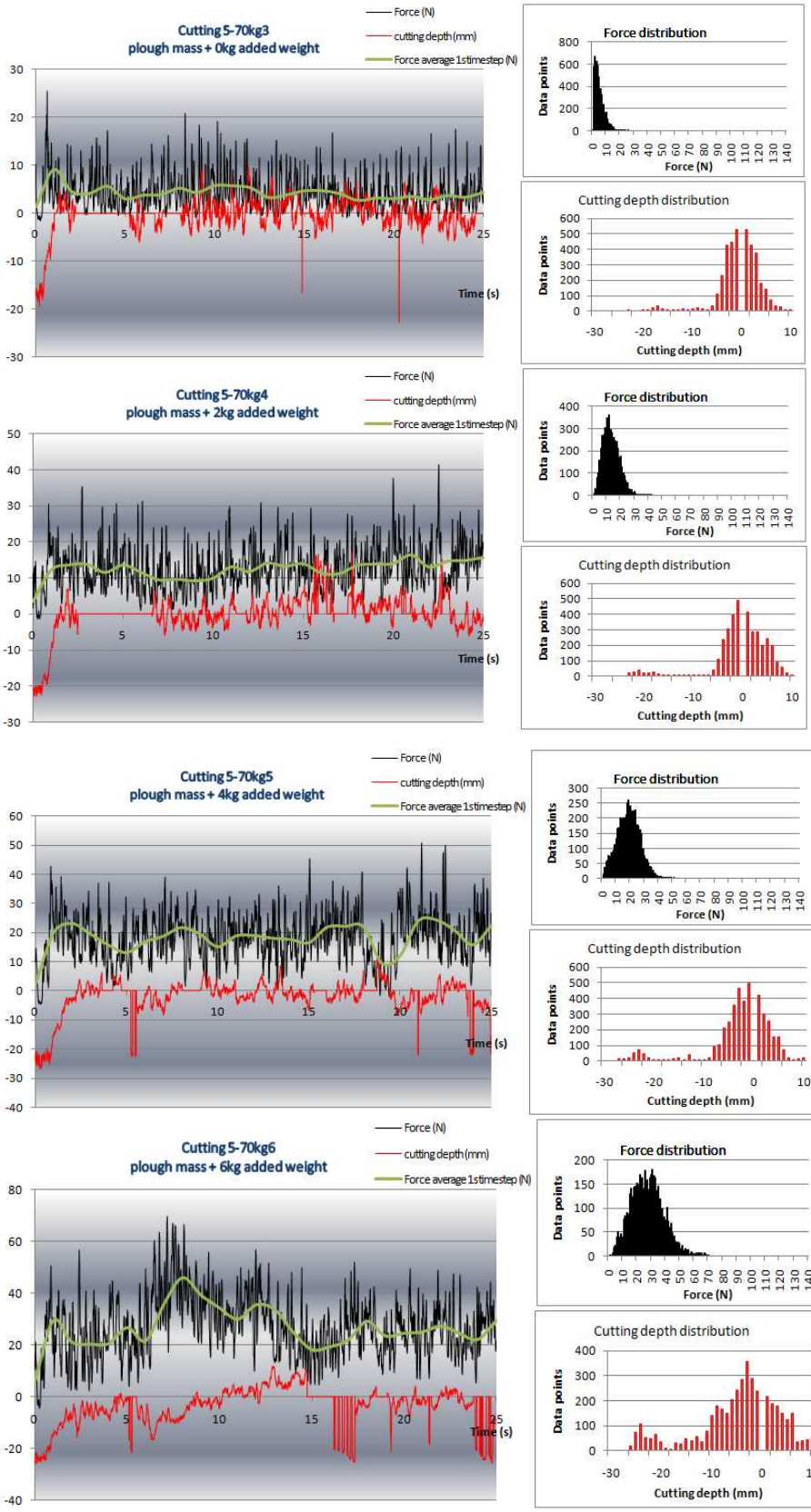
Cutting 5-70kg3
plough mass + 0kg added weight
Force (N)
cutting depth (mm)
Force average 1stimestep (N)
Time (s)
Force distribution
Data points
Force (N)
Cutting depth distribution
Cutting depth (mm)
Cutting 5-70kg4
plough mass + 2kg added weight
Cutting 5-70kg5
plough mass + 4kg added weight
Cutting 5-70kg6
plough mass + 6kg added weight

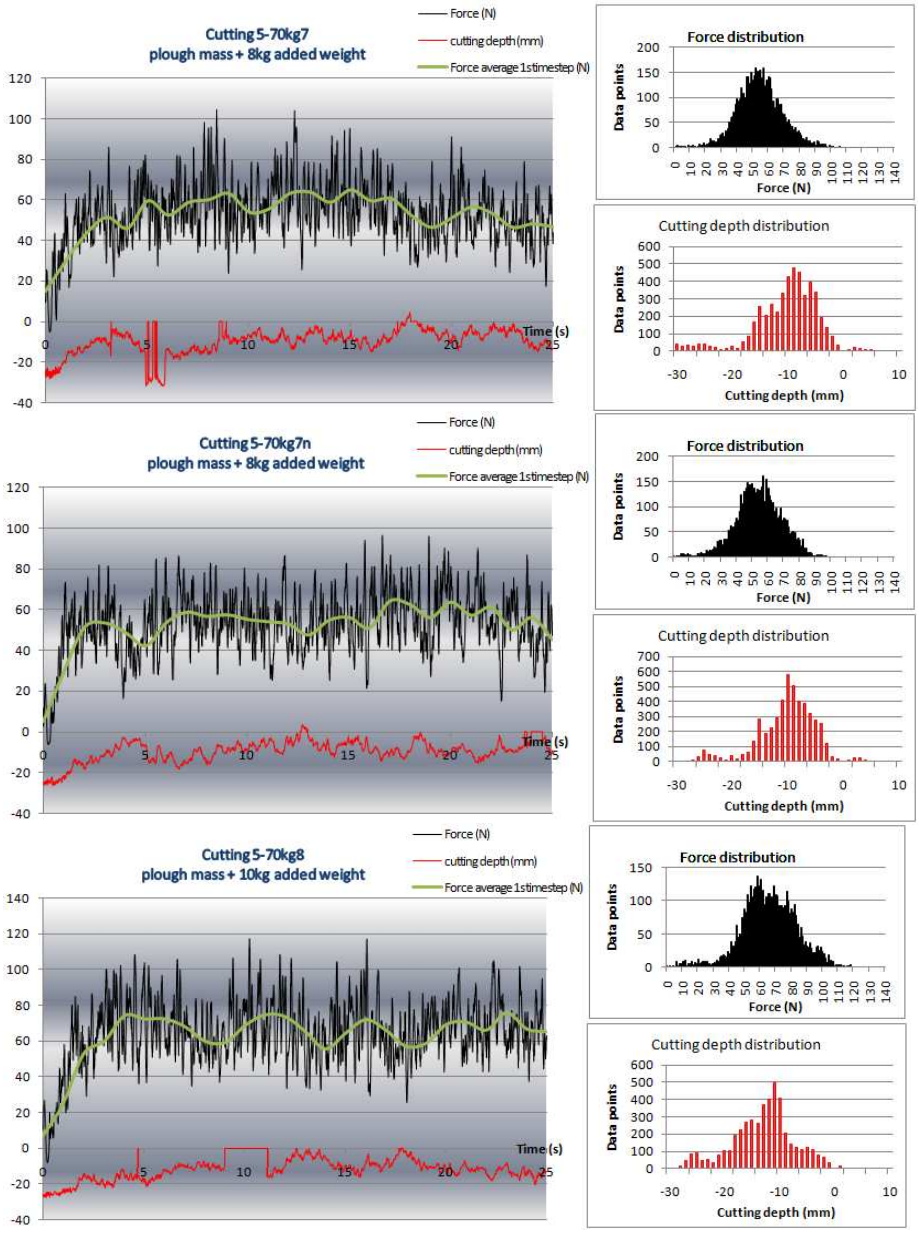
Cutting 5-70kg7
plough mass + 8kg added weight
Force (N)
cutting depth (mm)
Force average 1stimestep (N)
Time (s)
Force distribution
Data points
Force (N)
Cutting depth distribution
Cutting depth (mm)
Cutting 5-70kg7n
plough mass + 8kg added weight
Cutting 5-70kg8
plough mass + 10kg added weight

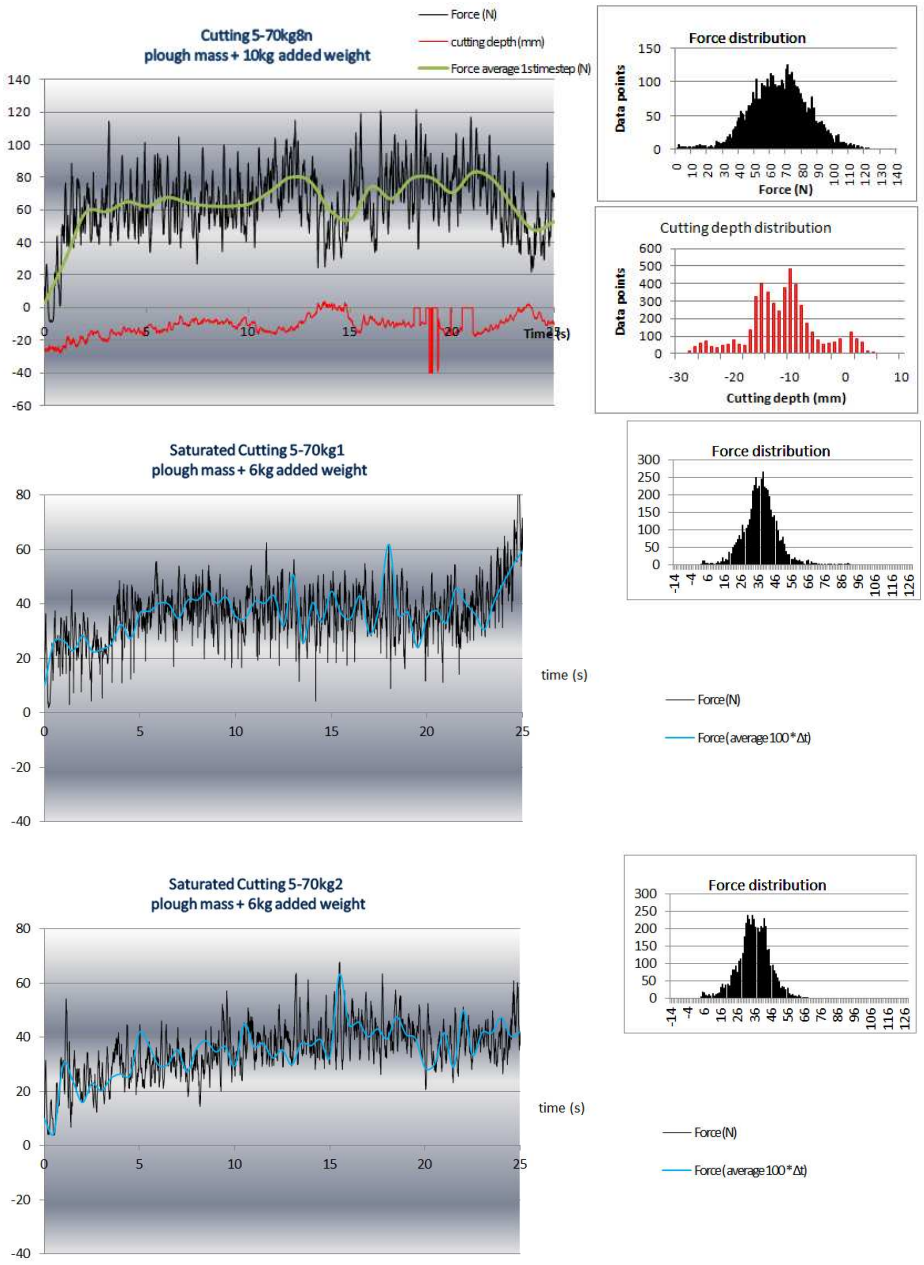
Cutting 5-70kg8n
plough mass + 10kg added weight
Force (N)
cutting depth (mm)
Force average 1stimestep (N)
Time (s)
Force distribution
Data points
Force (N)
Cutting depth distribution
Cutting depth (mm)
Saturated Cutting 5-70kg1
plough mass + 6kg added weight
time (s)
Force(N)
Force(average100*Δt)
Saturated Cutting 5-70kg2
plough mass + 6kg added weight

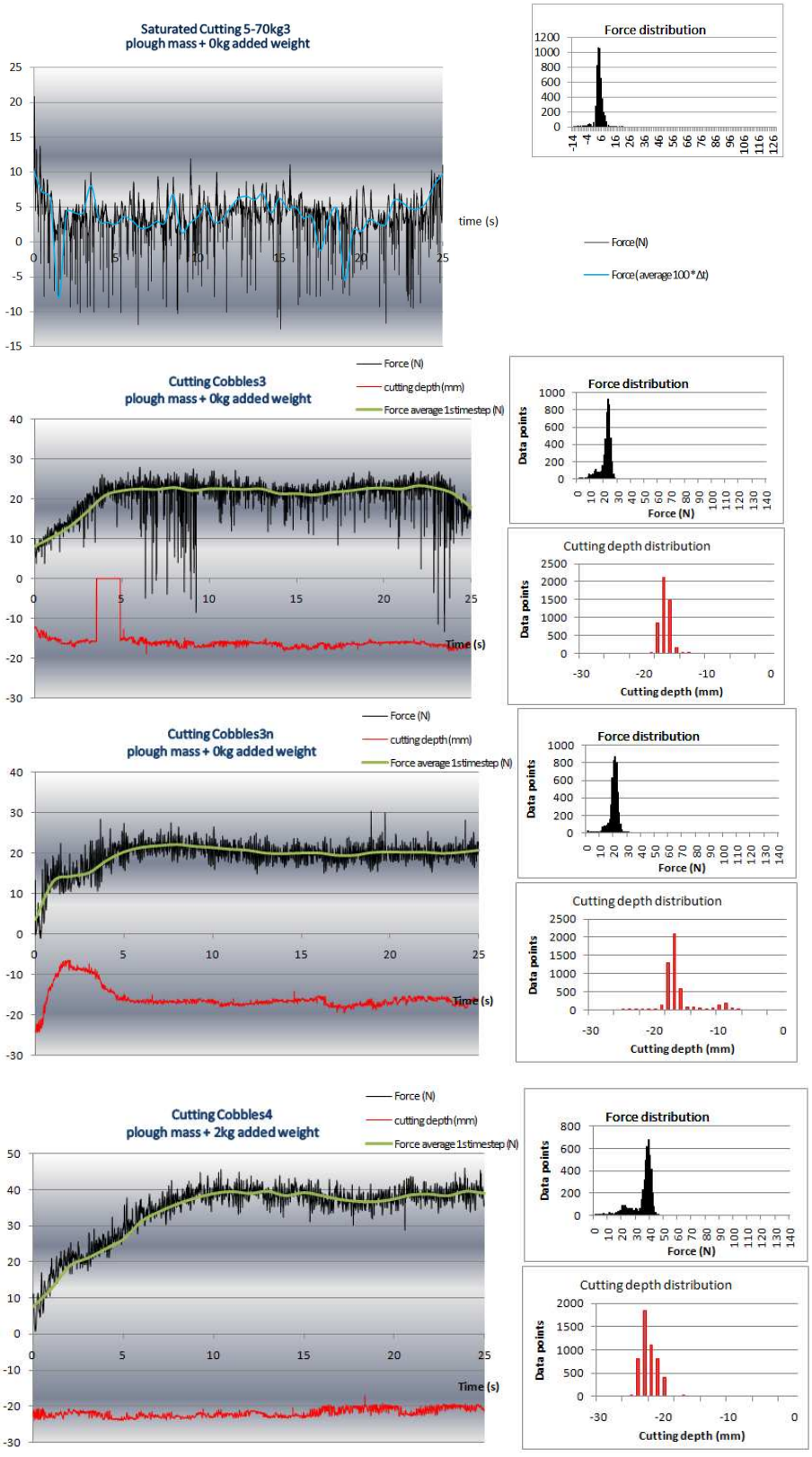
Saturated Cutting 5-70kg3
plough mass + 0kg added weight
time (s)
Force(N)
Force(average100*Δt)
Force distribution
Cutting Cobbles3
plough mass + 0kg added weight
Force (N)
cutting depth (mm)
Force average 1stimestep (N)
Time (s)
Force distribution
Data points
Force (N)
Cutting depth distribution
Cutting depth (mm)
Cutting Cobbles3n
plough mass + 0kg added weight
Cutting Cobbles4
plough mass + 2kg added weight

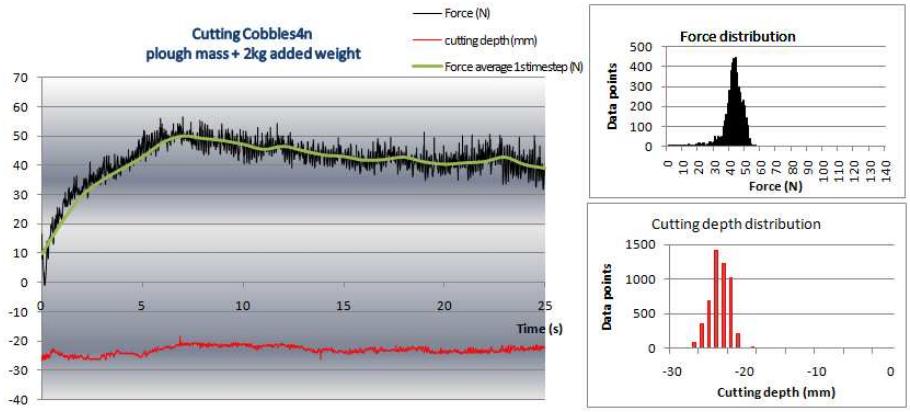
Cutting Cobbles4n
plough mass + 2kg added weight
Force (N)
cutting depth (mm)
Force average 1stimestep (N)
Time (s)
Force distribution
Data points
Force (N)
Cutting depth distribution
Cutting depth (mm)

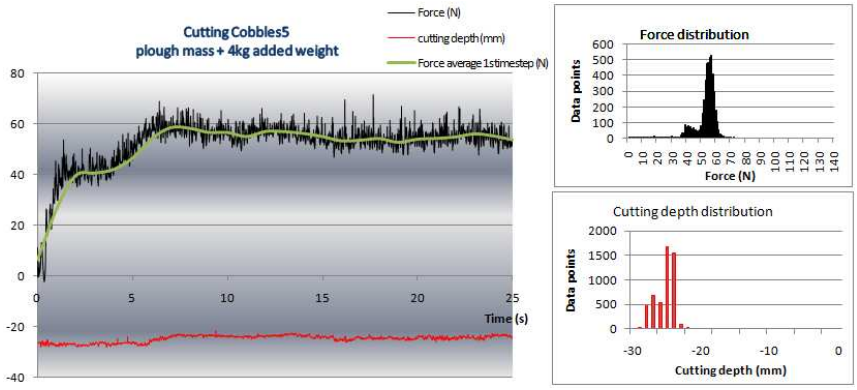
Cutting Cobbles5
plough mass + 4kg added weight
Force (N)
cutting depth (mm)
Force average 1stimestep (N)
Time (s)
Force distribution
Data points
Force (N)
Cutting depth distribution
Cutting depth (mm)

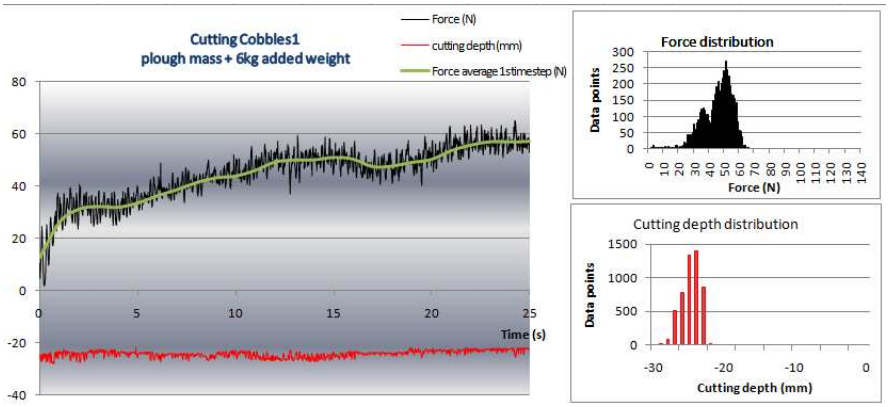
Cutting Cobbles1
plough mass + 6kg added weight
Force (N)
cutting depth (mm)
Force average 1stimestep (N)
Time (s)
Force distribution
Data points
Force (N)
Cutting depth distribution
Cutting depth (mm)

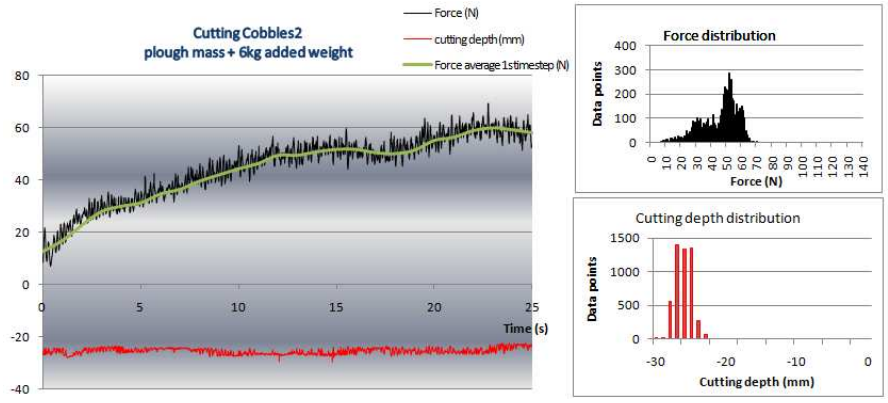
Cutting Cobbles2
plough mass + 6kg added weight
Force (N)
cutting depth (mm)
Force average 1stimestep (N)
Time (s)
Force distribution
Data points
Force (N)
Cutting depth distribution
Cutting depth (mm)

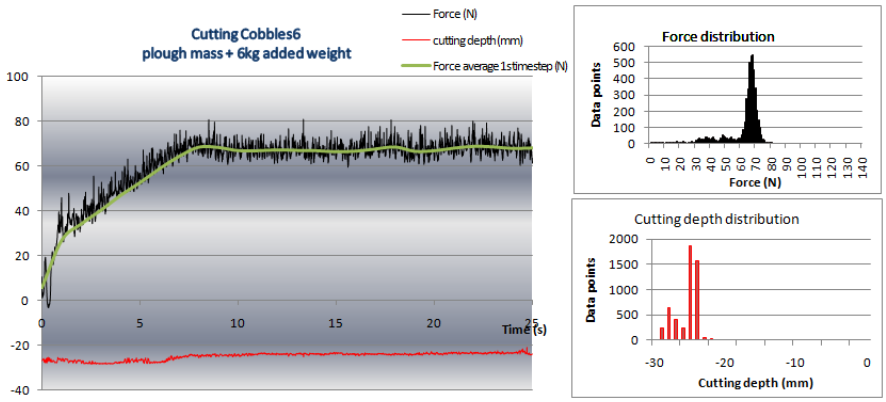
Cutting Cobbles6
plough mass + 6kg added weight
Force (N)
cutting depth (mm)
Force average 1stimestep (N)
Time (s)
Force distribution
Data points
Force (N)
Cutting depth distribution
Data points
Cutting depth (mm)

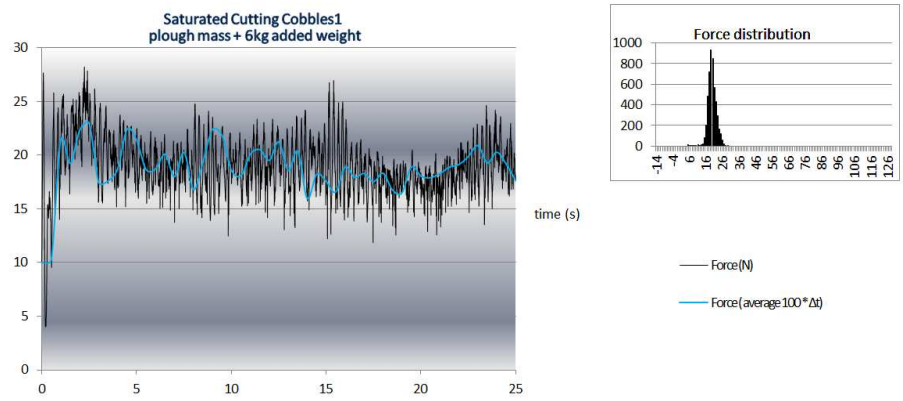
Saturated Cutting Cobbles1
plough mass + 6kg added weight
time (s)
Force distribution
Force(N)
Force(average 100*Δt)

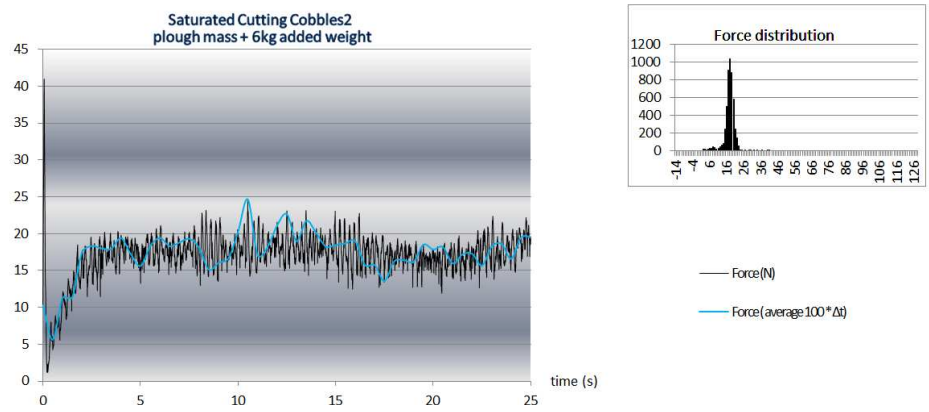
Saturated Cutting Cobbles2
plough mass + 6kg added weight
time (s)
Force distribution
Force(N)
Force(average 100*Δt)

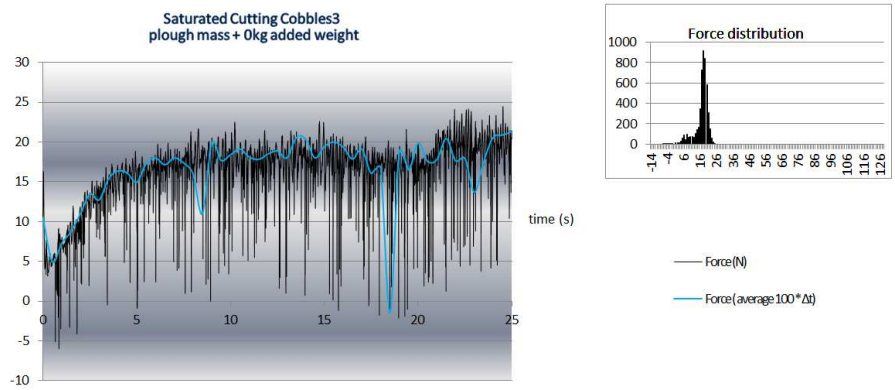
Saturated Cutting Cobbles3
plough mass + 0kg added weight
time (s)
Force distribution
Force(N)
Force(average 100*Δt)

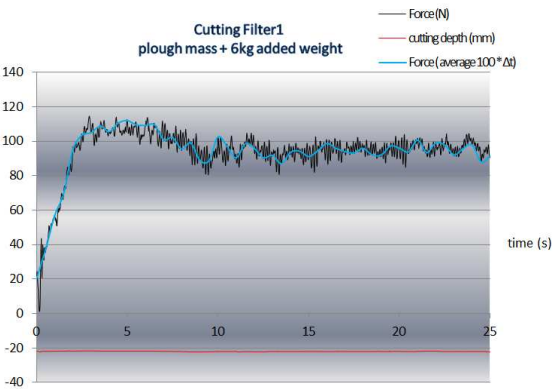
Cutting Filter1
plough mass + 6kg added weight
Force (N)
cutting depth (mm)
Force (average 100 * Δt)
time (s)

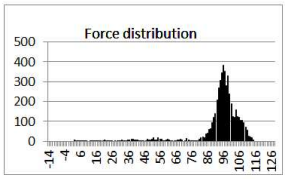
Force distribution

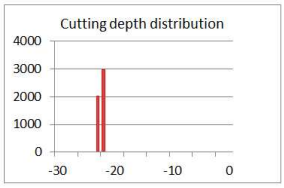
Cutting depth distribution

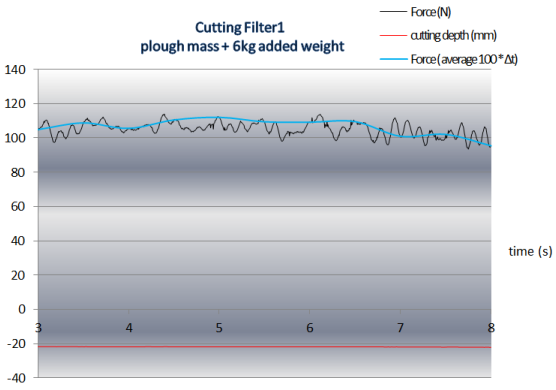
Cutting Filter1
plough mass + 6kg added weight
Force (N)
cutting depth (mm)
Force (average 100 * Δt)
time (s)

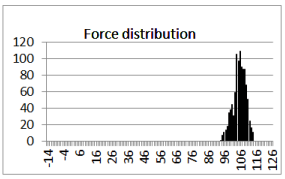
Force distribution

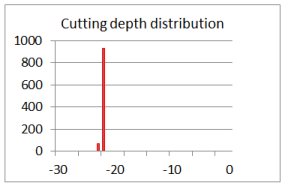
Cutting depth distribution

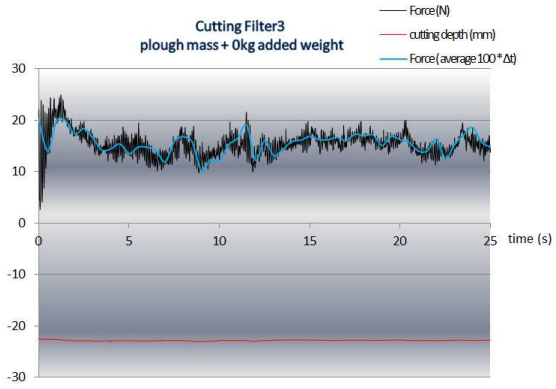
Cutting Filter3
plough mass + 0kg added weight
Force (N)
cutting depth (mm)
Force (average 100 * Δt)
time (s)

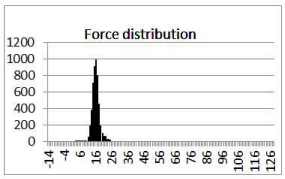
Force distribution

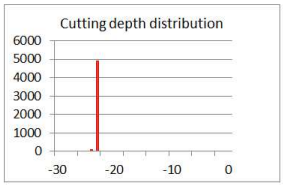
Cutting depth distribution

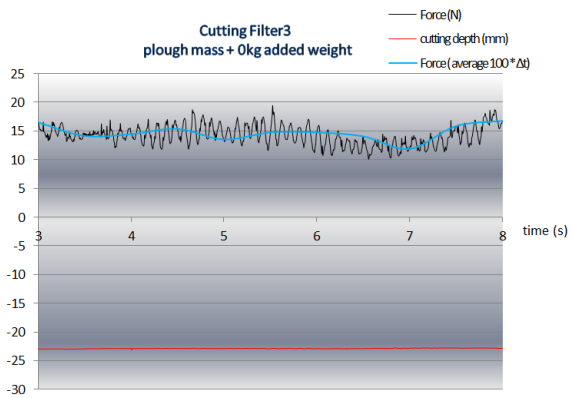
Cutting Filter3
plough mass + 0kg added weight
Force (N)
cutting depth (mm)
Force (average 100 * Δt)
time (s)

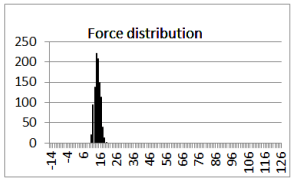
Force distribution

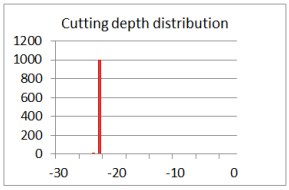
Cutting depth distribution

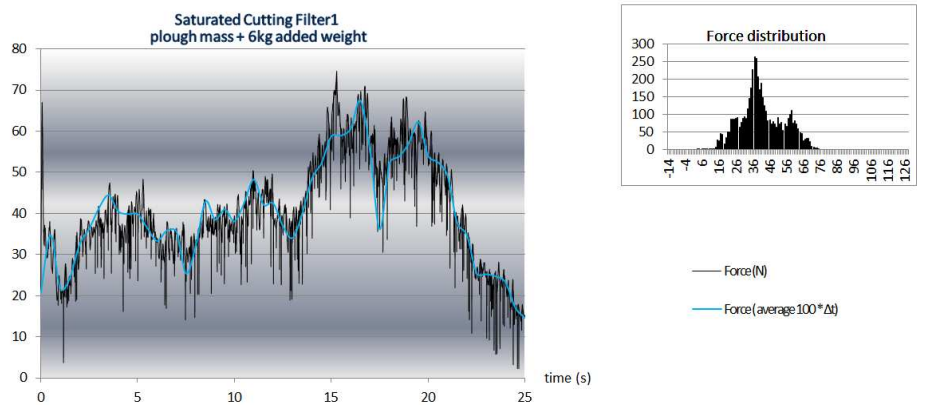
Saturated Cutting Filter1
plough mass + 6kg added weight
time (s)
Force distribution
Force (N)
Force (average 100 * Δt)

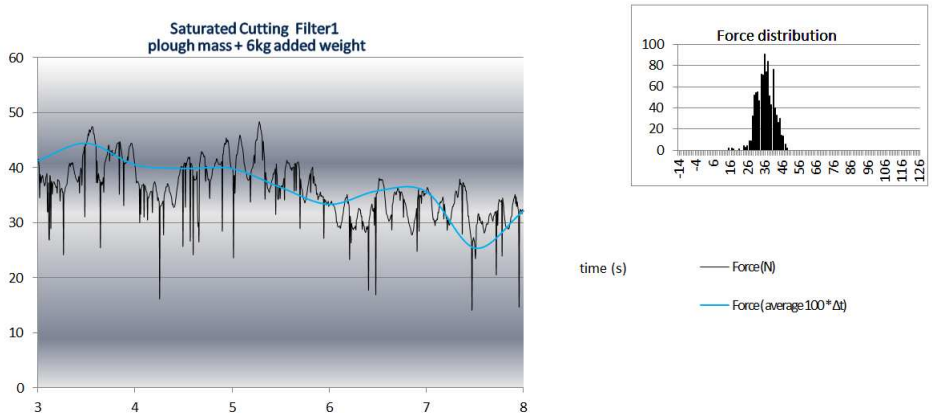
Saturated Cutting Filter1
plough mass + 6kg added weight
time (s)
Force distribution
Force (N)
Force (average 100 * Δt)

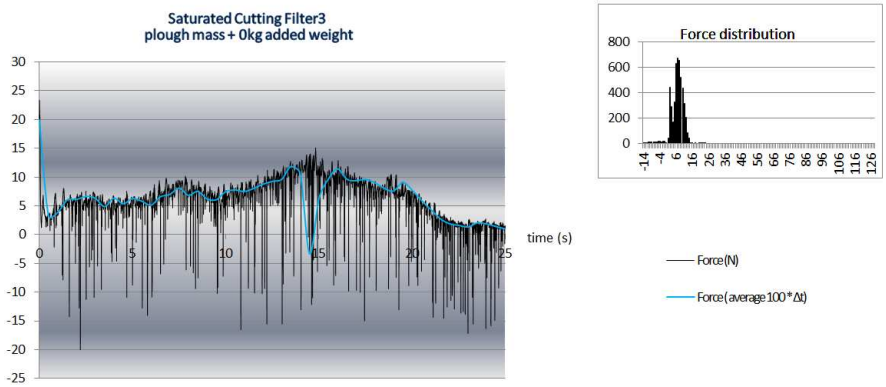
Saturated Cutting Filter3
plough mass + 0kg added weight
time (s)
Force distribution
Force (N)
Force (average 100 * Δt)

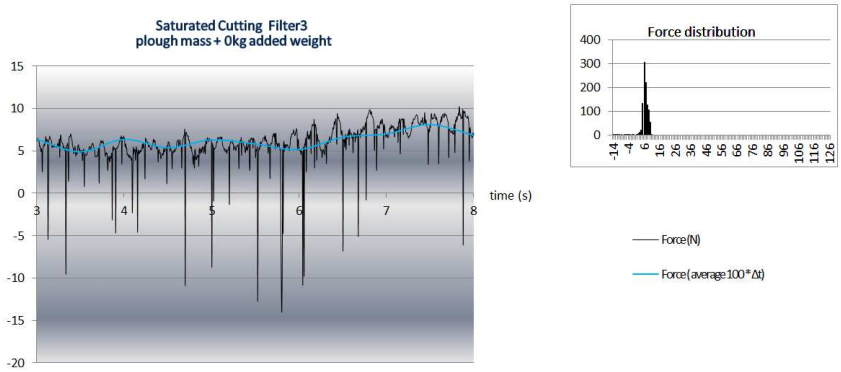
Saturated Cutting Filter3
plough mass + 0kg added weight
time (s)
Force distribution
Force (N)
Force (average 100 * Δt)

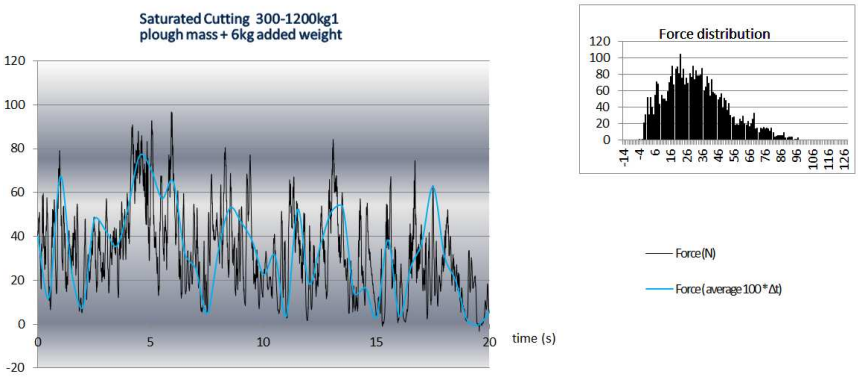
Saturated Cutting 300-1200kg1
plough mass + 6kg added weight
time (s)
Force distribution
Force (N)
Force (average 100 * Δt)

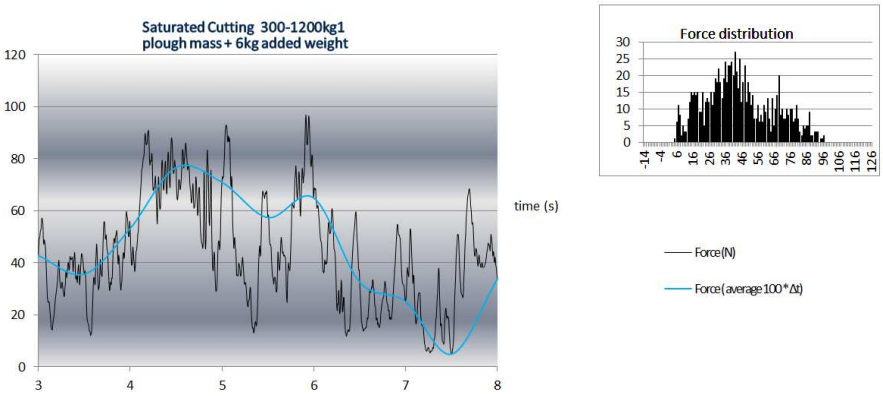
Saturated Cutting 300-1200kg1
plough mass + 6kg added weight
time (s)
Force distribution
Force (N)
Force (average 100 * Δt)

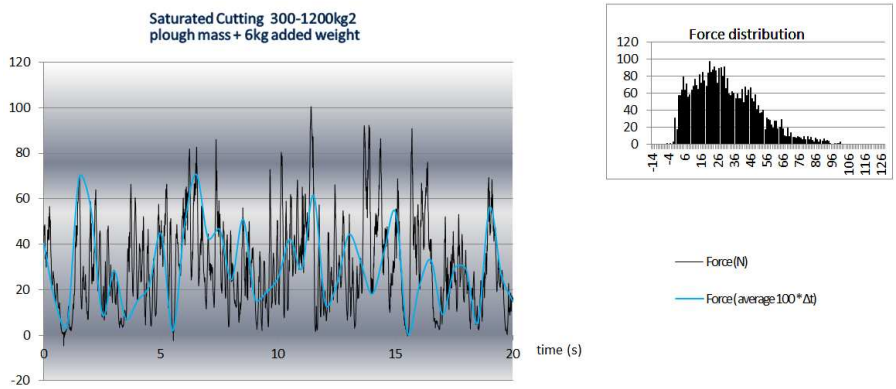
Saturated Cutting 300-1200kg2
plough mass + 6kg added weight
time (s)
Force distribution
Force (N)
Force (average 100 * Δt)

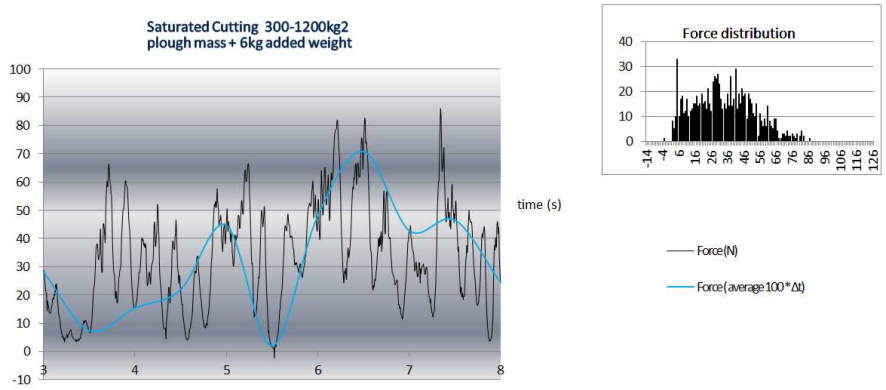
Saturated Cutting 300-1200kg2
plough mass + 6kg added weight
time (s)
Force distribution
Force (N)
Force (average 100 * Δt)